Generic Model for Predicting the Performance of Macro-Synthetic Fibre Reinforced Concrete for Industrial Flooring Applications.

by

Hermanus Lambertus Bester

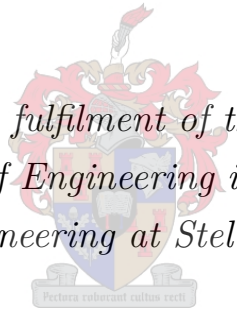

Thesis presented in fulfilment of the requirements for the degree of Master of Engineering in Civil Engineering in the Faculty of Engineering at Stellenbosch University

Department of Structural Engineering,
University of Stellenbosch,
Private Bag X1, Matieland 7602, South Africa.

Supervised by:
Prof. William Peter Boshoff

March 2017

Declaration

By submitting this thesis electronically, I declare that the entirety of the work contained therein is my own, original work, that I am the sole author thereof (save to the extent explicitly otherwise stated), that reproduction and publication thereof by Stellenbosch University will not infringe any third party rights and that I have not previously in its entirety or in part submitted it for obtaining any qualification.

Signature: .....

Date: March 2017

Abstract

The versatility and ready availability of concrete has ensured that this material will continue to be one of great and increasing importance for all types of construction (Domone, 2010). Due to its low tensile strength in comparison with its compressive strength, unreinforced concrete suffers from brittle failure in uni-axial or flexural tension. This drawback can be compensated for by the addition of fibres to the concrete in its fresh state to provide ductility to the brittle concrete matrix.

The primary objective of this study is to create generic models which can be implemented to predict the post-cracking performance of Macro-Synthetic Fibre Reinforced Concrete (MSFRC), specifically for industrial flooring applications. To develop the generic models, an extensive background study on FRC is conducted to identify possible factors influencing the performance of MSFRC. Concrete compressive strength, coarse aggregate size, coarse aggregate volume, fibre dosage, and mixing time of MSFRC in its fresh state are identified as the possible influencing factors. Research hypotheses are stated and investigated to determine which of the factors identified have a significant influence on the post-cracking performance of MSFRC, specifically for an experimental macro-synthetic fibre supplied by CHRYSO.

Generic linear models are derived to predict the residual flexural tensile strength of MSFRC at specific crack mouth opening displacements (CMOD) and are based on the macro-mechanical tests performed according to EN 14651 (European Norms, 2007). It is concluded that fibre dosage is the only identified factor indicating a significant influence on the residual flexural strength of MSFRC. It is also concluded that the limit of proportionality (LOP), which corresponds to the maximum stress between a CMOD of $0 - 0.05$ mm, is only influenced by the compressive strength.

Single-fibre pull-out tests (SFPOT) are performed to investigate the effect of compressive strength on the single-fibre performance of the CHRYSO macro-synthetic experimental fibre in its virgin and premixed fibre state. An increase in the performance is evident for the premixed fibres and can be attributed to the mixing process, causing a roughening of the fibre surface and ultimately increasing the fibre-matrix bond characteristics. It is established that compressive strength does not affect the single-fibre performance of the fibre in its virgin state. However, an increase in the performance of the premixed fibres is evident for a decrease in compressive strength, with the explanation of this phenomenon being unclear.

Simple- and multiple regression analyses are performed to statistically identify the factors that have a significant effect on the performance of MSFRC and to derive linear models predicting the

performance parameters. The regression analyses are based on the obtained macro-mechanical results. As from the visual inspection of the macro-mechanical results, the regression analyses concluded that fibre dosage is the only factor that has a significant effect on the residual flexural tensile strength of MSFRC, and compressive strength as the only factor that influences the LOP. Therefore, the models predicting the performance parameters associated with the residual flexural strength of MSFRC are based on the influence of fibre dosage, and the model predicting the LOP is based on the effect of compressive strength. The models can further be refined with additional experimental data, incorporating a Model Factor (MF) that takes account of additional variation experienced in the construction industry and determining partial material factors (γ_m) to derive suitable design values.

Opsomming

Die veelsydigheid en toeganklikheid van beton het verseker dat hierdie materiaal sal voortgaan om van groot en toenemende belang te wees vir alle vorme van konstruksie (Domone, 2010). Onbewapende beton ly aan bros faling in enkel-aksiale of buigspanning as gevolg van die materiaal se lae treksterkte in vergelyking met die druksterkte. Daar kan vir hierdie nadeel vergoed word deur die byvoeging van vesels tot die beton in die vars toestand om duktiliteit te verskaf aan die bros beton matriks.

Die primêre doel van hierdie navorsingsprojek is om generiese modelle te skep wat geïmplementeer kan word om die na-krakings-gedrag van Makro-Sintetiese Vesel Bewapende Beton (MSVBB) te voorspel, spesifiek met betrekking tot industriële vloer-toepassings. 'n Deeglike agtergrond studie oor Vesel Bewapende Beton (VBB) is uitgevoer om moontlike faktore wat die gedrag van MSVBB kan beinvloed, te identifiseer ten einde die generiese modelle te ontwikkel. Beton druksterkte, growwe aggregaat grootte, growwe aggregaat volume, vesel-volume, en die mengtyd van MSVBB in die vars toestand, is geïdentifiseer as moontlike faktore wat die gedrag van die materiaal kan beïnvloed. Navorsings hipoteses is gestel en ondersoek om vas te stel watter faktore 'n beduidende invloed het op die na-krakings gedrag van MSVBB, met inagneming van 'n eksperimentele makro-sintetiese vesel verskaf deur CHRYSO.

Generiese lineêre modelle is afgelei om die oorblywende buig-treksterkte van MSVVB te voorspel by spesifieke Kraak-Mond Opening Verplasings (KMOV) en is gebaseer op die makromeganiese toetse wat uitgevoer is vervolgens EN 14651 (European Norms, 2007). Vesel-volume is geïdentifiseer as die enigste faktor wat 'n beduidende invloed het op die oorblywende buig-treksterkte van MSVVB. Daar is ook bevind dat die Limiet van Proporsionaliteit (LVP), wat ooreenstem met die maksimum spanning tussen 'n KMOV van $0 - 0,05$ mm, slegs beïnvloed word deur die beton druksterkte.

Enkelvesel-uittrektoetse is uitgevoer om die effek van beton druksterkte op die enkel-vesel gedrag van die CHRYSO makro-sintetiese eksperimentele vesel, in die ongemengde en voorafgemengde vesel-toestand, te ondersoek. 'n Toename in die gedrag was merkbaar in die geval van die voorafgemengde vesel, en kan toegeskryf word aan die mengproses, wat veroorsaak dat die oppervlak van die sintetiese vesel beskadig word en uiteindelik die bindingseienskappe van die vesel-matriks positief beïnvloed. Daar is vasgestel dat beton-druksterkte nie die gedrag van die enkel-vesel beïnvloed in die ongemengde toestand nie. 'n Toename in die gedrag van die voorafgemengde vesel was merkbaar vir 'n afname in beton druksterkte.

Eenvoudige- en meervoudige regressie-analises is uitgevoer om die faktore wat 'n beduidende

invloed het op die gedrag van MSVBB, statisties te ontleed en te identifiseer, asook om lineêre generiese modelle te ontwikkel om die prestasie parameters te voorspel. Die regressie-ontledings is gebaseer op die driepuntbuig makro-meganiese resultate. In ooreenstemming met die gevolgtrekkings van die visuele inspeksie van die makro-meganiese resultate, het die regressie-ontledings getoon dat vesel-volume die enigste faktor is wat 'n beduidende effek het op die na-krakings gedrag van MSVVB, en druksterkte die enigste faktor is wat 'n beduidende effek het op die LVP. Dus is die liniêre modelle wat die prestasie parameters voorspel en verband hou met die na-krakings-gedrag van MSVBB, gebaseer op die invloed van vesel-volume, en die model wat die LVP voorspel gebaseer op die effek van beton-druksterkte. Die lineêre modelle kan verder verfyn word met bykomende eksperimentele data, asook deur 'n Model Faktor (MF) te inkorporeer wat additionele variasies in berekening bring as gevolg van onsekerhede in die konstruksie industrie. Parsïele materiaal faktore (γ_m) moet ook in ag geneem word om gepaste ontwerp-waardes te bepaal.

Acknowledgements

I would like to express my sincere gratitude to the following people for their support and assistance during the course of this study:

- My promoter and supervisor, Prof. Billy Boshoff, for his guidance and support throughout the course of the study period.
- The Civil Engineering laboratory and workshop staff at Stellenbosch University, for their assistance during the execution of the experimental work.
- Fibre and admixture supplier, CHRYSO, for their continual support and providing the opportunity to conduct this study.
- Laurent Bonafous, Noureddine Houhou, and Brenton Bouard from CHRYSO, providing valuable input throughout the study.
- My family and friends, especially my girlfriend Kent Stocken, for their unconditional love and support for the duration of my studies.
- Lastly, my Lord and Saviour providing me the strength and ability to complete my studies.

Contents

List of Figures

List of Tables

Nomenclature

b	Width of beam specimen (mm)
d	Diameter (mm)
d_e	Equivalent diameter (mm)
E_{mod}	Elastic modulus (GPa)
f_{cf}	Uni-axial tensile strength of concrete (MPa)
f_{ck}	Characteristic value
$f_{ck,c}$	Characteristic compressive cylinder strength of concrete at 28 days
$f_{ctk,fl}$	Characteristic flexural strength of plain concrete (MPa)
f_d	Design value
f_{LOP}	Strength corresponding to the maximum load achieved within a CMOD of $0 - 0.05$ mm (MPa)
$f_{LOP,ck}$	Characteristic value corresponding to the LOP (MPa)
f_R	Residual flexural tensile strength (MPa)
$f_{Rj,ck}$	Characteristic residual flexural tensile strength (j=$1, 2, 3, 4$) (MPa)
f_{R1}	Residual flexural tensile strength corresponding to a CMOD of 0.5 mm (MPa)
f_{R2}	Residual flexural tensile strength corresponding to a CMOD of 1.5 mm (MPa)
f_{R3}	Residual flexural tensile strength corresponding to a CMOD of 2.5 mm (MPa)
f_{R4}	Residual flexural tensile strength corresponding to a CMOD of 3.5 mm (MPa)
$F_{applied}$	Applied force (N)
$F_{fracture}$	Fibre fracture strength (N)
F_L	Maximum load in the CMOD interval $0 - 0.05$ mm (N)
F_{max}	Maximum single-fibre pull-out load (N)
F_R	Applied force at a specific CMOD

F_{ratio}	Ratio between the explained and unexplained variance according to the regression model
$F_{resistance}$	Resisting force (N)
h	Height of beam specimen (mm)
h_0	Notional size of the cross-section (mm)
h_{sp}	Distance between the tip of the notch and the top of the specimen (mm)
K	Workability factor
k_h	Coefficient depending on the notional size h_0
l	Span length (mm)
l_c	Critical fibre length (mm)
l_e	Embedment length (mm)
l_f	Fibre length (mm)
m	Mass of single fibre (g)
M_a	Mass of coarse aggregates in 1 kg/m^3 of concrete (kg)
M_n	Negative moment capacity (Nm)
M_p	Positive moment capacity (Nm)
r_f	Fibre radius (mm)
R^2	Coefficient of determination
$R_{e,3}$	Equivalent flexural tensile strength (MPa)
S	Surface-to-surface spacing between fibres (mm)
SS_M	Model sum of squares
SS_R	Sum of squared residuals
SS_T	Total sum of squares
t	Age of the concrete at a specific time (days)
t_s	Age of concrete at the beginning of drying shrinkage (days)
V_f	Fibre volume ratio (%)
y_0	Depth of neutral axis (mm)
Y	Observed values

$\bar{Y}$	Mean of the observed values
Y'	Predicted values
Z	Standard normal variable

List of greek symbols

α	Significance level
β	Coefficient reflecting the relative impact of an IV on the DV
β_R	Reliability index
γ_c	Partial safety factor for SFRC
γ_j	Regression coefficients (j=$0, 1, 2, ..., n$)
γ_M	Partial factor of material properties
ε	Elastic strain (μm)
ε_{ca}	Autogenous shrinkage strain (μm)
ε_{cd}	Drying shrinkage strain (μm)
$\varepsilon_{cd,0}$	Nominal unrestrained drying shrinkage strain (μm)
ε_{cs}	Total shrinkage strain (μm)
μ	Mean value
ξ	Random regression error term
ρ	Fibre material density (kg/m^3)
σ	Standard deviation
σ_f	Tensile stress of fibre (MPa)
σ_{R1}	Mean axial tensile strength corresponding to a CMOD of 0.5 mm (MPa)
σ_{R4}	Mean axial tensile strength corresponding to a CMOD of 3.5 mm (MPa)
$\sigma_w(w)$	Stress-crack opening relationship
τ	Interfacial shear bond stress (MPa)
ϕ	Angular deformation

Abbreviations

ACI	American Concrete Institute
ASTM	American Society for Testing and Materials
BSI	British Standards Institute
CBD	Compacted Bulk Density
C&CI	Cement and Concrete Institute
CE	European Conformity
CFR	CHRYSO Fluid Rescue
CMOD	Crack Mouth Opening Displacement
CMS	CHRYSO macro-synthetic experimental fibre
CPO134	CHRYSO Plast Omega 134
CoV	Coefficient of Variation
DV	Dependent Variable
EFNARC	European Federation of National Associations Representing for Concrete
EN	European Norms
ERMCO	European Ready Mixed Concrete Organisation
fib	International Federation for Structural Concrete
FM	Fineness Modulus
FRC	Fibre Reinforced Concrete
GFRC	Glass Fibre Reinforced Concrete
IQR	Inter Quartile Range
ISO	International Standards Organisation
ITZ	Interfacial Transition Zone
IV	Independent Variable

JCI	Japan Concrete Institute
LBD	Loose Bulk Density
LOP	Limit of Proportionality
LVDT	Linear Variable Displacement Transducer
MOR	Modulus of Rupture
MSFRC	Macro-Synthetic Fibre Reinforced Concrete
NFRC	Natural Fibre Reinforced Concrete
POD	Fibre Pull-Out Distance
PPC	Pretoria Portland Cement
RC	Reliability Class
RD	Relative Density
RDPT	Round Determinate Panel Tests
RFTS	Residual Flexural Tensile Strength
RILEM	International Union of Laboratories and Experts in Construction Materials, Systems, and Structures
RMSE	Root Mean Square Error
SANS	South African National Standards
SFPOT	Single-Fibre Pull-Out Tests
SFRC	Steel Fibre Reinforced Concrete
SNFRC	Synthetic Fibre Reinforced Concrete
TPBT	Three-Point Bending Test
TR	Technical Report

Chapter 1

Introduction

1.1 Overview

As construction works is constantly increasing across the world, concrete's availability and versatility have ensured that this material will continue to be of high importance (Domone, 2010). The tensile strength of concrete is much lower in comparison to its compressive strength and the material suffers brittle failure in uni-axial or flexural tension. This drawback has been compensated for by the addition of continuous high tensile strength steel bar reinforcing placed at the appropriate locations to withstand the imposed tensile and shear stresses. Significant disadvantages regarding steel reinforcing, such as being labour and time-intensive and having insufficient durability in corrosive environments, meant that fibre reinforced concrete (FRC) has been proposed and developed as a partial alternative. Fibres are discontinuous and commonly randomly distributed throughout the cement-based matrix. Therefore, fibres are not as efficient in withstanding the imposed tensile stresses, but because they tend to be more closely spaced than conventional reinforcement, they are better at controlling cracking (Bentur and Mindess, 2007).

FRC is a composite material characterised by a cement matrix and discrete fibres (discontinuous). Fibres can be made of either steel, polymers, carbon, glass or natural materials. It is known that the addition of fibres in concrete can improve its mechanical properties, i.e. the tensile and flexural behaviour. Unless a high percentage of fibres are added to the material, the compressive and elastic properties are not significantly affected (fib Special Activiy Group, 2010).

Macro fibres, i.e. fibres with an effective diameter of more than 0.3 mm (European Norms, 2006), have been used for some time in concrete applications where crack control and post-cracking performance are of importance. The typical application that make use of macro fibres is industrial concrete floors on grade. Synthetic fibre dosages generally range between 0.1 to 2% based on the total volume of the concrete produced (Zollo, 1997). These volumes are relatively small compared to conventional composites which are typically more than 60% by volume. The addition of macro fibres in concrete only starts having an effect once concrete has cracked, therefore the design has to include the post-cracking behaviour to utilise the fibres.

Using the Westergaard Theory to design floors on grade (the typical South African method), the addition of macro fibres have no effect, as this design method does not account for the post-cracking behaviour of concrete and any crack that occurs is seen as failure of the slab. Using the Yield-Line Theory approach, the post-cracking behaviour is taken into account by assuming that cracking does occur and it provides means for determining moments caused by loading by assessing the patterns of the yield-lines. Thus the addition of fibres will enhance the performance of a concrete floor on grade using the latter approach. A design code utilising the Yield-Line Theory is the Technical Report 34 (2013): *Concrete industrial ground floors*, issued by the Concrete Society UK.

The typical specification for determining the performance for FRC, is to declare the quantity of fibres to achieve residual (post-cracking) flexural strength f_R of 1.5 N/mm^2 at a crack mouth opening displacement (CMOD) of 0.5 mm and of 1.0 N/mm^2 at a CMOD of 3.5 mm (The Concrete Society, 2013). These specifications can be determined using a standard notched beam test in accordance with EN 14651: *Test method for metallic fibre concrete. Measuring the flexural tensile strength.* This test procedure is sophisticated and expensive and is also known to have a relative large scatter of results, resulting in unrealistic low characteristic values.

Recent work at Stellenbosch University has shown that the performance of macro synthetic fibre reinforced concrete (MSFRC) is dependent on a number of factors, including the mix design, coarse aggregate size and fibre type (Odendaal, 2015). It was also determined that the fibre bond to the concrete matrix, as determined by single fibre pull-out tests, is not a good indication of the post-cracking performance of MSFRC. There are mechanisms involved which are still not properly understood.

1.2 Problem statement

After more than 30 years of research and development, FRC is still not profoundly used in structural elements. One of the major obstacles identified preventing the implementation of the structural use of FRC is the lack of validated design and test methods (Vandewalle, 2000). The modelling of the post-cracking performance of MSFRC is of special interest as macro-synthetic fibres have been proposed with an aim of creating an alternative to steel fibres in structural applications, specifically slabs-on-grade. The lack of information regarding the post-cracking performance prediction of MSFRC based on the material characteristics of concrete supports the reason for the study.

1.3 Study objectives

The deliverable of this study is to development generic models for predicting the performance of MSFRC for industrial flooring applications, taking account of various material properties and the mixing process. The two objectives of this study are as follows:

1. Determining the factors influencing the performance of MSFRC for industrial flooring applications as well as quantifying their influence.
2. Creating generic models for predicting the performance of MSFRC based on material properties, fibre dosage, and various mixing procedures. These models must determine the residual flexural tensile strengths (MPa) at crack mouth opening displacements (CMOD) of 0.5 mm, 1.5 mm, 2.5 mm, and 3.5 mm respectively. The models would also determine the limit of proportionality (LOP) which corresponds to the maximum stress between a CMOD of $0 - 0.05$ mm. Note that these models are only calibrated for one experimental macro-synthetic fibre supplied by CHRYSO.

1.4 Scope of document

This thesis consists of six chapters and the outline of each chapter is as follows:

- Chapter 1 serves as an introduction and description of the study, stating the problem at hand, as well as the study objectives.
- Chapter 2 contains the literature review and theoretical background of FRC, the factors influencing the performance of FRC, globally available test methods to measure the performance of MSFRC, different methods for modelling the flexural behaviour of FRC, and the current applications of MSFRC.
- Chapter 3 describes the experimental framework of the study, including the research hypotheses, the mix design methodology, the different data collection methods measuring the macro-mechanical performance as well as the single-fibre performance, and an explanation of the modelling approach to determine the generic models predicting the performance of MSFRC considering the CMS fibre.
- Chapter 4 presents the results obtained for the evaluation of the macro-mechanical performance.
- Chapter 5 illustrates the results obtained for the evaluation of the single-fibre performance of the CMS fibre followed by a detailed discussion of the results.
- Chapter 6 presents the outcome of the simple- and multiple linear regression analyses as well as providing the linear models predicting the performance parameters.
- Chapter 7 concludes the thesis based on the results presented and the research documented. Future prospects and recommendations are also provided.

Chapter 2

Background of Fibre Reinforced concrete

This chapter provides a broad overview of fibre reinforced concrete (FRC). The chapter focusses on the mechanical behaviour of FRC as well as the factors influencing the performance of macro-synthetic fibre reinforced concrete (MSFRC). In addition, a description of the internationally acknowledged testing methods investigating the performance of FRC on macro-mechanical level is provided as well as the various applications of MSFRC.

2.1 Introduction to FRC

The term fibre reinforced concrete (FRC) is defined by the American Concrete Institute (ACI) as concrete containing dispersed, randomly orientated fibres. Fibrous materials have been used since ancient times to improve toughness and strength and to reduce cracking of brittle materials. Examples of this are the use of straw in clay bricks and hair in plaster (Perrie, 2009).

FRC has been developed as a partial alternative for conventional steel reinforcing. As fibres increase the residual strength of concrete in its cracked phase, FRC is becoming widely used in civil engineering (Buratti et al., 2011). To enhance the concrete toughness for structural applications, fibres with a high stiffness modulus can be used to substitute, partially or totally, conventional steel reinforcement. Other fibres, usually having a low stiffness modulus and a small size, can be used to reduce the shrinkage cracking of concrete (Prisco et al., 2009).

Over three decades have passed since the initiation of research and development of FRC. Information on the structural response of FRC elements was however mainly developed since 2000. Therefore, due to the lack of international building codes for FRC structural elements and standardised test methods, the use of FRC is still very limited with respect to its potential (Prisco et al., 2009). Several standards and publications have since been produced by various institutions, incl. the British Standards Institute (BSI), the American Society for Testing and Materials (ASTM), and the Concrete Society which details the usage of FRC. Early design considerations for steel fibre reinforced concrete (SFRC) were produced by the ACI Committee 544(1996) while RILEM TC162-TDF produced guidelines for typical structural elements. The International Federation for Structural Concrete (fib) has published the new *fib* Model Code (2010) that will be considered as the new reference document for Eurocode 2. This model code includes several

innovations and addresses among other topics, new materials for structural design, including FRC. The *fib* Model Code (2010) assist engineers to properly design FRC structural elements both at ultimate (ULS) and serviceability (SLS) limit states.

For most structural purposes, steel fibres are mostly considered over other fibres, but in recent times macro-synthetic fibres have been developed and proposed as an alternative. Experimentation with macro-synthetic fibres dates back to the 1960s, but more recent advances in production technologies and materials meant that MSFRC can provide concrete with post-cracking, load-bearing capacity and provide an alternative to SFRC in various applications. Initial interest in the use of MSFRC centred around its potential in sprayed concrete for tunnel linings, however examples of its use in ground-supported slabs and other applications are also available (The Concrete Society, 2007). The advantage of using macro fibres, which have similar dimensions to steel fibres used in bulk field applications, are that they are lightweight, cheaper, and inert, thus increasing the durability of structures compared to the use of steel fibres.

2.2 Overview of fibres

Cementitious materials are brittle and, if subjected to a tensile stress, the unreinforced matrix presents a limited elastic response which is quickly followed by micro-cracking, localised macro-cracking, and ultimately rupture. The introduction of various types of short fibres, does not significantly improve the elastic response, or stress at which cracking first occurs in the hardened material, but the benefit of the inclusion of fibres in the hardened material relate to its post-cracking state (The Concrete Society, 2007).

The addition of fibres into brittle materials has contributed immensely and has been a fundamental technology for millennia. In the Book of Exodus (Chapter 5, verse 6), the writer refers to the importance of straw in the making of bricks (Hannant, 1978). After the invention of the Hatschek process in 1898, the use of asbestos fibres in concrete began. In the past the use of asbestos cement construction products were widely used. However, its popularity decreased after it was proved to be carcinogenic and alternate fibre types were introduced throughout the 1960s and 1970s (ACI Committee 544, 2002).

In the modern era, fibres are incorporated in numerous materials used in the engineering profession to improve its properties. These enhanced properties include (ACI Committee 544, 2002):

- Tensile strength
- Compressive strength
- Elastic modulus
- Crack resistance and crack control
- Durability
- Fatigue life

- Impact- and abrasion resistance
- Shrinkage
- Expansion
- Thermal characteristics
- Fire resistance

The shortcomings of unreinforced concrete, i.e. a low tensile strength and low strain capacity at fracture, are traditionally overcome by the addition of steel reinforcing bars which are continuous and specifically located to optimise the performance. Fibres are discontinuous and generally distributed randomly throughout the matrix which can result in low fibre content in critical areas (ACI Committee 544, 2002). Therefore, fibres are mostly considered as secondary reinforcement and used in structural applications with conventional reinforcement, and should not be accounted for influencing the pre-cracking behaviour. However, it is possible for FRC to carry a higher flexural tensile load after cracking than before cracking.

Currently, there are numerous fibre types available for commercial and experimental use, and according to ACI Committee 544 (2002), there are four basic fibre categories:

- Steel fibre reinforced concrete (SFRC)
- Glass fibre reinforced concrete (GFRC)
- Natural fibre reinforced concrete (NFRC)
- Synthetic fibre reinforced concrete (SNFRC)

2.2.1 Steel fibres

Important fibre reinforcement properties are the fibre strength, stiffness, and the ability of the fibres to bond with the concrete matrix. The bond is dependant on the aspect ratio (ratio of length to equivalent diameter) of the fibre. Steel fibres have high strength and modulus of elasticity, and their bond to the concrete matrix is enhanced by mechanical anchorage or surface roughness. Steel fibres are also protected from corrosion by the alkaline environment of the cementitious matrix.

Steel fibres that are intended for reinforcing concrete are defined as short, discrete lengths of steel with an aspect ratio varying between 20 to 100, with any of several cross-sections. The length dimensions range from 6.4 to 76 mm (ACI Committee 544, 2002). The minimum tensile yield strength of steel fibres required by ASTM A820 is 345 MPa. According to EN $14889-1$, the typical modulus of elasticity for normal steel fibres is approximately 200 GPa. Figure 2.1 illustrates various steel fibre geometries.

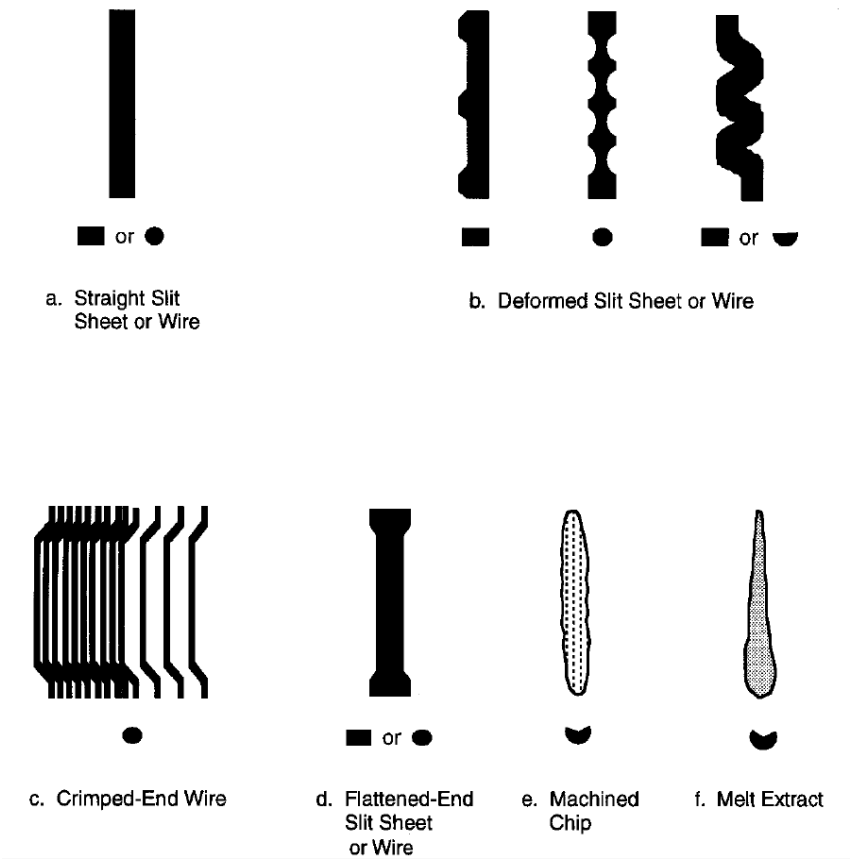

Figure 2.1: Various steel fibre geometries (ACI Committee 544, 2002)

For typical volume fractions, i.e. 0.25 to 1.5% of the volume concrete produced, the addition of steel fibres may reduce the slump value between 25 to 102 mm compared to a non-fibrous material. In addition to slump-loss, SFRC has the tendency to produce balling of fibres in the freshly mixed state. The addition of a high-range water-reducing admixture increase the workability of some harsh SFRC and has reduced the resistance to the use of SFRC (ACI Committee 544, 2002). In the hardened state, steel fibres improve the ductility of concrete under all modes of loading, but their effectiveness depend on the type and volume percentage of fibres present.

2.2.2 Glass fibres

In the early 1960s, research was performed on glass fibre reinforced cement paste. Most of this experimental work used regular borosilicate glass fibres (E-glass) and soda-lime-silica glass fibres (A-glass). It was however concluded that materials containing E-glass and A-glass as reinforcement, lost its strength rather quickly due to the high alkalinity of the matrix (pH $\geq$ 12.5). Thus, for long term use, E-glass and A-glass composites are unsuitable. Continued research in this field resulted in the development of a alkali resistant fibre (AR-glass fibre) which improved its durability. Compared to conventional concrete, the dimensional changes in GFRC can be considerably greater. Increased cyclical volumetric dimensional changes will occur if GFRC is exposed to normal moisture and temperature cycles (ACI Committee 544, 2002).

(a) Natural unprocessed straw fibre

(b) Natural processed sisal fibre

Figure 2.3: Natural fibres

AR-glass fibres are provided in two basic types, i.e. dispersible fibres and internal strands, as illustrated in Figure 2.2. The dispersible fibres disperse into individual monofilaments when mixed into the concrete. These fibres are considered to be micro-fibres and mostly used for plastic shrinkage control. The addition of this type of fibre ranges between 0.01 and 0.03% by volume. The internal strands refer to bundles of monofilaments that stay integral as bundles through mixing and into the final product. These strands are considered to be macro-fibres, and the addition ranges between 0.09 to 0.17% by volume. AR-glass fibre monofilaments are either 13 or 18 μm in diameter, with specific gravity of 2.7.

(a) Dispersible fibres

(b) Internal strands

Figure 2.2: Basic types of AR-glass fibres

2.2.3 Natural fibres

Little research about the use of natural fibres as reinforcement have been published. Using locally available manpower and technical capabilities, natural reinforcing can be produced at low levels of cost and energy. Generally, these fibres are referred to as unprocessed natural fibres. To enhance concrete's properties, different natural fibres, typically derived from wood by chemical processes, are also available. The most well known natural fibres are sisal, coconut, sugarcane bagasse, plantain, and palm (ACI Committee 544, 2002). Figure 2.3 illustrate examples of natural fibres.

The properties of NFRC are mainly affected by the type and length of the fibres, as well as the

Table 2.1: Properties of various synthetic fibre types (ACI Committee 544, 2002)

Fibre type	**Specific gravity**	**Tensile strength (MPa)**	**E_{mod} (GPa)**
Acrylic	1.16-1.18	268.91-999.78	13.79-19.31
Aramid I	1.44	2930.38	62.06
Aramid II	1.44	2344.30	117.22
Carbon, PAN HM	1.60-1.70	2482.20-3033.80	379.91
Carbon, PAN HT	1.60-1.70	3447.50-3999.10	230.29
Carbon, pitch GP	1.60-1.70	482.65-792.93	27.58-34.48
Carbon, pitch HP	1.80-2.15	1516.90-3102.75	151.69-482.65
Nylon	1.14	965.30	5.17
Polyester	1.34-1.39	227.54-1103.20	17.24
Polyethylene	0.92-0.96	75.85-586.08	5.00
Polypropylene	0.90-0.91	137.90-689.50	3.45-4.83

volume fraction. To improve the mechanical properties of the concrete matrix, the minimum fibre addition is approximately 3% by volume. The impact resistance is generally increased regardless of the fibre volume fraction and the compressive strength is not significantly affected, but the flexural and tensile strength are substantially increased (ACI Committee 544, 2002).

2.2.4 Synthetic fibres

Synthetic fibres are developed from research in the petrochemical and textile industries. SNFRC utilises fibres from various organic polymers which are available in a variety of formulations. According to EN $14889-2$, polymer fibres are straight/deformed pieces of extruded, orientated or cut material which can sufficiently be mixed into concrete or mortar. Table 2.1 illustrates various properties of different synthetic fibre types that have been tested and experimented on, in cement matrices.

Two general classes of synthetic fibres have emerged from research and development. Synthetic fibres are characterised in accordance with their physical form (European Norms, 2006):

- Class I:
  - (a) Micro-fibres: Diameter $<$ 0.3 mm; Monofilamented
  - (b) Micro-fibres: Diameter $<$ 0.3 mm; Fibrillated
- Class II:
  - Macro-fibres: Diameter $>$ 0.3 mm

Micro-synthetic fibres

Micro-synthetic fibres are referred to as synthetic fibres with a diameter (d) or equivalent diameter (d_e) of less than 0.3 mm. Since the mid 1980s, polypropylene micro fibres, which typically have lengths between 6 to 20 mm, have been used to modify the properties of concrete. These fibres are typically used in the range of 0.05 to 0.2% by volume, which equates to a dosage between 0.44 and 1.8 kg/m^3 (ACI Committee 544, 2002).

Typically, micro-synthetic fibres are produced from polypropylene and their cross-section is either circular, rectangular or elliptical. The cross-section, elastic modulus (E_{mod}), tensile strength and surface characteristics of the fibre, determines the bond between the fibres and the concrete matrix. The addition of micro-synthetic fibres can contribute to the resistance of plastic shrinkage and fire resistance, depending on the length and the fibre dosage (ERMCO, 2012). At high dosages, micro-synthetic fibre reinforced concrete will experience significant workability issues, thus micro fibres can only be utilised at low addition rates. An illustration of typical polypropylene micro-synthetic fibres is shown in Figure 2.4.

Figure 2.4: Polypropylene micro-synthetic fibres (ERMCO, 2012)

Macro-synthetic fibres

Since around the year 2000, macro-synthetic fibres, also referred to as structural synthetic fibres in literature, have been produced with the aim of substituting steel fibres in structural applications (Buratti et al., 2011). The addition of macro-synthetic fibres into the concrete matrix have a number of influences (ERMCO, 2012):

- Improve the toughness of hardened concrete
- Improve the impact resistance of concrete
- Increase the residual flexural tensile strength of concrete

The increased residual flexural tensile strength of MSFRC is a key parameter in measuring the performance. This parameter is dependent on the fibre type and dosage, as well as the properties of the concrete matrix itself.

Macro-synthetic fibres have diameters or equivalent diameters greater than 0.3 mm. These fibres have similar dimensions compared to steel fibres used structural elements, and incorporated at higher dosages than micro fibres. The maximum dosage of macro fibres is approximately 12 kg/m^3, which equates to about 1.35% by volume. Reports of experimental applications with macro-synthetic fibres dates back to the 1960s and recent interest in MSFRC has resulted in the production of fibres with higher stiffness moduli, typically ranging between 2 to 10 GPa, as well as the development of a variety of anchorage mechanisms to enhance bond (The Concrete Society, 2007).

Polypropylene fibres, which is one of the most commercially available synthetic fibres, are hydrophobic, which means that it does not absorb any water. Thus, in terms of physicochemical adhesion, there is no bond between polypropylene fibres and the cement gel and bonding occurs by means of mechanical interaction (ACI Committee 544, 2002). Actions such as fibre twisting and crimping increases the mechanical interaction. Polypropylene fibres have been suggested as a concrete additive since 1965 due to its low cost and abundantly availability, as well as its relative high tensile strength (Hannant, 1978).

Figure 2.5 illustrates two different types of macro-synthetic fibres. MS1 is a fibrillated polypropylene macro-synthetic fibre, and MS2 is a polystyrene macro-synthetic fibre. Figure 2.6 illustrates the physical difference between micro-synthetic and macro-synthetic fibres.

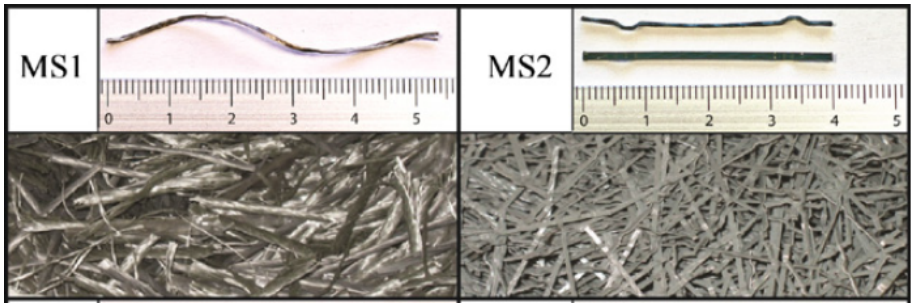

Figure 2.5: Two different macro-synthetic fibres (Buratti et al., 2011)

Figure 2.6: Physical difference between micro-synthetic and macro-synthetic fibres

2.3 Mechanical behaviour of FRC

The introduction of any fibre to concrete will not significantly affect, in its hardened state, the elastic response or the stress at which cracking occurs. Fibres are added with the purpose of affecting the post-elastic property changes, and the benefits of the inclusion of fibres relate to the post-cracking state of hardened concrete.

The behaviour of FRC is dependant on the structure of the composite. In order to analyse these composites, and to predict their performance, their internal structure must be characterised. The following components must be considered when analysing the mechanical behaviour of FRC (Bentur and Mindess, 2007):

- The structure of the cementitious matrix
- The shape and distribution of fibres
- The structure of the fibre-matrix interface

2.3.1 Structure of the cementitious matrix

The bulk cementitious matrix of FRC is not significantly different from that in other cementitious materials. The inclusion of fibres alter the micro-structure of the host cement paste matrix slightly. Micro-pores in the matrix are decreased in number and not appreciably in size, however the micro-pore surface and volume fractions increase due to the addition of fibres into the matrix. Many pores exist between the bulk matrix and the fibre surfaces where the properties

are dependant on the Water/Cement (W/C) ratio and the curing conditions. Decreasing the porosity can be achieved by a reduction in the W/C ratio (Beaudoin, 1990).

In FRCs, fibre volumes are typically restricted to less than 2% by volume of the concrete produced, and the fibres generally act as secondary reinforcement for the main purpose of crack control. The incorporation of fibres into the matrix and ensuring uniform dispersion of the fibres requires a dense micro-structure to provide effective reinforcement (Bentur and Mindess, 2007).

2.3.2 Shape and distribution of fibres

As outlined in the previous section, a wide range of fibres with different mechanical, physical, and chemical properties have been considered and used for the reinforcement of cementitious matrices. The shape of the individual fibres and their dispersion in the cementitious matrices must be considered when analysing the mechanical behaviour of FRC.

Individual fibres can be subdivided into two groups, i.e. discrete monofilaments, which are separated one from another (e.g. steel fibres), and fibre assemblies, which are generally made up of bundles of filaments, each with a typical diameter of 10 μm or less (e.g. polypropylene fibres). Monofilament fibres used in FRC are typically deformed into various configurations to improve the fibre-matrix interaction through mechanical anchoring. Bundled fibres do not disperse into their individual filaments and frequently maintain their bundled nature in the composite itself.

Generally, two different fibre reinforcement types exists: (1) *continuous reinforcement* (long fibres) which are added by different techniques, i.e. filament winding or layers of fibre mats, and (2) *discrete short fibres* which typically involves adding fibres, usually less than 50 mm long, into the matrix by methods such as spraying or mixing (Bentur and Mindess, 2007). The continuous form of reinforcement is less common in FRC composites which are usually reinforced with discrete, short fibres. The addition of discrete, short fibres is considered in this study. Figure 2.7 illustrates how reinforcement can be classified according to the dispersion of fibres in the matrix.

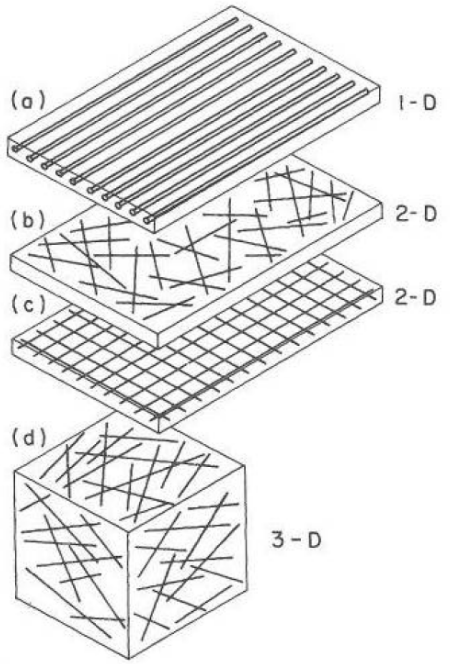

Figure 2.7: Classification of fibre arrangements (a) 1D, (b,c) 2D, and (d) 3D. Also distinguishes between continuous (a,c) and discrete, short fibres (b,d) (Bentur and Mindess, 2007)

In the case of discrete short fibres the dispersion in the matrix is rarely completely uniform and a more random orientation can be assumed. If the ratio of the fibre length to thickness of the composite is sufficiently large, it can be assumed that the fibres will have a 2D distribution as illustrated in Figure 2.7(b), which is usually the case in thin components. 2D distribution can also be promoted in thicker components with the use of external vibration. This will also promote anisotropic behaviour. The distribution and the uniformity of discrete fibres is affected by the mixing and consolidation process, and a complete uniform distribution cannot be achieved (Bentur and Mindess, 2007). These effects must be considered in structural applications where variation in fibre distribution in larger components may result in considerably variability in the mechanical properties of the composite. The distribution of fibres can typically be explained according to the dosage of fibres and the size of the specimens, as well as the workability of the composite in its fresh state and the method of compaction. Figure 2.8 is a nomograph illustrating the relationship between the fibre diameter and spacing and yields either the fibre count, or the surface area of fibres per unit volume of the composite, for unit lengths of fibres.

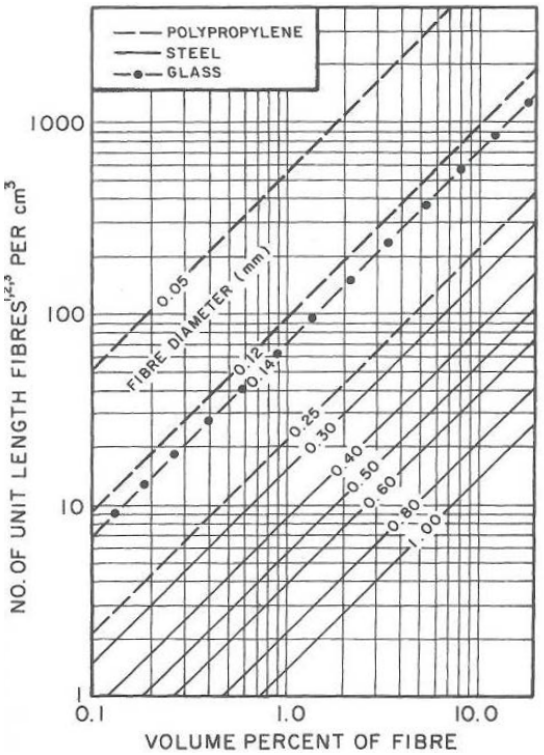

Figure 2.8: Number of fibres per unit volume, or surface area of fibres per unit volume, as a function of the volume percent of fibres and the fibre geometry(Bentur and Mindess, 2007)

2.3.3 Structure of the fibre-matrix interface

With the addition of fibres into the concrete matrix, the composite is characterised by an Interfacial Transition Zone (ITZ) between the matrix and the fibres. Away from the ITZ, the micro-structure of the paste is much different than the bulk paste. Depending on the type of fibre and the production technology, the size and nature of the transition zone will vary and can in some instances change considerably with time (Bentur and Mindess, 2007).

It is acknowledged that the properties of the fibre-matrix interface have a significant influence on the mechanical behaviour of cement composites. Predicting the strength of these composites, the shear-deformation behaviour of the ITZ is of critical importance. Several attempts have been made to determine the shear strength of the ITZ, which typically relied on techniques involving the pull-out of one or more fibres from the matrix (Beaudoin, 1990). Thus, the fibre-matrix bond and the debonding process across the interface need to be taken into consideration when analysing the mechanical behaviour of FRC.

During a single fibre pull-out test of a fibre embedded in a cement matrix, many modes of failure are possible. The ultimate failure mode is dependant on various interfacial bond conditions. Figure 2.9 illustrates the development of an interfacial shear stress (τ) between the matrix and a fibre when a force is transferred from the matrix to the fibre.

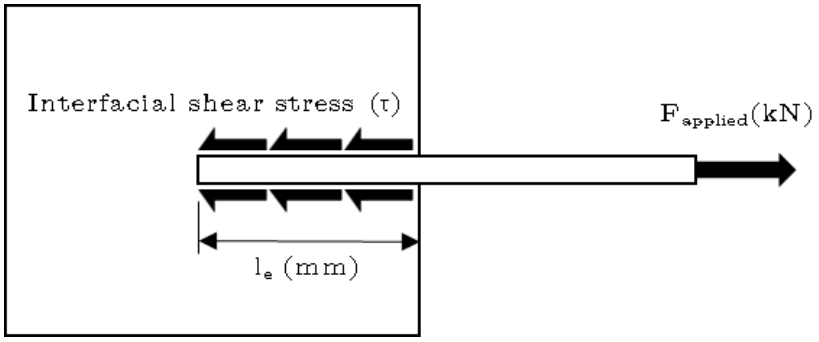

Figure 2.9: The development of an interfacial shear bond stress after an force has been applied to a fibre reinforced composite

The shear stress over the embedment length of the fibre (l_e) offers a resisting force ($F_{resistance}$) and is defined as:

$$F_{resistance} = \tau \cdot \pi \cdot d_e \cdot l_e \tag{2.1}$$

where:
d_e = equivalent fibre diameter

Fracture of a fibre is an undesirable occurrence. The fracture of fibres initiates at some flaw(s) and can be written as:

$$F_{fracture} = \sigma_f \cdot (\frac{\pi \cdot d_e^2}{4}) \tag{2.2}$$

where:
σ_f = ultimate fibre tensile strength

The most common way in which FRC fail, is fibre pull-out. This failure mode will occur if $F_{resistance}<F_{fracture}$. If $F_{resistance}>F_{fracture}$, fibre fracture will occur, which will lead to brittle failure of the composite (Beaudoin, 1990).

When the embedment length of a fibre (l_e) is less than a certain critical length (l_c), the fibre will debond instantly and pull out when the load required to break the adhesion at the interface is reached. When $l_e > l_c$, fibres will tend to fail in tension with no debonding. When the tensile strength of the fibre is greater than the load required to break the adhesion at the interface, the fibre will debond and pull-out regardless of its length. The critical length of a fibre (l_c) is defined as (Beaudoin, 1990):

$$l_c = \frac{d \cdot \sigma_f}{2 \cdot \tau} \tag{2.3}$$

Several techniques exist to enhance the interfacial bond stress (τ) between the fibre and the matrix. Some techniques make use of macroscopic processes such as fibre deformation, while other techniques involves microscopic changes such as modification of the ITZ or the fibre surface.

The ITZ densification techniques employ the addition of silica fume to the cement matrix. Significant bond strength enhancement is provided by this technique, but due to the chemical inertness of polymeric synthetic fibres, this technique is limited to composites reinforced with metal and carbon fibres only. For low-surface-energy polymer fibres, fibre deformation and fibre surface modification has indicated to be more effective in improving the interfacial bond stress and enhancing mechanical bond. Fibre deformation include fibrillation, crimping and twisting of fibres, as well as the addition of buttons at the end of the fibres. Fibre surface modification utilises plasma treatment to improve the interfacial bond stress (τ) in composites reinforced with polymeric fibres. Hydrogen atoms are removed from the fibre and replaced with polar groups by implementing this technique. An enhancement in the reactivity and an improved adhesion between the fibre and the matrix is the result (Singh et al., 2004).

2.3.4 Fibre-matrix interaction

The inclusion of fibres in the concrete matrix affects the properties of concrete in both the freshly mixed and hardened states, often in an opposite sense. The following factors describe this statement:

- Fibre content
- Fibre aspect ratio

By increasing the fibre content, it naturally tends to improve the properties of FRC in its hardened stated, but decreases mixture fluidity in the freshly mixed state. A critical fibre volume is generally prescribed to ensure uniform fibre distribution and a mixture that can be properly consolidated. This shortcoming indicates that the potential enhancement of the properties in the hardened state of FRC cannot be fully achieved either due to non-uniform fibre distribution or incomplete consolidation, or a combination of these effects.

The effect of the fibre aspect ratio, which refers to the ratio of fibre length to the diameter for straight circular fibres, also influences the freshly mixed and hardened states of FRC. Long slender high-aspect-ratio fibres provides better reinforcing effectiveness and greater potential property enhancement of FRC in the hardened state, but are more difficult to process in the freshly mixed state compared to the same amount of short thick low-aspect-ratio fibres (Bentur and Mindess, 2007).

It is therefore important to consider the effects of the addition of fibres to the concrete matrix. A low fibre content and a low fibre aspect ratio have the least adverse effects on the properties of FRC in the freshly mixed state but provide minor property enhancement in the hardened state, while high fibre content and a high fibre aspect ratio offer the opposite. Therefore, the various fibre-matrix interactions that affects the behaviour of FRC in the freshly mixed and hardened

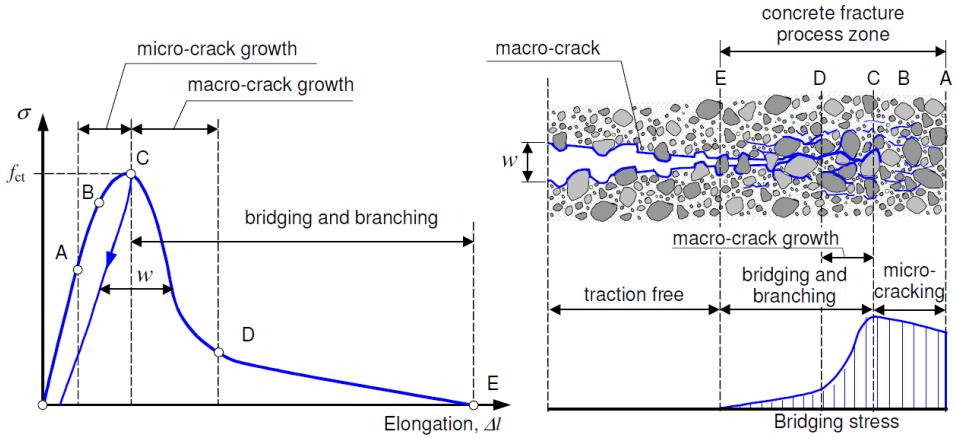

Figure 2.10: Aggregate bridging mechanism in uni-axial tension and the resulting stress-crack opening relationship (Löfgren, 2005)

states have to be considered and is often compromised in terms of placeability, final property enhancement, and miscibility (Bentur and Mindess, 2007). Factors influencing the fibre-matrix interactions in the freshly mixed and hardened states of MSFRC are discussed in Section 2.6.

2.3.5 Fibre-crack bridging mechanism

As aforementioned, the effect of fibres only initiates after the concrete matrix has cracked. Due to the addition of fibres, FRC composites do not break in a brittle matter after the initiation of the first crack. This effect increases the fracture energy or toughness of the composite. In addition to the effect of fibres, the cracking of the matrix contributes to the energy which is dissipated due to the bridging of aggregates.

When a crack occurs in conventional concrete, the coarse aggregates tend to bridge the crack. This crack however propagates through the interface between the aggregate and the matrix. Figure 2.10 illustrates the aggregate bridging mechanism.

Referring to Figure 2.10, internal cracks starts to grow at the ITZ between the cement paste and the coarse aggregate at Point A which finally get into the Mortar B. Localisation of cracks start at the peak Stress C and further propagates in an unstable manner which results in macro-cracks starting to propagate through the specimen, leading to a stress Drop D (Löfgren, 2005).

Depending on the crack width, there are two possibilities in a FRC composite, i.e. a combined bridging effect of coarse aggregates and fibres and the fibre bridging mechanism. When concrete cracks, stresses are transferred from the matrix to the fibres. The fibres bridge the crack and the opening rate of the crack is reduced, thus reducing the stress intensity at the crack tip. Due to the fibre bridging mechanism, the composite indicates a high energy absorption during crack propagation as the crack width increases with time. The fibre bridging mechanism is influenced by the following factors:

- Nature of the fibre/matrix interface

- Fibre aspect ratio
- Geometry of the fibre
- Concrete matrix composition
- Orientation of fibres
- Fibre volume

Thus, for fibres to stabilise crack propagation, the fibre-matrix bond of cement-based composites is of great importance. Investigating the fibre bridging mechanism, single-fibre pull-out test are typically performed (Bentur and Mindess, 2007). However, in reality, fibres are randomly orientated and numerous researchers have investigated the effect of the inclination of fibres at different angles to understand the totality of the pull-out behaviour.

2.3.6 Pre-cracked behaviour of FRC

Due to the low volume of fibres added to the concrete matrix (maximum 1.3% for macro-synthetic fibres), the uncracked strength of FRC is dependant on the strength of the concrete matrix. This suggests that, prior to cracking, the material properties and the material proportions influence the uncracked behaviour.

During the early stages of loading and prior to the onset of cracking, the interaction between the fibre and the matrix is usually assumed to behave elastically with a consequent linear distribution of stress and strain, so the standard elastic bending formula is applicable when determining the maximum flexural stress. The validity is reached at the onset of cracking, and the stress calculated at this point according to the specific loading applied, span and size of the specimen is the first-crack strength and is referred to as the modulus of rupture (MOR) (Bentur and Mindess, 2007). Standardised three-point bending tests are commonly used to determine the MOR and as aforementioned, simple beam theory is used to determine the flexural stress at first crack. Figure 2.11 illustrates four different stages of the flexural load-deflection response which exhibits a strain softening behaviour of a steel-fibre-reinforced concrete beam. It is evident that the first stage illustrates a linear load-deflection relationship for the stage prior to the first crack.

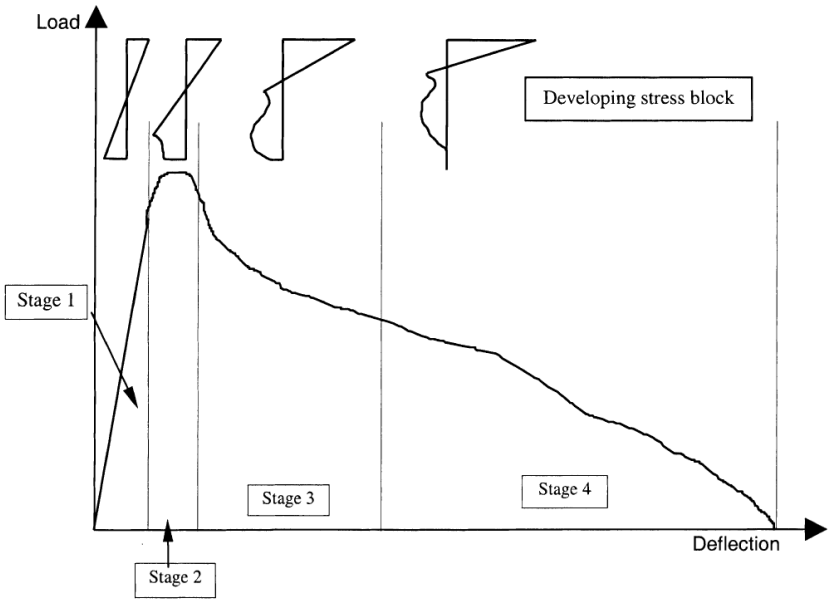

Figure 2.11: Relationship between the different stages of the flexural load-deflection response of a steel-fibre-reinforced concrete beam (Robins et al., 2001)

For commonly used macro-synthetic fibre dosages, the pre-cracking tensile strength is not influenced. However, an large fibre dosage can cause a decrease in the MOR, as the workability of the composite is affected and consequently include an unwanted amount of air while casting (Buratti et al., 2011). Other research have however suggested that, for higher fibre content composites made with steel or carbon fibres, the fibre characteristics can affect the first-crack flexural strength (Bentur and Mindess, 2007). Figure 2.12 illustrates this affect.

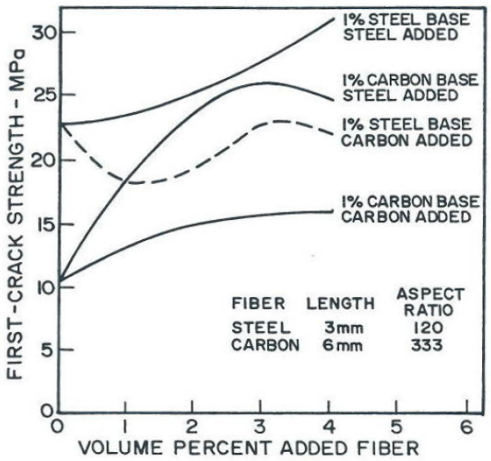

Figure 2.12: Effects of fibre type and content on first-crack flexural strength with steel and carbon fibres (Bentur and Mindess, 2007)

2.3.7 Post-cracking behaviour of FRC

Preventing or controlling tensile cracking in concrete structures is the most critical application of fibres (Oh et al., 2005). The post-cracking residual tensile strength, which is an important

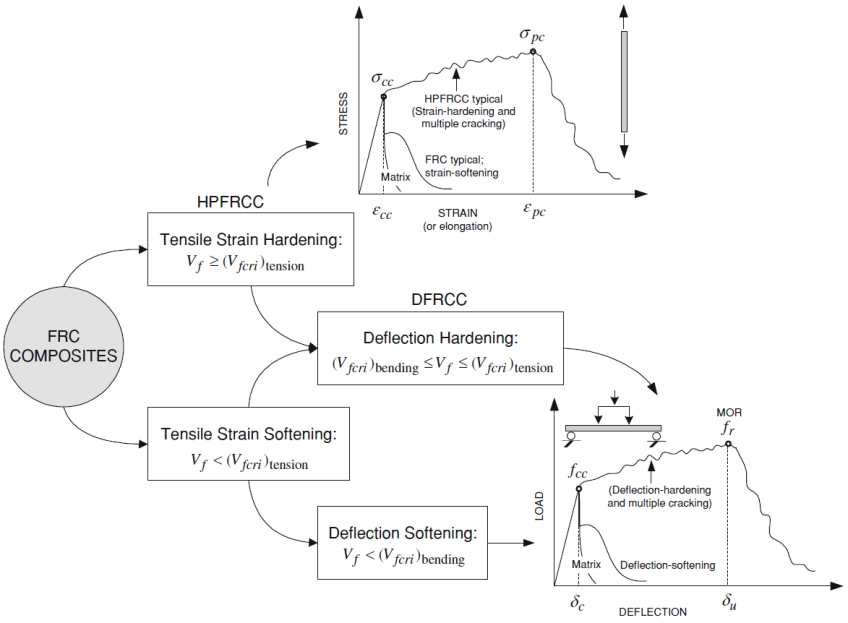

Figure 2.13: Depiction of the softening and hardening behaviour of FRC (Prisco et al., 2009)

design parameter for FRC structures, is the mechanical property mostly influenced by fibre reinforcement.

Due to the well known difficulties in performing uni-axial tensile tests, flexural bending tests with notched beams are typically performed to analyse the post-cracking behaviour of FRC. When FRC cracks, the load carried by the concrete is transferred from the matrix to the fibres and, depending on the volume of fibres, the physical properties of the fibres and the matrix as well as the bond between the two, the composite will either experience a deflection-softening or a deflection-hardening behaviour (The Concrete Society, 2007). If fibres can carry a larger load than the composite material prior to cracking, deflection-hardening occurs and deflection-softening occurs in the opposite manner. Figure 2.13 illustrates the hardening and softening behaviour of FRC composites subjected to a tensile force and to a flexural force. From Figure 2.13 it is evident that a posibility exists for a softening material in tension to experience a hardening behaviour in bending. This is due to the linear variability of the strain profile along the uncracked cross-section in flexural bending tests that favours a more stable propagation of cracks (Prisco et al., 2009).

The addition of fibres to the concrete matrix significantly increases the energy absorption capability of the composite, which can be determined by calculating the area under the load-deflection graph. The resultant composite can thus exhibit considerable ductility, often termed 'toughness'. The addition of macro-synthetic fibres generally tends to exhibit deflection-softening behaviour due to their low stiffness.

2.3.8 Mechanical behaviour according to TR 34

Technical Report No. 34 (TR34) was published by the Concrete Society as a design and construction tool for concrete industrial flooring applications. In 1988 the first edition was published and soon became recognised globally.

The first edition took account of the quick development of new construction techniques and gave guidance on thickness design of concrete industrial ground floors. The second and third editions, published in 1994 and 2003 respectively, continued to update these techniques and provide guidance to current knowledge and practice. Since 2003, ground-supported floors designed and constructed in accordance with TR34 have provided sufficient performance. The fourth edition, published in 2013, is a result of thorough review of all the aspects of floor design and construction since the previous edition (The Concrete Society, 2007).

The design guidelines provided in these reports have been based largely on steel fabric floors with sawn joints and on 'jointless' steel-fibre-reinforced ground-supported floors. Notably, the design guidance in the third and fourth edition has been expanded to include guidance on the design of MSFRC.

The third edition of the TR34 states that, considering MSFRC, certain dosages of structural fibres will provide suitable values of $R_{e,3}$, which is a measure of the ductility of the composite and typically referred to as the equivalent flexural strength, and determined experimentally, using a three-point bending test, as for SFRC. The $R_{e,3}$ value is the average load applied as the beam deflects to 3 mm, expressed as a ratio of the load measured at the occurrence of the first crack. The fibre dosage should be sufficient to provide a $R_{e,3}$ value of at least 0.3, otherwise the composite should be treated as plain concrete. If sufficient ductility can be demonstrated, i.e. a $R_{e,3}$ value ≥ 0.3, the same design equation to calculate the residual positive (sagging) moment capacity (M_p) can be used for MSFRC as for SFRC (The Concrete Society, 2003):

$$M_p = \frac{f_{ctk,fl}}{\gamma_c} \cdot R_{e,3} \cdot \frac{h^2}{6} \tag{2.4}$$

where:
$f_{ctk,fl}$ = characteristic flexural strength of the plain concrete (MPa)
γ_c = partial safety factor for SFRC
h = overall slab thickness (mm)

While fibres increase the toughness of the composite, they do not affect the cracking stress, i.e. an increase the negative (hogging) moment capacity (M_n), and can be calculated as (The Concrete Society, 2003):

$$M_n = \frac{f_{ctk,fl}}{\gamma_c} \cdot \frac{h^2}{6} \tag{2.5}$$

The fourth edition states that macro-synthetic fibres, in accordance with EN 14889, provide post-cracking or residual moment capacity. According to this edition, the fibre supplier is required to supply the quantity of fibres necessary to achieve a residual flexural strength (f_R) of 1.5 N/mm^2 at a crack mouth opening displacement (CMOD) of 0.5 mm and of 1.0 N/mm^2 at a CMOD of 3.5 mm.

The effect of the fibres on the strength of MSFRC have to be determined using a standard notched beam test in accordance with EN 14651. During this test method, four loads are reported, i.e. F_{R1}, F_{R2}, F_{R3}, and F_{R4}, corresponding to the applied load at CMODs of 0.5, 1.5, 2.5, and 3.5 mm, respectively. A typical applied load (F_R) versus CMOD is illustrated in Figure 2.14.

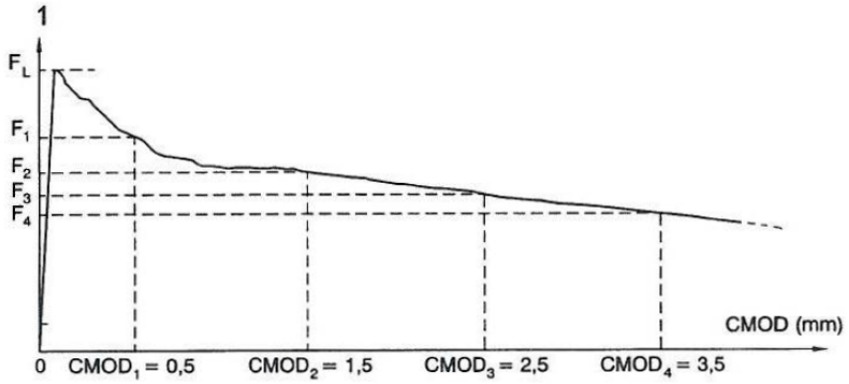

Figure 2.14: Typical load-CMOD graph (European Norms, 2007)

From the load-CMOD response, a residual flexural tensile strength (f_R) is determined for each load and can be calculated as:

$$f_R = \frac{3}{2} \cdot \left(\frac{F_R \cdot l}{b \cdot h_{sp}^2}\right) \tag{2.6}$$

where:
F_R = applied load at considered stage
l = span length of specimen
b = width of specimen
h_{sp} = depth of the section to the tip of the notch

Four values f_{R1}, f_{R2}, f_{R3}, and f_{R4}, corresponding to the measured applied loads F_{R1}, F_{R2}, F_{R3}, and F_{R4}, are reported for each test. The method to determine the residual moment capacity from these measurements is explained referring to a document prepared by the RILEM committee, TC 162-TDF(2002). At ultimate limit state (ULS), the calculation of the ultimate moment capacity is dependant on the mean axial tensile strengths for each of two crack widths. These strengths are σ_{R1} and σ_{R4} corresponding to CMOD of 0.5 mm and 3.5 mm respectively, and can be calculated as:

$$\sigma_{R1} = 0.45 \cdot f_{R1} \tag{2.7}$$

$$\sigma_{R4} = 0.37 \cdot f_{R4} \tag{2.8}$$

It is assumed that the axial tensile strength at the tip of the crack is σ_{R1} and, conversely, at the tension face it is assumed to be σ_{R4}, with a triangular distribution between the two points. Figure 2.15 illustrates the assumed stress and strain distribution.

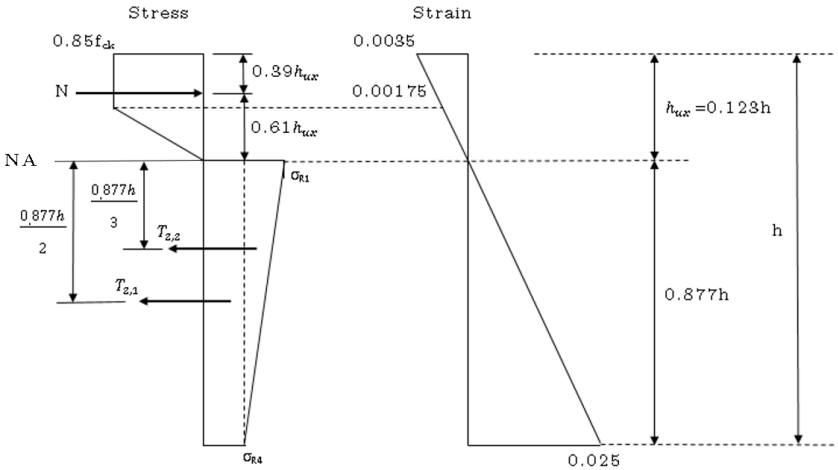

Figure 2.15: Stress block for fibre reinforced concrete (The Concrete Society, 2013)

From Figure 2.15 and taking moments about the centroid of the compression zone (N), the ultimate moment capacity can be calculated as:

$$M_u = \frac{h^2}{\gamma_m}(0.29 \cdot \sigma_{R4} + 0.16 \cdot \sigma_{R1}) \tag{2.9}$$

where:
h = height of the specimen
γ_m = partial material safety factor

Note that this is a simplified and conservative calculation of M_u. An iterative process can be followed to calculate a more accurate value of M_u which is less conservative.

2.3.9 Classification of FRC

Residual flexural tensile strengths f_{R1} and f_{R3} can be used to characterise the residual strength of FRC for SLS and ULS analysis, according to the fib Model Code (2010). To additionally simplify the classification of FRC, the material behaviour at ULS can be related to the behaviour of the material at SLS using the f_{R3}/f_{R1} ratio.

The post-cracking residual strength of FRC can be classified by using two parameters. The first parameter is a number representing the f_{R1} class, while the second parameter is a letter representing the f_{R3}/f_{R1} ratio.

The strength interval for $f_{R1,ck}$ (characteristic value of f_{R1}) is defined by two subsequent numbers in the series:

- 1.0; 1.5; 2.0; 2.5; 3.0; 4.0; 5.0; 6.0; 7.0; 8.0 (MPa)

While the letters a, b, c, d, and e correspond to the residual strength ratios:

- 'a' if $0.5 \leq f_{R3,ck}/f_{R1,ck} \leq 0.7$
- 'b' if $0.7 \leq f_{R3,ck}/f_{R1,ck} \leq 0.9$
- 'c' if $0.9 \leq f_{R3,ck}/f_{R1,ck} \leq 1.1$
- 'd' if $1.1 \leq f_{R3,ck}/f_{R1,ck} \leq 1.3$
- 'e' if $1.3 \leq f_{R3,ck}/f_{R1,ck}$

Although this classification accurately represent the most common cases of FRC exhibiting strain-softening behaviour, it can also be adopted for strain-hardening FRCs. Figure 2.16 illustrates a composite having a $f_{R1,ck} = 2.2$ MPa and a $f_{R3,ck} = 1.8$ MPa which is classified as '2b'.

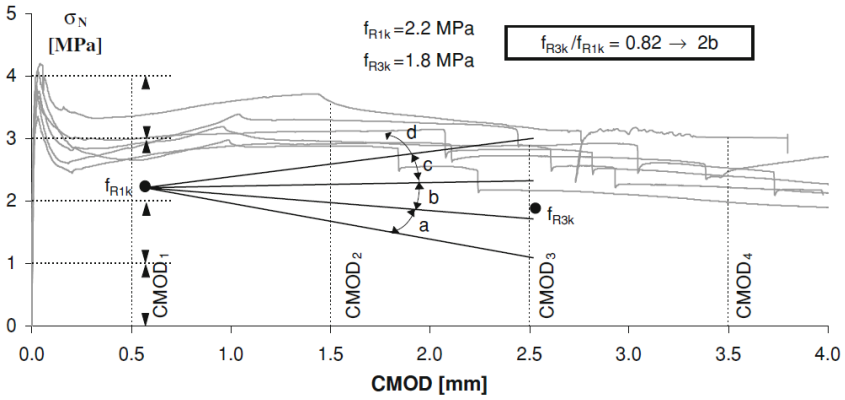

Figure 2.16: Example of FRC classification (Prisco et al., 2009)

Since it is of critical importance that brittleness must be avoided in structural behaviour, fibre reinforcement can be used to substitute conventional reinforcement (considering ULS), if the following relationships are fulfilled:

- $f_{R1,ck}/f_{LOP,ck} > 0.4$
- $f_{R3,ck}/f_{R1,ck} > 0.5$

where:
f_{Lk} = Characteristic value of the nominal strength, corresponding to the peak load (or the highest load within the interval $0 - 0.05$ mm), determined according to EN 14651.

It is important to note that this classification is not compatible with Technical Report 34 (TR34), as the TR34 requires the values f_{R1} and f_{R4}, and not f_{R1} and f_{R3} which is considered for this classification process.

2.4 Test methods measuring the performance of MSFRC

For FRC to be used effectively and economically in practice, the assessment of the properties of FRC is of critical importance. Methods commonly used to determine the properties of conventional concrete are applicable to investigate the properties, which are largely matrix dependant, such as compressive strength. Test methods which are somewhat different from those used for plain concrete are, however, required to evaluate the the properties of FRC which are more dependant on the presence of fibres and the fibre-matrix interface (Bentur and Mindess, 2007)

It is these properties that are of significant interest as they represent areas in which the addition of fibres to the composite experience a notable increase in its properties. These properties are primarily toughness (energy absorption capability), crack-control, and impact resistance of the composite (Bentur and Mindess, 2007).

In this section a brief review of the general test methods evaluating the freshly mixed properties of FRC, as well as a comprehensive review of the available test methods measuring the flexural performance of FRC in its hardened state, is provided.

2.4.1 Freshly mixed properties of FRC

Test methods used to evaluate the properties of FRC in its freshly mixed state are primarily for the following characteristics (Bentur and Mindess, 2007):

- Workability of the mix
- Content of fibres in the freshly mixed state

The workability of FRC in its freshly mixed state is the evaluation of its ability to be mixed, handled, transported, and, which is the critical characteristic, placed and consolidated with a minimum loss of homogeneity and minimal entrapped air. Various test methods are available to evaluated one or more of these characteristics (ACI Committee 544, 1999). The slump test and the Vebe test are briefly discussed as they are the more common tests conducted to measure the workability.

The slump test, in accordance with EN $12350-2$, is the oldest and most common test to evaluate the workability, but because it is a static test, it is not a good indicator of the workability of FRC (Bentur and Mindess, 2007). If however, it can be established that a FRC mixture has adequate handling and placing characteristics for a certain slump, the slump test can be implemented as a quality assurance test to evaluate the consistency of FRC (ACI Committee 544, 1999).

The Vebe test, in accordance with EN 12350 − 3, is a method used to determine the behaviour of concrete subjected to an external vibration. This method is acceptable for determining the workability of FRC placed using vibration. This test method adequately evaluates the ability of concrete, which is subjected to vibration, to flow, as well as to assess the ease with which entrapped air can be removed. It should however be noted that the Vebe test is not as convenient as the slump test for field use (ACI Committee 544, 1999).

For the purpose of uniformity and quality assurance in FRC, the fibre content of FRC in its freshly mixed state is a significant parameter. To determine the fibre content, wash-out tests are typically considered. This method is more efficient if the matrix is a mortar, due to the ability of the mortar to wash away when placed in a mesh-basket, while the fibres are retained on the mesh. A standard method published by the Japan Concrete Institute, JCI-SF 7, can be implemented to determine the fibre content (Bentur and Mindess, 2007).

2.4.2 Flexural behaviour of FRC using static test methods

An uni-axial tensile test requires a pure and uniform tensile stress applied to a concrete specimen. This is, however, difficult to achieve. In addition to this, and due to the fact that the stress is acting over the whole cross-section, there exists a much higher probability for a weak link to form which will instigate the first crack. The result is lower tensile strength than obtained in a flexural tensile test, as well as providing less accurate results. Since the uni-axial tensile test is more difficult to perform, flexural tests are performed to evaluate the mechanical behaviour of FRC (ERMCO, 2012).

Static mechanical tests are performed to evaluate the flexural behaviour of FRC. To evaluate the flexural behaviour of FRC, the complete stress-strain curve, or alternatively the load-deflection curve, needs to be measured. The interpretation of these curves in the post-cracking zone represents the strain capacity and the toughness of the composite, thus providing an indication of the quality of the material referring to its crack control capability. A reliable curve in the post-cracking zone is of critical importance, thus the use of a rigid testing machine with a closed loop testing configuration is recommended (Bentur and Mindess, 2007).

2.4.2.1 Three-point bending test

The fourth edition of TR34, as well as the fib Model Code (2010), recommends that the nominal properties of a FRC composite under flexure must be determined by performing a three-point bending test on a notched beam, in accordance with EN 14561. Figure 2.17 illustrates the setup of the three-point bending test.

Beams consisting of a 150x150 mm cross-section, with a span length of 500 mm, and a total length not less than 550 mm and not exceeding 700 mm, are to be used as standard test specimens. The shape and size of the specimens are acceptable for concrete with a maximum aggregate size not exceeding 32 mm, and fibres not longer than 60 mm. A notch with a width

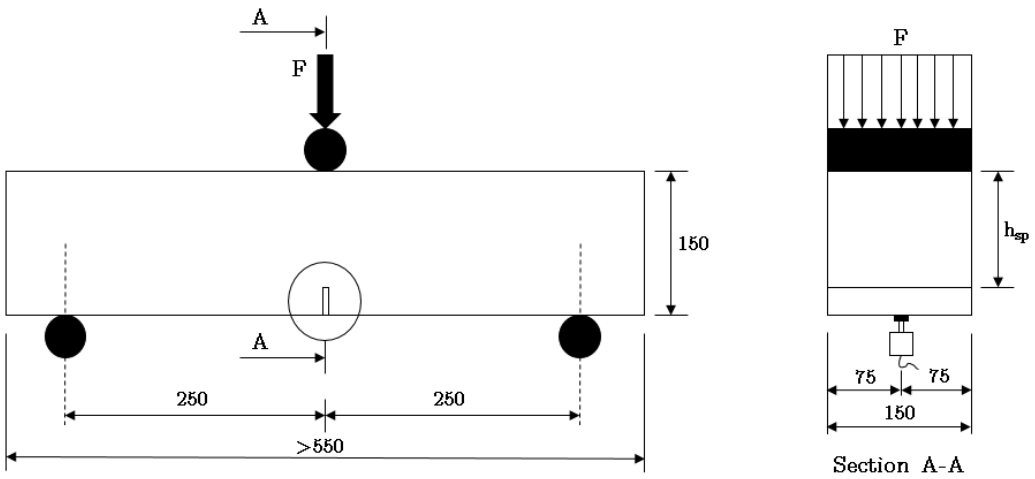

Figure 2.17: Setup of the three-point bending test according to EN 14651

not exceeding 5 mm is required, with the unnotched distance h_{sp}, referring to Figure 2.17, equal to 125 mm $\pm$ 1 mm. Tests must be performed 28 days after casting, using a testing machine capable of producing a constant rate of increase of deflection (δ) or CMOD of the specimen using a closed loop configuration. If the testing machine controls the rate of increase of the CMOD, the machine must be operated at a constant rate of 0.05 mm/min for CMOD from 0 to 0.1 mm, whereafter the machine must be operated at a constant rate of 0.2 mm/min until the end of the test. The test must not be terminated at a CMOD value less than 4 mm. Tests completed during which the crack started outside the notch, must be rejected (European Norms, 2007).

The following characteristic values can be determined from this test method:

- Limit of proportionality (LOP)
- Residual flexural tensile strengths at different CMODs

The CMOD is a value measured in millimetres (mm) and is taken at the bottom surface of the specimen. If the line of measurement is at a distance y below the bottom of the test specimen, the following expression must be used to determine the CMOD derived from the measured value CMOD_y:

$$CMOD = CMOD_y \cdot (\frac{h}{h+y}) \tag{2.10}$$

where:
h = total depth of the test specimen
y = distance below the bottom of the test specimen where the measurement is taken

The limit of proportionality (LOP) is calculated using the load value F_L which corresponds to the maximum load in the CMOD interval $0 - 0.05$ mm. The following expression can be used to determine the LOP:

$$f_{LOP} = \frac{3}{2} \cdot (\frac{F_L \cdot l}{b \cdot h_{sp}^2}) \tag{2.11}$$

where:
f_{LOP} = Strength corresponding to the maximum load achieved within a CMOD of $0 - 0.05$ mm (MPa)
l = span length (mm)
b = width of the specimen (mm)
h_{sp} = distance between the tip of the notch and the top of the specimen (mm)

The residual flexural tensile strengths are calculated using the applied loadings at specified CMODs, as illustrated in Figure 2.14. The calculation of the critical residual flexural tensile strengths, at different CMODs, is covered in Section 2.3.8. The following equation must be implemented:

$$f_{R,j} = \frac{3}{2} \cdot (\frac{F_j \cdot l}{b \cdot h_{sp}^2}) \tag{2.12}$$

where:
$f_{R,j}$ = residual flexural tensile strength corresponding with CMOD = CMOD$_j$ (j = $1, 2, 3, 4$) (MPa)
F_j = applied loading corresponding with CMOD = CMOD$_j$ (j = $1, 2, 3, 4$) as illustrated in Figure 2.14 (N)

Previous research has indicated that the scatter of results is profound when the test method, prescribed by EN 14651, is implemented (Buratti et al., 2011). The scatter of the results strongly depends on the type, and the dosage, of fibres, and is a result of the small number of fibres crossing the crack surface, as well as the small crack surface aiding a high statistical variability. Due to the more homogeneous distribution and higher amount of macro-synthetic fibres over the fracture surface, the scatter of results in the post-cracking region for MSFRC is much smaller than for SFRC (Buratti et al., 2011).

2.4.2.2 Four-point bending test

The flexural performance of FRC can also be evaluated using a four-point bending test, also referred to as the third-point loading bending test. This test method can be performed in accordance with ASTM C78 (ASTM Committee, 2010b). Figure 2.18 illustrates the typical setup considering the four-point bending test according to ASTM C78 (2010).

This standard implements two proposed specimen sizes, i.e. a 100x100x350 mm beam with a span equal to 300 mm, and a 150x150x500 mm beam with a span equal to 450 mm. This test method, however, only allows the calculation of the modulus of rupture (MOR):

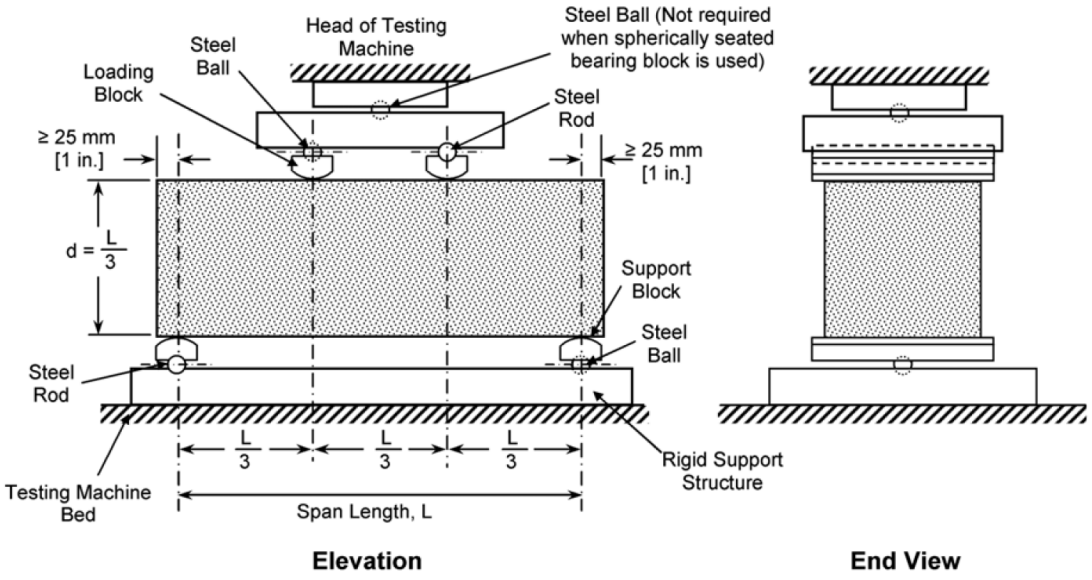

Figure 2.18: Setup of the four-point bending test according to ASTM *C*78 (2010)

$$MOR = \frac{F \cdot l}{b \cdot d^2} \tag{2.13}$$

where:
MOR = modulus of rupture (MPa)
F = maximum load carried by specimen (N)
b = width of specimen (mm)
d = depth of specimen (mm)

Several other ASTM standards evaluating the flexural performance of FRC, use the identical test setup as ASTM C78 (2010) and is briefly discussed. Implementing ASTM C1018 (1997), a specimen with a size of 100x100x350 mm, is tested under four-point bending employing the test setup according to ASTM C78 (2010). This test method defines various toughness indices as a ratio of the area beneath the load-deflection curve to a certain deflection, as well as the area beneath the curve to the first crack. In addition to the toughness indices, residual strengths, representing the average post-cracking load the specimen can achieve over a certain deflection interval, are calculated from the toughness indices. This test method suffers, however, from a number of shortcomings, e.g. the test results are strongly influenced by the test procedure and different toughness values and residual strengths can be a result of a slight change in the determination of the first crack strength and deflection measurements (Bentur and Mindess, 2007). Due to its shortcomings, this test method has been withdrawn and effectively replaced by ASTM C1609 (2013).

ASTM C1609 (2013) provides a test method, implementing the test setup equivalent to that provided in ASTM C78 (2010), to calculate the first-peak and peak loads, as well as the corresponding stresses. It also provides the determination of the residual flexural tensile strengths at specified deflections, as calculated in Section 2.4.2.1, as well as the composites toughness based

on the area beneath the load-deflection curve up to a certain deflection. Two preferred specimen sizes of 100x100x350 mm, or 150x150x500 mm, are used and measures the deflection up to at least l/150 of the span length (l) (ASTM Committee, 2013).

ASTM C1399 (2010) also provides a standard to evaluate the flexural performance and determine the residual flexural tensile strengths of FRC. According to this method, a specimen, with a size of 100x100x350 mm, is loaded in a similar manner as prescribed according to ASTM C78 (2010). An initial load is applied until the specimen begins to crack. The load is released and the cracked specimen is reloaded to get a reloaded-deflection curve. The average residual strength of the specimen over a deflection range of 0.5 to 1.25 mm can then be determined, using the reloaded curve (ASTM Committee, 2010a).

According to SANS 5864 (SABS Standards Division, 2006b), the use of the four-point bending test will most likely yield flexural strengths which is lower than that of the three-point bending test. Instead of applying a force at a particular point, there exists a wider range of area for cracking to occur under third-point loading and the selection of a weaker spot along the span for the crack to occur is more prominent.

2.4.2.3 Round Determinate Panel Test (RDPT)

Evaluating the post-cracking behaviour of FRC performing either of the test methods described previously, a large scatter of results can be expected. This is due to the non-uniform fibre distribution and small crack area. One of the possible solution to avoid this large scatter of results is to increase the crack area. This can be achieved by implementing ASTM C1550 (2012) to determine the flexural performance of FRC (Vandewalle et al., 2008).

ASTM C1550 (2012) requires a standard round panel test to be performed on specimens with a diameter of 800 mm and a thickness of 75 mm. The panels must be supported on three symmetrically arranged pivot points on a pitch circle diameter of 750 mm. A central point load, with a hemispherical end, is then applied to these panels. This test method is controlled by means of central displacement. A test sample which fails by means of three evenly sized cracks between the supports are classified as successful. Figure 2.19 illustrates the typical setup for the RDPT according to ASTM C1550 (2012).

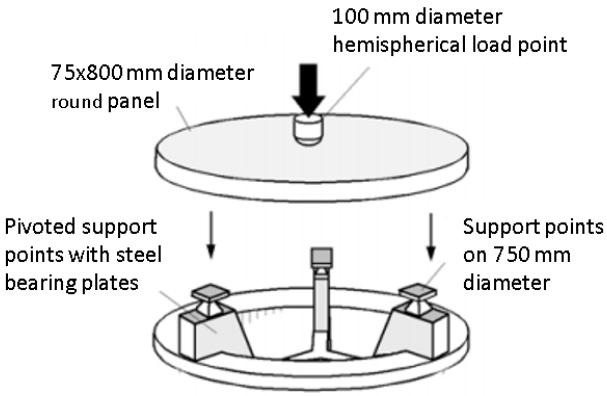

Figure 2.19: Setup of the round determinate panel test (RDPT) according to ASTM C1550 (2012)

The RDPT evaluates the flexural behaviour of FRC and determines the toughness of the composite expressed as the energy absorption capability in the post-cracking range. The performance of the composite is quantified by the energy absorbed between the onset of the applied loading and specific central deflection. Due to the significantly higher crack area of the RDPT, test results vary between 5 to 10%, which is considerably lower than typical variations observed in three-point bending tests which is between 20 to 30% (Vandewalle et al., 2008). The RDPT is specifically of interest for applications with thin elements, for example wall elements, shotcrete, etc.

2.4.2.4 Plate test

The European Federation of National Associations Representing for Concrete (EFNARC) (EFNARC, 1996) recommends the implementation of a plate test to evaluate the flexural performance of FRC. As for the RDPT, the plate test evaluate the composite's performance by characterising its energy absorption capacity (Gopalaratnam and Gettu, 1995).

EFNARC (1996) specifies that a test plate, with dimensions 600x600x100 mm and simply supported along all four its edges, using a 500x500 mm span, must be subjected to a centre point load through a contact surface area of 100x100 mm at a rate of 1.5 mm/min. Figure 2.20 illustrates the basic test setup for the plate test.

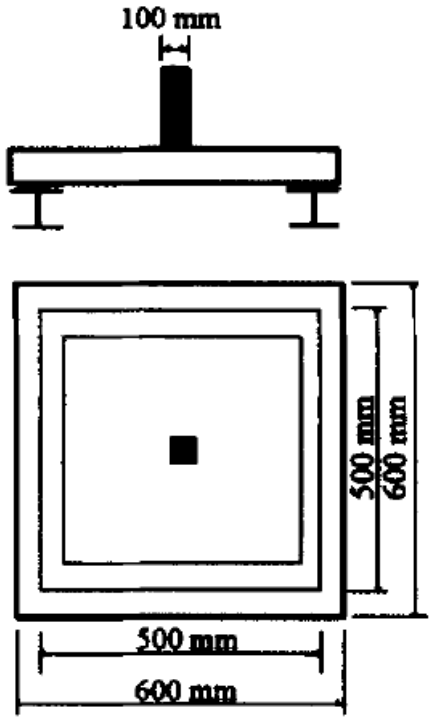

Figure 2.20: Test setup used for the plate test (Gopalaratnam and Gettu, 1995)

The result of the test is a plot of the load against the central deflection. The energy absorption capacity is then determined, as for the RDPT, by calculating the area under the load-deflection curve. The energy absorbed, up to a central deflection of 25 mm, is required. The performance of the composites can then be classified according to different classes for specific energy absorption capacities, as illustrated in Table 2.2

Table 2.2: Toughness classification according to energy absorption capacity (Gopalaratnam and Gettu, 1995)

Toughness classification	**Energy absorption (J) for deflection up to 25 mm**
a	500
b	700
c	1000

2.5 Time-dependant behaviour of FRC

As fibres only influence the performance after the first crack has formed, the time-dependent behaviour of FRC must be explained in its cracked state. However, a brief overview of the time-dependant behaviour of normal cement-based composites is provided to explain the mechanisms involved in causing time-dependant behaviour.

2.5.1 Time-dependent behaviour of normal cement-based composites

Under constant temperature and stress, concrete experience a gradual increase in deformation. When serviceability, durability and long-term performance of concrete structures are of concern, shrinkage and creep are very important factors to consider (Kovler, 1995).

Shrinkage of concrete is independent of stress and is a time-dependent volume change due to a number of mechanisms. The movement of water in both the fresh, and hardened states of concrete, has been identified as being the primary mechanism responsible for shrinkage (Neville, 2011). Four phenomena have been identified as the mechanisms of shrinkage on macro level, i.e. drying shrinkage, hardening shrinkage (chemical shrinkage), autogenous shrinkage and carbonation shrinkage (Boshoff, 2007).

When a cement-based material is allowed to dry, i.e. the internal relative humidity is higher than the ambient relative humidity, the migration of water is initiated and the volume, or length change, is defined as drying shrinkage. During the first stage of drying shrinkage, free water in the capillary pores are lost, which has little, to no effect, on the measured shrinkage. However, as drying continues, absorbed water stored in the capillary pores and gel is withdrawn and causes shrinkage of the unrestrained hydrated cement paste.

Hardening shrinkage (chemical shrinkage) occurs mostly in the plastic state of concrete and can be defined as the volume change of cement-based materials due to chemical reactions taking place during the hydration of cement. The possible volume reduction due to the hydration process can be explained due to the solidification of free water. However, in the hardened state of the material, the solidification does not have a significant effect on the macroscopic length, or volume change, as most of the chemical shrinkage is accommodated by internal porosities.

Autogenous shrinkage is defined as macroscopic length, or volume change, when water transport is not allowed to, or from, the cement paste, but extracted from the capillary pores and gel due to the hydration of the unhydrated cement particles. This extraction causes autogenous shrinkage and is also referred to as self-desiccation. In the past, volume change during the drying of cement-based materials has been attributed solely to drying shrinkage. However, at low water/cement ratios, less true drying shrinkage is measured and higher autogenous shrinkage. It has been shown that at a W/C ratio as low as 0.17, all the volume and length change can be attributed to autogenous shrinkage with true drying shrinkage not playing a role (Tazawa and Miyazawa, 1995).

Due to CO_2 from the ambient environment reacting with hydrated cement paste in the surface region of cement-based materials, carbonation shrinkage occurs. Due to the fact that the first step of the reaction involves dissolving CO_2 in the pore water, nearly no carbonation shrinkage would occur if the pores are either saturated or empty (Perrie, 2009).

As mentioned above, creep is also an important factor to consider when the time-dependent behaviour of cement-based materials are to be understood. Creep is the tendency of materials to deform gradually under a sustained load. Sometimes creep can be beneficial to structural engineers as it leads to redistribution of stresses within structures, whereas, in other cases, it

can lead to adverse effects. These effects can involve excessive deflections and elongation and/or shortening of concrete structures (Babafemi and Boshoff, 2015). The consequences of creep can have dramatic influences, rendering structures to be unserviceable with time which leads to great economic losses. The combination of three mechanisms can describe creep of cement-based materials (Boshoff, 2007).

Firstly, creep is initially caused by the migration of water in the capillary pores in the cement matrix. The movement is induced when stress is applied to the material. Secondly, the breaking and re-establishing of bonds on the micro-level initiates creep. When stress is applied to the material, it is believed that the gel structure within the matrix collapses when internal stress peaks are formed. Due to the continuation of the hydration process, the micro-structure is redefined and serves as an explanation for the permanent deformation associated with creep. Lastly, in high stress conditions, the formation of micro cracks in the matrix cause non-linearity of creep. The micro cracks are formed due to internal stress peaks which exceeds the fracture strength. These cracks may grow and connect under a sustained load and even cause a global material failure on macro-level. This fracture is referred to as creep fracture (Boshoff, 2007).

2.5.2 Time-dependent behaviour of cracked FRC

Much still remains unknown regarding the creep behaviour of FRC. As mentioned, fibres only influence the performance once concrete has cracked, thus the time-dependent behaviour of FRC are discussed in its cracked state.

With the addition of fibres, the weakness of concrete in tension has greatly been curtailed. Several studies on the creep of concrete have predominately focussed on compressive creep. A comparison between the coefficient describing compressive and tensile creep have been researched, and it is suggested that the mechanisms involved for creep in compression differs from that in tension (Gilbert et al., 2011). The limited number of research on uniaxial tensile creep has to do with the technicalities of the experimental setup, i.e. the load transmitting mechanism (stress concentration) as well as the boundary condition (moment transmission). Limited research can also be found on the time-dependent uniaxial tensile behaviour of cracked FRC.

Some research has been published on the uniaxial tensile creep of FRC in its cracked state. Zhao et al. (2014) investigated SFRC and Boshoff et al. (2009) investigated micro synthetic FRC. The variables considered during the work of Zhao et al. (2014), were the critical load level and the precracked width. From prisms, cylindrical specimens were cored and subjected to a creep load equal to 30%, and increased to 60%, of the average residual strength of each specimen after being cracked to a width of 0.05 and 0.2 mm. After an 3 month period, Zhao et al. (2014) documented that the crack opening was similar as the instantaneous deformation, proven it to be an elastic deformation. The results from the work indicated that, at 30% of the maximum pre-cracking load, the delayed crack opening did not exceed 0.25 mm. It was also reported that, for specimens whose load were increased to 60% of the maximum pre-cracking load, an increase in creep was also observed. Referring to the time-dependent crack opening of cracked FRC, it is suggested that the load level is a very important consideration.

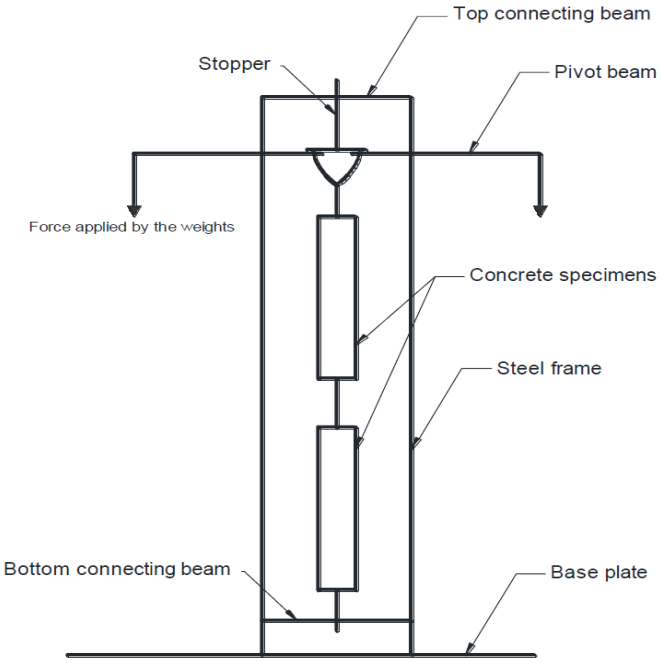

Figure 2.21: Uniaxial tensile creep frame with specimens in series (Babafemi and Boshoff, 2015)

Babafemi and Boshoff (2015) investigated the time-dependent flexural creep behaviour of cracked MSFRC as the addition of macro-synthetic fibres can have a larger crack width increase as opposed to cracked SFRC. Investigating the residual behaviour of MSFRC, uniaxial tensile tests were performed. The residual strengths were of importance as the uniaxial tensile creep loads were based on them. The uniaxial tensile creep frame considered in the work of Babafemi and Boshoff (2015), is illustrated in Figure 2.21.

Five load levels were investigated, i.e. 30%, 40%, 50%, 60%, and 70% of the residual tensile strength. The deformation was measured using two LVDTs on each specimen and included basic creep, drying creep, crack widening and drying shrinkage. The actual creep deformation was calculated by subtracting the drying shrinkage from the total creep.

At all the stress levels investigated, an increase in the CMOD was evident right after applying the creep loads. After two weeks of continued loading, an increase in crack opening was reported at a decreasing rate for all samples. Table 2.3 presents the results of the creep at 30, 90, and 180 days, as well as the instantaneous creep. The percentage difference in the CMOD between 30-90 days and 90-180 days are also shown.

Table 2.3: Uniaxial tensile creep results (Babafemi and Boshoff, 2015)

Stress level (%)	$CMOD_{inst}$ (mm)	$CMOD_{creep(30)}$(mm)	$CMOD_{creep(90)}$(mm)	$CMOD_{creep(180)}$(mm)	$CMOD_{(30-90)}$(%)	$CMOD_{(90-180)}$(%)
30	0.017	0.357	0.546	0.65	53	19
40	0.042	0.517	0.791	1.12	53	42
50	0.070	0.655	0.960	1.25	47	30
60	0.150	1.343	2.190	3.67	63	68
70	0.280	1.737	3.280	5.71	89	74

From the results reported by Babafemi and Boshoff (2015), the $CMOD_{inst}$ and $CMOD_{creep}$ increased with the applied creep load and the specimen's age. For each of the stress levels investigated, the $CMOD_{creep}$ was higher than the $CMOD_{inst}$. It should also be noted that MSFRC indicated as experiencing creep at a low stress level of 30% of the average residual tensile strength. At stress levels of 60% and 70%, the time-dependent crack opening is more profound.

It can be concluded that the creep of cracked MSFRC is dependent on the stress level. An increase in the creep load will cause a more severe time-dependent crack opening. Creep fracture occurred at stress levels in excess of 60% and 70% before unloading, thus creep fracture should be considered when using MSFRC. Babafemi and Boshoff (2015) also reported that the distribution and number of fibres crossing the cracked plane is responsible for variability and severity of the time-dependent crack opening.An lower time-dependent crack opening is experienced for an increase in the amount of fibres bridging the cracked surface.

2.6 Influencing factors on the performance of MSFRC

This section reports on the factors influencing the performance of MSFRC. It is known that the constituent material's characteristics, including their respective volumes, influence the performance of FRC in its fresh and hardened state. Fibre geometry, fibre dosage, the mechanical and physical properties of the fibres, the fibre-matrix interfacial bond characteristics, as well as the mechanical properties of the matrix, significantly affects the performance of MSFRC.

2.6.1 Effect of mix design parameters

Generally, no changes to conventional concrete mix proportions have to be made when adding fibres at a dosage of approximately 0.25% or less by volume, as far as the binder content as well as the fine and coarse aggregate ratios are concerned. The water content may need to be adjusted depending on the fibre type and volume, or ideally the addition, or increase, of a water-reducing admixture is prescribed to maintain the workability, slump, and W/C ratio (ACI Committee 544, 2008).

When adding fibres at a dosage of more than 0.25% by volume, the mix proportions needs to be adjusted. The paste content and the fine aggregate volume have to be increased. The maximum grain size must be reduced due to the decrease in available space when larger dosages of fibres are added. The cohesion of the composite must also be increased to prevent segregation.

The larger the paste content of the matrix, i.e. the phase of the matrix within which the fibres can move and rotate, the better the workability for any specific fibre content. The paste consistency is of critical importance and the determining factor characterising the consistency is the paste viscosity. The viscosity is governed by the W/C ratio, the dosage of a water-reducing admixture, and the amount, and type, of filler incorporated, such as fly ash, slag, or silica fume. The volume of paste needed for a specific type and dosage of fibres to produce a certain level of

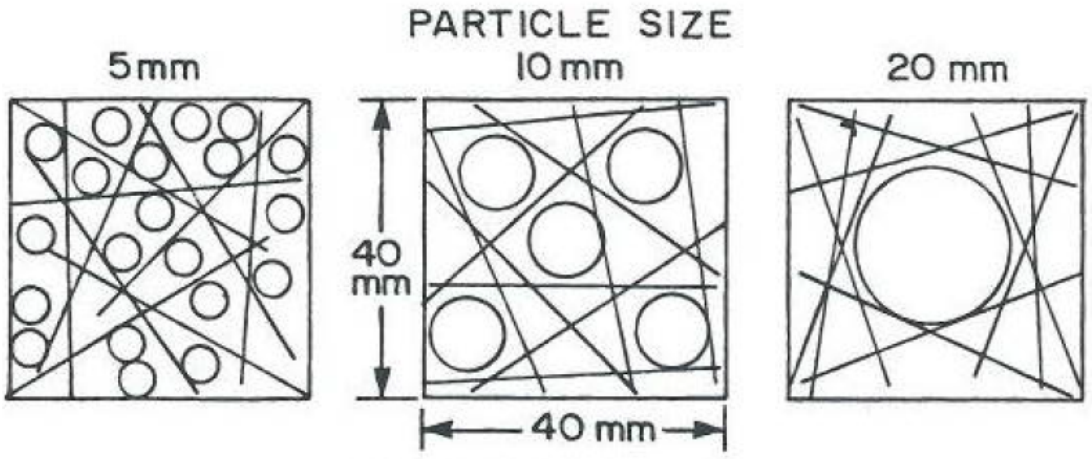

Figure 2.22: Effect of coarse aggregate particle size on fibre distribution (Hannant, 1978)

workability, decreases as the consistency of the paste increases. It should be noted that excessive fluidity may cause segregation, and loss of workability, due to particle interference (Bentur and Mindess, 2007).

Figure 2.22 illustrates the effect an increase in coarse aggregate particle size has on fibre distribution. It can be concluded, from Figure 2.22, that an increase in the particle size will ensure a less uniform fibre distribution and will result in fewer fibres bridging the cracks to provide post-cracking load carrying capacity. From previous research concluded at Stellenbosch University (Odendaal, 2015), round determinate panel tests (RDPT), completed according to ASTM $C1550$ (2012), indicated a decrease in energy absorbed when the nominal aggregate particle size was increased. Notched beam tests, completed according to EN 14561 (2007), did however not indicate a particular trend for the effect of coarse aggregate particle size on the $R_{e,3}$ value. The reason for this discrepancy between the two test methods still has to be established. It can however be concluded that larger particle sizes will occupy more crack area, thus distributing fibres more unevenly which results in areas with few to no fibres, ensuring a worse performance (Odendaal, 2015).

From literature, several models have been developed to calculate the average spacing between fibres, taking account of the fibre length, equivalent fibre diameter, and the fibre volume ratio. These spacings can be used to determine the maximum particle size. Some of these models are:

1. McKee (1969):

$$S = \sqrt[3]{\frac{25 \cdot \pi \cdot d^2 \cdot l}{V_f}} - d \tag{2.14}$$

2. Romualdi and Mandel (1964):

$$S = (13.8 \cdot d \cdot \sqrt{\frac{1}{V_f}}) - d \tag{2.15}$$

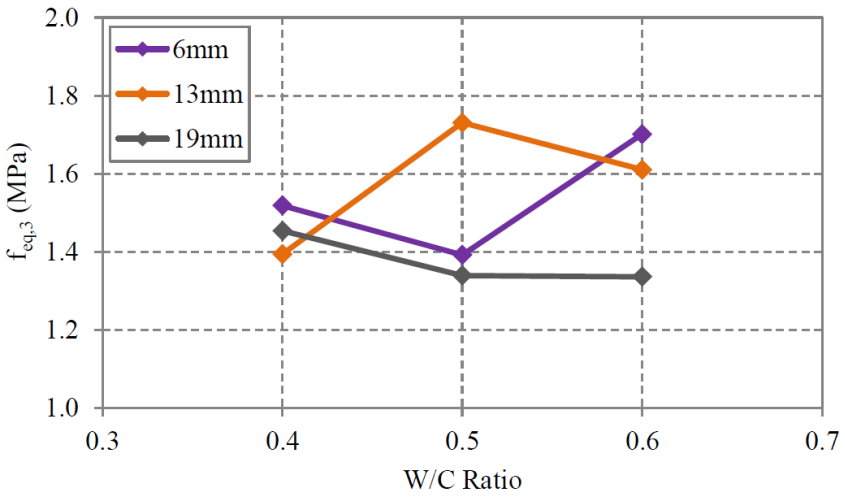

Figure 2.23: Equivalent flexural tensile strengths for various W/C ratios at different nominal coarse aggregate sizes (Odendaal, 2015)

3. Kobayashi and Cho (1976):

$$S = (5 \cdot \sqrt{\frac{\pi}{\frac{0.002 \cdot l}{d} + 0.4}} \cdot \frac{d}{\sqrt{V_f}}) - d \tag{2.16}$$

where:
S = surface-to-surface spacing between neighbouring fibres (mm)
l = fibre length (mm)
d = fibre diameter (mm)
V_f = fibre volume ratio (%)

Another factor that affects the post-cracking behaviour of MSFRC, is the W/C ratio. From previous research concluded at Stellenbosch University, notched beam tests, completed according to EN 14561, indicated that an increase in the W/C ratio resulted in an increase in the $R_{e,3}$ value. This is rather misleading, as the equivalent flexural strength ($f_{eq,3}$) remained relatively constant for an increase in the W/C ratio, illustrated in Figure 2.23, but the modulus of rupture (MOR) decreased due to the weakened cement matrix as a result of the additional free water at higher W/C ratios, as depicted in Figure 2.24 (Odendaal, 2015). The decreasing MOR resulted in an increase in the $R_{e,3}$ value. This, however, does not suggest that the post-cracking performance of MSFRC increases with an increase in the W/C ratio. From the documented research, it can be concluded that, considering notched beam tests, it seems that the performance is not influenced by the W/C ratio. Conversely, other researchers have found that an increase in the W/C ratio causes a decrease in the post-cracking performance of FRC (Lin, 1992).

Round determinate panel tests (RDPT), completed according to ASTM $C1550$ (2012), indicated a decrease in energy absorbed for an increase in the W/C ratio. A possible explanation for this effect is a reduction of fibre bond stress with an increased W/C ratio (Odendaal, 2015). The reason for the different trend, considering the two different test methods, is not known.

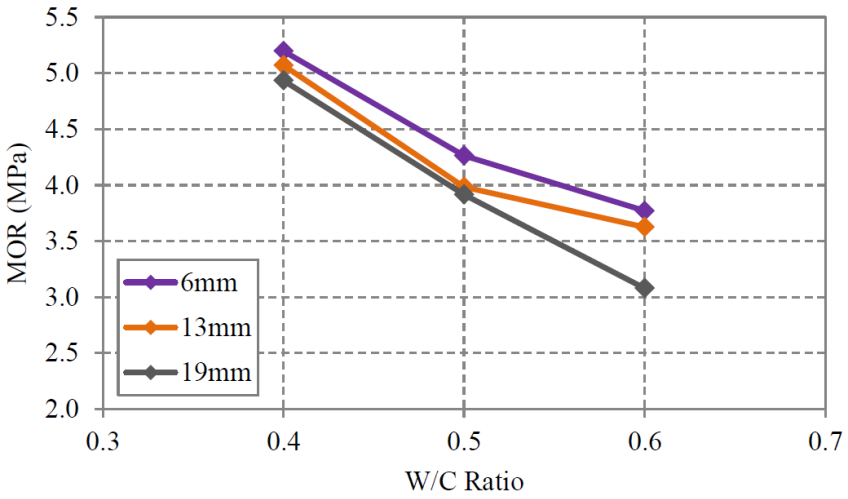

Figure 2.24: MOR for various W/C ratios at different nominal coarse aggregate sizes (Odendaal, 2015)

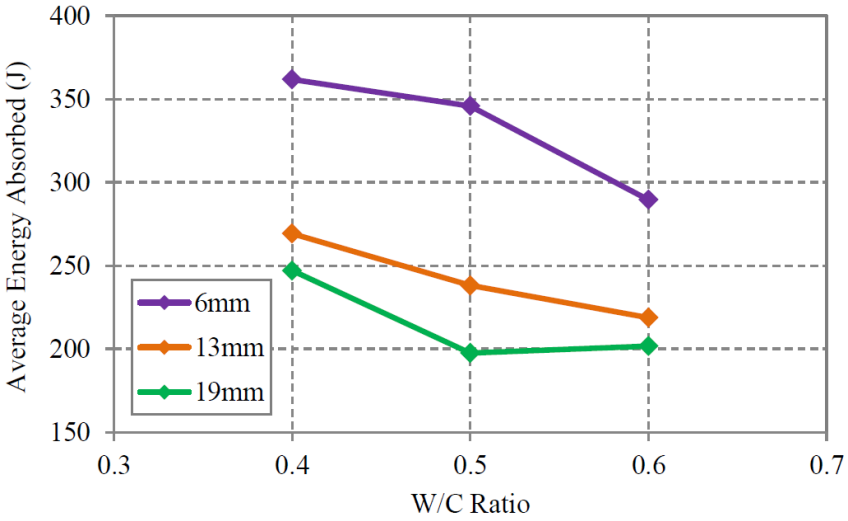

Figure 2.25: Average energy absorbed according to RDPT for various W/C ratios considering different nominal coarse aggregate sizes (Odendaal, 2015)

Figure 2.25 illustrates the effect on the energy absorption capability of MSFRC, by increasing the W/C ratio for various coarse aggregate sizes.

2.6.2 Effect of fibre properties and volume

For any type of fibre to be effective in reinforcing brittle cementitious matrices, the fibres must have suitable intrinsic material properties. The following properties must be considered (Bentur and Mindess, 2007):

- Tensile strength
- Ductility
- Elastic modulus

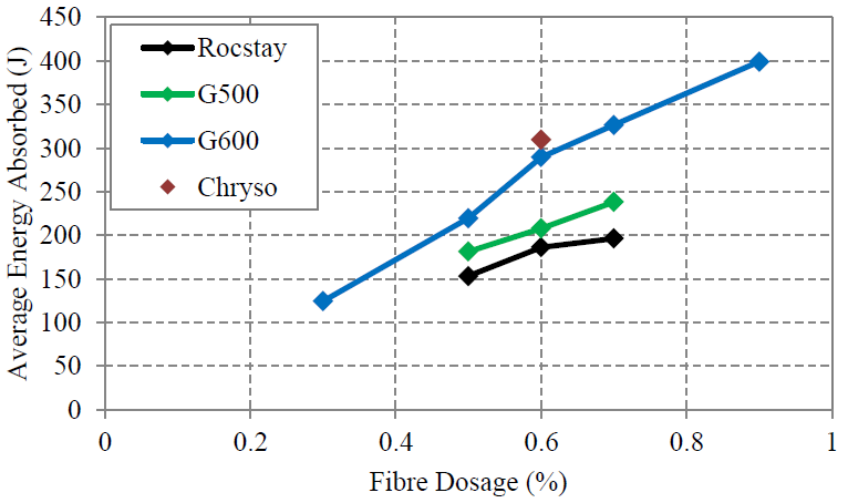

Figure 2.26: Average energy absorbed for different fibre types and fibre dosages (Odendaal, 2015)

- Elasticity
- Poisson's ratio

The tensile strength of the fibre must be greater than that of the matrix itself, since the effective load-bearing area of the fibres is much less than the corresponding area of the matrix. To enhance the energy absorption capability of the composite, the fibre must be able to withstand strains well in excess of the cracking strain experienced by the cement-based matrix. The composite will also experience less strain after the matrix have cracked if the elastic modulus of the fibre is higher relative to that of the matrix. The effectiveness of the fibre reinforcing will reduce if the fibres are not truly elastic and are prone to creep under normal or elevated temperatures. In this case the composite will tend to experience stress relaxation when loaded prior to cracking, and time-dependant strain after cracking. Fibres with a Poisson's ratio greater than $0.20 - 0.25$ are more prone to contract laterally under tensile stresses, more than the matrix, and tear away from the matrix. This adversely affects the adhesive bond between the fibre and the matrix. Ultimately, the potential of fibre reinforcement depends strongly of the interfacial shear bond between the fibre and the matrix and whether failure occurs by fibre pull-out or fibre fracture (Bentur and Mindess, 2007).

From previous research concluded at Stellenbosch University (Odendaal, 2015), the increase of the fibre dosage results in the increase of the post-cracking performance of MSFRC. Round determinate panel tests, completed according to ASTM C1550, suggested that an increase in the fibre dosage indicated a linear increase in the average energy absorbed, as illustrated in Figure 2.26. Notched beam tests, completed according to EN 14561, also showed an increase in the equivalent flexural tensile strength, and $R_{e,3}$ value, with an increase in fibre dosage, as illustrated in Figure 2.27. A higher fibre dosage will ensure more fibres bridging the cracks, resulting in a higher residual load carrying capacity. It should be noted that various macro-synthetic fibre types were used in the research documented by Odendaal, 2015, supplied by various suppliers.

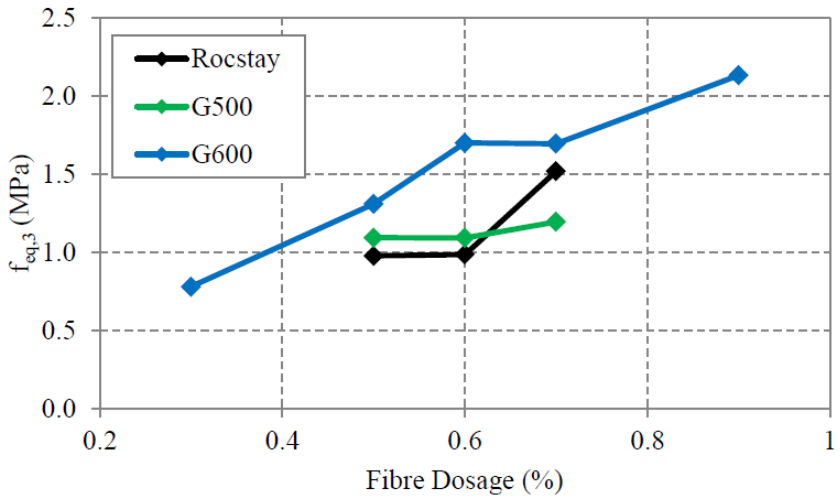

Figure 2.27: Equivalent flexural strength for different fibre types and fibre dosages (Odendaal, 2015)

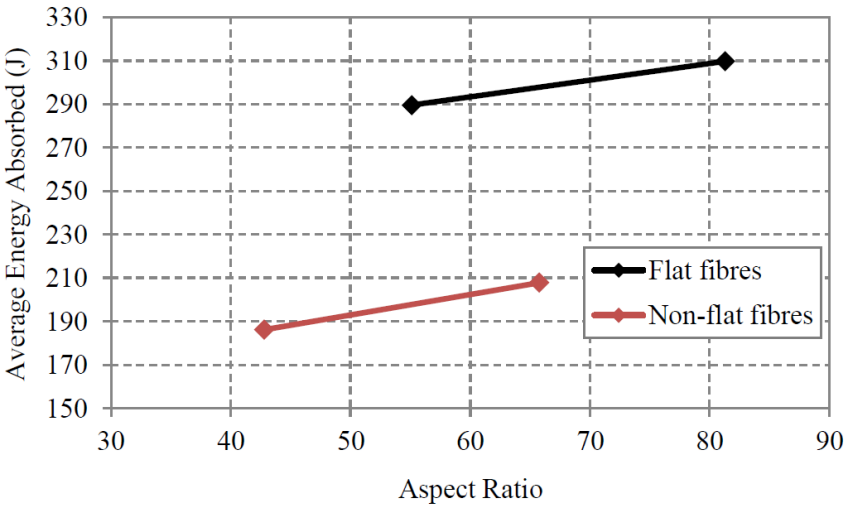

Figure 2.28: Effect of fibre type and aspect ratio on the average energy absorbed (Odendaal, 2015)

Fibre geometry also affects the post-cracking performance of MSFRC. According to previous research, flat fibres with a rectangular cross-section performs better than non-flat crimped fibres, and fibres with similar shapes and tensile strengths may exhibit more or less the same behaviour, although their bond stresses differ significantly (Odendaal, 2015). The fibre aspect ratio also plays a role in the post-cracking performance, with an increase in the performance corresponding to an increase in the fibre aspect ratio. Figure 2.28 illustrates these effects, according to the average energy absorbed.

2.7 MSFRC for industrial flooring applications

In recent times, the use of macro-synthetic fibres in concrete slabs-on-grade, as well as a suited replacement for steel fibres or traditional steel fabric, has become one of its primary applications.

Industrial concrete slabs-on-grade has two primary functions, i.e. transferring sustained loads to the soil without structural failures or excessive settlements, and providing an acceptable surface where operations can be carried out in a productive and safely manner (Neal, 2002). Most industrial floors is provided with sufficient reinforcement to control the size and amount of cracks. Standardised welded steel mesh has been the conventional choice for reinforcing industrial concrete slabs-on-grade, but recently, with the construction world developing with a rapid rate, the use of fibres in slabs-on-grade has significantly increased. Industrial concrete slabs-on-grade, roads and other slab elements are responsible for implementing nearly 65% of fibres produced worldwide (Labib and Eden, 2006).

For most structural applications of FRC, steel fibres are mostly considered. More recently, macro-synthetic (structural) fibres have been incorporated in structural applications. The lighter weight, lower abrasion, and sufficient structural performance are making macro-synthetic reinforcement an economic alternative. In a recent study by Murugesan and Rajpurohit, 2015, the cost benefit considering SFRC to conventional concrete for industrial floors was reported, and indicated, an approximate saving of 10% of the overall slab cost. As macro-synthetic fibres are more cost effective than steel fibres, the use of MSFRC would indicate an even larger percentage.

A recent study by Bothma (2013), investigated the use of macro-synthetic fibres in the design of concrete floors on grade. The aim of the study was to investigate two different design methods for slabs-on-grade, i.e. the Westegaard theory, which is an elastic theory and excludes the effect of fibres since it defines failure when any form of cracking occurs, and the Yield-line theory, which is a plastic theory. Failure is still defined once the first crack on the top surface of the slab occurs, considering the Yield-line design theory, but the ductility gained from the fibres are included reaching higher positive moments after first cracks occurred on the bottom of the slab. These moments are calculated as illustrated in Section 2.3.8.

From the results presented by Bothma (2013), using the Westegaard design theory, thicker design depths (22.5% more) were needed for slabs compared to the design depths calculated according to the Yield-line theory. This indicates that the Yield-line theory is more effective, from a design perspective, since it provides for thinner slabs while still complying with the requirements for both the ultimate and serviceability limit states.

It can be concluded that the use of macro-synthetic fibres are beneficial for concrete slabs-on-grade, from a performance and economical point of view. However, due to the perceived uncertainty over the ability of macro-synthetic fibres to replace steel fabric or steel fibre reinforcement, structural fibres are not commonly used, and the need for extensive research is clear.

2.8 Other applications of MSFRC

The use of FRC has increased steadily since its introduction into the construction world in the 1960s. Roughly 80 million m^3 of FRC are produced annually since 2001, with the main applications being slabs-on-grade (60%), shotcrete (25%), pre-cast structural members (5%),

and the rest of the fraction distributed amongst a number of speciality structural forms (Bentur and Mindess, 2007).

Despite the effectiveness of the addition of fibres to a cementitious matrix, such as providing crack resistance and control, and significantly increasing the residual strength in the post-cracking region, ensuring a more ductile material as oppose to conventional concrete which suffers brittle failure, the implementation of fibres in truly structural applications are still very limited. This may be explained due to the fact that most structural design codes for concrete are primarily based on concrete strength, i.e. the maximum load an element can withstand, as the principal design parameter rather than concrete toughness. Recently, RILEM Committee TC162-TDF developed a detailed procedure for designing according to flexural loading, which includes the post-peak behaviour of SFRC (Vandewalle, 2000).

Despite the absence of design provisions in building codes, FRC is being used in a variety of structural applications worldwide. The principal applications of MSFRC are listed below other than concrete slabs-on-grade (The Concrete Society, 2007):

1. **Sprayed concrete:**
   Macro-synthetic fibre reinforced sprayed concrete has the potential, and is well suited, to ground support applications where large movements and gross deformations are acceptable, at least in the short term, such as mining or tunnelling. The movements and deformations may ignite cracking in the sprayed concrete, but due to the addition of macro-synthetic fibres, the material may have significant toughness or residual strength beyond the onset of cracking, to control and accommodate the movements.

2. **Composite floors with profiled metal sheeting:**
   Recently, synthetic fibre reinforced composite slab solutions have been developed which incorporates the use of a specific combination of steel sheeting and synthetic fibres. Fibres have been used to replace the typical welded fabric reinforcement, which is used in composite floors, for the purpose of crack control, load distribution and fire resistance. For successful incorporation of macro-synthetic fibres in composite construction, serviceability requirements is of critical importance.

3. **Cast in-situ concrete:**
   Examples where MSFRC are used in cast in-situ applications includes tunnel linings, railway applications, marine/coastal applications, walls, and water-retaining structures. In tunnel linings, macro-synthetic fibres have been incorporated to avoid the use of crack control fabric, leading to cost and time savings, as well as avoiding the risk of corrosion. For railway applications, macro-synthetic fibres have been chosen in preference to traditional reinforcement due to the concern that steel would affect the induction loop. In various marine/coastal applications, macro-synthetic fibres have been used to avoid the major task of fixing large areas of steel to irregular profiles, as well as enhancing the impact resistance of sea walls and avoiding the risk of corrosion. In water-retaining structures, macro-synthetic fibres have been used for crack-control.

4. **Precast concrete:**
   In various precast concrete applications, macro-synthetic fibres have been used to replace conventional reinforcement, either to carry the in-service loads, or to accommodate stresses induced during manufacture, handling, storage, transport, and installation. Some applications include paving flags, pipes and ancillary products, and other applications such as piles and precast staircases.

2.9 Concluding summary

Over three decades have passed since the initiation of the modern era of research and development of FRC. Although the use of FRC for structural applications is continuously increasing, it is still very limited with respect to its potential, due to the lack of international building codes for FRC structural elements.

Determining the factors influencing the performance of MSFRC was done by analysing literature as well as unpublished tests completed at Stellenbosch University (Odendaal, 2015) and CHRYSO. Several works have been published on the performance of MSFRC, suggesting that the constituent material's characteristics, including their respective volumes, influence the performance of FRC in its fresh and hardened state. Other factors including fibre geometry, fibre dosage, the mechanical and physical properties of the fibres, the fibre-matrix interfacial bond characteristics, as well as the mechanical properties of the matrix, significantly affects the performance of MSFRC. Numerous test methods are also available to quantify the performance of MSFRC, with the three-point bending test being the most popular due to its useful design parameter as well as being prescribed by the TR 34 manual.

While much still remains unknown about the mechanisms and behaviour of MSFRC and despite the absence of design provisions in building codes, macro-synthetic (structural) fibres are being used and implemented in a variety of structural applications worldwide, primarily as a replacement for steel fibres or traditional steel fabric in concrete slabs-on-grade. From a performance and economical point of view, an increasing demand for the use of MSFRC in the industry exists. It was also evident from the literature available regarding the topic at hand, extensive research is required to promote MSFRC into the competitive construction industry.

Chapter 3

Experimental Framework

This chapter provides information regarding the different research hypotheses, as well as the analysis procedures used to investigate the different research hypotheses. The characteristics of the materials considered and a detailed description of the mix design methodology implemented are also provided. Additionally, the experimental framework adopted to investigate the macro-mechanical and single-fibre performance of the CHRYSO macro-synthetic experimental (CMS) fibre is described in detail. Special attention is provided on the specimen preparation and the test methods implemented for the Three-Point Bending Test (TPBT) and Single-Fibre Pull-Out Test (SFPOT).

3.1 Research hypotheses

Generating different research hypotheses is part of the first objective of this study, as stated in Section 1.3. The data obtained during the investigation of the different hypotheses is used to accept or reject the influence of a number of factors and to create the proposed generic models predicting the post-cracking performance of MSFRC.

From previous research, a number of influencing factors are identified that influence the performance of MSFRC. From these identified factors, the following hypotheses are constructed:

1. Specifying the cement type and water/cement (W/C) ratio are more influential than specifying the compressive strength of MSFRC.
2. The use of smaller coarse aggregate sizes have a positive effect on the post-cracking performance of MSFRC.
3. Increasing the mortar volume, i.e. decreasing the volume of coarse aggregates, has a positive effect on the post-cracking performance of MSFRC.
4. Increasing the fibre dosage has a positive effect on the post-cracking performance of MSFRC.
5. The mixing process has an significant effect on the performance of MSFRC. Increasing the mixing time will ensure better fibre distribution and increase fibre damage, which will

improve the post-cracking performance of MSFRC.

3.2 Mix design methodology

Industrial concrete flooring incorporating macro-synthetic fibres is the largest applications of MSFRC, thus the mixes used during this study is designed to represent typical surface bed concrete mixes. To successfully design these mixes, the various mix design parameters for industrial concrete flooring had to be understood.

According to ACI Committee 302 (1997), the design strength (28 day characteristic strength) can vary between 21 to 55 MPa, depending on the class of floor. Typically in South Africa, the strength of surface beds vary between 25 to 50 MPa. A CEM I or CEM II cement type is typically prescribed with a maximum of 20% replaced with an extender, i.e. either fly ash or slag. Due to the availability issues regarding a CEM I in South Africa, a 52.5N CEM II cement was mostly considered throughout the study. A 42.5N CEM III cement was, however, also considered and tested to evaluate Hypothesis 1.

For industrial flooring applications, it is recommended that the coarse aggregate size must be maximised to decrease the required water content, reducing the amount of shrinkage strain. It is generally recommended that the water content should not exceed 180 l/m^3. Typically, the coarse aggregate size must be smaller than 25% of the floor thickness, with a maximum nominal size of 37.5 mm. Due to the poor grading of the large size aggregates, the coarse aggregates are typically blended with a smaller size aggregate, for example a 9.5mm or 13.2mm stone, to improve the grading as well as the workability of the mix. For the fine aggregate, a dune sand blended with a crusher dust (typically 40:60 ratio), is recommended. According to ACI Committee 544 (2008), it is recommended that the mix designs should be modified to include a maximum of 55% coarse aggregate content by total volume of aggregates (coarse and fine aggregates).

In South Africa, the typical target slump for concrete surface beds is 75 mm, with an acceptable range between 50 to 100 mm. However, the inclusion of macro-synthetic fibres in a concrete mix results in a reduction of slump. From previous research, it is suggested that for every 1.5 kg/m^3, the slump reduces with approximately 25 mm (Odendaal, 2015). Thus, by incorporating fibres, the concrete mix must be designed for a higher slump value.

Table 3.1 indicates the various mix design parameters that is considered throughout the course of this study.

Due to the vast amount of mix parameters considered throughout this study, the mix design process is complex. Conventional mix design processes, i.e. the C&CI method which is derived from ACI Standard 211.12-91, and the nominal 'eye-ball' mix design process are difficult to implement to ensure appropriate mixes incorporating all of the variables. Brenton Brouard, the Technical Manager of Concrete for CHRYSO South Africa, proposed a method which he refers to as the 'Incremental Method' (Bouard, 2015). The basic approach of the so-called Incremental

Table 3.1: Mix design parameters

Mix design parameters	**Lower limit**	**Min**	**Center**	**Max**	**Higher limit**
Cube target strength (MPa)	25	30	40	50	60
Fibre dosage (kg/m^3)	2.5	3	4	5	5.5
Slump (mm)	50		100		150
Nominal coarse aggregate size (mm)	19		26.5		37.5
Coarse aggregate volume (l/m^3)	350		400		450
Mixing time (min)	5	10	20	30	60
Admixture (Plasticiser)	Dosage adjusted to control workability				
W/C ratio	0.4				0.8
Water content (l/m^3)	170				
Cement type and class	42.5N CEM III & 52.5N CEM II				

Method is to initially design the concrete mix 'too wet.' The water content can then be reduced with increments of 5 to 10 l/m^3. Throughout the process the W/C ratio, as well as the coarse aggregate volume, stays constant and only the volume of fine aggregates is adjusted. The number of increments depend on the workability and consistency of the mix. Increments are added until a suitable slump is achieved.

Due to the high number of mix variations and alterations, the reference mix design is of critical importance. With trial and error, as well as the use of the Incremental Method, a reference mix was developed.

3.3 Hypotheses analysis procedure

The analysis procedure of this project included mix variations and alterations to investigate the research hypotheses stated in Section 3.1. Mix variations were applied to determine the effect of the cement type and class, compressive strength (varying W/C ratios), coarse aggregate size (mm), mortar volume (coarse aggregate volume (l/m^3)), fibre dosage (kg/m^3), as well as the mixing time (min) and the mixing procedure (mixer type). Unless otherwise stated, the following were cast from each mix:

- Six beams (150x150x700 mm each)
- Four cubes (100x100x100 mm) or three cubes (150x150x150 mm) for nominal coarse aggregate sizes $>$ 19.5 mm

Various mixes were designed to quantify the effect of the identified influencing factors. Unless otherwise stated, a W/C ratio of 0.55 was considered. A water reducing agent (lignosulphonate-based plasticiser) was added to the mixes to control workability. The following mix variations

were made:

1. The first hypothesis states that the specification of the cement type and the W/C ratio are more influential than specifying the compressive strength of the concrete. The following cement types and classes were considered:

   - 42.5N CEM III
   - 52.5N CEM II

   The following W/C ratios were considered for each cement type:

   - 0.4
   - 0.45
   - 0.5
   - 0.55
   - 0.6
   - 0.65
   - 0.7
   - 0.75
   - 0.8

   *Note: When varying the W/C ratio, the water content remained constant (170 l/m^3) and the cement content was adjusted accordingly. The coarse aggregate volume was also kept constant (400 l/m^3), thus adjusting the fine aggregate content accordingly. A constant fibre dosage of 4 kg/m^3 was considered.

2. The second hypothesis states that a smaller coarse aggregate size will ensure a better post-cracking performance of MSFRC. The following nominal coarse aggregate sizes were considered:

   - 19 mm
   - 26.5 mm
   - 37.5 mm

   *Note: Measuring the effect of the aggregate size, a constant W/C ratio of 0.55 and a fibre dosage of 4 kg/m^3 were considered. The coarse aggregate volume remained constant (400 l/m^3).

3. The third hypothesis states that increasing the mortar volume, i.e. decreasing the coarse aggregate volume, will have a positive effect on the post-cracking performance of MSFRC. To investigate the effect of varying the coarse aggregate volume on the performance of

MSFRC, tests were completed for each nominal coarse aggregate size (19 mm, 26.5 mm, and 37.5 mm) at the following volumes:

- 350 l/m^3
- 400 l/m^3
- 450 l/m^3

*Note: A constant W/C ratio of 0.55 and a fibre dosage of 4 kg/m^3 were considered.

4. The fourth hypothesis states that an increase in the fibre dosage will have an positive effect on the performance of MSFRC. The following fibre dosages were considered:

   - 2.5 kg/m^3
   - 3.0 kg/m^3
   - 3.5 kg/m^3
   - 4.0 kg/m^3
   - 4.5 kg/m^3
   - 5.0 kg/m^3
   - 5.5 kg/m^3

   *Note: Initially, a constant W/C ratio of 0.55 was considered. Various fibre dosages (3, 4, and 5 kg/m^3), at W/C ratios of 0.45 and 0.65, were also considered to investigate the effect on the post-cracking performance by increasing the compressive strength for the specific fibre dosages. A constant coarse aggregate size (19 mm) and coarse aggregate volume (400 l/m^3) were considered.

5. The fifth hypothesis states that increasing the mixing time of the initial mixing process would ensure better fibre distribution and increase fibre surface damage, thus increasing the performance of MSFRC. The following mixing times were investigated:

   - 5 min
   - 10 min
   - 20 min
   - 30 min
   - 60 min

   *Note: A constant W/C ratio of 0.55 and a fibre dosage of 4 kg/m^3 were considered. A constant coarse aggregate size (19 mm) and coarse aggregate volume (400 l/m^3) were considered. It should be noted, for the prolonged mixing times, the addition of a slump revival admixture (superplasticiser) was necessary to control the workability of the mixes.

All the tests were repeated using a 310 litre tilting-drum mixer to compare the results to the results obtained for the 120 litre pan mixer.

3.4 Material characteristics

To measure the performance of macro-synthetic fibre reinforced concrete (MSFRC), it is important that the material properties of the components of the composite, are fully known and understood. This section presents the material properties of the constituent materials.

3.4.1 Cement

Two cement types were considered, i.e. a 52.5 N CEM II/A-L (limestone extender content between 6 to 20%) and a 42.5 N CEM III/A (blastfurnace slag content between 35 to 65%) cement, both supplied by Pretoria Portland Cement (PPC), with a relative density of 3.14 and 3.05 respectively. Table 3.2 illustrates the typical composition of the two cement types.

Table 3.2: Average composition of 52.5N CEM II and 42.5N CEM III cement

	SiO^2	**Al^2O^3**	**Fe^2O^3**	**Mn^2O^3**	**TiO^2**	**CaO**	**MgO**	**SO^3**	**K^2O**	**Na^2O**	**NaK**
52.5 N CEM II (%)	18.7	4.3	2.9	0.1	0.2	63.4	1.0	2.2	0.7	0.2	0.7
42.5 N CEM III (%)	23.0	8.5	2.8	0.1	0.4	51.0	5.3	1.9	0.7	0.3	0.7

3.4.2 Fine aggregates

According to Technical Report 34 (The Concrete Society, 2003), fine aggregate grading should conform to Grades C (coarse), M (medium), or F (fine) according to Table 4 of BS 882:1992 for flooring applications, as illustrated in Table 3.3. Fine aggregate gradings at the coarse end of Grade C, or the fine end of Grade F, should be avoided.

According to Craig Mills, Regional Technical Manager of Lafarge South Africa, a dune sand blended with a crusher sand, typically 40%:60% ratio, is recommended for industrial flooring applications, rather than river sand due to a retardation effect as a result of the organic content of river sand (Mills, 2015). When crushed sand is used, either on its own or in combination with other sands, the proportion of the combined sand passing the 75 μm sieve by mass, should not exceed 9% according to BS 882:1992. For this project, the fine aggregate gradation limits according to ACI Committee 302 (1997) was considered, as it is prescribed specifically for concrete Class 7 floors, i.e. floors that are used for heavy-duty, industrial-type applications, subject to heavy traffic and impact. Table 3.4 illustrates the specifications for fine aggregate gradation according to ACI.

Table 3.3: Fine aggregate gradation limits according to BS 882:1992

	Percentage passing (%)		
Sieve size (mm)	**Grade C**	**Grade M**	**Grade F**
10	100	100	100
5	89-100	89-100	89-100
2.36	60-100	65-100	80-100
1.18	30-90	45-100	70-100
0.6	15-54	25-80	55-100
0.3	5-40	5-48	5-70
0.15	0-15	0-15	0-15

Table 3.4: Fine aggregate gradation according to ACI Committee 302 (1997)

Sieve size (mm)	**Percent passing (%)**
4.75	85-100
2.36	80-90
1.18	50-75
0.6	30-50
0.3	10-20
0.15	2-5

To determine the gradation of the fine aggregates, i.e. the dune sand as well as the crusher sand, a sieve analysis was performed according to SANS 201:2008. Figure 3.1 illustrates the gradation of the dune sand and crusher sand respectively.

A fineness modulus (FM) of 1.61 and 3.95 was calculated for the dune and crusher sand respectively. For the combined gradation, an initial 53%:47% ratio between dune and crusher sand, was considered. This ratio was determined by considering a FM of 2.7 for the fine aggregate. However, after preliminary tests, an optimal ratio of 60%:40% between dune and crusher sand was chosen due to an increase in the amount of fines passing the 150 and 75 μm sieves, improving the cohesion of the mix.

Figure 3.2 illustrates the grading of the combined fine aggregate, comparing it to the higher and lower limits according to ACI Committee 302 (1997). From the figure, it is evident that the combined fine aggregate grading is slightly below the lower limit of the 2.36 mm sieve, and slightly above the limits of the 0.6 and 0.3 mm sieves. Due to the fact that these margins are relatively small, it was assumed that the gradation of the combined fine aggregate was

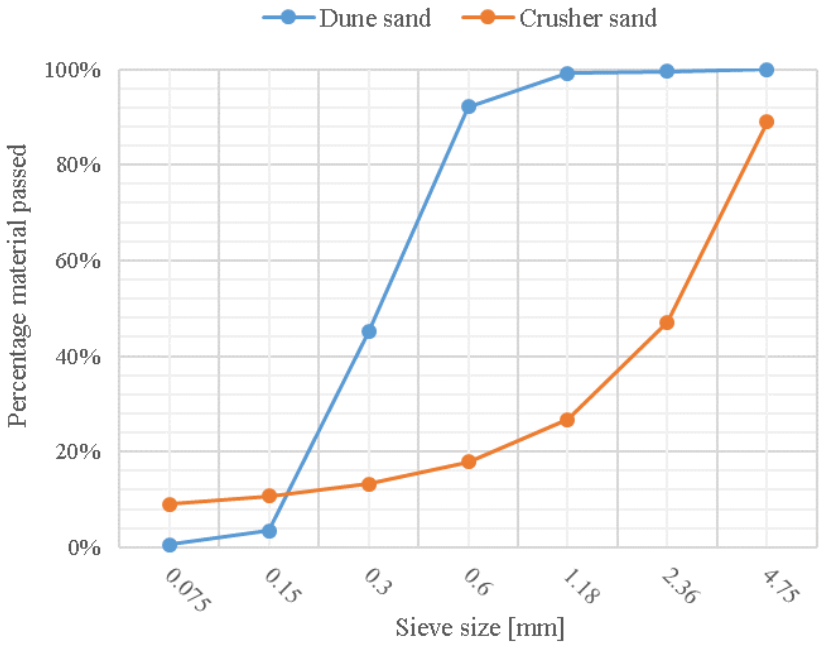

Figure 3.1: Dune and crusher sand sieve analysis

acceptable. The properties of the fine aggregates are summarised in Table 3.5. The particle relative densities (RD) were determined in accordance with SANS 5844:2014 (SABS Standards Division, 2014), and the bulk densities (LBD and CBD) were calculated according to SANS 5845:2006 (SABS Standards Division, 2006a).

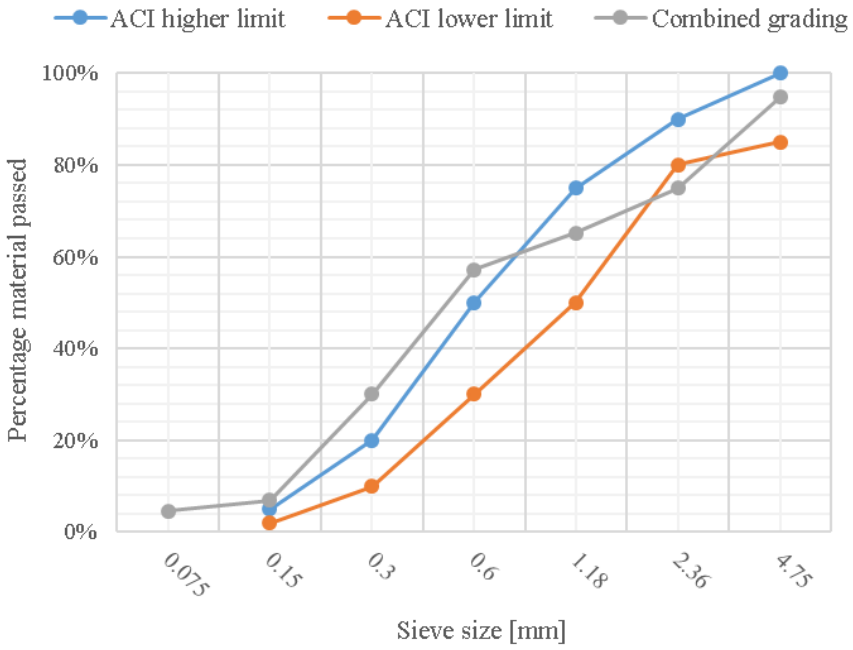

Figure 3.2: Grading of combined fine aggregate compared with limitations according to ACI Committee 302, 1997

Table 3.5: Summary of fine aggregate properties

Type	**FM**	**RD**	**LBD (kg/m^3)**	**CBD (kg/m^3)**
Dune sand	1.61	2.61	1487	1572
Crusher sand	3.95	2.72	1504	1610

3.4.3 Coarse aggregates

The coarse aggregates considered throughout the duration of this study is known as Greywacke stone (metamorphic rock type), also referred to as Malmesbury shale, and is characterised by its angular shape and grey colour.

To determine the gradation of the coarse aggregates considered in this study, i.e. nominal coarse aggregate sizes of 19 mm, 26.5 mm and 37.5 mm, sieve analyses were performed according to SANS 201:2008. Figure 3.3 illustrates the gradation of the 19 mm, 26.5 mm, and the 37.5 mm coarse aggregates respectively. The properties of the coarse aggregates are summarised in Table 3.6. As for the fine aggregates, the particle relative densities (RD) were determined according to SANS 5844:2014, and the bulk densities (LBD and CBD) were calculated according to SANS 5845:2006.

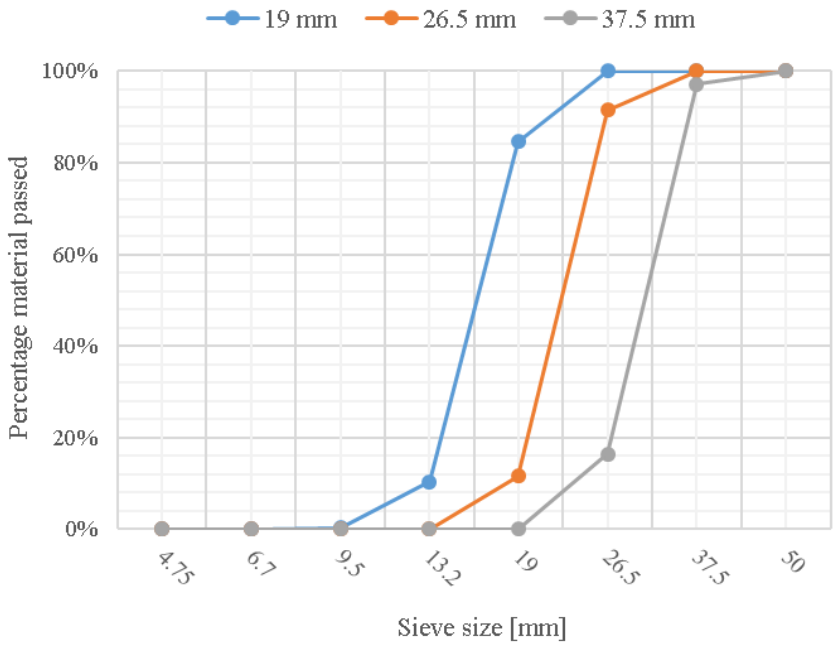

Figure 3.3: Coarse aggregates gradation

Table 3.6: Summary of coarse aggregate properties

Nominal size	**RD**	**LBD** (kg/m^3)	**CBD** (kg/m^3)
19 mm	2.72	1396	1492
26.5 mm	2.72	1379	1454
37.5 mm	2.73	1376	1482

3.4.4 Macro-synthetic fibre

The fibre considered throughout the course of this study was an experimental macro-synthetic fibre supplied by CHRYSO. The fibre is produced using a high tensile strength raw material, i.e. polypropylene. The fibres were supplied in a collated, fibrillated form, with a twisted profile and a rectangular cross-section. The intent of the twisted fibre profile is to enhance the mechanical interlock between the fibre and the matrix, as no bond between the fibre and the cement gel exists and bonding occurs by means of mechanical interaction.

Figure 3.4 illustrates the collated, fibrillated fibre, as well as the monofilament fibre with its twisted configuration. Table 3.7 provides the properties of the CMS fibre, as obtained from the supplier.

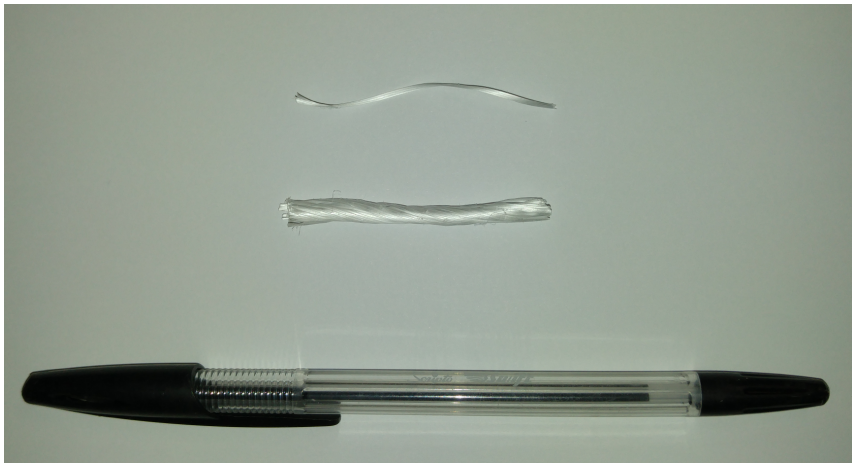

Figure 3.4: CHRYSO macro-synthetic experimental (CMS) fibre

Table 3.7: Properties of the CMS fibre

Colour	White
Specific gravity	0.92
Length (l)	50 mm
Diameter (d)	1.3 mm
Aspect ratio (l/d)	38.5
Tensile strength	600 MPa
Young modulus	5 GPa
Chemical resistance (alkali)	High
Melting point	160°C
Flash point	590°C

3.4.5 Admixtures

To provide suitable workability to all concrete mixes considered, the incorporation of an admixture, i.e. a water reducing agent, was necessary. The dosage of the admixture was adjusted to provide suitable workability and consistency as necessary. Workability and consistency were measured using a slump test in accordance to EN $12350-2$ (2009).

The plasticiser considered throughout this study was a new generation water reducing agent supplied by CHRYSO, with a trade name CHRYSO Plast Omega 134 (CPO134). The admixture conforms to European Conformity (CE) marking, as well as to NF 085 certification. The plasticiser is based on hybrid polymer technology and the synthesis of the molecules provide a wide dosage range, high water reduction power, slump retention, and homogeneous concrete. Table 3.8 provides the properties of the plasticiser as obtained from the supplier.

Due to the mixing process (specifically for prolonged mixing times exceeding 10 minutes), the concrete mixes experienced a loss of workability. For the mixes to retain a suitable slump and workability after the prolonged mixing times, i.e. 10, 20, 30, and 60 minutes respectively, a slump revival admixture was used.

The slump revival admixture considered in this study is a high range water reducing superplasticiser supplied by CHRYSO, with a trade name CHRYSO Fluid Rescue (CFR). CFR is manufactured in accordance to EN $934-2$, EN $934-3$, and ASTM C494, and is a new generation polymer based on modified phosphonates. The use of CFR results in plastic conditions being maintained for an extended time period. Table 3.9 provides the properties of CFR as obtained from the supplier.

Table 3.8: Properties of the CHRYSO Plast Omega 134 plasticiser

Physical state	Liquid
Colour	Brown
Specific gravity	1.11
pH	6.0 ± 2.0
Cl^- ions content	$< 0.10\%$
Na_2O equivalent	$< 2\%$
Dry extract (halogen)	30.5% ±1.1%
Dry extract (EN 480-8)	30.7% ±1.1%

Table 3.9: Properties of the CHRYSO Fluid Rescue superplasticiser

Physical state	Liquid
Colour	Milky cream
Specific gravity	1.03
pH	7.0 ± 2.0
Cl^- ion content	<0.1%
Na_20 equivalent	<1.0%

3.5 Macro-mechanical performance evaluation

This section provides information regarding the concrete mix proportions, as well as the specimen preparation, considered for the macro-mechanical investigations. A detailed explanation of the considered test setup, i.e. the three-point bending test (TPBT), implemented to investigate and provide the performance parameters, is provided. A detailed explanation of other macro-mechanical performance evaluation methods, including the shrinkage measurement test as well as Computed Tomography (CT) scans, are also provided.

3.5.1 Concrete mix proportions

To quantify the influence of all the variables to predict the performance of MSFRC for industrial flooring applications, it was important that the mix designs portrayed suitable concrete mixtures. It was important that all the mix designs fell within the specifications for typical concrete surface bed mixtures.

Important aspects of these mix designs were to maximise the coarse aggregate size and volume,

as well as minimising paste volume to decrease the amount of shrinkage that would commence. However, with the incorporation of macro-synthetic fibres, paste volume plays an important role due to the increased surface area that must be covered.

Typically, water content for industrial floors do not exceed 180 l/m^3. According to Craig Mills, Regional Technical Manager of Lafarge South Africa, coarse aggregate content varies between 950 to 1200 kg/m^3, based on coarse aggregates with a relative density (RD) of 2.7 (Mills, 2015). Calculating the required coarse aggregate content according to the method prescribed by the Cement and Concrete Institute (C&CI), the following equation is implemented:

$$M_a = CBD \cdot (K - 0.1 \cdot FM) \tag{3.1}$$

where:
M_a = mass of stone in 1 m^3 of concrete (kg)
CBD = Compacted bulk density of coarse aggregate (kg/m^3)
K = Workability factor
FM = Fineness modulus of fine aggregate

Table 3.10 indicates the required coarse aggregate content for the various nominal coarse aggregate sizes according to Equation 3.1. The workability factor depends on the required slump range, as well as the nominal coarse aggregate size. According to Perrie (2009), the K factor for the considered coarse aggregate sizes are 0.94, 1.00, and 1.05 respectively, considering an approximate slump range between 75-150 mm.

Table 3.10: Coarse aggregate content according to C&CI

Nominal size	**CBD (kg/m^3)**	**K**	**FM**	**M$_a$ (kg/m^3)**
19 mm	1492	0.94	2.70	999
26.5 mm	1454	1.00	2.70	1062
37.5 mm	1482	1.05	2.70	1156

The required coarse aggregate volume for each nominal coarse aggregate size according to C&CI are within the suggested range. Therefore, considering a coarse aggregate content varying between 950 to 1200 kg/m^3, which equates to approximately 350-450 l/m^3, a reference mix design is determined considering a coarse aggregate volume of 400 l/m^3. For the reference mix design, a W/C ratio of 0.55 is chosen. As determined from the gradation of the fine aggregate, a 60%:40% ratio between dune and crusher sand is chosen. The reference mix design is indicated in Table 3.11.

Table 3.11: Reference mix design

Constituent	**Mass (kg/m^3)**	**RD**	**Volume (l/m^3)**
Water	170	1	170
Cement (52.5N CEM II)	309.09	3.14	98.44
Coarse aggregate (19 mm, 26.5 mm, 37.5 mm)	1088	2.72	400
Fine aggregate: Dune sand (60%)	519.23	2.61	198.94
Fine aggregate: Crusher sand (40%)	360.74	2.72	132.63
Total	**2447.06**		**1000**

Table 3.12 summarises the adjustments made for each material constituent according to each research hypotheses. The adjustments corresponds to the hypotheses analysis procedure mentioned in Section 3.3.

Table 3.12: Summary of material constituents adjustments for the analyses of each research hypothesis

	Water content (l/m^3)	**W/C ratio**	**Coarse aggregate size (mm)**	**Coarse aggregate volume (l/m^3)**	**Fine aggregate volume (l/m^3)**	**Fibre dosage (kg/m^3)**	**Mixing time (min)**
Hypothesis 1	constant (170)	adjusted (0.4-0.8)	constant (19)	constant (400)	adjusted accordingly	constant (4)	constant (2)
Hypothesis 2	constant (170)	constant (0.55)	adjusted (19, 26.5, 37.5)	constant (400)	constant (327.22)	constant (4)	constant (2)
Hypothesis 3	constant (170)	constant (0.55)	adjusted (19, 26.5, 37.5)	adjusted (350-450)	adjusted accordingly	constant (4)	constant (2)
Hypothesis 4	constant (170)	constant (0.55)	constant (19)	constant (400)	adjusted accordingly	adjusted (2.5-5.5)	constant (2)
Hypothesis 5	constant (170)	constant (0.55)	constant (19)	constant (400)	constant (327.22)	constant (4)	adjusted (5-60)

3.5.2 Specimen preparation and curing

Using the reference mix design indicated in Table 3.11 and the adjustments made according to Table 3.12, beam specimens measuring 150x150x700 mm were prepared. According to the TR34 (2013), twelve beam specimens are required for each batch to establish the design parameters. However, for the purpose of this study and the limited time frame, it was decided to cast six specimens per batch. Steel moulds with the aforementioned dimensions, as shown in Figure 3.5a, were used for the preparation of the beams. Prior to mixing, the moulds were oiled with mould release oil. The moulds were filled in the sequence documented by EN 14651 (2007) as

(a)

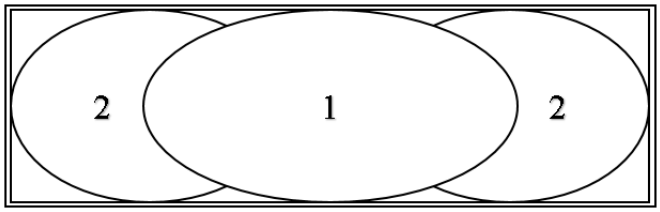

(b)

Figure 3.5: (a) 150x150x700 mm Steel mould and (b) Sequence of filling the mould

illustrated in Figure 3.5b. After the moulds were filled to approximately 90% of the height, a poker vibrator was used to ensure adequate compaction. The mould was topped-up by adding fresh MSFRC while being compacted. Subsequently, the casting face was trowelled using a hand-trowel.

A 120 litre concrete pan mixer (Figure 3.6a) was used for the preparation of a 110 litre mix for each batch of MSFRC. It should be noted that a 310 litre tilting-drum mixer (Figure 3.6b) was considered to compare with the results obtained considering the pan mixer as stated in Section 3.3.

(a) Pan mixer

(b) Tilting-drum mixer

Figure 3.6: Mixer types used during study

Both concrete mixers were rinsed with water and dried with industrial tissue paper prior to mixing to remove any additional water and to ensure the same conditions for each mix. The materials were batched by weight and were added in the order of sand, cement, stone. These constituent materials were dry-mixed for 30 seconds before the addition of the mixing water. After the introduction of the mixing water, the materials were allowed to mix for a further 30 seconds before the addition of the water-reducing agent (plasticiser). An additional 2 minutes

were allowed for the materials to mix after the addition of the plasticiser to ensure a homogenous concrete mixture. The introduction of the fibres commenced subsequently and were carefully sprinkled into the mixer over a period of approximately 30 seconds to prevent fibre-ball formation. The MSFRC mixture was allowed to mix for an additional 2 minutes after the last fibres were added to ensure thorough distribution of the fibres within the mixture.

Mix control was conducted by measuring the workability of the MSFRC in its fresh state for each mix and performing compressive strength tests on cubes at 28 days after casting. The workability tests consisted of slump tests in accordance to EN 12350−2 (2009) and the compressive strength tests were conducted on four control cubes measuring 100x100x100 mm for each batch according to EN 12390−3 (2009) and EN 12390−4 (2009). For nominal coarse aggregate sizes larger than 19 mm, compressive strength tests were conducted on three control cubes measuring 150x150x150 mm.

All specimens were de-moulded ±24 hours after being casted and directly placed in temperature controlled curing tanks with a temperature of 25°C. Figure 3.7 illustrates the upright position of the beams for the duration of the curing process. All specimens were cured for 27 days before removal from the curing tanks for testing. The beam specimens were removed, not less than 3 days before testing, rotated over 90° around their longitudinal axis to a non-casting face, and wet-notched using a 3.5 mm thick diamond-tipped concrete blade through the width of each specimen at mid-span. The depth of the notch was 25 ± 1 mm. The beam specimens were re-immersed into the curing tanks after being notched until the date of testing.

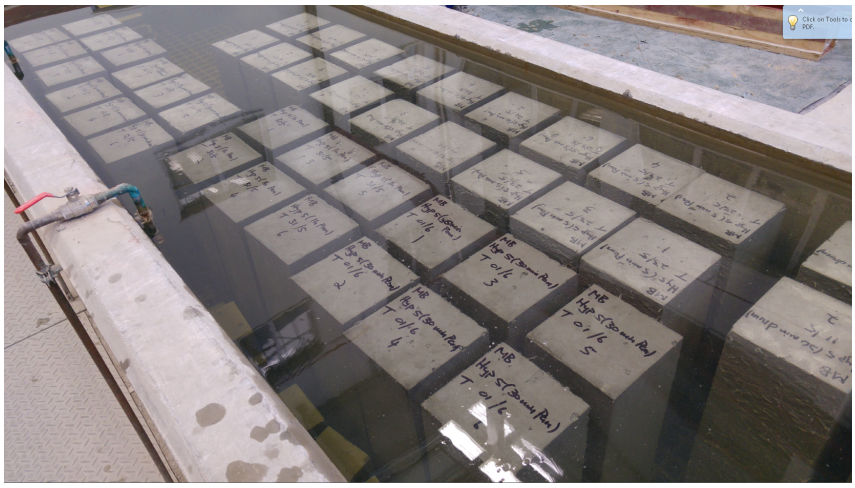

Figure 3.7: Position of beam specimens for the duration of the curing process

Prior to testing (±2 hours), beam specimens were removed from the curing tanks and prepared by positioning two knife-edges (as described in EN 14651 (2007), 10 mm apart, along the notch at mid-width of each test specimen using a high-strength exopy glue. The function of the knife-edges was to mount the displacement transducer measuring the CMOD. Figure 3.8 illustrates the position of the knife-edges on each test specimen.

Figure 3.8: Position of knife-edges on beam specimens

3.5.3 Three-Point Bending Test setup

Due to the complex behaviour of FRC, the setup for most test methods measuring the macro-mechanical properties are sophisticated, time consuming, and expensive. Although there are several tests used to quantify the behaviour of FRC, the two most practical methods for measuring the macro-mechanical performance of MSFRC are the Three-Point Bending Test (TPBT), due to its familiarity in the field, and the Round Determinate Panel Test (RDPT), due to its apparent low scatter of results. During this project, TPBTs were performed according to EN 14651, as prescribed by TR34. This method provides for the determination of the limit of proportionality (LOP) and the residual flexural tensile strengths at specific crack mouth opening displacements (CMOD).

TPBTs were conducted using an Instron 2000KPX universal material testing machine. The machine have a capacity of 2 MN. A load cell with a capacity of 250 kN, instead of 2 MN, was used to ensure sufficient accuracy. Transferring the load applied by the actuator to the test sample, two supporting rollers and one loading roller, located at mid-span, was used. The span length between the two supporting rollers was 500 mm. A crack opening displacement gauge extensometer with a 10 mm gauge length, and a 4 mm travel, was attached to measure the crack mouth opening displacement (CMOD). The clip gauge was mounted at mid-width and along the longitudinal axis of each specimen, to ensure that the distance between the bottom of the specimen and the line of measurement was close to 5 mm. Figure 3.9 illustrates the arrangement of the displacement transducer, clipped between two knife-edges.

A closed loop control was used by controlling the CMOD rate. Up until a CMOD of 0.1 mm, the machine was operated at a CMOD rate of 0.05 mm/min, where after it increased to a constant rate of 0.2 mm/min. The test procedure was terminated at a CMOD of 4.2 mm. Due to the nature of the adopted test setup, the response was received in the form of a load-CMOD curve. From the response, the LOP as well as the residual flexural tensile strengths at a CMOD of 0.5 mm, 1.5 mm, 2.5 mm, and 3.5 mm were determined. The adopted TPBT is illustrated in Figure 3.10.

Figure 3.9: Arrangement of displacement transducer for measuring CMOD

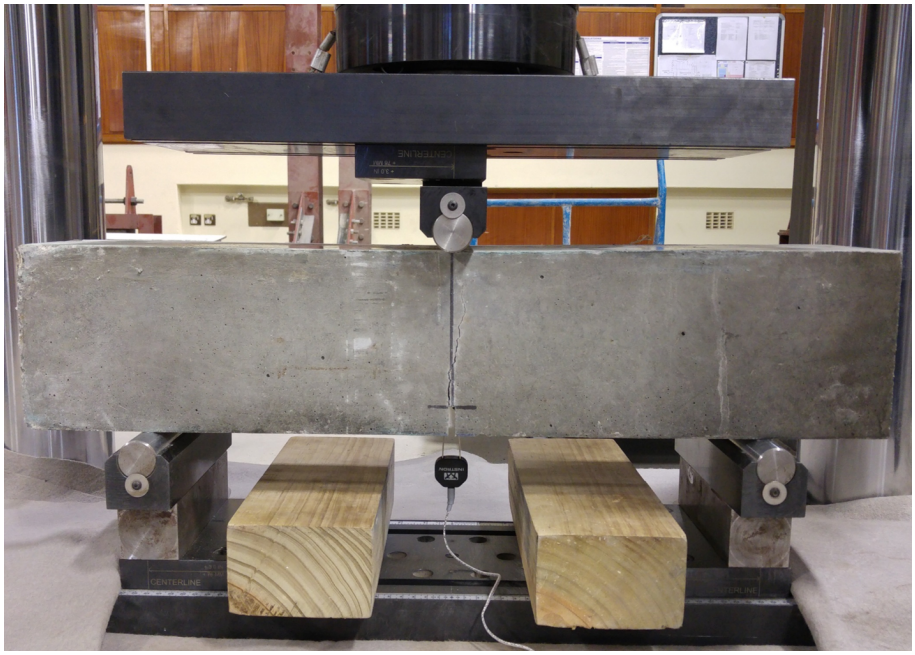

Figure 3.10: Adopted Three-Point Bending Test setup

3.5.4 Shrinkage test

As time-dependent behaviour of concrete is an important factor when referring to concrete flooring, shrinkage deformation of MSFRC is studied, partly in accordance to BS ISO 1920 – 8 (British Standards Institution, 2009). Shrinkage measurements were conducted on a number of

samples over a period of 91 days, incorporating a range of fibre dosages.

Three fibre dosages were considered in this study, namely 2.5 kg/m^3, 4.0 kg/m^3, and 5.5 kg/m^3 respectively. The results were compared to the shrinkage deformation measured for a reference concrete without fibre addition, as well as the shrinkage deformation predicted according to EN 1992-1-1 (2004). The concrete mix proportions considered for the mixes incorporating different fibres dosages, as well as the reference mix, are stated in Section 3.5.1.

Eight beam specimens, i.e. two specimens for each fibre dosage and two specimens for the reference mix, measuring 100x100x500 mm, were prepared for conducting the shrinkage measurements. Steel moulds with the aforementioned dimensions were used for the preparation of the beams. All specimens were de-moulded ±24 hours after being cast and directly placed in a temperature controlled room with a temperature of 24 ± 0.5°C and a relative humidity of 65 ± 1%. To ensure that no restraint exists which may influence the shrinkage measurements, all the specimens were placed in an upright position throughout the testing period as illustrated in Figure 3.11.

Figure 3.11: Position of shrinkage measurement samples during testing period

Before the specimens were placed in the curing room, three pairs of shrinkage targets, 100 mm apart, were positioned on each face of the specimens, excluding the casting face, with the use of a positioning apparatus. The use of the positioning apparatus ensured that the initial position of all the targets were identical. A digital dial gauge was used to measure the relative displacements between the targets. The first reading was taken ±24 hours after the targets were affixed. To obtain the zero setting of the digital dial gauge, the positioning apparatus was used as a reference bar. Figure 3.12 illustrates the considered positioning apparatus, as well as the

digital dial gauge used to obtain the shrinkage measurements.

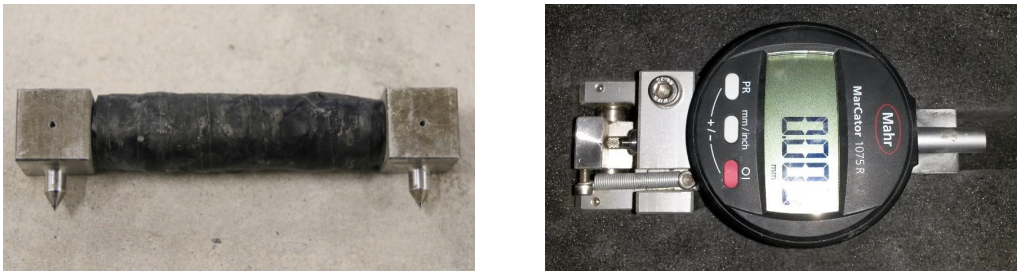

(a) (b)

Figure 3.12: (a) Shrinkage targets positioning apparatus and (b) Digital dial gauge

Subsequent shrinkage measurement readings were taken at 48 and 72 hours after the targets were positioned on the specimens. Thereafter readings were taken at 5, 7, 9, 12, 16, 21, 27, 35, 49, 56, 62, 71, and 91 days after the specimens were prepared. Three shrinkage readings (one reading per side) were taken per specimen and the average reading was used to represent the shrinkage measurement for each specimen. Furthermore, these values were used to calculate the average shrinkage representing a particular group for a specific fibre dosage and the reference mix.

3.5.5 Computed Tomography (CT) scans

An industrial Computed Tomography (CT) scanner was used to provide scans that allows for 2D and 3D analysis of the inside of any object in a non-destructive manner. The principle of measurement is similar to medical Computed Axial Tomography (CAT) scanners. A sample is exposed to an accumulation of x-rays and, using a sensor on the other side, the absorbed radiation is measured. A full 3D image is possible by repeating the procedure from various angles around the object. Small density differences and atomic number of the scanned sample is the primary functions of this technique. The measurement principle is illustrated in Figure 3.13.

The CT scans can be used to investigate and identify the porosity of materials, as well as cracks, transitions or inclusions in materials. The scans can also be used to study density variations within the material and compile a 3D Computer-Aided Drawing (CAD) surface or volume data set of the scanned sample.

For the purpose of this study, CT scans are used to investigate the effect of coarse aggregate size on fibre distribution and fibre volume fraction within the scanned samples. As the CT scanner is dependent on density differences and due to the low relative density of the CMS fibre (0.92), the size of the scanned objects was restricted to 50x50x50 mm cubes to ensure sufficient amount and intensity of x-rays to penetrate the samples.

Three samples for each considered nominal coarse aggregate size, i.e. 19 mm, 26.5 mm, and 37.5 mm, with a fibre dosage of 4 kg/m^3, were scanned and analysed. One beam specimen with

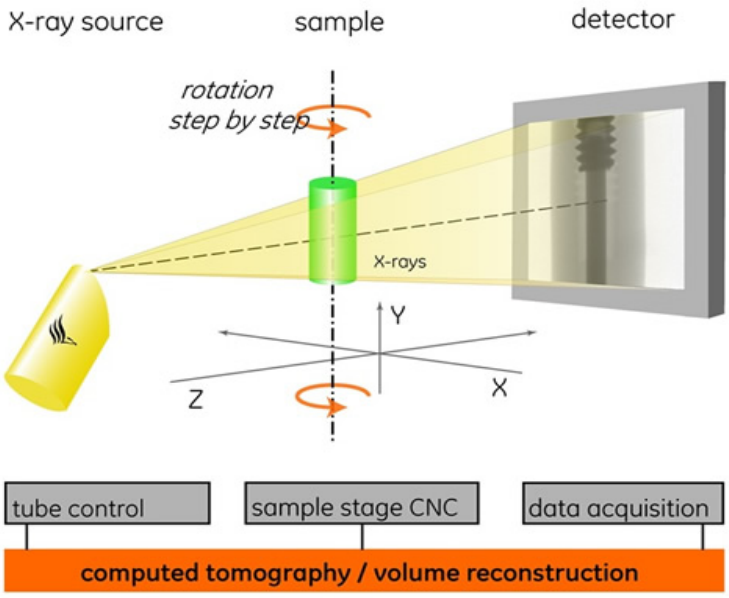

Figure 3.13: CT scanner measurement principle (Central Analytical Facility, 2012)

measurements 150x150x350 mm was prepared for each nominal coarse aggregate size. The mix proportions considered were as stated in Section 3.3 for testing the influence of coarse aggregate size on the performance of MSFRC. Three 50x50x50 mm cubes were cut from the centre of each beam to exclude the effect of the boundaries and corners of the mould on the distribution and orientation of the fibres. A concrete sawing machine with a 3.5 mm thick diamond-tipped blade was used.

A General Electric Phoenix V|Tome|X L240/NF180 tube was used for conducting the scans. The x-ray settings were 160 kV and 250 microA, and 3200 images were taken in a full rotation at a acquisition time of 500 ms per image and a voxel size of 50 μm. Detector shift was activated to minimise ring artefacts and scan time was around 50 minutes per scan. The analysis of the scans were completed using Volume Graphics VGStudio Max 3.0 software package.

3.6 Single-fibre performance evaluation

Single-fibre pull-out tests (SFPOT) have been considered to model the failure of a composite material since the 1950s (DiFrancia et al., 1996). This test can be performed to determine the maximum pull-out force, average bond stress, and critical length of the fibre type being investigated.

Investigation of the performance of the CMS fibre on single-fibre level is of interest to determine whether concrete compressive strength has an influence on the single-fibre performance. A distinction was also made between the performance of the fibre in its virgin and premixed fibre state to investigate the effect of the mixing process which causes roughening of the fibre surface. Single-fibre pull-out tests (SFPOT) were performed to provide information regarding the interfacial bond resisting fibre-pullout for the CMS fibre at various W/C ratios.

(a) (b)

Figure 3.14: (a) Samples for CT scans and (b) Position of sample being scanned

This section provides information regarding the concrete mix proportions used for the single-fibre investigation, as well as the specimen preparation. A detailed explanation of the SFPOT setup is also provided.

3.6.1 Concrete mix proportions

The concrete constituents considered for the investigation of the CMS fibre on single-fibre level, are described and provided in Section 3.4. To investigate the effect of concrete compressive strength on the fibre-pullout resistance, three W/C ratios were considered, i.e. 0.45, 0.55, and 0.65.

The reference concrete mix design, stated in Table 3.11, was also considered for the single-fibre performance investigations. Adjustments to the reference mix design were made to incorporate the three different W/C ratios. The water content and the coarse aggregate content was kept constant and the cement content, as well as the fine aggregate content, was adjusted accordingly.

A 52.5N CEM II/A-L cement type, as described in Section 3.4.1, was considered for the single-fibre performance investigation. Greywacke coarse aggregate, with a nominal size of 19 mm, was used throughout the single-fibre performance investigation. A plasticiser, i.e. the CPO134, as described in Section 3.4.5, was added to provide suitable workability. Table 3.13 indicates the considered mix designs for the various W/C ratios.

Table 3.13: Mix designs for the investigation on single-fibre level

	Mass (kg/m^3)		
Constituent	**W/C = 0.45**	**W/C = 0.55**	**W/C = 0.65**
Water	170	170	170
Cement (52.5N CEM II)	378	309	262
Coarse aggregate (19 mm)	1088	1088	1088
Fine aggregate: Dune sand (60%)	478	519	543
Fine aggregate: Crusher sand (40%)	332	361	377

3.6.2 Specimen preparation and curing

To investigate the effect of concrete compressive strength and the mixing process on the single-fibre performance, single CMS fibres were embedded in its virgin and premixed fibre state. The virgin state refers to the appearance of the fibre as received from the supplier and the premixed state refers to the appearance of the fibre as a result of the mixing process considering a pan mixer and a normal mixing time, i.e. a mixing time of two minutes after the addition of the final fibre. Figure 3.15 illustrates the visual difference between the CMS fibre in its virgin and premixed fibre state.

(a) (b)

Figure 3.15: (a) Virgin fibre state and (b) Premixed fibre state

The same methodology for preparing specimens to undergo single-fibre performance evaluation, as documented by Lerch (2016), was considered. Typical concrete cube moulds, with dimensions measuring 100x100x100 mm, were divided into four equal compartments using a wooden separator preparing specimens with dimensions measuring 39x39x100 mm. Using mould release

oil, the moulds, along with the wooden separator, were oiled prior to mixing.

To prepare the specimens undergoing single-fibre performance evaluation, a 10 litre concrete mix was prepared for each W/C ratio. The same mixing procedure was adopted for the single-fibre investigation as mentioned in Section 3.5.2. All the premixed fibres used for the single-fibre performance evaluations were premixed at a W/C of 0.55 and were rinsed with water directly after mixing concluded to retain only the roughened fibres.

The embedment length of all the fibres were taken as half the fibre length, i.e. 25 mm. This length was chosen as it represents the maximum length of the fibre which could be embedded on either side of a potential crack. The fibres were embedded to the pre-marked embedment lengths by hand with great care and as straight as possible. Due to the low flexural stiffness of the CMS fibre, and to simplify the insertion process of the fibres into the specimens, the prepared concrete mixes were sieved through a 2.36 mm sieve to eliminate the coarse aggregate content which causes the non-stiff fibres to bend within the concrete matrix. Removing the coarse aggregates also ensured that the fibres were in continuous contact with the surrounding concrete paste, eliminating possible weak spots which could cause additional variability in the test results.

Four specimens containing virgin fibres and four specimens containing premixed fibres were prepared for each W/C ratio. A schematisation of the single-fibre specimen preparation adopted from Lerch (2016), is provided in Figure 3.16. Four control cubes, with dimensions measuring 50x50x50 mm, were additionally prepared for each considered W/C ratio, according to EN 12390-3 (2009) and EN 12390-4 (2009), to measure the compressive strength for each batch using a Contest material testing machine with a capacity of 2000 kN. The single-fibre specimens, together with the control cubes, were demoulded ±24 hours after being cast and directly placed in a temperature controlled curing tank with a water temperature of 25°C. All the specimens were left to cure for an additional 27 days before testing.

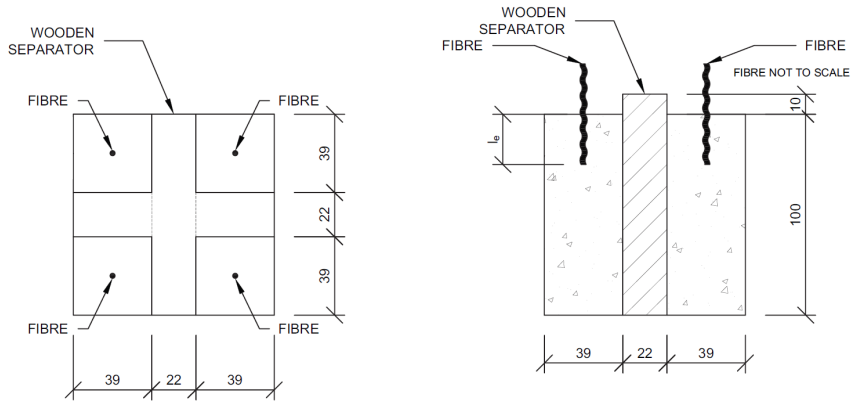

Figure 3.16: Single-fibre specimen preparation methodology adopted by Lerch (2016)

3.6.3 Single fibre pull-out test setup

The single-fibre pull-out test (SFPOT) setup considered in this study was adopted from the work documented by Lerch (2016). Prior to testing, the SFPOT specimens were removed from the curing tanks and left to climatise for ±1 hour before commencing with the tests.

SFPOTs were conducted using a Zwick Z250 universal testing machine with a capacity of 250 kN. Two hydraulic clamps were used to ensure that the SFPOT specimens, as well as the system gripping the single-fibre, were firmly kept in position. A fibre-clamp consisting of two 40x8 mm flat mild steel plates and tightened using two 6 mm bolts, were attached to the fibre-gripping system. The steel plates were used to grip the fibre portion extending above the hardened cement paste as close as possible to the surface of the cement paste to ensure consistency, as illustrated in Figure 3.17. A load-cell with a capacity of 500 kg was used to measure the pull-out force. Two linear variable displacement transducers (LVDTs), each having a range of 50 mm, were used to measure the pull-out displacement on either side of the fibre. The average of the two LVDT readings represented the true pull-out displacement of the fibre.

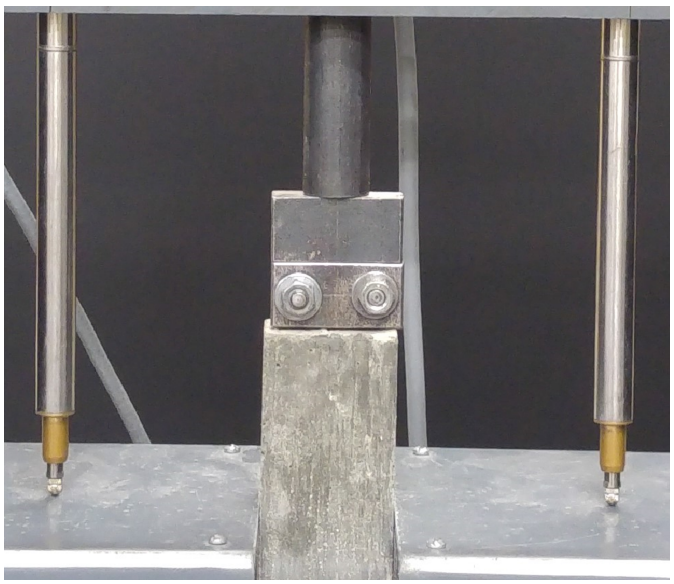

Figure 3.17: SFPOT fibre-clamp setup

The SFPOTs were controlled using a crosshead displacement rate of 0.2 mm/s. Placing the SFPOT specimens into the testing grips, the single-fibre is subjected to a small compressive force due to the nature of the test setup. This force causes the fibre to bend imperceptibly, causing inaccurate and inconsistent results. A small pre-load of 5 N was applied to the test method to eliminate these small compressive forces. Figure 3.18 illustrates the SFPOT setup, as adopted from Lerch (2016).

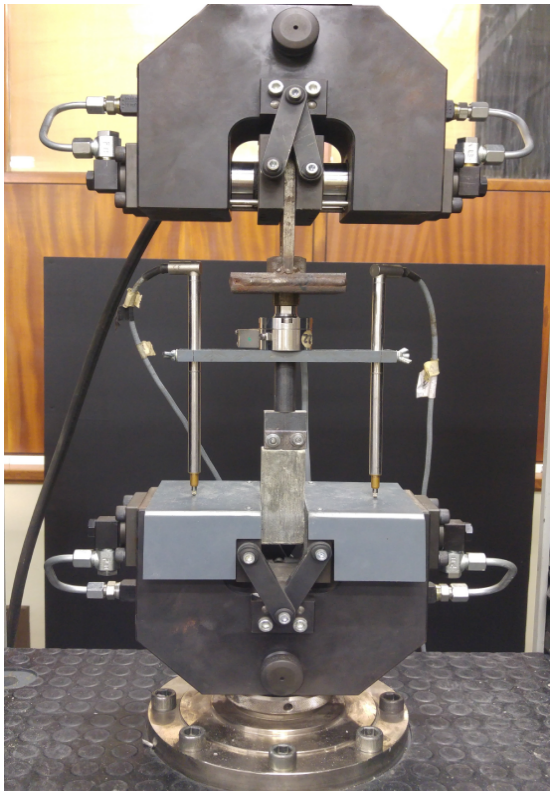

Figure 3.18: Single-fibre pull-out test (SFPOT) setup adopted from Lerch (2016)

3.6.4 Scanning electron microscopy (SEM) imaging

A scanning electron microscope produces high-resolution images by scanning a sample with a focused beam of electrons. Information regarding the sample's surface topography and the composition can be acquired through the electrons which interacts with the atoms in the sample.

Scanning electron microscopy (SEM) images of the CMS fibre were taken to illustrate the effect of mixing time on fibre damage. Individual SEM images of the fibre in its virgin and premixed state for the various mixing times (considering the laboratory pan mixer), stated in Section 3.3, were compiled and compared with one another. Imaging of the samples were accomplished using a Zeiss MERLIN Field Emission Scanning Electron Microscope and Zeiss SmartSEM software.

Before commencing with the SEM imaging, the different samples were mounted on a stub with double sided carbon tape and coated with a thin ($\pm$10 nm thick) layer of gold, using an Edwards S150A Gold Sputter Coater, making the sample surface electrically conductive. Secondary electron (SE Type 1) images were captured using a Zeiss SE1 (inLens) detector and represent the surface structure of the samples. Beam conditions during surface analysis were 5 kV and approximately 250 pA, and the working distance from the microscope pole piece was less than 4 mm during the acquisition.

3.7 Concluding summary

This chapter presents the research hypotheses investigated during the course of the project. A detailed description of the material characteristics and the experimental framework adopted for the investigation of the macro-mechanical, as well as the single-fibre performance of the CMS fibre, is provided.

The concrete mix proportions, specimen preparation and adopted test methods measuring the macro-mechanical and the single-fibre performance are described in detail. The macro-mechanical performance evaluation consisted of three-point bending tests according to EN 14651, as well as shrinkage measurement comparisons and computed tomography (CT) scans providing additional information.

SFPOTs were used to investigate the influence of compressive strength on the single-fibre performance of the CMS fibre in its virgin and premixed fibre state. Scanning electron microscopy (SEM) imaging was used for the visual assessment of the CMS fibre considering various mixing times. The procedure of analysis, adopted to interpret the SEM images, is also provided.

Chapter 4

Macro-Mechanical Results

This chapter reports on the macro-mechanical performance of concrete reinforced with the CHRYSO macro-synthetic experimental (CMS) fibre. The results obtained from investigating the research hypotheses are used to draw conclusions from and create generic linear models predicting the performance of macro-synthetic fibre reinforced concrete (MSFRC).

The three-point bending test (TPBT) is adopted as the primary macro-mechanical performance indicator in this study. The effect of compressive strength, nominal coarse aggregate size, coarse aggregate volume, fibre dosage, and prolonged mixing times (considering two mixer types) on the performance parameters, i.e. the limit of proportionality (LOP) and the residual flexural tensile strengths (f_{R1}, f_{R2}, f_{R3}, and f_{R4}), are investigated and reported here. Shrinkage tests were performed to investigate the influence of an increase in fibre dosage on the drying shrinkage of MSFRC. Computed tomography (CT) scans were performed to provide information regarding the effect of coarse aggregate size on fibre distribution and to determine the fibre volume fraction within the scanned samples to compare with the theoretical fibre dosage.

To create the linear generic models predicting the performance parameters of MSFRC, simple- and multiple linear regression analyses are performed to statistically investigate the effect of each independent variable and exclude the variables not having a significant influence on the performance parameters. It is important to note that the conclusions drawn in this chapter is based on the output of the TPBTs and the results of the statistical analyses are used for creating the generic models predicting the performance parameters as presented in Chapter 6.

4.1 Compressive strength test results

Compressive strength tests were completed at 28 days for each MSFRC batch as a measure of quality control. This section illustrates the results obtained from the various compressive strength tests according to each research hypothesis, as well as a discussion on the influence of each independent variable. The compressive strength results for each sample are provided in Appendix A.1. It should be noted that the error bars indicated for each data point illustrates the standard deviation for each set of tests.

Figure 4.1 illustrates the effect of W/C ratio on the compressive strength of MSFRC for the

two cement types used in this study. As expected, an increase in W/C ratio caused a decrease in compressive strength for both cement types. It is evident that the 52.5N CEM II cement exhibited a higher average compressive strength for most of the W/C ratios compared to the 42.5N CEM III cement. However, the gradient of the trend line associated with the 42.5N CEM III cement, is less acute compared to the 52.5N CEM II cement, indicating a more gradual loss in compressive strength for an increase in W/C ratio. According to Vijaya Gowri et al. (2016), a high volume slag concrete exhibits a more gradual loss in compressive strength for an increase in W/C ratio, compared to an ordinary concrete. For a W/C ratio ≥ 0.70, the average compressive strength for the 42.5N CEM III cement is slightly higher or very similar to the 52.5N CEM II cement. This repercussion can be explained due to the blastfurnace slag content (between $35 - 65\%$) of the 42.5N CEM III cement.

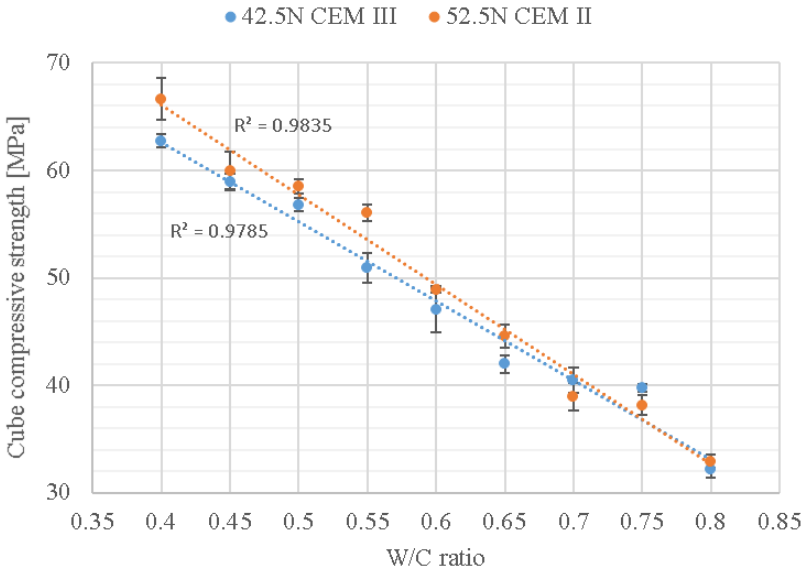

Figure 4.1: Cube compressive strength test results - Hypothesis 1

Figure 4.2 illustrates the effect of coarse aggregate size on the compressive strength of MSFRC for a coarse aggregate volume of 400 l/m^3. It can be concluded that an increase in nominal coarse aggregate size indicates a decrease in the average compressive strength. This result can explained due to the packing density of the concrete matrix. Figure 4.3 illustrates the cube density measured for each nominal coarse aggregate size. It is evident that a decrease in cube density occurred for an increase in nominal coarse aggregate size. A smaller nominal coarse aggregate size typically improves the packing density of the matrix, ultimately increasing the compressive strength of the concrete.

It should be noted that the larger coarse aggregate sizes, i.e. the 26.5 mm and 37.5 mm nominal coarse aggregate sizes, experienced a more substantial standard deviation. The larger standard deviation is a result of the larger coarse aggregate size, negatively affecting the homogeneity of the concrete samples.

Figure 4.4 illustrates the effect of coarse aggregate volume on the compressive strength of MS-

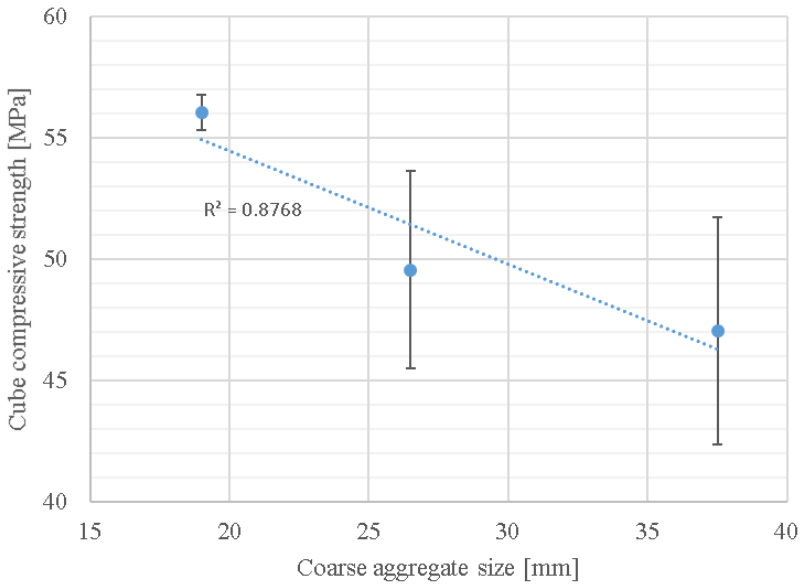

Figure 4.2: Cube compressive strength test results - Hypothesis 2

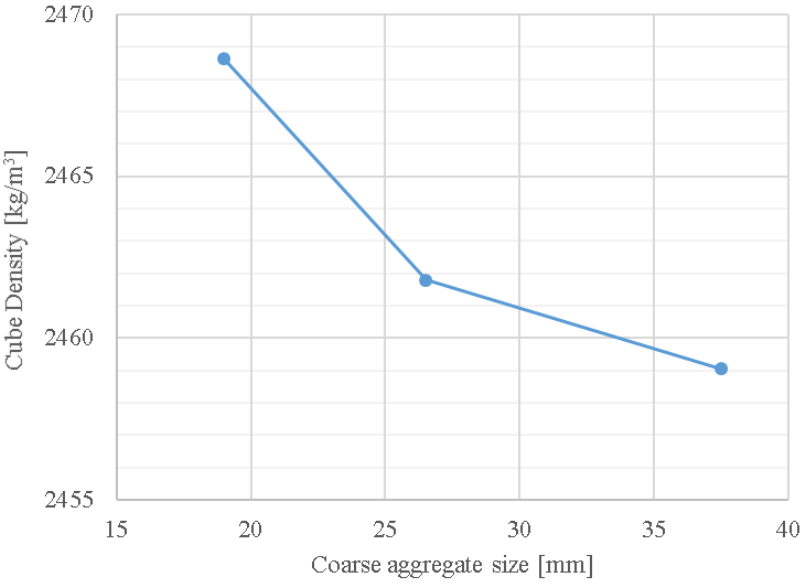

Figure 4.3: Cube densities (kg/m^3) corresponding to the different nominal coarse aggregate sizes at a volume of 400 l/m^3

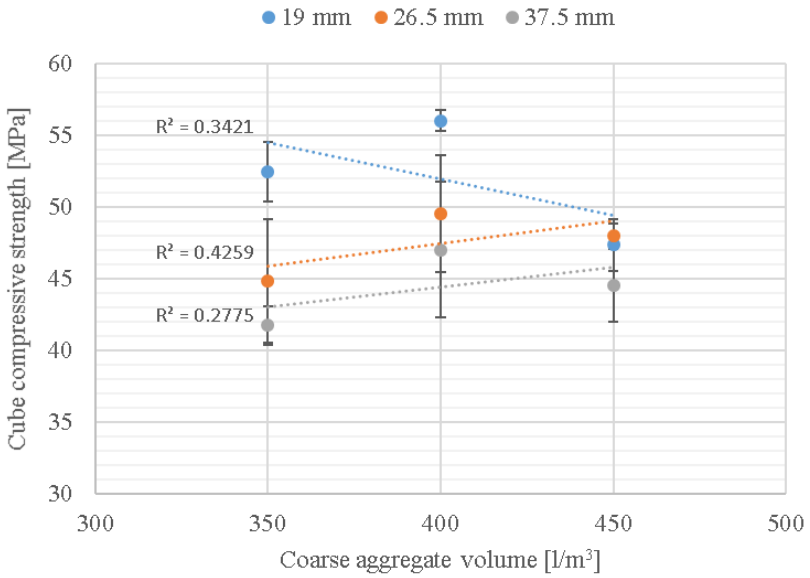

Figure 4.4: Cube compressive strength test results - Hypothesis 3

FRC. The effect of coarse aggregate volume is investigated for all three nominal coarse aggregate sizes used in this study. It should be noted that the linear trend lines illustrating the general trend of compressive strength for an increase in the coarse aggregate volume for each nominal aggregate size, are misleading. Referring to all three nominal coarse aggregate sizes, it is evident that an optimal coarse aggregate volume of 400 l/m^3 can be identified and a decrease in the average compressive strength was experienced for both an increase and decrease in coarse aggregate volume of 50 l/m^3. According to Stock et al. (1979), compressive strength decreases for an increase in the paste content, providing an explanation for the lower average compressive strength experienced for a coarse aggregate volume of 350 l/m^3. Larrard (1999) documented that the coarse aggregate volume effect can be masked by the increase of entrapped air when workability decreases. Thus, for the decrease in the workability experienced for the higher coarse aggregate volume (450 l/m^3), the increase of entrapped air, ultimately decreasing the cube densities as illustrated on Figure 4.5, caused a decrease in the compressive strength.

Figure 4.6 illustrates the effect of fibre dosage on the compressive strength of MSFRC. From literature, different results on the effect of fibre dosage on the compressive strength of FRC are found. From previous research documented by Zollo (1984), the addition of synthetic fibres (0-0.3%) had a negative influence on the compressive strength. Mindess and Vondran (1988) reported that, by incorporating 0.5% fibres by volume, the compressive strength could be improved by as much as 25%.

From Figure 4.6 it is evident that the addition of the CMS fibre for fibre volumes ranging between 0.27 to 0.60% (2.5 to 5.5 kg/m^3), increased the compressive strength. The increasing compressive strength trend can perhaps be attributed to the increased plasticiser dosage incorporated for an increase in fibre dosage to control the workability of the mixes rather than the effect of the fibres. The general mechanism of a plasticiser is to provide cement particles with a highly negative charge to repel the particles due to the same electrostatic charge and provide more

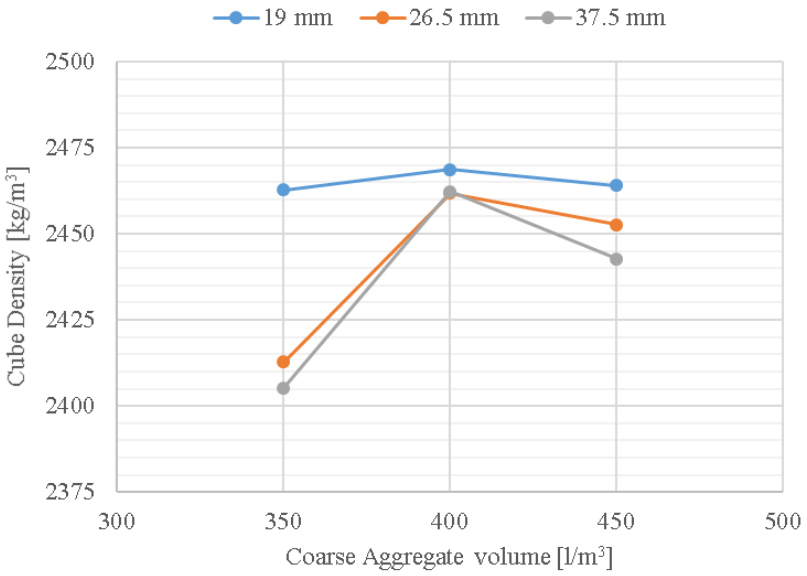

Figure 4.5: Cube densities (kg/m^3) corresponding to the different coarse aggregate volumes for each nominal coarse aggregate size

water by deflocculating the cement particles. Therefore, an increase in the dosage does not only provide more water for the hydration process, but also accelerate it, ultimately improving the compressive strength. It should however be noted that the average compressive strength decreased for fibre dosages larger than 4.0 kg/m^3. The decrease in compressive at high fibre dosages can be explained due to the increased void content and decreased concrete density.

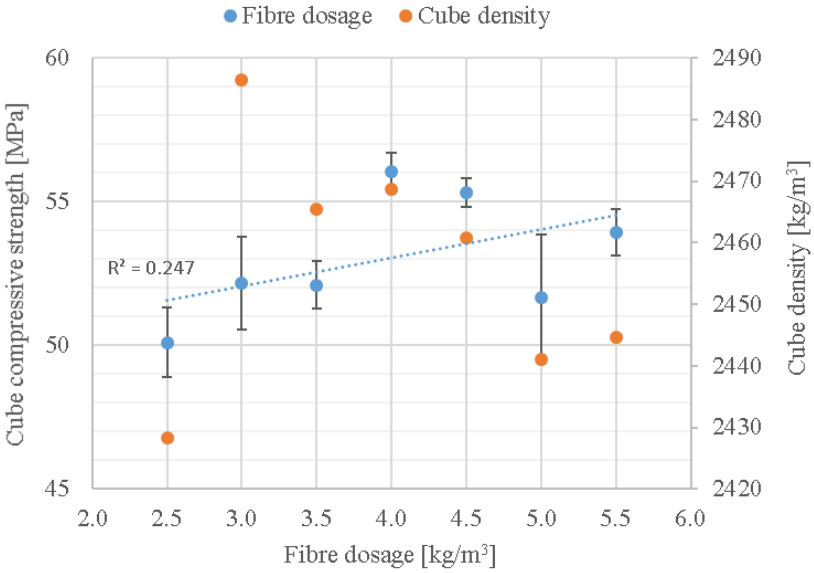

Figure 4.6: Cube compressive strength test results - Hypothesis 4

Figure 4.7 illustrates the effect of mixing time on the compressive strength of MSFRC. The effect of mixing on the compressive strength was investigated for both mixer types used in this

study. It is evident from Figure 4.7 that the average compressive strength, corresponding to the pan mixer, was higher for each mixing time investigated.

The increase in compressive strength corresponding to an increase in mixing time for both mixer types can largely be attributed to the loss of water associated with longer mixing times due to evaporation and absorption. The loss of water lowers the W/C ratio which ultimately increase the compressive strength and the LOP. As mentioned in Section 3.4.5, a slump revival admixture was also incorporated into the mixes to retain a suitable slump and workability after the prolonged mixing times. A high range water reducing superplasticiser (CFR) was added at different dosages to control the workability. For the pan mixer, a higher dosage of the slump revival admixture was required due to its higher mechanical performance and since more water evaporated from the more open pan mixer compared to the tilting-drum mixer, resulting in an enhanced loss of workability. From the data provided by the supplier, a 10% increase of the 28 day compressive strength could be expected after the addition of 1 l/m^3 CFR. As aforementioned, the addition of a plasticiser, or in this case a superplasticiser, results in an increase of the compressive strength. It should be noted that the same compressive strength for both mixer types was documented for a mixing time of 5 minutes due to the same dosage of CHRYSO Fluid Rescue (CFR).

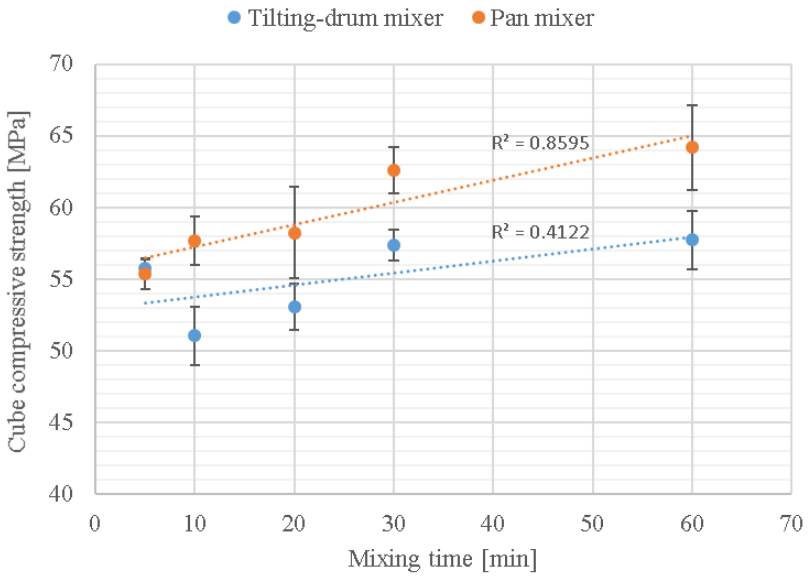

Figure 4.7: Cube compressive strength test results - Hypothesis 5

4.2 Three-point bending test results

The three-point bending test (TPBT) is adopted as the primary test method measuring the macro-mechanical performance of MSFR. This section illustrates the performance in terms of the limit of proportionality (LOP) as well as the residual flexural tensile strengths at specific crack mouth opening displacements (CMODs). The results presented in this section are used in the statistical analyses, presented in Chaper 6, to determine the generic models predicting the

performance of MSFRC. The TPBT results for each set of tests are presented in Appendix A.2.

It should be noted that the results presented in this section are the average values, with the error bars indicating the standard deviation experienced for each set of tests. Data not representing the typical trend was excluded from the results in a sufficient and unbiased manner. Tukey's graphical procedure (boxplot) was used for flagging observations as outliers (Tukey, 1977). Observations were classified as non-representative when falling outside the intervals:

$$\begin{aligned} &Q_1 - g \cdot (IQR) \\ &Q_3 + g \cdot (IQR) \end{aligned} \tag{4.1}$$

where:
Q_1 = First quartile
Q_3 = Third quartile
IQR = Inter Quartile Range $(Q_3 - Q_1)$

A common value for g is 1.5 for flagging observations as outliers or 3.0 for flagging observations as "far out." However, Hoaglin and Iglewicz (1987) used simulation to convert the boxplot outlier labeling rule to a formal outlier identification testing procedure to find the value of g as a function of the sample size (n). Hoaglin and Iglewicz (1987) concluded that a value of $g = 2.2$ is satisfactorily for identifying outliers in normally distributed data for small sample sizes $(n < 20)$. Thus, for the purpose of this study, a value of $g = 2.2$ was considered to identify non-representative data as each batch of tests consisted of six specimens.

4.2.1 Limit of proportionality (LOP) results

The effect of each independent variable on the LOP is illustrated and discussed in this section. The LOP corresponds to the maximum stress experienced between a CMOD of $0 - 0.05$ mm. Commonly, the modulus of rupture (MOR), which corresponds to the first crack strength of a specimen and is defined as the stress in a material just before it yields in a flexure test, is often used instead of the LOP due to the similar definitions of the terms. It is possible for the LOP and the MOR to be equal if the maximum stress between a CMOD of $0 - 0.05$ mm corresponds to the first crack strength of the specimen.

Figure 4.8 illustrates the effect of compressive strength on the LOP for both cement types used in this study. It is evident that an increase in the compressive strength results in an increase in the LOP for both cement types. From Figure 4.8, it should however be noted that the LOP corresponding to the 42.5N CEM III cement exceeds the LOP corresponding to the 52.5N CEM II cement. The increase in the LOP for the 42.5N CEM III cement is also more profound. These results can be explained due to the high blastfurnace slag content of the 42.5N CEM III cement. According to the Slag Cement Association (SCA) (2013), the use of slag as part of the cementitious material in a concrete mix enhances the strength of the concrete, particularly the

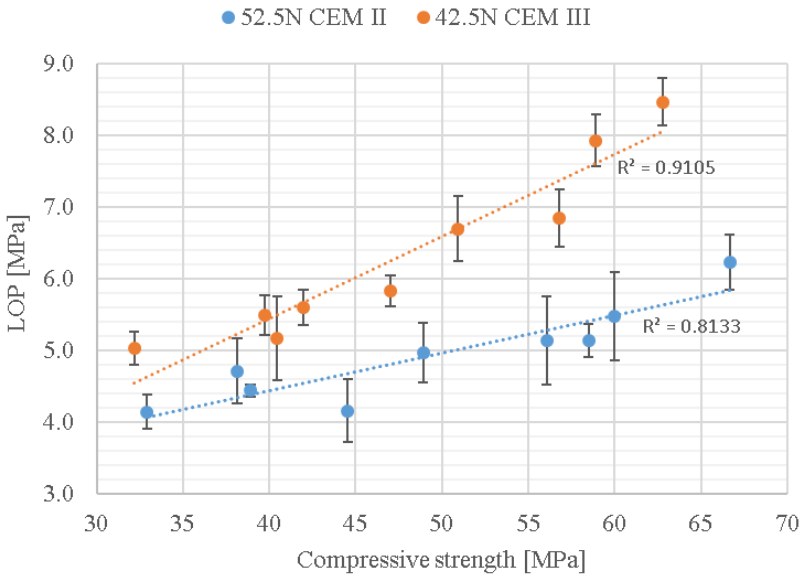

Figure 4.8: Limit of proportionality - Hypothesis 1

Table 4.1: Flexural strength of both cement types according to EN 196-1

Cement type	**Sample no.**	**F_{max} (N)**	**R_f (MPa)**	**Average (MPa)**
42.5N CEM III	1	3319.69	9.07	8.93
	2	3424.70	9.36	
	3	3178.11	8.35	
52.5N CEM II	1	3201.91	8.75	8.40
	2	2844.35	7.78	
	3	3173.85	8.68	

flexural strength. When portland cement reacts with water, it forms calcium silicate hydrate (C-S-H) and calcium hydroxide ($Ca(OH)_2$). The slag reacts with water and the $Ca(OH)_2$, which is a by-product of the cement hydration process and do not contribute to the strength, to form additional C-S-H crystals which provides the strength. The improved flexural strength is attributed to the increased denseness of the concrete paste matrix due to the additional C-S-H crystals, as well as an improved paste-aggregate bond.

Cement mortar tests according to EN 196-1 (European Norms, 2005) were performed to verify the results presented in Figure 4.8. Table 4.1 indicates the comparison between the 28 day flexural strength (R_f) for both cement types. It can be concluded that the average flexural strength of the 42.5N CEM III cement exceeds the 52.5N CEM II cement, verifying the results presented in Figure 4.8. It can thus be concluded that compressive strength significantly effects the LOP of MSFRC, but the extent is dependent on the cement type and class, with a cement extended with blastfurnace slag indicating an improved LOP.

The relationship between the LOP and coarse aggregate size for MSFRC, for a coarse aggregate volume of 400 l/m^3, is illustrated in Figure 4.9. From the graph, it is evident that an increase in the nominal coarse aggregate size tends to decrease the LOP for MSFRC. This behaviour is expected, as an increase in coarse aggregate size would negatively effect the packing density of the concrete matrix as well as influencing the compaction of the mix, decreasing the flexural performance as a weaker bond exits between larger particles compared to smaller particles due to a smaller surface area-to-volume ratio (Quiroga and Fowler, 2004). It should however be noted that a slight increase in the LOP is illustrated for an increase in nominal coarse aggregate size between 19 and 26.5 mm with a substantial decrease in LOP between nominal coarse aggregate sizes 26.5 and 37.5 mm. No clear conclusion can be provided for the slight increase in LOP between coarse aggregate sizes 19 and 26.5 mm. The large scatter of results experienced due to the TPBT setup is believed to be a possible explanation. It is also evident that all three points are within experimental uncertainty of the first point. Therefore, no clear conclusion can be drawn regarding the influence of an increase in nominal coarse aggregate size on the LOP of MSFRC.

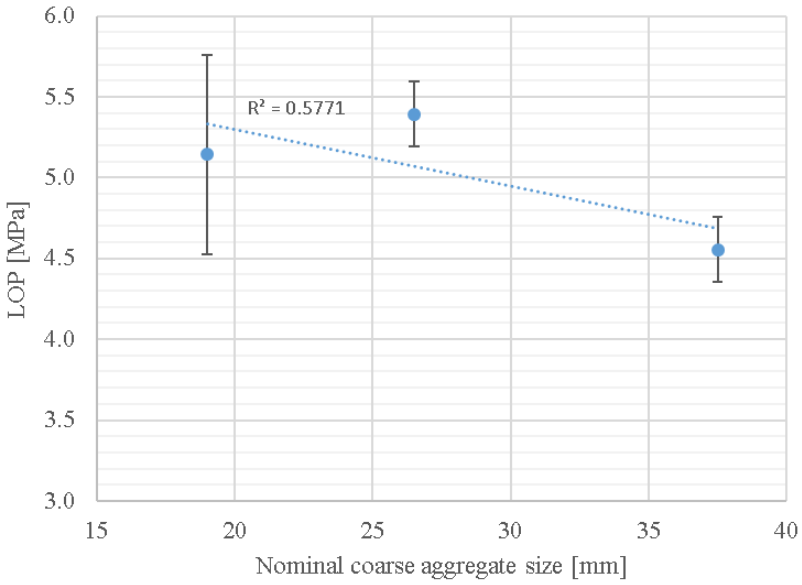

Figure 4.9: Limit of proportionality - Hypothesis 2

Figure 4.10 illustrates the relationship between the LOP and the coarse aggregate volume for MSFRC. It is evident that no clear trend exists for an increase in coarse aggregate volume for all three nominal coarse aggregate sizes investigated although the trend lines indicate a positive trend for an increase in coarse aggregate volume. It should be noted that a large standard deviation was experienced by investigating the effect of coarse aggregate volume. As mentioned previously, the large scatter of results can be attributed to the TPBT setup. This drawback is a result of the small crack-area (125x150 mm) available during execution of the TPBTs, varying the number of coarse aggregates, as well as fibres, bridging the induced crack. From the data presented, it can be concluded that coarse aggregate volume does not significantly influence the LOP. However, an improved test method with a lower scatter of results should be implemented

to investigate the effect of coarse aggregate volume on the LOP of MSFRC.

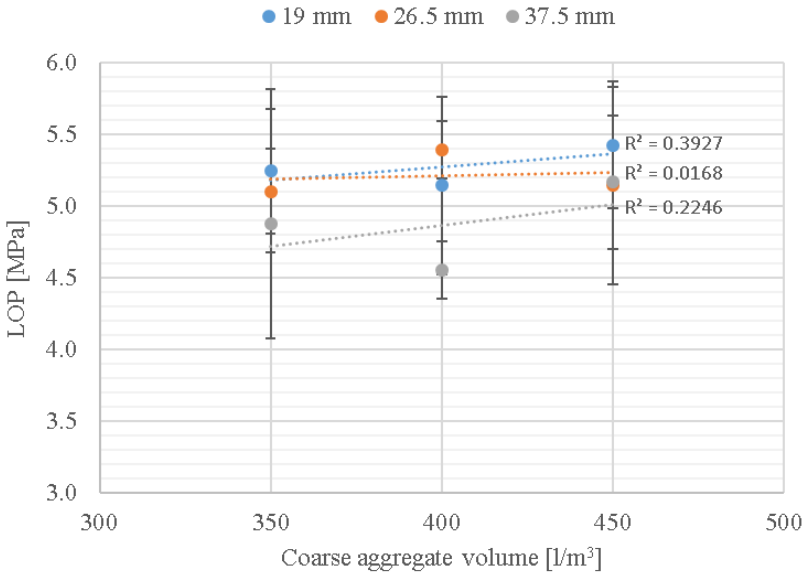

Figure 4.10: Limit of proportionality - Hypothesis 3

Figure 4.11 illustrates the effect of fibre dosage on the LOP of MSFRC. It was expected that fibre dosage would have a negligible effect on the LOP as the addition of fibres only influences the post-cracking (residual) strength of concrete (Buratti et al., 2011). According to Figure 4.11 it is should however be noted that an increasing trend exits for an increase in fibre dosage. The trend can be attributed to the increased plasticiser dosage incorporated for an increase in fibre dosage to control the workability of the mixes. An increased plasticiser dosage ultimately increases the compressive strength, which increases the LOP as illustrated in Figure 4.8.

Once again a large scatter of results are presented as illustrated by the error bars and can be attributed to the TPBT setup. From the data presented in Figure 4.11, it should also be noted that the data point corresponding to the lowest fibre dosage (2.5 kg/m^3) and the highest fibre dosage (5.5 kg/m^3) do not fit the general trend. The increased LOP at the low fibre dosage can be attributed to the increased average beam density. Conversely, the decrease in the LOP at the high fibre dosage can be attributed to the decreased average beam density due to an increase in void content.

The relationship between mixing time, for both mixer types used in this study, and the LOP for MSFRC is illustrated in Figure 4.12. For both mixer types, a similar increasing trend for the LOP is presented. The increasing trend is not attributed to an increase in mixing time, but rather to the increased loss in water associated with prolonged mixing times due to evaporation and absorption, which ultimately lowers the W/C ratio and increases the strength and LOP, as well as an increase in the slump revival admixture (superplasticiser) dosage. As mentioned in Section 3.4.5, a slump revival admixture (CFR) was incorporated at different dosages to retain a suitable slump and workability after the prolonged mixing times. The additional superplasticiser increased the compressive strength as illustrated in Figure 4.7, ultimately increasing the LOP.

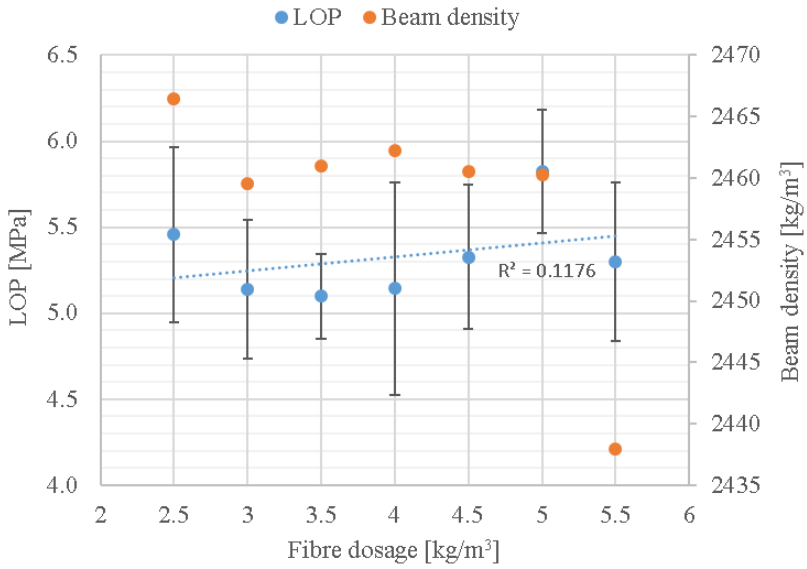

Figure 4.11: Limit of proportionality - Hypothesis 4

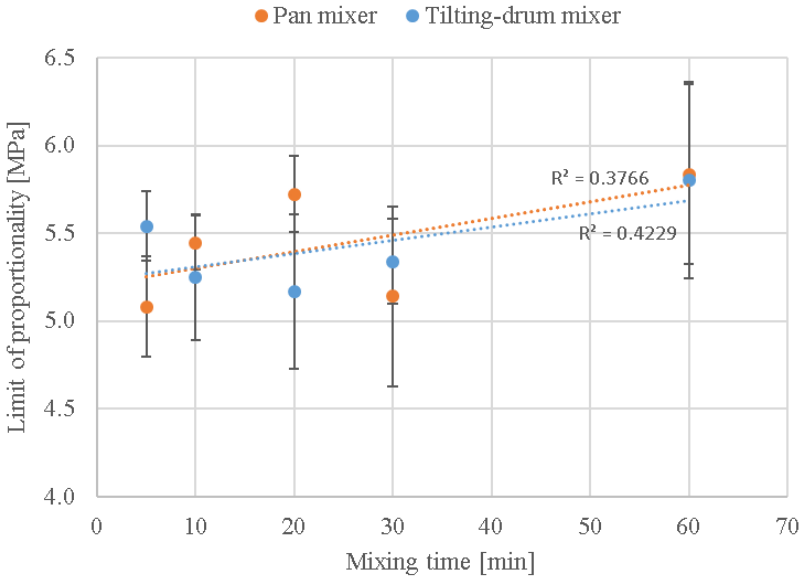

Figure 4.12: Limit of proportionality - Hypothesis 5

4.2.2 Residual flexural tensile strength (RFTS) results

The post-cracking performance of MSFRC is investigated in terms of the RFTSs, i.e. f_{R1}, f_{R2}, f_{R3}, and f_{R4} corresponding to CMODs of 0.5, 1.5, 2.5, and 3.5 mm. The RFTS at CMODs of 0.5 (f_{R1}) and 3.5 mm (f_{R4}) are of significant interest according to TR34. RFTS at CMODs of 1.5 (f_{R2}) and 2.5 mm (f_{R3}) are typically utilised in the design approach for punching shear for slabs-on-grade, which is not applicable to MSFRC, but only SFRC. Nevertheless, the effect of each independent variable, on each residual flexural tensile strength, is presented and discussed

in this section.

Figure 4.13 illustrates the comparison between the typical TPBT output for plain concrete and MSFRC, with a fibre addition of 4 kg/m^3, for the reference mix design indicated in Table 3.11. It is evident that macro-synthetic fibre addition does not affect the MOR, as concrete must crack before the addition of any reinforcement can have an effect (The Concrete Society, 2013). However, it can be concluded that the residual strength is significantly influenced by the addition of macro-synthetic fibres, indicating an increased residual strength at each CMOD in the post-cracking region. It should be noted that the RFTS of MSFRC decreases with an increase in crack opening as the fibres undergo pull-out during an increase in crack widening, resulting in less fibres bridging the crack plane, ultimately decreasing the residual strength.

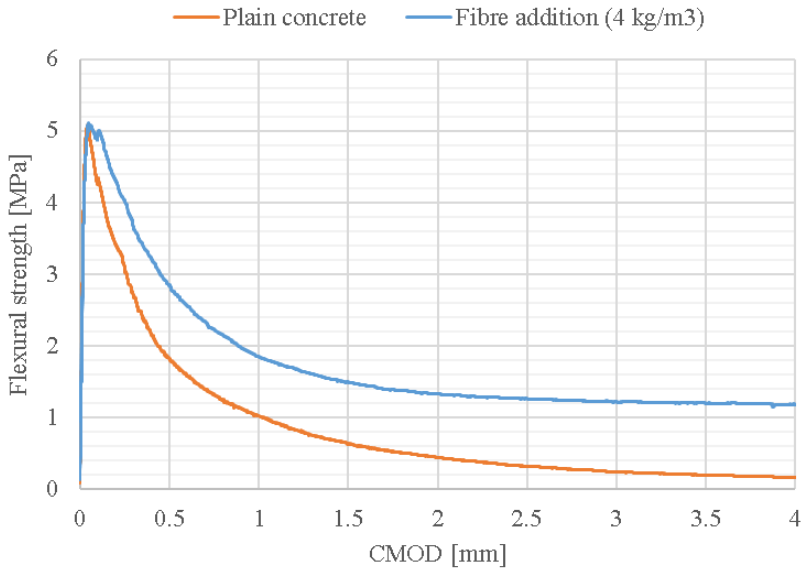

Figure 4.13: Typical TPBT output illustrating the comparison between plain concrete and MSFRC

Figure 4.14 illustrates the effect of compressive strength on the RFTS. The effect of both cement types used in this study are illustrated, with Figure 4.14a indicating the effect of the 42.5N CEM III cement, and Figure 4.14b indicating the effect of the 52.5N CEM II cement.

From Figure 4.14 it is evident that f_{R1} is slightly influenced by compressive strength, indicating an upward trend for an increase in compressive strength for both cement types. The increasing trend can be attributed to an improved and more favourable bond between the fibres and the concrete matrix due to an increased density for an increase in compressive strength as depicted in Figure 4.15. The higher densities can be attributed to the increased denseness of the concrete paste matrix due to the higher cement content corresponding to a decrease in the W/C ratio. From Figure 4.15, it is also evident that nearly the same trend occurred for both cement types, indicating that the use of blastfurnace slag as an extender does not affect the concrete density. From the results depicted in Figure 4.14 it is evident that the type of cement does not significantly effect f_{R1}, contradicting the results illustrated in Figure 4.8, indicating an improved performance

considering the 42.5N CEM III cement.

Referring to f_{R2}-f_{R4}, it can be concluded that compressive strength has a negligible effect. The negligible effect can be attributed to an increase in crack widening. As the pull-out resistance of the CMS fibre is dependent on the bond between the fibre and the concrete matrix due to the absence of mechanical interlocking, an increase in CMOD decreases the bond area of fibre-to-matrix, reducing the effect of an increase in compressive strength. It can also be concluded that cement type does not affect f_{R2}-f_{R4}.

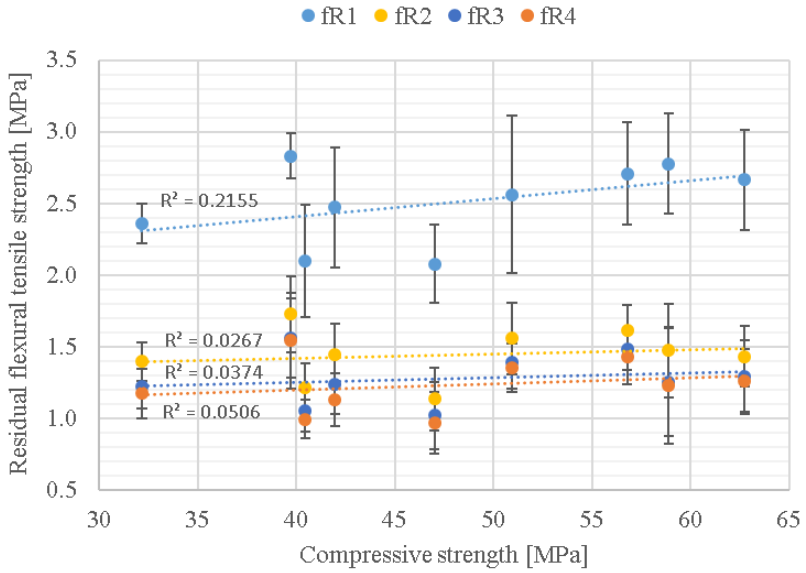

(a) Cement type - 42.5N CEM III

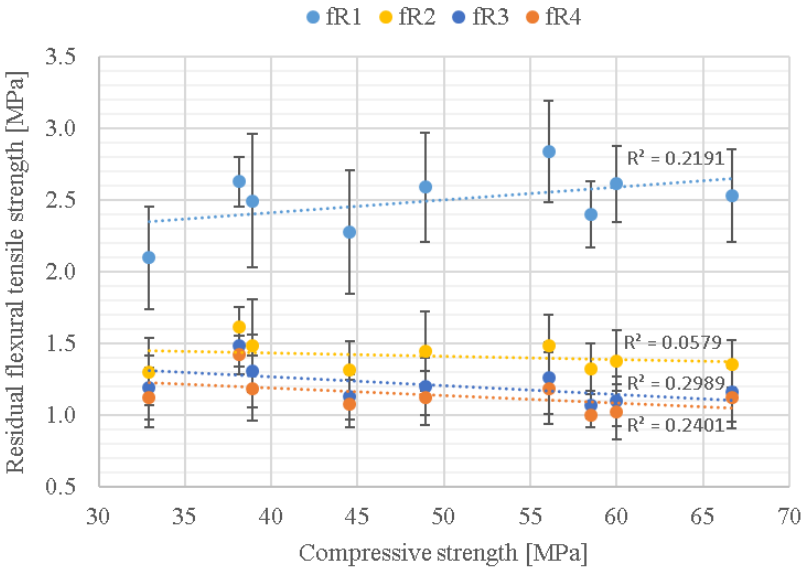

(b) Cement type - 52.5N CEM II

Figure 4.14: Residual flexural tensile strength results - Hypothesis 1

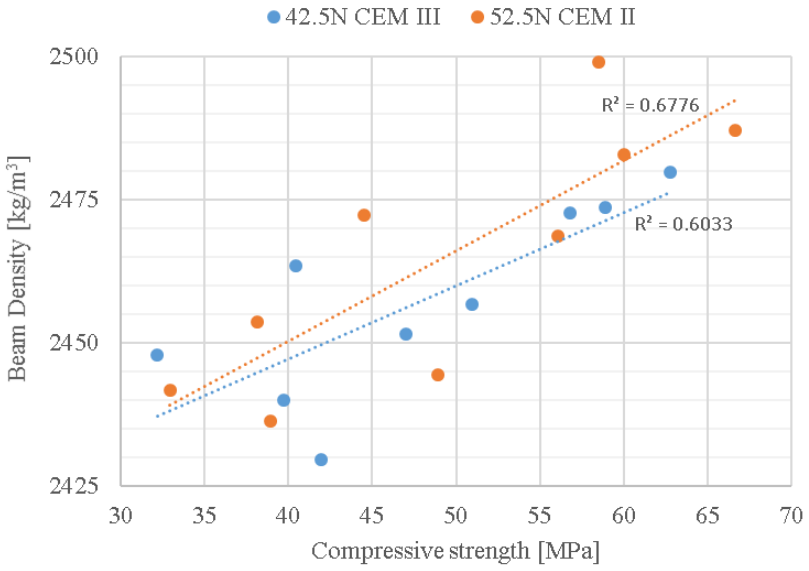

Figure 4.15: Comparison between density (kg/m^3) and compressive strength (MPa)

Figure 4.16 depicts the relationship between f_{R1}–f_{R4} and coarse aggregate size. It can be concluded that an increase in nominal coarse aggregate size has a negative effect on f_{R1}, indicating a decreasing trend. A larger nominal coarse aggregate size negatively influences fibre distribution (Beaudoin, 1990), causing fewer fibres to bridge the crack plane, ultimately decreasing the residual strength. It is also evident that the effect of nominal coarse aggregate size on f_{R2}-f_{R4} is negligible for the nominal sizes considered in this study.

It should however be noted that a slight increase in the RFTS is illustrated for an increase in nominal coarse aggregate size from 19 to 26.5 mm with a decrease in RFTS evident between nominal coarse aggregate sizes 26.5 and 37.5 mm. No clear conclusion can be provided for the slight increase between coarse aggregate sizes 19 to 26.5 mm. The large scatter of results due to the TPBT setup is believed to be a possible explanation.

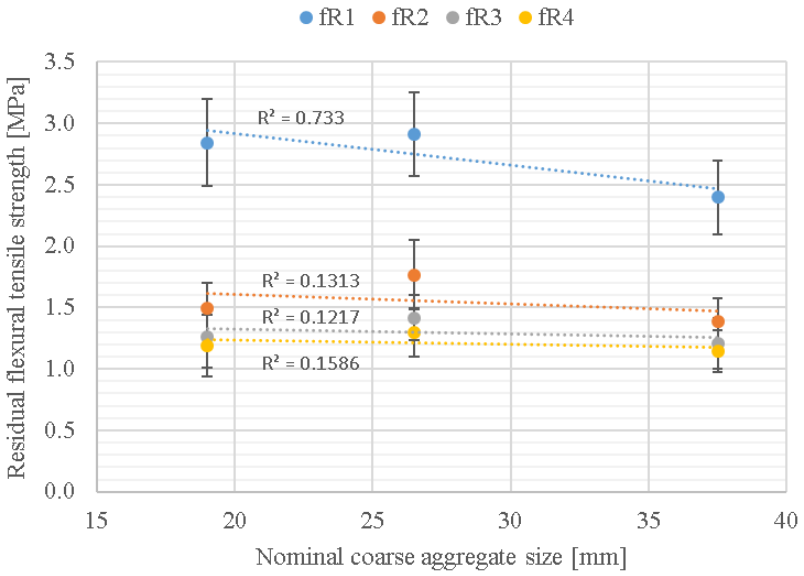

Figure 4.16: Residual flexural tensile strength results - Hypothesis 2

Figure 4.17 depicts the relationship between f_{R1} to f_{R4} and coarse aggregate volume for all three nominal coarse aggregate sizes used in this study. Initially it was expected that an increase in coarse aggregate volume would cause a decrease in the RFTS. An increase in coarse aggregate volume results in a decrease of the available paste for the macro-synthetic fibres to be distributed, reducing the amount of fibres bridging the crack plane and ultimately decreasing the RFTS. For the same fibre dosage, an increase in coarse aggregate volume might also induce fibre balling due to the decreased paste volume, causing a non-uniform distribution of the fibres within the matrix.

Figure 4.17 depicts a contradicting relationship. Figure 4.17a and Figure 4.17c illustrates an increasing trend for f_{R1} to f_{R4}, where an increase in coarse aggregate volume for a nominal coarse aggregate size of 26.5 mm, as illustrated in Figure 4.17b, has a negligible effect on the RFTS. These contradicting results can be attributed to the TPBT setup, as previously mentioned. The small crack-area available during the execution of the TPBTs, significantly affected the results, varying the number of coarse aggregates, as well as fibres, bridging the induced crack plane. From the data presented, it can be concluded that a slight increase in RFTS is evident for an increase in coarse aggregate volume, however, a better test method with a larger crack-area must be implemented to investigate the influence of coarse aggregate volume on the RFTS.

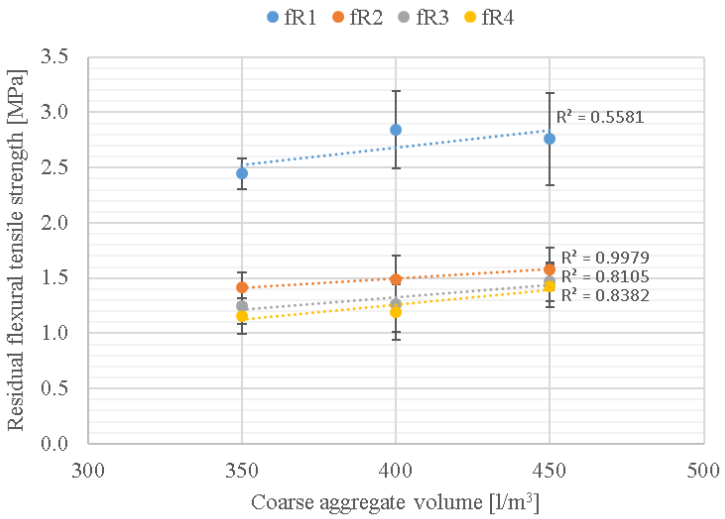

(a) 19 mm nominal coarse aggregate size

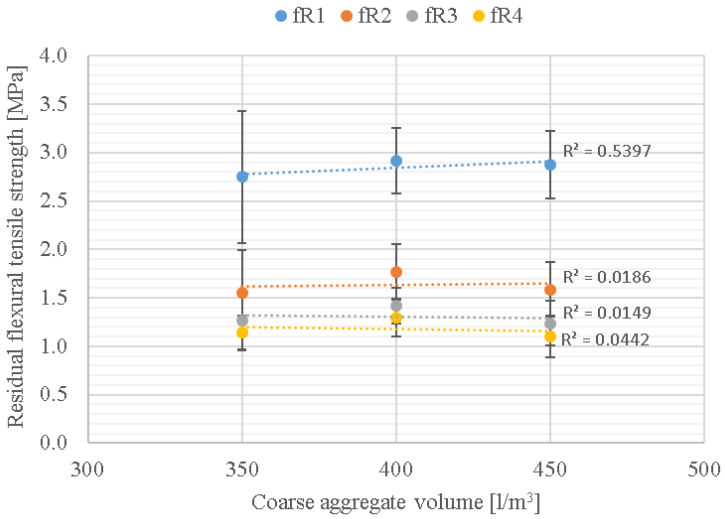

(b) 26.5 mm nominal coarse aggregate size

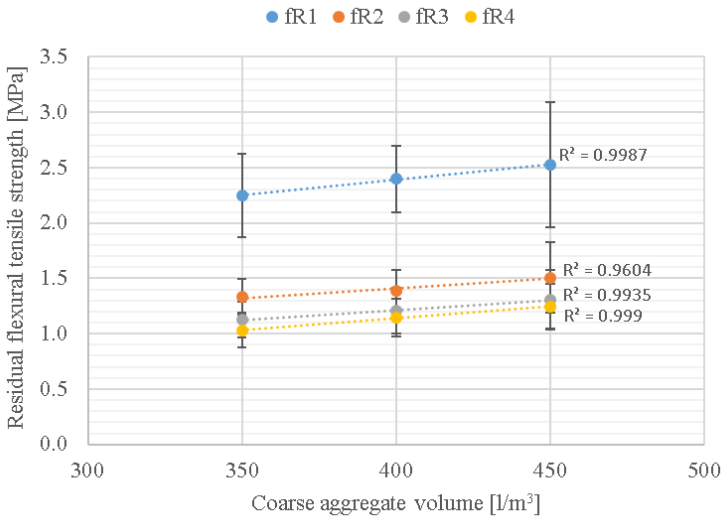

(c) 37.5 mm nominal coarse aggregate size

Figure 4.17: Residual flexural tensile strength results - Hypothesis 3

Figure 4.18 illustrates the relationship between f_{R1} to f_{R4} and fibre dosage. As expected, an increase in fibre dosage resulted in an increase in RFTS for f_{R1} to f_{R4}, with a similar degree of improvement as depicted by the trend lines. An increase in fibre dosage results in an increased amount of fibres bridging the crack plane, ultimately improving the RFTS at each CMOD in the post-cracking region. Similarly as the influence of fibre dosage on the LOP depicted in Figure 4.11, the results presented at the low (2.5 kg/m^3) and high (5.5 kg/m^3) fibre dosages do not fit the general trend. The increased RFTS at the low fibre dosage can be attributed to the increased average beam density. Conversely, the decrease in the RFTS at the high fibre dosage can be attributed to the decreased average beam density due to an increase in void content.

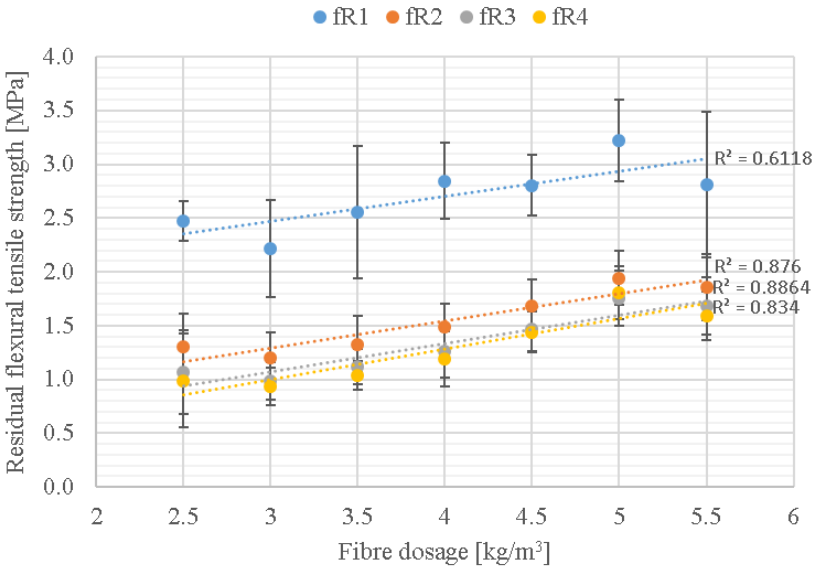

Figure 4.18: Residual flexural tensile strength results - Hypothesis 4

The effect of mixing time on f_{R1} to f_{R4}, for both mixer types, is illustrated in Figure 4.19. From Figure 4.19a, it is evident that the effect of mixing time on performance parameter f_{R1} is negligible for a pan mixer. Referring to f_{R2}-f_{R4}, it can be concluded that mixing time, for a pan mixer, has a significant decreasing affect, indicating a similar declining trend as depicted by the trend lines. It should be noted that an initial increase in the residual performance for f_{R1}-f_{R4} is illustrated for a mixing time between $5 - 10$ minutes, where after the performance decreases, indicating an optimal mixing time of 10 minutes. Initially, it was expected that an increase in mixing time would ensure better fibre distribution and increase fibre damage, enhancing the bond between the synthetic fibre and the concrete matrix, ultimately improving the RFTS. For a mixing time up until 10 minutes the initial expectation was proven correct, however, for prolonged mixing times extending 10 minutes, the CMS fibre started deteriorating, reducing its tensile capacity, and ultimately decreasing the residual strength.

Figure 4.19b illustrates the relationship between mixing time and f$_{R1}$ to f_{R4} for a tilting-drum mixer. A tilting-drum mixer was considered to simulate the mixing process experienced in a ready-mix truck. From Figure 4.19b it is evident that the effect of mixing time on f_{R1}-f_{R4} is

negligible. It can be concluded that the mixing process for a tilting-drum mixer did not enhance, nor decrease, the residual performance and the effect can be neglected.

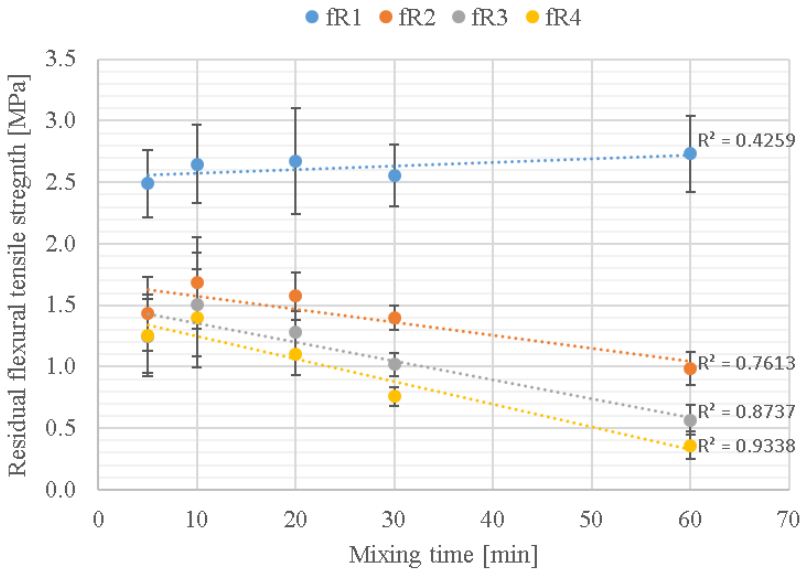

(a) Pan mixer

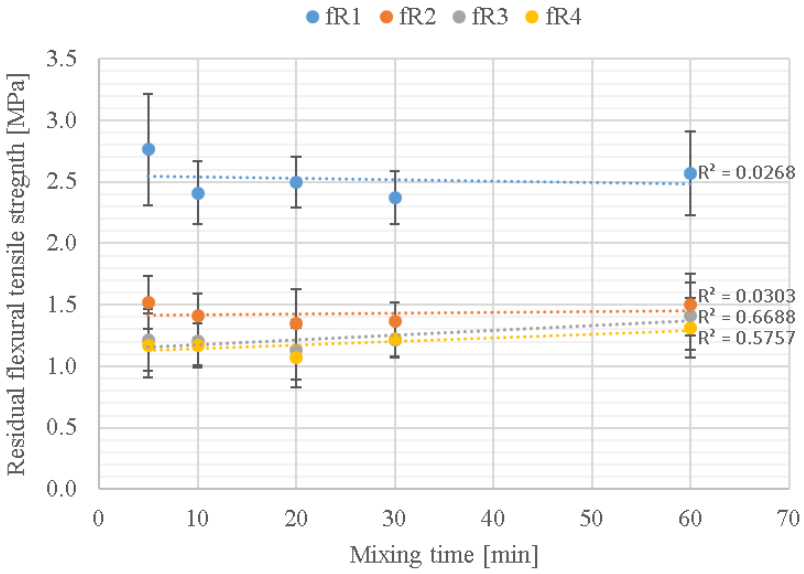

(b) Tilting-drum mixer

Figure 4.19: Residual flexural tensile strength results - Hypothesis 5

4.3 Shrinkage test results

Shrinkage measurements were conducted over a period of 91 days. It is important to note that these measurements included the total shrinkage measurement, including drying shrinkage and autogenous shrinkage. However, at the considered W/C ratio of 0.55, the effect of autogenous shrinkage would not considerably influence the shrinkage measurements, and it can be assumed

that the shrinkage measurements represent the deformation due to drying shrinkage. At lower W/C ratios, volume and length change can be attributed to autogenous shrinkage, due to water transport not being allowed to or from the cement paste, but extracted from the capillary pores.

The obtained shrinkage measurements are also compared to the shrinkage deformation predicted according to EN 1992-1-1 (British Standards Institution, 2004). According to EN 1992-1-1, the total shrinkage strain is dependent on two factors, i.e. drying shrinkage strain and autogenous shrinkage strain. The drying shrinkage strain is a function of the migration of water through the hardened concrete specimen and the autogenous shrinkage is a linear function of the concrete strength. The following equation represents the total shrinkage strain according to EN 1992-1-1:

$$\varepsilon_{cs} = \varepsilon_{cd} + \varepsilon_{ca} \tag{4.2}$$

where:
ε_{cs} = total shrinkage strain
ε_{cd} = drying shrinkage strain
ε_{ca} = autogenous shrinkage strain

As mentioned above, the autogenous shrinkage strain was disregarded due to the considered W/C ratio, thus the total shrinkage strain according to EN 1992-1-1 was calculated by disregarding the autogenous shrinkage strain. The development of the drying shrinkage strain, in time, was calculated using the following equation:

$$\varepsilon_{cd}(t) = \beta_{ds}(t, t_s) \cdot k_h \cdot \varepsilon_{cd,0} \tag{4.3}$$

where:
$\beta_{ds}(t, t_s) = \frac{t - t_s}{(t - t_s) + 0.04\sqrt{h_0^3}}$
t = age of the concrete at the considered time (days)
t_s = age of concrete at the beginning of drying shrinkage (normally at the end of curing)
$h_0 = (2 \cdot A_c)/u$

- A_c is the cross-sectional area and u is the perimeter of the part of the cross-section exposed to drying

k_h = coefficient depending on the notional size h_0 according to Table 3.3 in EN 1992-1-1
$\varepsilon_{cd,0}$ = nominal unrestrained drying shrinkage which is dependent on the relative humidity (%) and the concrete compressive strength (MPa) and was calculated as follows:

- $\varepsilon_{cd,0} = 0.85[(220 + 110 \cdot \alpha_{ds1}) \cdot exp(-\alpha_{ds2} \cdot \frac{f_{cm}}{f_{cmo}})] \cdot 10^{-}6 \cdot \beta_{RH}$
- $\beta_{RH} = 1.55[1 - (\frac{RH}{RH_o})^3]$

  where:

- f_{cm} = Mean compressive strength (MPa)
- f_{cmo} = 10 MPa
- α_{ds1} = 4 for cement Class N
- α_{ds2} = 0.12 for cement Class N
- RH = Ambient relative humidity (%)
- RH_o = 100%

To determine the maximum drying shrinkage strain, all the specimens were immediately exposed to drying shrinkage, therefore t_s were taken as 0. The cross-section for all the specimens were 100x100 mm, and the perimeter of the cross-section exposed to drying was equal to 4x100 mm, which provided a notional size of 50 and a k_h coefficient of 1.0 according to Table 3.3 in EN 1992-1-1. The average cube compressive strength of the reference concrete was 56.2 MPa and the approximate relative humidity was 65%, which provided a nominal unrestrained drying shrinkage ($\varepsilon_{cd,0}$) of 321 $\mu\varepsilon$.

The average shrinkage strain determined for each particular group, as well as the total shrinkage strain calculated according to EN 1992-1-1, is illustrated in Figure 4.20.

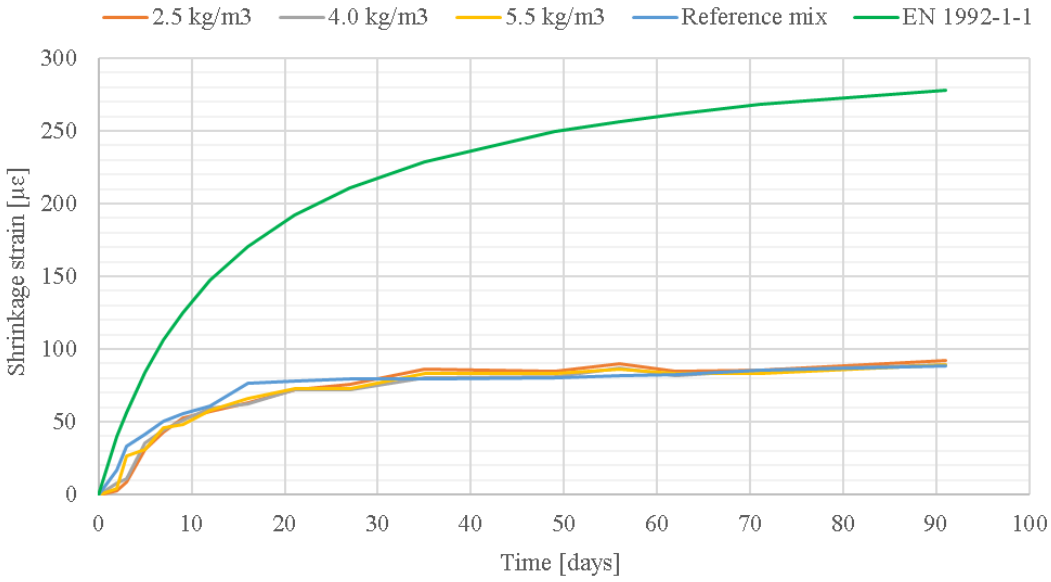

Figure 4.20: Comparison between the average shrinkage strain for various fibre dosages, a reference concrete as well as the shrinkage strain according to EN 1992-1-1

From Figure 4.20, it is evident that the addition of the CMS fibre, at the considered dosages, had a negligible effect on the shrinkage strain compared to the strain measured for the reference concrete mix. The slight anomalies in the measurements is a result of the changes in the temperature/humidity of the climate controlled room where the shrinkage measurement tests were carried out. It can also be concluded that the shrinkage strain predicted by EN 1992-1-1 overestimated the true shrinkage strain. The overestimation can perhaps be attributed to coarse

aggregate size and volume not being accounted for in the prediction model. Due to the large nominal coarse aggregate size (19 mm) and relative high coarse aggregate volume (400 l/m^3) considered in this study, a lower drying shrinkage strain can be expected. It is also evident that the average shrinkage-time relationship has not reached equilibrium, as the graphs illustrate an increasing trend up until 91 days.

4.4 Computed Tomography (CT) scan results

This section presents the results obtained from the CT scans. The CT scans provided information regarding the effect of coarse aggregate size on fibre distribution and determined the fibre volume fraction within the scanned samples to compare with the theoretical fibre dosage.

Figure 4.21 to Figure 4.23 represent the results of the CT scans for each nominal coarse aggregate size. It should be noted that the colour of the fibre volumes, illustrated on the images, exhibit various volumes, with a scale provided in ascending order from bottom to top.

From Figure 4.21, it is evident that a relative homologous distribution of fibres exits considering the 19 mm nominal coarse aggregate size. Due to the nature of the fibre, the fibre orientation is dependent on the distribution of the aggregates within the matrix, thus a critique conclusion on the orientation of the fibres cannot be made due to the considered sample size. It is evident, from Figure 4.21b and Figure 4.21c, that air voids are included in the detected fibre volumes. The air voids can be identified as the small detected volumes attached to the fibres. These air voids could not be excluded from the analyses, as they are connected to the fibres and by removing the voids from the analysis, the fibre attached to the void would also be removed, providing an inaccurate representation of the amount of fibre volumes within the scanned samples.

Referring to Figure 4.22, a less homologous fibre distribution exits between the three scanned samples considering, the 26.5 mm nominal coarse aggregate size. It is evident that the increase in coarse aggregate size had an influence on the distribution of the fibres within the matrix, with Figure 4.22a portraying a lower visible fibre volume within the scanned sample, compared to the higher and bundled fibre volume illustrated by Figures 4.22b and 4.22c. The inclusion of air voids in the detected fibre volumes is once again visible in Figures 4.22b and 4.22c, and could not be removed without removing the fibres attached to the voids.

Figure 4.23 depicts the effect of a 37.5 mm nominal coarse aggregate size. It is evident that the larger 37.5 mm nominal coarse aggregate size had a worse effect on the fibre distribution, exhibiting a non-homologous distribution with an increased amount of visible voids presented in the scanned samples. Once again, these voids can be identified as the small detected volumes attached to the fibres. The increased amount of voids can be contributed to the bundled distribution of the fibres within the matrix. It should be noted that the sample presented in Figure 4.23c is not completely symmetrical, due to a single coarse aggregate which de-bonded in the preparation process.

From the CT scans presented, it can be concluded that an increase in coarse aggregate size affect

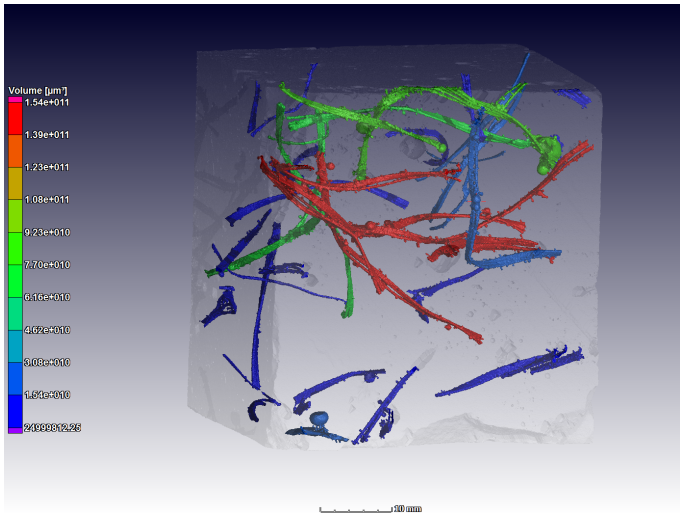

(a) Sample 1

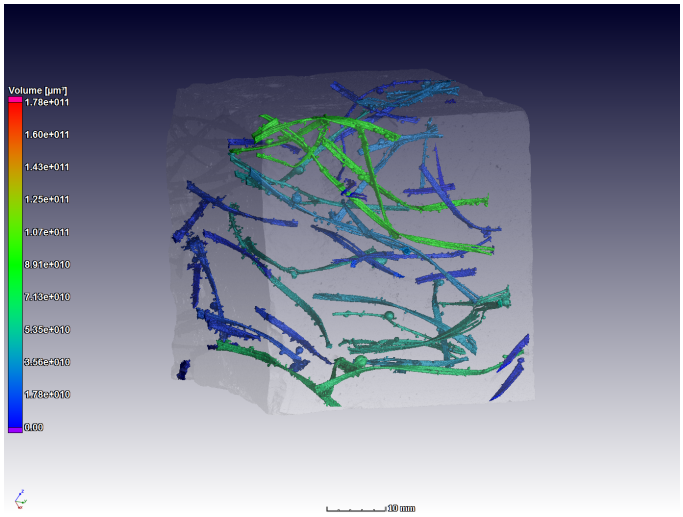

(b) Sample 2

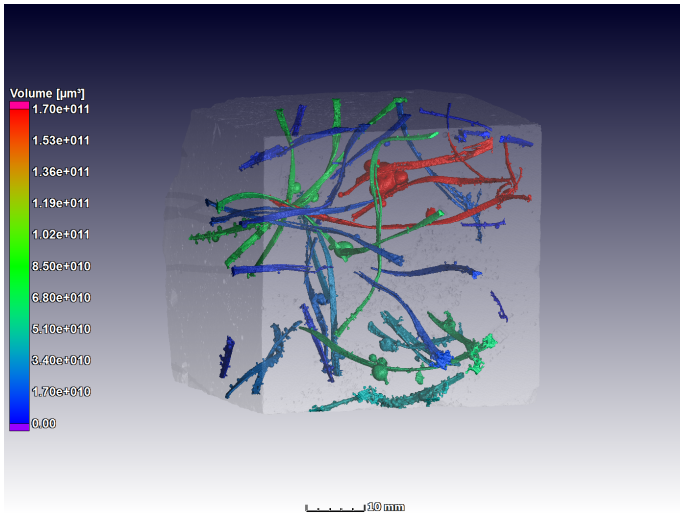

(c) Sample 3

Figure 4.21: CT scan images - 19 mm nominal coarse aggregate size

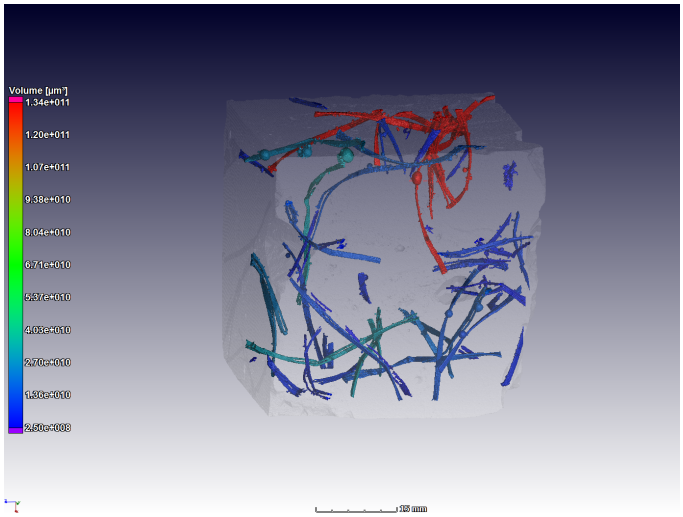

(a) Sample 1

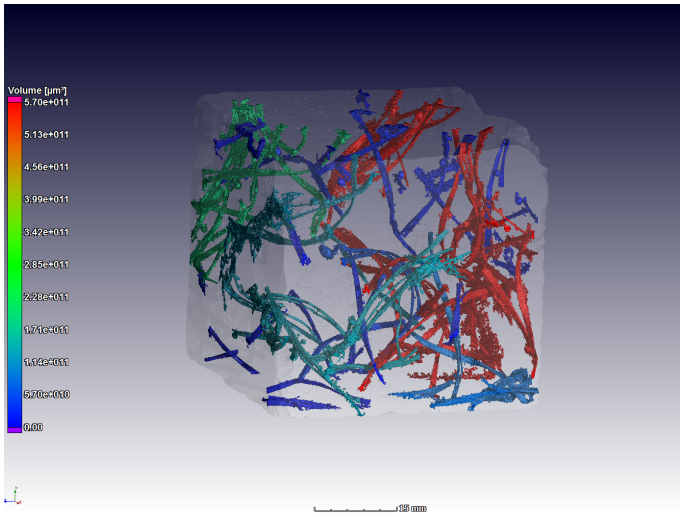

(b) Sample 2

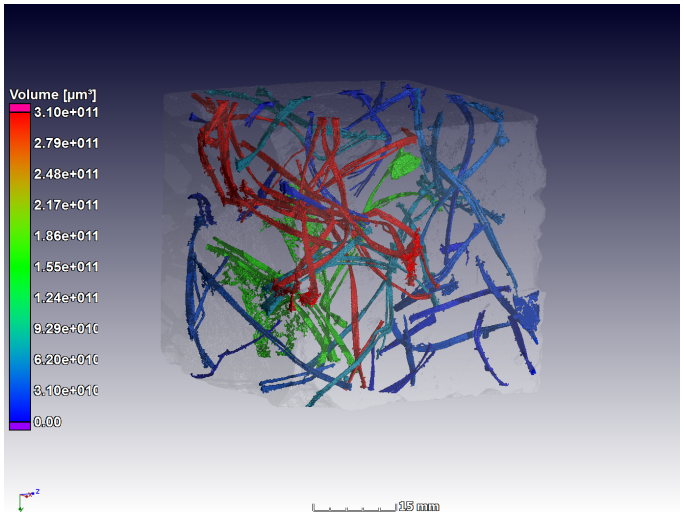

(c) Sample 3

Figure 4.22: CT scan images - 26.5 mm nominal coarse aggregate size

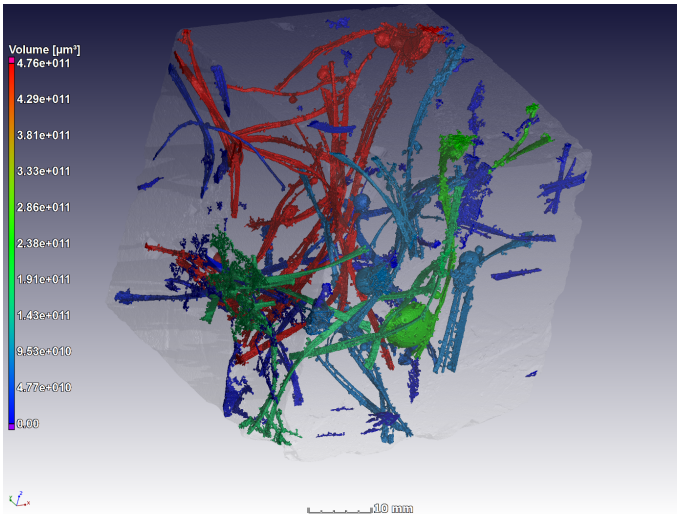

(a) Sample 1

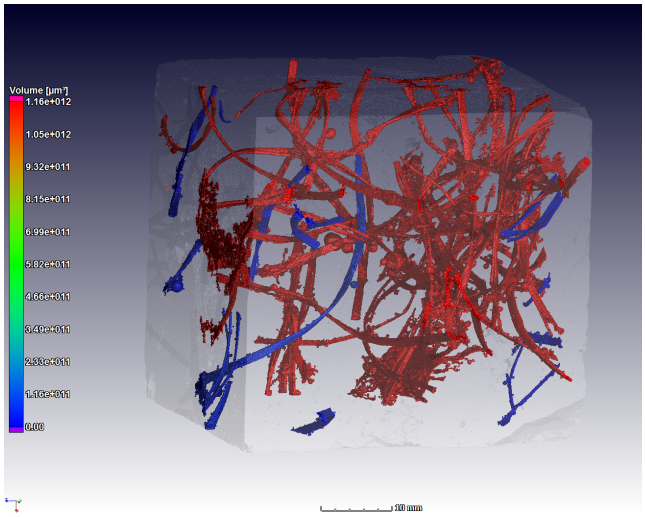

(b) Sample 2

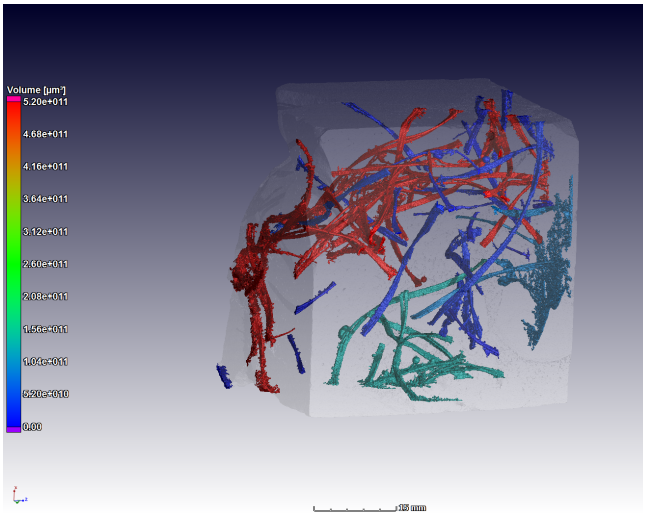

(c) Sample 3

Figure 4.23: CT scan images - 37.5 mm nominal coarse aggregate size

the fibre distribution within the concrete matrix, yielding a more prominent non-homologous fibre distribution and an increase in air voids of the MSFRC matrix. The fibre volume analysis of the scanned samples are presented in Table 4.2.

Table 4.2: CT scan fibre volume analysis

Nominal coarse aggregate size (mm)	Sample no.	Material volume (μm^3)	Fibre volume (μm^3)	Fibre volume ratio (%)	Theoretical volume ratio (%) (Fibre dosage = 4 kg/m^3)	Difference (% points)	Average difference (% points)
19	1	1.11E+14	5.11E+11	0.460	0.435	0.026	0.089
	2	1.14E+14	5.84E+11	0.512	0.435	0.077	
	3	1.13E+14	6.78E+11	0.600	0.435	0.165	
26.5	1	1.31E+14	5.30E+11	0.405	0.435	-0.030	0.340
	2	1.28E+14	1.44E+12	1.125	0.435	0.690	
	3	1.31E+14	1.04E+12	0.794	0.435	0.359	
37.5	1	1.22E+14	1.52E+12	1.246	0.435	0.811	0.615
	2	1.16E+14	1.29E+12	1.112	0.435	0.677	
	3	1.29E+14	1.02E+12	0.791	0.435	0.356	

According to Table 4.2 the average difference between the theoretical volume ratio of fibres considered for the investigation and the detected fibre volume ratios in the scanned samples, increased with an increase in nominal coarse aggregate size. The same theoretical volume ratio was considered for all the specimens, indicating that an increase in the nominal coarse aggregate size yields an increase in void content for MSFRC.

Figure 4.24 illustrates the average beam density versus the different nominal coarse aggregate sizes of the samples tested measuring the macro-mechanical performance according to Hypothesis 2, as stated in Section 3.3. From Figure 4.24, it can be concluded that an increase in coarse aggregate size yields an increase in the void content present in the MSFRC matrix, ultimately decreasing the density.

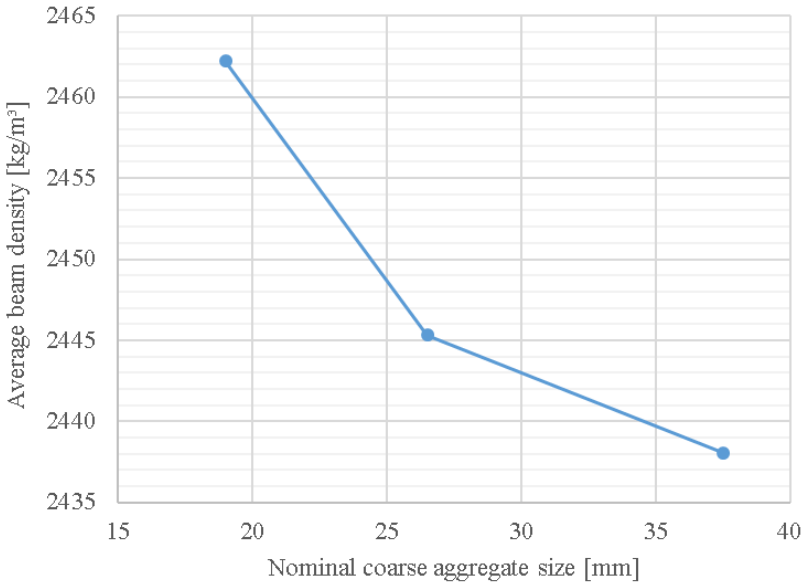

Figure 4.24: Average beam density versus nominal coarse aggregate size for a constant fibre dosage (4 kg/m^3)

4.5 Concluding summary

This chapter reported on the macro-mechanical performance of the CMS fibre. The macro-mechanical performance evaluation consisted of compressive strength tests, TPBTs, shrinkage tests and CT scans.

The following enumeration contains a summary of the conclusions drawn from the compressive strength tests:

1. A decrease in the compressive strength occurred for an increase in the W/C ratio for both considered cement types.
2. A decrease in the compressive strength occurred for an increase in nominal coarse aggregate size.
3. An optimal coarse aggregate volume of 400 l/m^3 was identified. A decrease in the compressive strength occurred for both an increase and decrease in coarse aggregate volume of 50 l/m^3.
4. A decrease in compressive strength occurred at high fibre dosages ($>$ 4.0 kg/m^3) due to a decrease in the cube densities.
5. Mixing time had a negligible affect on the compressive strength.

The results obtained according to the TPBTs are used to investigate the stated research hypotheses. The following enumeration contains a summary of the effect of the various influencing factors on the performance parameters:

1. Compressive strength significantly affected the LOP, but the extent is dependent on the cement type and class, with a cement extended with blastfurnace slag indicating an improved LOP. A slight increase in f_{R1} occurred for an increase in compressive strength. Referring to performance parameters f_{R2}-f_{R4}, compressive strength showed a negligible effect.
2. An increase in nominal coarse aggregate size tended to decrease the LOP as well as performance parameter f_{R1}. Referring to performance parameters f_{R2}-f_{R4}, coarse aggregate size showed a negligible effect.
3. An increase in coarse aggregate volume indicated an insignificantly effect on the LOP, but indicated a positive effect on f_{R1}-f_{R4}. It is concluded that a better test method should be considered to investigate the influence of coarse aggregate volume due to the large scatter of results.
4. Fibre dosage showed a negligible effect on the LOP. However, fibre dosage significantly affected f_{R1}-f_{R4}, with an increase in fibre dosage resulting in an increase in the RFTSs.
5. Mixing time showed a negligible effect on the LOP. Referring to f_{R1}, mixing time showed a insignificant effect for both mixer types. Referring to the pan mixer, f_{R2}-f_{R4} is significantly

decreased for prolonged mixing times exceeding 10 minutes. Conversely, mixing time showed a negligible effect on f_{R2}-f_{R4} for a tilting-drum mixer.

Shrinkage tests and CT scans were performed to provide additional information regarding the performance of the CMS fibre. From the shrinkage tests it is evident that the addition of the CMS fibre, at various dosages, does not significantly affect the shrinkage strain compared to that of plain concrete. The CT scans illustrated that an increase in the nominal coarse aggregate size increased the amount of voids present in the matrix and also contributed to a more bundled fibre distribution. It is also recommended that investigations consisting of only three data points should be increased. Interpretations of some of the datasets with three points, i.e. the effect of nominal coarse aggregate size and coarse aggregate volume, are dubious especially when the standard deviation of a point is so large that the other two points fall within this range.

Chapter 5

Single-fibre results

This chapter reports on the results obtained during the investigation of the influence of compressive strength on the single-fibre performance of the CHRYSO macro-synthetic experimental (CMS) fibre. The results include observations according to the single-fibre pull-out tests (SFPOT), as well as an analysis of the effect of mixing time with the aid of scanning electron microscopy (SEM) images.

The SFPOT results are discussed with regard to the peak loads resisted and the interfacial bond stress. The fibres were embedded either in its virgin or premixed state, i.e. undergoing mixing prior to embedment. Consequently, the results obtained for the virgin and premixed fibres are compared in order to firstly, establish the effect of compressive strength, and secondly the effect of fibre mixing on the single-fibre performance of the CMS fibre.

As for the macro-mechanical results, the conclusions are based on the average values of the observed data. Each set of tests consisted of four readings. The average of the four readings is used to represent the outcome of each data set. The error bars depicted on the graphs illustrate the standard deviation for each set of tests. The results for each sample which underwent single-fibre evaluation are provided in Appendix B.

5.1 Single fibre pull-out test results

The frictional and mechanical bond between synthetic fibres and the concrete matrix is the dominating bond in the post-cracking region, which enhances the toughness of FRC, and is thus of great interest (Domone, 2010). When fibres are incorporated in concrete and the concrete starts to crack, the load is transferred from the concrete matrix to the fibres bridging the crack opening. For equilibrium to be satisfied, a gripping force applied by the matrix onto the embedded fibre surface must be exerted to counteract the applied force, causing fibre pull-out in the form of a bond stress at the fibre-matrix interface. The interfacial bond stress is assumed to follow a constant shear stress distribution along the fibre length. Considering this assumption as well as assuming a circular cross-section of the fibre, Equation 5.1 can be derived:

$$\pi \cdot r_f^2 \cdot \sigma_f = 2 \cdot \pi \cdot r_f \cdot \tau \cdot l_f \tag{5.1}$$

where:
r_f = fibre radius
σ_f = tensile stress in fibre at a distance x from the fibre end
τ = interfacial bond stress along the length of the fibre
l_f = fibre length

By rearranging Equation 5.1, the interfacial bond stress at fibre pull-out can be determined considering Equation 5.2.

$$\tau = \frac{F_{max}}{\pi \cdot d_f \cdot l_e} \tag{5.2}$$

where:
F_{max} = maximum pull-out force
d_f = fibre diameter
l_e = fibre embedment length

An equivalent fibre diameter can be calculated if the considered fibre has an irregular cross-section. EN 14889-2 (European Norms, 2006) proposes Equation 5.3 to determine the equivalent diameter.

$$d_{eq} = \sqrt{\frac{4 \cdot m \cdot 10^6}{\pi \cdot l_d \cdot \rho}} \tag{5.3}$$

where:
d_{eq} = equivalent fibre diameter
m = mass of single-fibre (accurate to 0.001 g)
l_d = developed fibre length (accurate to 0.01 mm)
ρ = fibre material density

To investigate the effect of compressive strength on the single-fibre performance of the CMS fibre, three W/C ratios are considered, i.e. a W/C ratio of 0.45, 0.55, and 0.65. Table 5.1 indicates the average compressive strengths of the mortar samples for each W/C ratio. Appendix B.1 provides the compressive strength results of each mortar sample.

Table 5.1: Single-fibre mortar compressive strength results

W/C ratio	**Density (kg/m^3)**	**Compressive strength (MPa)**	**Standard deviation (MPa)**	**CoV (%)**
0.45	2232.35	71.78	6.06	8.4
0.55	2137.52	56.39	1.32	2.3
0.65	2179.10	50.35	2.52	5.0

The load corresponding to the elastic bond experienced during single-fibre pull-out can be distinguished as the peak load from the single-fibre pull-out response. As the pull-out resistance of a fibre is dependent on the surface area in direct contact with the hardened paste matrix, a result comparison can only be attained by converting the peak loads to interfacial bond stresses.

Figure 5.1 illustrates the pull-out force versus pull-out displacement of the CMS fibre in its virgin state for each W/C ratio. It should be noted that the graphs are in terms of the pull-out load resisted and not the interfacial bond stress. From Figure 5.1 it is clear that all the fibres pulled out and did not experience fibre fracture. For each specimen a maximum pull-out force (F_{max}) was reached, after which the resisting force decreased corresponding to a decrease in the fibre embedment length. It should be noted that the response of Sample 4, corresponding to a W/C ratio of 0.55, is significantly lower comparing to the rest of the samples in the set. Subsequently, this result was excluded from the analysis and could be attributed to the variable nature of the test. It is also evident that the single-fibre pull-out response of the virgin CMS fibre at a W/C ratio of 0.55 is different compared to a W/C ratio of 0.45 and 0.65. Not a clear conclusion could be drawn to explain this phenomenon. One possible explanation could be the variability associated with the test method. More samples for each W/C ratio should be tested to verify the single-fibre pull-out response of the CMS fibre in its virgin state at all the considered W/C ratios.

Figure 5.2 illustrates the pull-out force versus pull-out displacement of the CMS fibre in its premixed state for each W/C ratio. As previously mentioned, a premixed time of two minutes was implemented after the addition of the last fibre to the concrete mix. It is evident that there exits a larger variation in the responses of the CMS fibre in its premixed state for each W/C ratio which can be attributed to the premixing process, affecting each sample differently. It should also be noted that the response of Sample 2, corresponding to a W/C ratio of 0.45, and Sample 4, corresponding to a W/C ratio of 0.55, is significantly lower than the rest of the samples in their respective sets. As mentioned previously, these results were excluded from the analyses.

The response of Sample 3 (W/C ratio = 0.55) and Sample 4 (W/C ratio = 0.65) illustrates the occurrence of fibre fracture. In this case, the resisting force provided by the bond stress across the embedment length is greater than the force required for fibre fracture. This results in the sharp drop experienced by these samples as the tensile strength of the fibre was exceeded, causing fibre fracture. The fibres which experienced fibre fracture were disregarded in the calculation of the average interfacial bond stress experienced by the respective fibres.

Figure 5.3 illustrates the average peak load and Figure 5.4 illustrates the average interfacial bond stress experienced by the CMS fibre in its virgin and premixed state for each W/C ratio. The SFPOT results for each sample are provided in Appendix B.2.

From the single-fibre performance of the CMS fibre depicted in Figures 5.3 and 5.4, it is evident that an increase in the W/C ratio, i.e. a decrease in the concrete compressive strength, did not significantly influence the maximum pull-out load, and therefore the bond stresses, of the fibre in its virgin state. The bond between the fibre and the hardened paste matrix is dependent

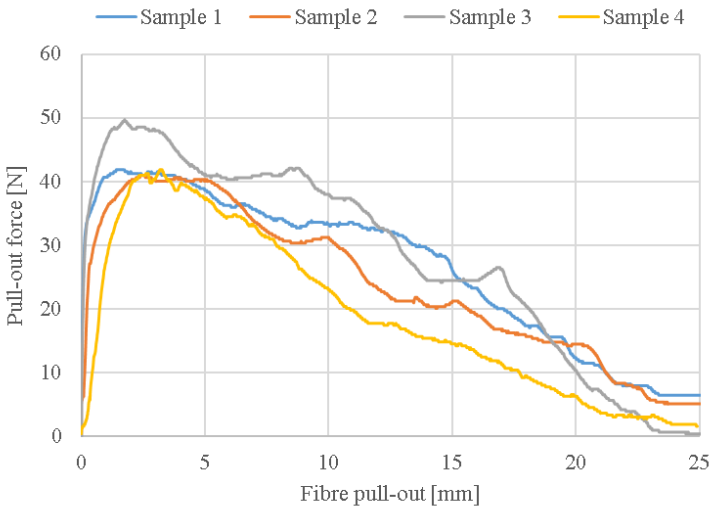

(a) W/C ratio = 0.45

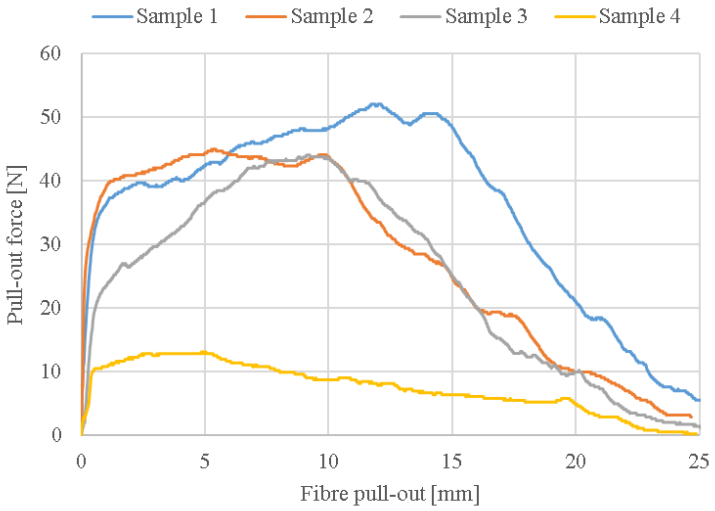

(b) W/C ratio = 0.55

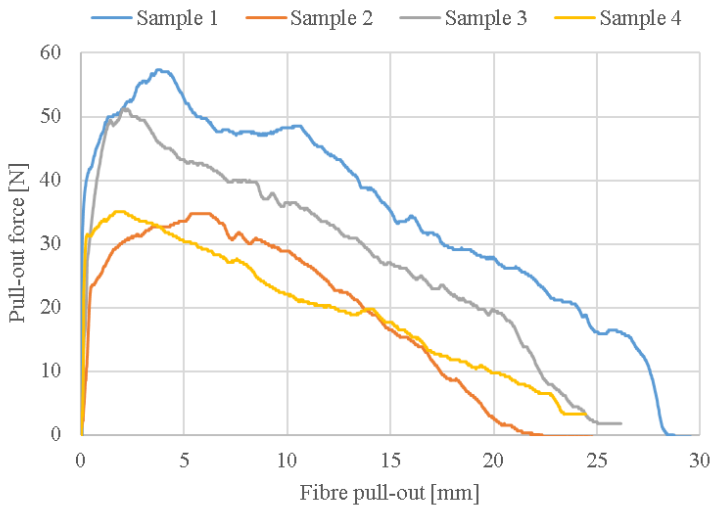

(c) W/C ratio = 0.65

Figure 5.1: Pull-out force versus pull-out displacement for the CMS fibre in its virgin state

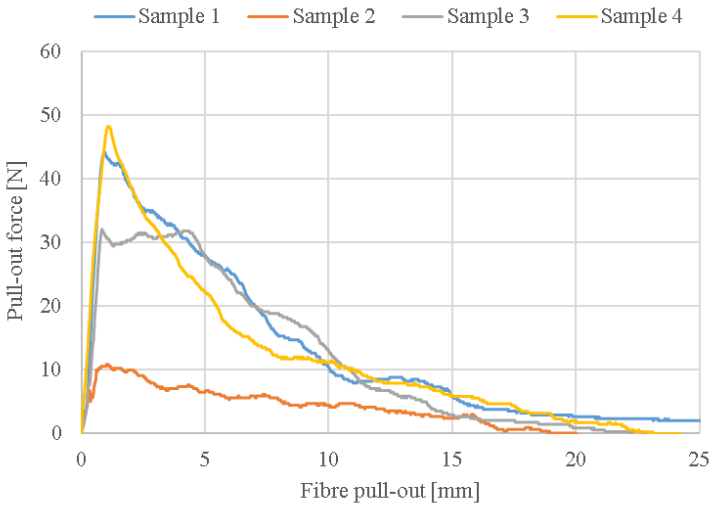

(a) W/C ratio = 0.45

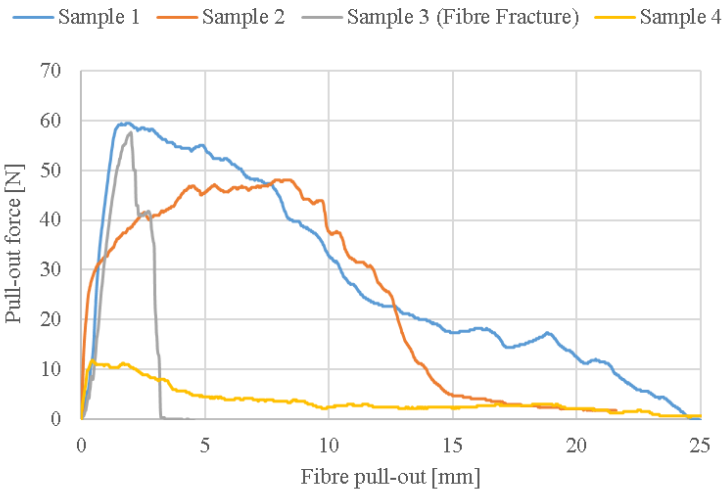

(b) W/C ratio = 0.55

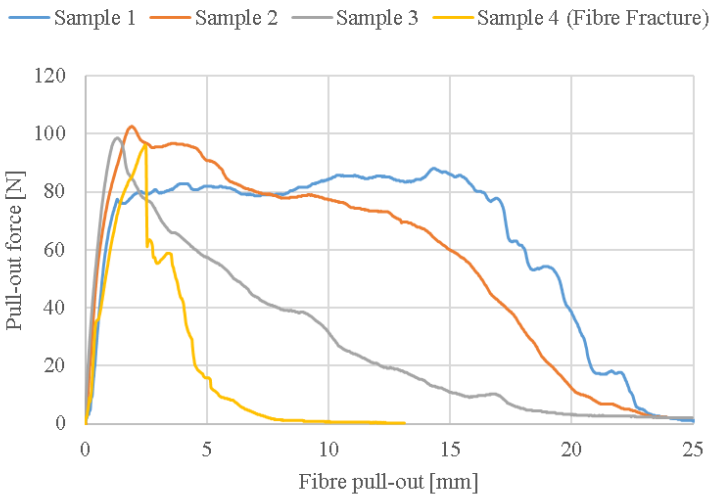

(c) W/C ratio = 0.65

Figure 5.2: Pull-out force versus pull-out displacement for the CMS fibre in its premixed state

on mechanical interlock and due to the flat and smooth surface of the fibre in its virgin state, an increase in compressive strength did not improve the performance of the fibre on single-fibre level. The insignificant influence of compressive strength could also be attributed to the chemical inertness of the CMS fibre and the fibre being hydrophilic. Odendaal (2015) reported that the influence of a changing W/C ratio is limited to flat fibres and not consistent for untreated fibres and that the single-fibre performance of untreated flat and non-flat fibres are not influenced for a W/C ratio between 0.4 to 0.6, but perhaps influenced by surface treatment.

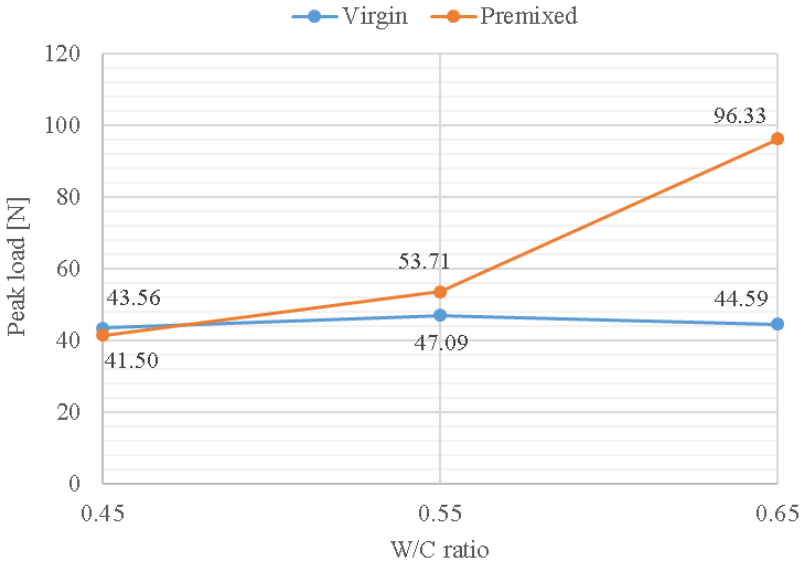

Figure 5.3: Single-fibre peak load experienced by the CMS fibre in its virgin and premixed state

From Figure 5.4 it is evident that the interfacial bond stress of the CMS fibre in its premixed state, increased for each W/C ratio. As reported by Lerch (2016), flat synthetic fibres with no significant deformations in its premixed state exhibit an increase in pull-out resistance as a result of premixing. The surface roughening caused by premixing can be regarded as the primary bond mechanism and is responsible for an enhanced fibre-matrix interlock.

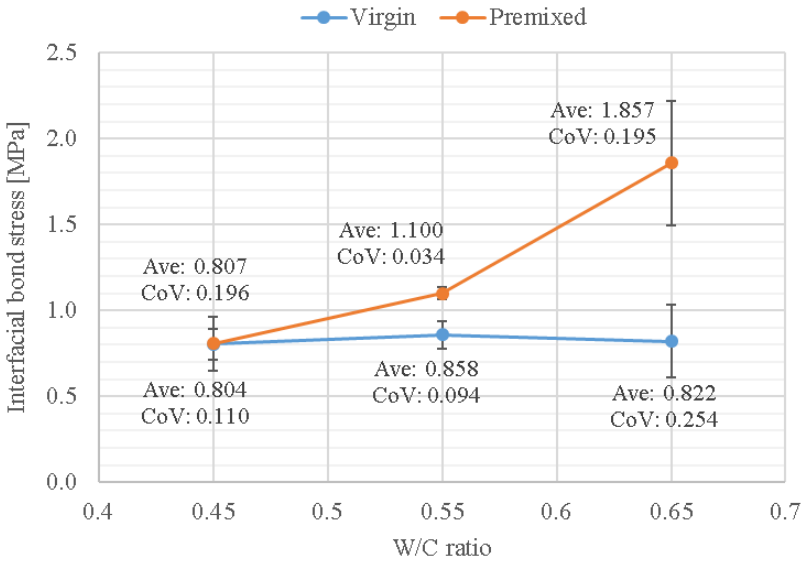

Figure 5.4: Single-fibre interfacial bond stress experienced by the CMS fibre in its virgin and premixed state

Table 5.2 indicates the comparison of the average interfacial bond stress experienced by the CMS fibre in its virgin and premixed state for the each W/C ratio.

Table 5.2: Comparison between the interfacial bond stress experienced by the fibre in its virgin and premixed state

W/C ratio	**Interfacial bond stress (MPa)**		**Percentage increase (%)**
	Virgin	**Premixed**	
0.45	0.804	0.807	0.37
0.55	0.858	1.100	28.21
0.65	0.822	1.857	125.91

According to Table 5.2 an increase in the percentage increase experienced in the interfacial bond stress for a decrease in compressive strength. These results are contradictory, as it was expected that the premixed fibres would experience a decrease in interfacial bond stress with an increase in W/C ratio due to a denser cement matrix and better fibre-matrix bond brought by a higher cement content. From the results presented, it is evident that other factors caused an increase in the interfacial bond stress experienced by the CMS fibre on a single premixed-fibre level for a decrease in compressive strength.

No research has been documented which could provide a possible explanation for the increase in the single-fibre pull-out resistance of macro-synthetic fibres for an increase in the W/C ratio. A possible explanation for the increase in the performance can be attributed to the increase in

the fine aggregate content due to the decrease in cement content associated with an increase in the W/C ratio. Due to the larger particle sizes of the fine aggregates compared to the cement particles, more severe surface roughening of the synthetic fibres would be experienced in the premixing process with an increase in the fine aggregate volume. This explanation is however only speculation, as all the fibres used in this investigation were premixed at one W/C ratio. Therefore, further research should be conducted to investigate this phenomenon.

It should also be noted that high Coefficient of Variations (CoV) (>0.10) are indicated for all data points on Figure 5.4, except the data points corresponding to a W/C ratio of 0.55. Thus, to draw indisputable conclusions on the effect of compressive strength on the single-fibre performance of macro-synthetic fibres in its premixed state, more samples should be prepared and tested to create a larger sample size due to the higher variability experienced by the uncontrollable surface roughening caused by the premixing process.

The results of the fibre in its premixed state also does not correlate with the macro-mechanical results presented in Chapter 4 which illustrated that performance parameters f_{R2}-f_{R4} were not linked to the W/C ratio, with f_{R1} slightly influenced by compressive strength. To compare the SFPOT results and the macro-mechanical results, the interfacial bond stress of the fibre in its virgin and premixed state at fibre pull-out distances (POD) of 0.5, 1.5, 2.5, and 3.5 mm respectively, is compared to the f_{R1}-f_{R4} results for each W/C ratio. The physical significance of comparing the bond stress of the CMS fibre to the residual flexural performance parameters is to determine whether the flexural performance could be compared to the tensile performance of the fibre. The comparison between the SFPOT results and the macro-mechanical results for each W/C ratio is illustrated in Figure 5.5. It should be noted that the average of each set of tests, excluding specimens which were identified as outliers or specimens that underwent fibre fracture, was used to represent the interfacial bond stress at the different PODs.

According to Figure 5.5, no specific relationship exists between the interfacial bond stress and the residual flexural tensile strength of the CMS fibre at fibre PODs equal to the specified CMODs. Figures 5.5b and 5.5c indicates an improved interfacial bond stress for the fibre in its premixed state comparing to the virgin fibre. Figure 5.5c also depicts a much improved interfacial bond stress of the fibre in its premixed state, with the bond stress exceeding the residual flexural tensile strengths at PODs of 1.5, 2.5, and 3.5 mm respectively. It should also be noted that while the residual flexural tensile strengths decreased for an increase in the CMOD for each W/C ratio, the interfacial bond stress for the fibre in its virgin and premixed state has not reached its maximum at the considered PODs.

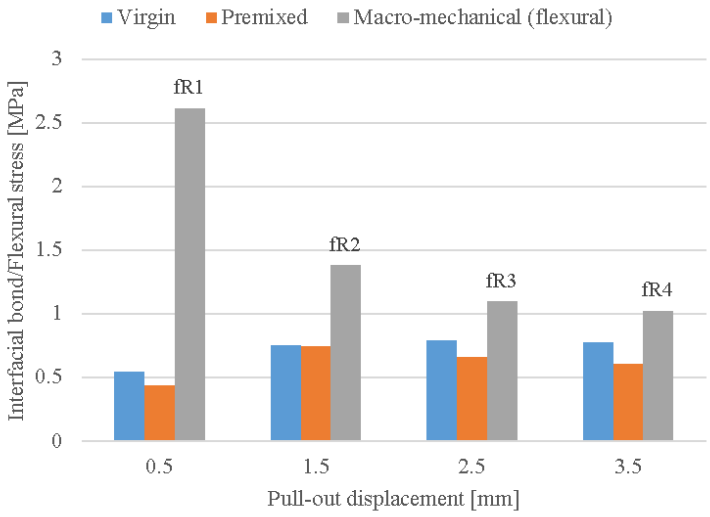

(a) W/C ratio = 0.45

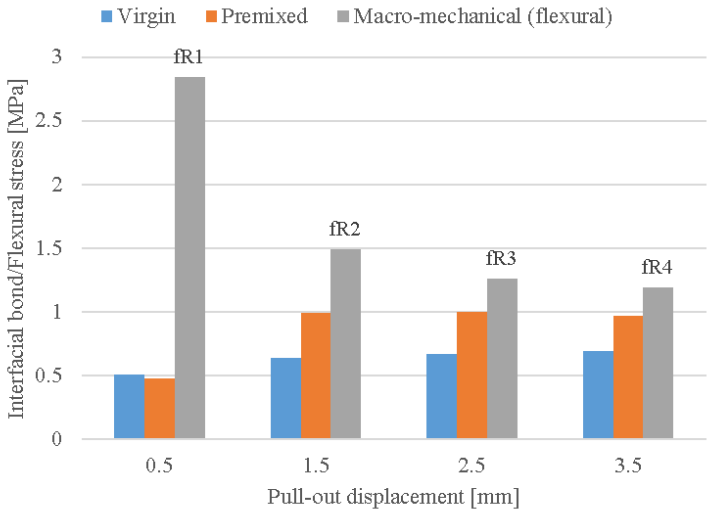

(b) W/C ratio = 0.55

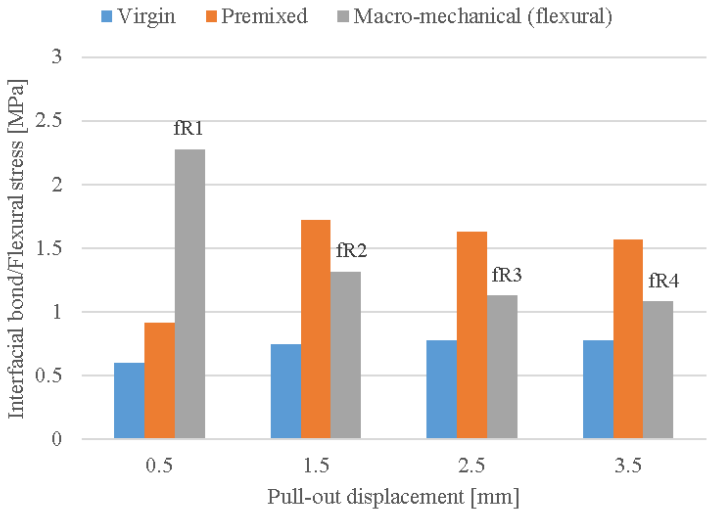

(c) W/C ratio = 0.65

Figure 5.5: Comparison between the SFPOT results and the macro-mechanical results

5.2 Scanning Electron Microscopy (SEM) results

Scanning electron microscopy (SEM) images of the CMS fibre were used as a surface analysis tool and taken to illustrate the effect of mixing time and mixing process on fibre surface damage. The SEM images provides valuable information regarding the fibre geometry and are used for the surface analysis of the CMS fibre subjected to the various mixing times and compared to the fibre in its virgin state.

The following figures illustrates the comparison between the fibre under SEM conditions and the physical appearance of the fibre. Figure 5.6 depicts the surface of the CMS fibre in its virgin state in the absence of any surface roughening.

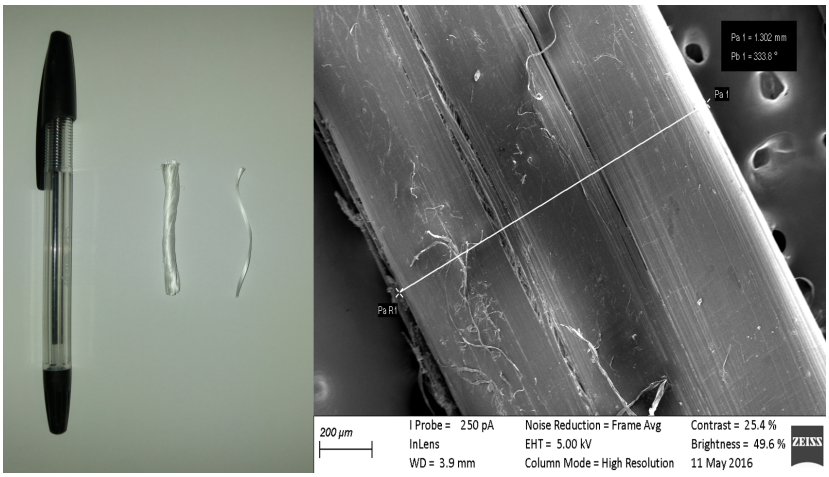

Figure 5.6: Comparison between the physical appearance and the SEM image of the fibre in its virgin state

The premixing affect of a pan mixer is shown in Figures 5.7 to 5.12 and depicts the premixed fibre surface after the different mixing times.

Figure 5.7: Comparison between the physical appearance and the SEM image of the fibre after a mixing time of 2 minutes

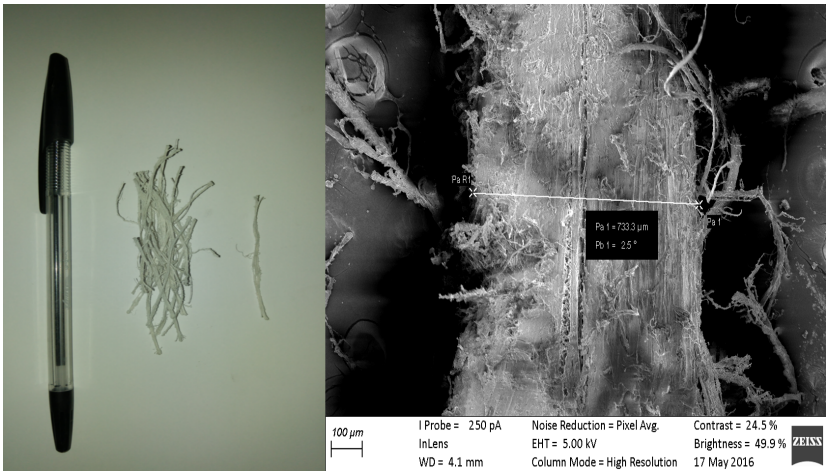

Figure 5.8: Comparison between the physical appearance and the SEM image of the fibre after a mixing time of 5 minutes

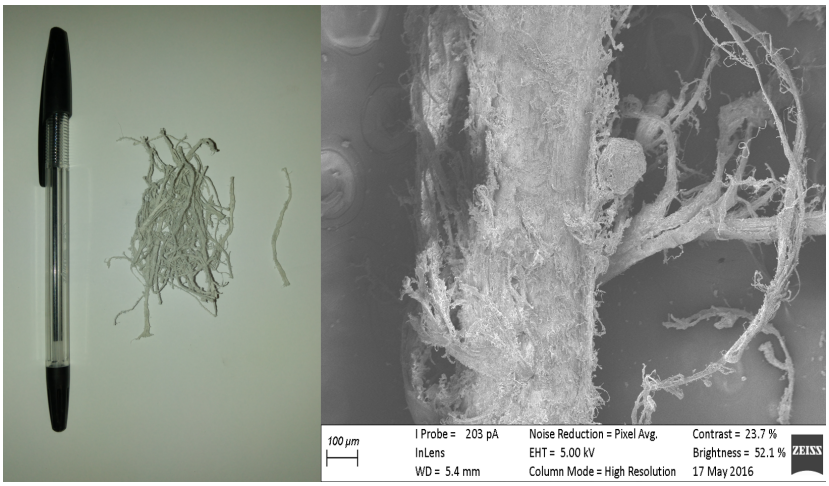

Figure 5.9: Comparison between the physical appearance and the SEM image of the fibre after a mixing time of 10 minutes

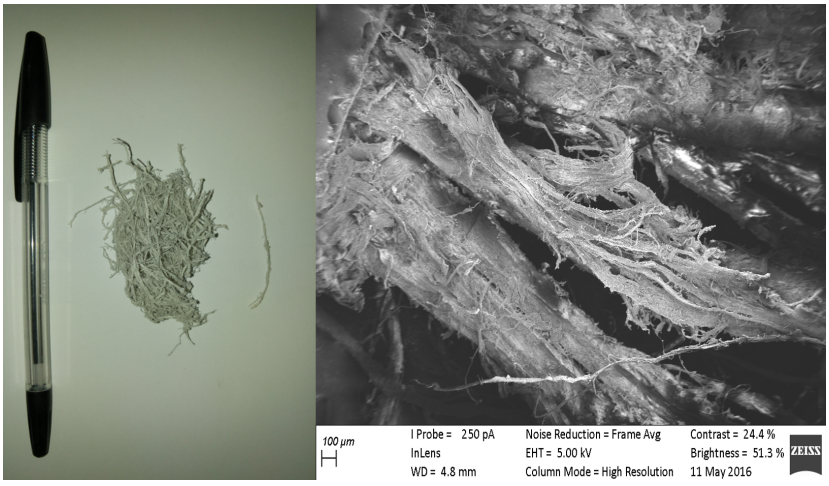

Figure 5.10: Comparison between the physical appearance and the SEM image of the fibre after a mixing time of 20 minutes

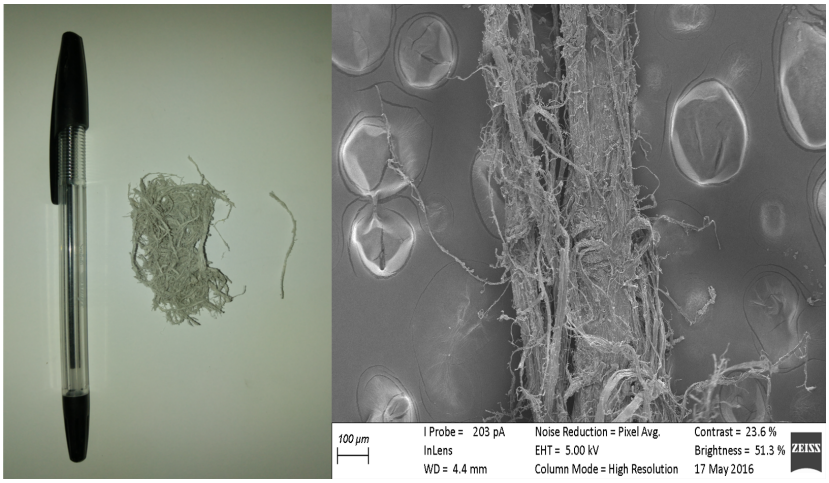

Figure 5.11: Comparison between the physical appearance and the SEM image of the fibre after a mixing time of 30 minutes

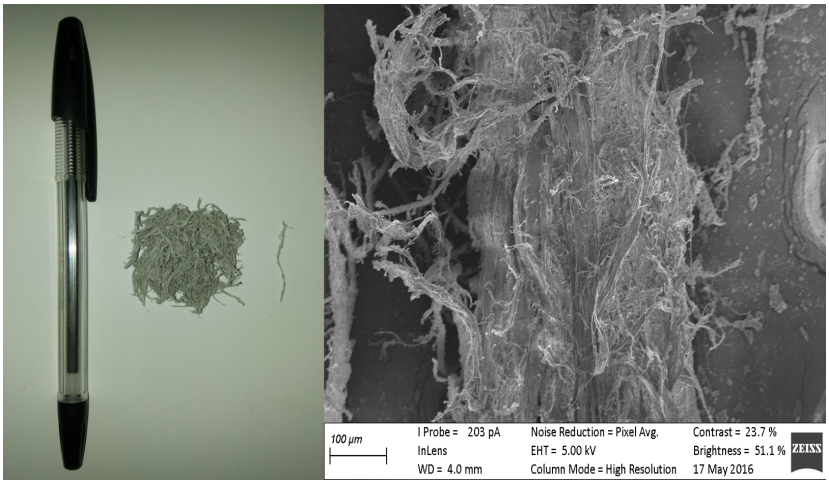

Figure 5.12: Comparison between the physical appearance and the SEM image of the fibre after a mixing time of 60 minutes

From the TPBT results presented in Section 4.2, it is evident that the different mixing times for the tilting-drum mixer showed a negligible effect on the residual flexural performance of MSFRC. Figure 5.13 depicts the premixed surface of the fibre after a mixing time of 60 minutes in a tilting-drum mixer.

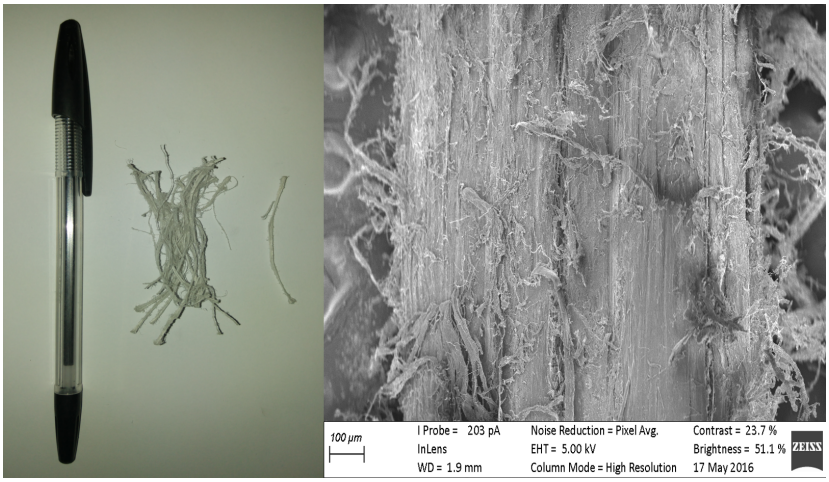

Figure 5.13: Comparison between the physical appearance and the SEM image of the fibre after a mixing time of 60 minutes in a tilting-drum mixer

The SEM images of the individual fibre surfaces indicates the extent of the surface damage caused by an increase in mixing time for a pan mixer. Comparing the SEM images of the CMS fibre in both fibre states, the premixed fibres are characterised by significant surface roughening, fine scrapings and a decrease in fibre length. In the bottom left corner of each SEM image, a scaling bar is presented indicating a constant magnification of 100 μm. It is also important to note that the working distance, being the distance between the microscope-lens and the specimen, was less than 4 mm during the acquisition of the images.

At first it was anticipated that macro-synthetic fibres would exhibit an increase in interfacial bond with the surrounding concrete matrix with an increase in mixing time due to fibre surface damage, while a poor interfacial bond would exits with little fibre surface damage. From the TPBT results presented in Section 4.2 it was evident that an increase in the residual flexural performance of the CMS fibre exits for a mixing time up to 10 minutes for a pan mixer. For the mixing times exceeding 10 minutes, a substantial decrease in the residual flexural performance occurred.

From previous research (Lerch, 2016), it was documented that the performance of macro-synthetic fibres with flat profiles are susceptible to premixing, stating that premixing flat macro-synthetic fibres considerably influences the bond characteristics and that provided surface corrugations do not significantly affect the fibre-matrix interaction of flat fibres, but rather the surface roughening caused by the premixing process. The same explanation can be provided for the increase in the performance up until a mixing time of 10 minutes.

From the SEM images it is evident that the width of the fibres decreased with an increase in mixing time and that extensive fibre deterioration occurred for mixing times exceeding 10 minutes, thus having a negative impact on the performance as indicated in Section 4.2. The increased mixing times caused the fibrillated CMS fibre to break down into its individual fibrils and the tensile strength of the fibre contributing to the performance was significantly decreased. Referring to the SEM image shown in Figure 5.13, it is evident that the surface damage and the

deterioration of the CMS fibre are less susceptible to the mixing process considering a tilting-drum mixer due to the lower mechanical performance of the mixer, providing a reason for the negligible influence an increase in mixing time had on the residual flexural performance of the CMS fibre for a tilting-drum mixer.

5.3 Concluding summary

The SFPOT results revealed that a change in compressive strength does not influence the pull-out resistance of the CMS fibre in its virgin state. This can be attributed to the smooth surface of the fibre in its virgin state, providing a lack of mechanical interlock between the fibre and the concrete matrix. The insignificant influence of compressive strength could also be attributed to the chemical inertness of the CMS fibre and the fibre being hydrophilic.

Furthermore, it is shown that an increase in the pull-out resistance occurred for the CMS fibre in its premixed state in contrast to its virgin state for a W/C ratio of 0.55 and 0.65. The enhanced interlock can be attributed to the surface roughening of the fibres caused by premixing and can be regarded as the primary mechanism responsible for the better bond exhibited by flat macro-synthetic fibres. It is also indicated that a decrease in compressive strength positively effected the interfacial bond stress experienced by the CMS fibre in its premixed fibre state. A possible explanation for the increased performance can be attributed to the increase in fine aggregate volume associated with an increase in the W/C ratio which can cause more severe surface roughening of the synthetic fibre, enhancing the bond of the fibre to the cement matrix and ultimately improving the pull-out resistance. It is concluded that further research should be conducted to investigate this phenomenon. It is also concluded that there is no significant relationship between the single-fibre performance and the macro-mechanical performance of the CMS fibre.

The SEM images revealed that extensive deterioration and damage of the fibre surface occurred for mixing times exceeding 10 minutes for a pan mixer. The increased mixing times caused the fibre to break up into its individual fibrils, decreasing the tensile strength of the fibre contributing to the flexural performance. It is also evident that the CMS fibre is less susceptible to the mixing process for a tilting-drum mixer due to its less severe mechanical performance compared to a pan mixer.

Chapter 6

Linear models predicting the performance of MSFRC

This chapter reports on the results of simple- and multiple regression analyses used to investigate the relationships between the independent variables (IVs) and each dependent variable (DV) and ultimately to determine generic models predicting the performance of macro-synthetic fibre reinforced concrete (MSFRC). The outcome of the regression analyses are based on the macro-mechanical results presented in Chapter 4.

6.1 Regression Analysis

The second objective of this study entailed the development of generic models predicting the performance, i.e. the residual flexural tensile performance, of MSFRC at specified crack mouth opening displacements (CMOD) of the CHRYSO macro-synthetic experimental (CMS) fibre.

The generic models predicting the performance of MSFRC are based on the identified independent variables (IV) having a significant effect on each performance parameter, i.e. f_{R1}, f_{R2}, f_{R3}, f_{R4} and f_{LOP}. A regression analysis is a technique implemented to explore the relationships between a single dependent variable (DV) and one or more IVs. The objective of a regression analysis is predicting the dependent variable by using the IVs whose values are known. Table 6.1 indicates the dependent and independent variables considered for the regression analyses.

A regression analysis assumes that the mean of a random variable Y is related to an IV x by considering a straight-line relationship. For a simple linear regression analysis, the expected value of Y for each value of x is:

$$E(Y|x) = \gamma_0 + \gamma_1 \cdot x \tag{6.1}$$

The intercept is given by γ_0. The slope (γ_1) is known as the regression coefficient. Only the mean of Y is a linear function of x and the actual observed value does not fall precisely on a straight line. Generalising this problem to a probabilistic linear model, it is assumed that the expected value of Y is a linear function of x, but considering a fixed value of x, the actual value of Y is determined by the linear model plus a random error term:

Table 6.1: Dependent and independent variables considered for the regression analyses

Dependent Variables (DV)	f_{R1}
	f_{R2}
	f_{R3}
	f_{R4}
	f_{LOP}
Independent Variables (IV)	Compressive strength (MPa)
	Nominal coarse aggregate size (mm)
	Coarse aggregate volume (l/m^3)
	Fibre dosage (kg/m^3)
	Mixing time (min)

$$Y = \gamma_0 + \gamma_1 \cdot x + \xi \tag{6.2}$$

The random error term (ξ) has a mean of zero and an unknown variance (σ^2). The random errors arising from the various observations are assumed to be uncorrelated random variables.

As for this study, many applications involve situations in which there exits more than one IV. A multiple linear regression analysis considers two or more IVs (x_n) in the prediction of the DV (Y) and can be described using Equation 6.3.

$$Y = \gamma_0 + \gamma_1 \cdot x_1 + \gamma_2 \cdot x_2 + \cdots + \gamma_n \cdot x_n + \xi \tag{6.3}$$

The parameters γ_j (j=0, 1, ..., n) are referred to as the regression coefficients and represents the expected change in Y per unit change in x_n when all the remaining IVs x_m ($m \neq n$) are held constant. By performing a multiple linear regression analysis, the simple linear regression model is expanded by adding IV(s) which indicates the greatest additional predictive power.

To explore the multiple linear regression analyses, various methods can be considered. The coefficient of determination (R^2) serves as a substantial analysis tool and was considered in this study. R^2 represent the amount of variance in the outcome that can be explained by the regression model relative to how much variation there existed using the mean value. As a percentage, it represents the percentage of variation in the outcome that can be explained by the regression model. It also represents the combined effect of the entire variate, i.e. one or more independent variable plus the intercept, in predicting the dependent variable. The R^2 value ranges from 1.0 (perfect prediction) to 0.0 (no prediction) and is calculated as follows:

$$R^2 = \frac{SS_M}{SS_T} \tag{6.4}$$

where:
SS_M = Model sum of squares
SS_T = Total sum of squares

To determine SS_T, the differences between the observed values and the mean value for each DV must be calculated. SS_T is equal to the summation of the squared differences. The model sum of squares (SS_M) is determined by calculating the difference between SS_T and the sum of squared residuals (SS_R). SS_R corresponds to the differences between the observed values and the predicted values according to the regression model can be determined by the summation of the squared differences.

The F_{ratio} test is also implemented as a comparative tool. The test is based on the ratio of the improvement due to the model (SS_M) and the difference between the observed values and the values predicted by the model (SS_R). Rather than using the sum of squares, the mean sum of squares (MS) are used in the F_{ratio} test. For calculating the mean sum of squares it is necessary to divide by the degrees of freedom:

$$\begin{aligned} MS_M &= \frac{SS_M}{df_M} \\ MS_R &= \frac{SS_R}{df_R} \end{aligned} \tag{6.5}$$

where:
df_M = Number of estimated coefficients (including intercept) - 1
df_R = Sample size - Number of estimated coefficients (including intercept)

$$F_{ratio} = \frac{MS_M}{MS_R} \tag{6.6}$$

Dividing each sum of squares by its appropriate degree of freedom, results in variance estimation. MS_M is the variance explained by the regression model, while MS_R is the unexplained variance. If the ratio between the explained and the unexplained variance is high, the regression variate is of significant value in explaining the dependent variable.

Interpreting the statistical significance of each IV required a specified acceptable level of statistical error. The most common approach is to specify the level of Type I error (α-value) which is the probability of rejecting the null hypothesis, also referred to as a false positive. By specifying an α-value, an acceptable limit for error is set and indicates the probability of concluding that significance exists for the various IVs (Montgomery and Runger, 2007). An α-value of 0.05 was considered throughout the regression analyses, suggesting that an IV with a P-value $\leq$ 0.05 indicated as having a significant influence on the considered dependent variable.

Due to variation in response scale and variability across variables, direct interpretation about the effect of variables is problematic. Standardisation is used to convert independent variables to

a common scale and variability when performing a multiple linear regression analyses, the most common being a mean of zero and a standard deviation of one (Hair et al., 2010). In this way, all variables are comparable. Not only does a multiple regression analysis provide regression coefficients, it also provides coefficients resulting from the analysis of standardised data termed beta (β) coefficients. The beta coefficients eliminate the problem of dealing with different units of measurement and reflect the relative impact a change in one standard deviation in either IV has on the DV.

Initially, simple linear regression analyses are performed for between each DV and IV individually, to gain insight and explore the relationships between the separate variables. Multiple linear regression analyses are performed following the simple linear regression analyses to identify the IVs having the most significant effect on the DVs, and to determine a linear model predicting the various DVs based on the output of the multiple linear regression analyses. The regression analyses are completed using a statistical analysis software package STATISTICA v13. The package provides comprehensive array of data analysis, data management, data visualisation, and its techniques included a wide selection of predictive modelling.

6.2 Simple linear regression analysis results

This section presents the results obtained and includes a detailed discussion of the simple linear regression analyses. To investigate the separate relationships between each IV and DV, the probability of rejecting the null hypothesis for a specified α-level is of special interest. An α-level of 0.05 is considered throughout the regression analyses, indicating an IV with a P-value ≤ 0.05 as having a significant influence.

Table 6.2 provides the significance (P-value) of each IV for each DV. A comprehensive indication of the simple linear regression results are presented in Appendix A.3. It should be stated that the results presented in Table 6.2 are based on the average values of the observed data, and not the raw data values. As each set of tests consisted of six specimens, the average of each set is used in the regression analyses. The average values are considered to appropriately represent the result of each set, as the large variation experienced between the raw data values are not attributed to the variation in the material properties, but rather the implemented test setup as the small crack-plane utilised a large variation in results. The large variation between the raw data values would unfairly influence the outcome of the regression analyses as the analyses are sensitive to the differences between the observed data values and the predicted values. Appendix A.3 does however present a comparison between the simple linear regression analyses implementing the raw data values and the average values.

Table 6.2: P-values of each IV according to the simple linear regression analyses considering a α-level of 0.05

Independent Variable	**P-values**				
	f_{R1}	f_{R2}	f_{R3}	f_{R4}	f_{LOP}
Compressive strength - 42.5N CEM III (MPa)	0.208	0.675	0.618	0.561	0.000065
Compressive strength - 52.5N CEM II (MPa)	0.204	0.533	0.128	0.181	0.0009
Coarse aggregate size (mm)	0.346	0.764	0.773	0.739	0.451
Coarse aggregate volume (l/m^3)	0.245	0.435	0.142	0.282	0.471
Fibre dosage (kg/m^3)	0.043	0.002	0.0002	0.0012	0.640
Mixing time - Tilting-drum mixer (min)	0.792	0.779	0.091	0.137	0.235
Mixing time - Pan mixer (min)	0.233	0.054	0.0198	0.0074	0.319

From Table 6.2 it is evident that fibre dosage is the IV indicating the most significant influence on f_{R1} to f_{R4}. It can also be concluded that mixing time, considering a pan mixer, indicates as having a significant influence on f_{R3} and f_{R4}, with a close-to-significant effect (p-value = 0.054) on f_{R2}. Compressive strength, for both cement types, was the only independent variable having a significant influence of f_{LOP}.

The simple linear regression results support the macro-mechanical results illustrated in Section 4.2, with fibre dosage indicating a definite effect on f_{R1} to f_{R4}, and compressive strength indicating a definite effect on f_{LOP}. It should however be noted that while some of the results presented in Section 4.2 indicated several IVs as having an effect on the DVs, the variability of those results influenced the outcome of the simple linear regression analyses, ultimately indicating a non-significant effect. From the results presented in Appendix A.3, it should be noted that compressive strength, considering the raw data values, indicated as having a significant effect on f_{R1}, f_{R3}, and f_{R4}. Due to these contradicting results, additional tests were completed for W/C ratios between 0.45 to 0.65 (increments of 0.05), at fibre dosages ranging between 3.0 to 5.0 kg/m^3 (increments of 0.5), to enlarge the data set representing the influence of compressive strength and fibre dosage on the DVs. The results of the additional tests are presented in Section 6.3, due to the effect depending on multiple variables.

6.3 Multiple linear regression analysis results

To create generic models for predicting the post-cracking performance of MSFRC, multiple linear regression analyses are performed to analyse the relationships between the IVs and the DVs. Due to the nature of the study consisting of more than one IV, a multiple linear regression analysis is deemed adequate as it considers the effect of two or more IVs in predicting the DV. The

objective of the multiple linear regression analyses is to use the IVs whose values were known to predict the DVs.

The results of the simple linear regression analyses, as indicated in Section 6.2, gave an indication of the separate effect of the IVs on each DV. However, the effect of the interaction between the various IVs is not considered in the simple linear regression analyses. The interaction between the IVs is important to consider, as it is possible that their combined effect was greater than the sum of their separate effects, creating a synergy. On the contrary, a possibility also existed that the interaction between the IVs caused the opposite of a synergy, i.e. producing a combined effect worse than the sum of their separate effects.

The first step of the multiple linear regression analyses is to perform a univariate test of significance for each DV. The univariate test of significance takes account of the effect of all IVs and identifies the IVs with the most significant effect. A restricted parameterisation test, i.e. a solution process considering the effect of all the IVs, is followed by a best subset solution, which assesses the fit of the regression model using ordinary least squares (Mallow's C_p) to find the best model involving a set of the IVs, and a forward stepwise solution (if necessary) to eliminate the IVs which does not have a significant effect on the DVs. The restricted parameterisation test also determined the regression parameter estimates, as well as the significance of each regression model. Appendix A.4 provides a comprehensive comparison between the multiple regression analyses.

As for the simple linear regression analyses, the multiple linear regression analyses are based on the average values from the observed data. It should be noted that the observed data corresponding to the 42.5N CEM III cement, as well as mixing time corresponding to the pan mixer, are excluded from the multiple linear regression analyses. The 42.5N CEM III results are excluded due to the 52.5N CEM II cement being the reference cement type. The data corresponding to mixing time for a pan mixer are excluded due to the observed data from the tilting-drum mixer corresponding to the reference mixing time of 5 minutes. The effect of mixing time is also better represented by the results corresponding to the tilting-drum mixer, due to the nature of the mixing process being comparative with a ready-mix truck.

Table 6.3 indicates the significance of each IV on the DVs according to the univariate tests of significance, implementing an α-level of 0.05. As shown in the simple linear regression analyses, fibre dosage (kg/m^3) is the only IV indicating a significant influence on f_{R1} to f_{R4}. It can also be concluded that compressive strength (MPa) is the only IV having a significant influence on f_{LOP}. Appendix A.4 provides a comprehensive comparison between the univariate tests of significance for each DV. It is important to note that the outcome of the various multiple linear regression analyses are based on a primary interaction between all the IVs. Secondary affects, i.e. the secondary interactions between IVs, are excluded from the analyses due to the limited time frame of the study. To simplify the investigations, reference levels for each IV are chosen, providing more data points at specific levels. For an absolute accurate outcome of the multiple linear regression analyses,the secondary interactions between the IVs should also be investigated, which will require tests other than the chosen reference levels for each IV.

Table 6.3: P-values of each IV according to the univariate tests of significance considering a α-level of 0.05

Independent Variable	**P-values**				
	f_{R1}	f_{R2}	f_{R3}	f_{R4}	f_{LOP}
Compressive strength (MPa)	0.164	0.837	0.065	0.164	0.000026
Coarse aggregate size (mm)	0.914	0.743	0.416	0.275	0.631
Coarse aggregate volume (l/m^3)	0.194	0.405	0.165	0.262	0.563
Fibre dosage (kg/m^3)	0.007871	0.000029	0.000000	0.000001	0.912
Mixing time (min)	0.362	0.649	0.282	0.352	0.616

From the multiple linear regression results it is evident that all of the DVs are dependent on a single IV. Table 6.4 provides the regression model parameter estimates for each DV. The solution process implemented for each DV, as well as the identified IV predicting the DV, are also presented. It is important to note that the regression models are calculated, and is valid, for fibre dosages between 2.5 and 5.5 kg/m^3 and compressive strengths for a 52.5N CEM II cement with W/C ratios ranging between 0.4− and 0.8. A comprehensive comparison between the regression model parameter estimates for each DV is presented in Appendix A.4.

Table 6.4: Summary of the regression model parameter estimates

Dependent Variable	**Solution process**	**Independent Variable**	**Regression model parameters**	
			Intercept	**Regression coefficient (γ)**
f_{R1}	Best subset solution	Fibre dosage (kg/m^3)	1.567	0.249
f_{R2}	Best subset solution	Fibre dosage (kg/m^3)	0.470	0.251
f_{R3}	Forward stepwise solution	Fibre dosage (kg/m^3)	0.045	0.303
f_{R4}	Best subset solution	Fibre dosage (kg/m^3)	-0.098	0.321
f_{LOP}	Best subset solution	Compressive strength (MPa)	2.641	0.050

Table 6.5 provides a comparison between the significance of each regression model corresponding the different solution processes for each DV. It is evident that the coefficient of determination (R^2), representing the percentage variation explained by the regression models, decreased by implementing the solution process used to determine the final regression model for each DV. The decreased R^2 values can be attributed to the insignificant IVs being excluded in the final regression models, ultimately decreasing the percentage variation explained by the models. It should also be noted that the percentage variation explained by the regression models for f_{R2} to f_{R4}, and f_{LOP}, are much higher than for f_{R1}, suggesting that the excluded IVs notably influenced f_{R1}.

An increase in the F_{ratio}, which represents the ratio between the explained and unexplained variance associated to the regression models, is also evident for each DV according to Table 6.5. The increase in the F_{ratio} suggests that the regression variate is of significant value in explaining the DV, ultimately improving the predictive ability of each model.

Table 6.5: Significance of the regression models considering the various solution processes

Dependent Variable	**Solution process**	**R^2 (%)**	**F_{ratio}**	**P-value**
f_{R1}	Restricted parameterisation	38.4	2.745	0.045
	Best subset	25.9	9.075	0.006
f_{R2}	Restricted parameterisation	56.5	5.726	0.002
	Best subset	54.4	31.028	0.000
f_{R3}	Restricted parameterisation	72.6	11.655	0.000
	Best subset	70.0	18.709	0.000
	Forward stepwise	64.7	47.712	0.000
f_{R4}	Restricted parameterisation	68.5	9.567	0.000
	Best subset	62.2	42.748	0.000
f_{LOP}	Restricted parameterisation	61.1	6.919	0.001
	Best subset	59.7	38.481	0.000

As mentioned in Section 6.2, the influence of a change in compressive strength on f_{R1} is further investigated as a result of the simple linear regression analysis results. The low coefficient of determination (R^2) of the regression model predicting f_{R1}, shown in Table 6.5, supports the reason for conducting an expanded investigation. A multiple linear regression analysis is conducted to investigate the influence of compressive strength and fibre dosage for W/C ratios of 0.45, 0.55 and 0.65, at fibre dosages of 3.0, 4.0, and 5.0 kg/m^3, respectively. Table 6.6 provides the significance of compressive strength and fibre dosage on f_{R1} separately, as well as the regression model significance considering both compressive strength and fibre dosage to predict f_{R1}. Appendix A.2 provides a comprehensive comparison between the additional TPBT results. Referring to the data presented in Appendix A.2, it should be noted that the data for a fibre dosage of 4 kg/m^3 and a W/C ratio of 0.55, is as presented in Appendix A.2.

Table 6.6: Significance of compressive strength and fibre dosage on f_{R1}

Independent Variables	**Univariate test of significance**	**Regression model significane**		
	P-values	**R^2 (%)**	**F_{ratio}**	**P-value**
Compressive strength (MPa)	0.338735	81.3	13.077	0.0065
Fibre dosage (kg/m^3)	0.002475			

The results presented in Table 6.6 supports the results presented in Table 6.3, indicating fibre dosage as the only IV having a significant influence on f_{R1}. It should however be noted that that an improved R^2 is calculated, 81.3% versus 25.9%, indicating an improved percentage of the variation being explained by the regression model by incorporating the effect of compressive strength and fibre dosage. For the purpose of this study, the regression models predicting the performance parameters are based on the IVs having a definite effect (p-value ≤ 0.05) on the DV, therefore excluding the effect of compressive strength in the regression model predicting f_{R1}.

Figure 6.1 illustrates the relationship between f_{R1} and a change in the LOP. After the obtained results and according to the scatter plot, it seems from a visual inspection that a relationship exists between a change in the LOP and f_{R1}, with an increase in the f_{R1} corresponding to an increase in the LOP. However, the relative low R^2 value indicates that the relationship is not that strong.

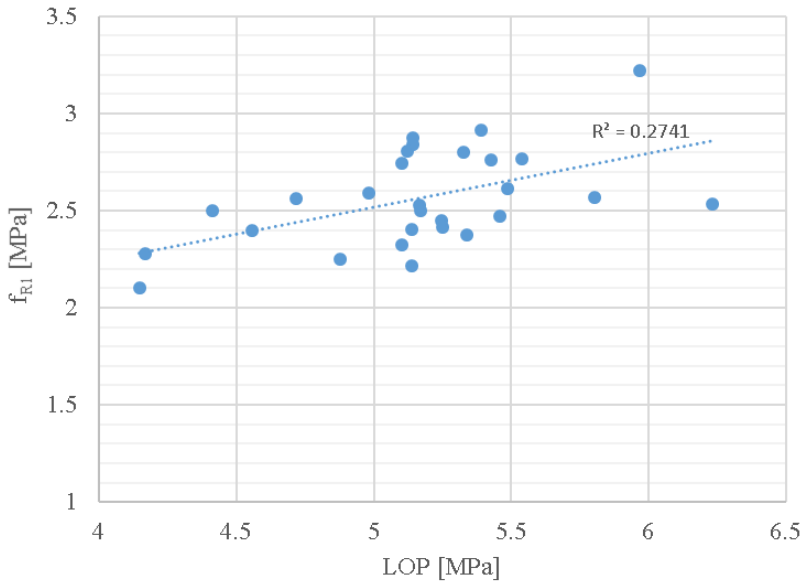

Figure 6.1: Relationship between f_{R1} and a change in the LOP

A multiple regression analysis is performed to investigate the relationship between f_{R1} to f_{R4} and the influence of a change in the LOP and fibre dosage, which is identified as an IV having a significant influence on the residual flexural strength of MSFRC. Additional tests were completed

to provide a complete data set to investigate the relationship. As the LOP is dependent on the compressive strength, the additional tests consisted of mixes with a W/C ratio varying between 0.45 and 0.65 (increments of 0.05) and a fibre dosage ranging between 3 and 5 kg/m^3 (increments of 0.5). A comprehensive comparison between the TPBT results for the additional tests is provided in Appendix A.2.

The results of the multiple regression analysis is provided in Table 6.7. The significance of the two independent variables considered is of concern, thus the p-values for each DV is used as a comparative measurement. Supporting the results presented in Table 6.3, fibre dosage is identified as having a signicant influence of f_{R1} to f_{R4} and a change in the LOP does not have a significant influence on each of the residual strengths. The statistical analysis of the data therefore does not correlate with the visual inspection of the results which indicated a relationship between specifically f_{R1} and a change in the LOP. As previously mentioned, only IVs having a definite effect (p-value ≤ 0.05) on the DVs are considered in the regression models. Thus, for the purpose of this study, it can be concluded that f_{R1} to f_{R4} are only significantly influenced by the fibre dosage.

Table 6.7: Comparison between the significance of fibre dosage and the LOP on the performance parameters according using a multiple regression analysis

Independent Variable	**P-values**			
	f_{R1}	f_{R2}	f_{R3}	f_{R4}
Fibre dosage (kg/m^3)	0.00014	0.00002	0.00003	0.00004
Limit of proportionality (MPa)	0.27699	0.37810	0.20563	0.11846

Table 6.8 summarises the equations of the regression models for each performance parameter developed according to the multiple regression analyses. The standard deviation (σ) of each regression model, also referred to as the root mean square error (RMSE) of the estimate, is also presented in Table 6.8 and is calculated as follows:

$$\sigma_x = RMSE = \sqrt{\frac{\Sigma(Y - Y')^2}{N - 2}} \tag{6.7}$$

where:
Y = observed data values
Y' = predicted value
N = sample size

Equation 6.7 is an unbiased estimate of the standard deviation of the variations in the observed data not explained by the respective regression models. The regression models strive to minimise the sum of the squared deviations of the prediction, thus the standard deviation of the regression

models is closely related to the sum of the squared residuals, which is the difference between the observed data and the predicted values, therefore also referred to as the mean square error between the values. It should be noted that the sum of the squared residuals is divided by $(N-2)$ due to an additional degree of freedom for error being used by estimating two parameters, i.e. the slope and the intercept, rather than only a single degree of freedom (mean) being used in fitting the data to the model. Appendix C provides a comprehensive comparison between the observed and the predicted values according to the linear regression models for each performance parameter.

Table 6.8: Summary of the regression models for predicting the performance parameters

Performance Parameter	$\sigma_{\mathbf{x}}$ **(MPa)**	**Linear regression model**
f_{R1}	0.219	$0.249 \cdot Fibre\ dosage\ (kg/m^3) + 1.567$
f_{R2}	0.119	$0.251 \cdot Fibre\ dosage\ (kg/m^3) + 0.470$
f_{R3}	0.116	$0.303 \cdot Fibre\ dosage\ (kg/m^3) + 0.045$
f_{R4}	0.130	$0.321 \cdot Fibre\ dosage\ (kg/m^3) - 0.098$
f_{LOP}	0.305	$0.05 \cdot f_{cu}\ (MPa) + 2.641$ • f_{cu} = cube compressive strength

6.4 Adjusted regression models

During the course of the study, all the tests were executed and performed under controlled laboratory conditions. It is acknowledged that construction works suffers from a number of uncertainties at all stages of the execution process. Some of these uncertainties and variations can never be completely eliminated and must therefore be taken into account in the design values. According to Holicky, 2009, the following types of uncertainties can usually be identified:

- Natural randomness of material properties, actions and geometric data
- Statistical uncertainties due to limited available and reliable data
- Gross errors in design, execution, and operations of structures
- Lack of knowledge of the behaviour of new materials in real conditions

To include the variations experienced in the construction industry, the standard deviation (σ) and ultimately the regression models predicting the performance parameters, are adjusted. The regression model for each performance parameter is adjusted and calibrated by implementing a Model Factor (MF). As a general rule, additional variations between 5 and 15%, due to uncertainties in the construction industry, must be incorporated in the design values. It is assumed that the mean values (μ) of the performance parameters obtained in the industry are the same as under controlled laboratory conditions as the additional variation is attributed to

uncontrollable uncertainties and not variation in the material properties. Thus, the MF consisted of a μ-value of 1 and three different standard deviations (σ_y), i.e. 0.05 (5%), 0.10 (10%), and 0.15 (15%), respectively. Three different σ_y values are considered to illustrate the affect of an increase in the additional variation. The following equation is applied to calibrate the regression models accounting for the additional variations:

$$f_{calibrated}(\mu_{xy}, \sigma_{xy}) = MF(\mu_y, \sigma_y) \cdot f_{model}(\mu_x, \sigma_x) \tag{6.8}$$

where:
$\mu_{xy} = \mu_x \cdot \mu_y$ (Holicky, 2009)
$\sigma_{xy} = \mu_x \cdot \mu_y \cdot \sqrt{w_x^2 + w_y^2 + w_x^2 \cdot w_y^2}$ (Holicky, 2009)
w = coefficient of variance = σ/μ

The calculation procedures for determining the mean value (μ_{xy}) and the standard deviation (σ_{xy}) of the calibrated regression models are provided in Table 6.9. It should be noted that the standard deviations shown in Table 6.8 (σ_x), and the aforementioned standard deviations due to the additional uncertainties and variations in the industry (σ_y), are used to calculate the standard deviation of the calibrated models (σ_{xy}). Fibre dosage (kg/m^3) is represented by the symbol F_d.

Table 6.9: Calibrated regression models - Mean value (μ_{xy}) and standard deviation (σ_{xy})

Performance Parameter	$\boldsymbol{\mu_{xy}}$ **(MPa)**	$\boldsymbol{\sigma_{xy}}$ **(MPa)**
f_{R1}	$(0.249 \cdot F_d + 1.567) \cdot (1)$	$\mu_{xy} \cdot \sqrt{(\frac{\sigma_x}{0.249 \cdot F_d + 1.567})^2 + (\frac{\sigma_y}{1})^2 + (\frac{\sigma_x}{0.249 \cdot F_d + 1.567})^2 \cdot (\frac{\sigma_y}{1})^2}$
f_{R2}	$(0.251 \cdot F_d + 0.47) \cdot (1)$	$\mu_{xy} \cdot \sqrt{(\frac{\sigma_x}{0.251 \cdot F_d + 0.47})^2 + (\frac{\sigma_y}{1})^2 + (\frac{\sigma_x}{0.251 \cdot F_d + 0.47})^2 \cdot (\frac{\sigma_y}{1})^2}$
f_{R3}	$(0.303 \cdot F_d + 0.045) \cdot (1)$	$\mu_{xy} \cdot \sqrt{(\frac{\sigma_x}{0.303 \cdot F_d + 0.045})^2 + (\frac{\sigma_y}{1})^2 + (\frac{\sigma_x}{0.303 \cdot F_d + 0.045})^2 \cdot (\frac{\sigma_y}{1})^2}$
f_{R4}	$(0.321 \cdot F_d - 0.098) \cdot (1)$	$\mu_{xy} \cdot \sqrt{(\frac{\sigma_x}{0.321 \cdot F_d - 0.098})^2 + (\frac{\sigma_y}{1})^2 + (\frac{\sigma_x}{0.321 \cdot F_d - 0.098})^2 \cdot (\frac{\sigma_y}{1})^2}$
f_{LOP}	$(0.05 \cdot f_{cu}(MPa) + 2.641) \cdot (1)$	$\mu_{xy} \cdot \sqrt{(\frac{\sigma_x}{0.05 \cdot f_{cu}(MPa) + 2.641})^2 + (\frac{\sigma_y}{1})^2 + (\frac{\sigma_x}{0.05 \cdot f_{cu}(MPa) + 2.641})^2 \cdot (\frac{\sigma_y}{1})^2}$

Besides calibrating the mean regression models to incorporate the uncertainties and larger variations experienced in the construction industry, the characteristic regression models (f_{ck}) are calculated which forms part of the design process. The characteristic regression models are defined as the models predicting the performance parameters with an exceedance probability of 95%, suggesting that no more than 5% of the predicted values are below the characteristic values. The characteristic regression models are determined assuming a Gaussian normal distribution with a standard normal variable (Z) of 1.645, which corresponds to an exceedance probability of 95%. Figure 6.2 illustrates the probability density function associated with the implemented standard normal variable.

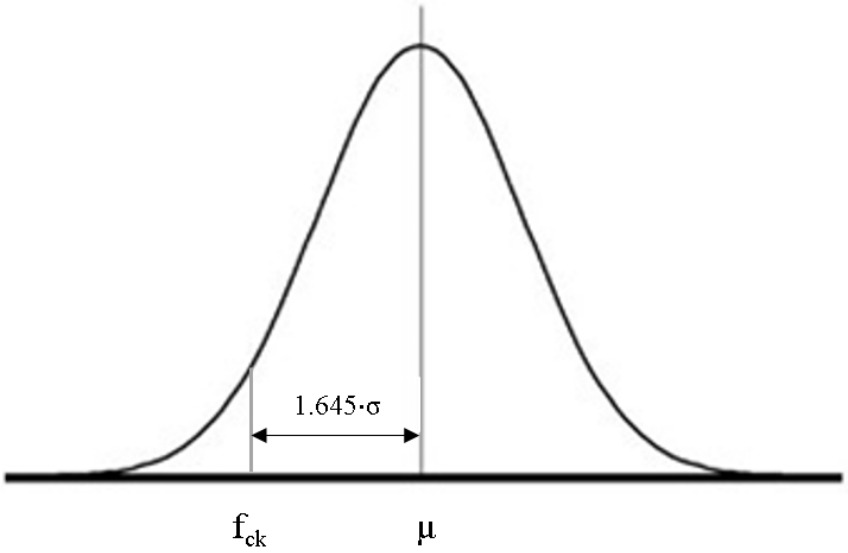

Figure 6.2: Probability density function for a Z-value of 1.645

The characteristic regression models are determined by implementing the following equation:

$$f_{ck}(\mu_{xy}, \sigma_{xy}) = \mu_{xy} - (1.645 \cdot \sigma_{xy}) \tag{6.9}$$

Figure 6.3 illustrates the comparison between the mean regression models, as presented in Table 6.8, and the characteristic mean regression models (f_{ck}) for each performance parameter, as calculated by implementing Equation 6.9 for the laboratory results (lab) and the three additional standard deviations (%). An important observation from the figures presented below is that the regression models predicting f_{R1} to f_{R4} are valid for a fibre dosage between 2.5 and 5.5 kg/m^3, and the regression models predicting f_{LOP} are illustrated for a cube compressive strength between 35 and 65 MPa. Appendix A.4 provides a comparison between the adjusted regression model parameters for each performance parameter.

From the illustrated comparisons, it is evident that a higher level of conservatism is achieved with an increase in the additional standard deviation. It should however be mentioned that the higher additional standard deviations may unfairly decrease the regression model parameters, presenting overly conservative models. The exact amount of additional variation that should be accounted for, especially for MSFRC, is however still unclear and it is recommended that further research should be done to investigate the additional variations and reliability for MSFRC. For the purpose of this study, the adjusted regression models which included the additional standard deviations, are calculated and illustrated primarily as a comparative measure. Table 6.10 presents a comparison between the linear mean regression models and the linear characteristic regression models for each performance parameter. It is important to note that no additional standard deviation are added to the characteristic regression models presented in Table 6.10 and the standard deviations of each performance parameter, as presented in Table 6.8, are considered and implemented using Equation 6.9 to determine the characteristic models.

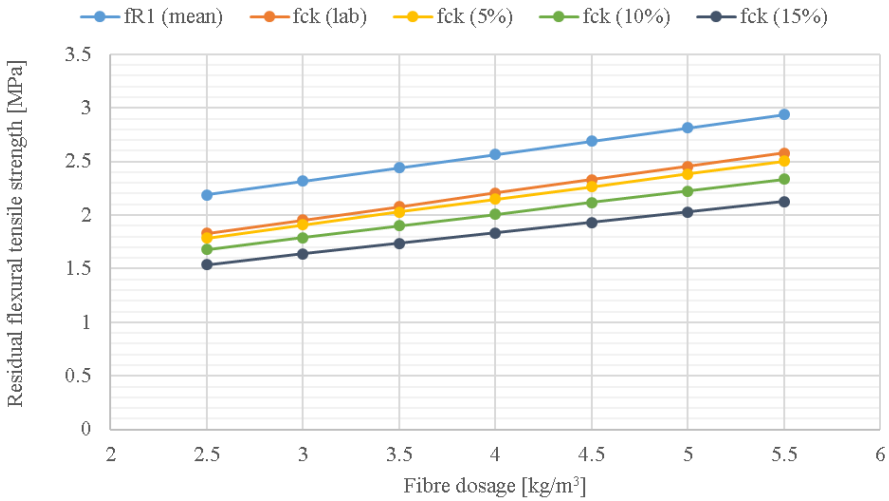

(a) f_{R1}

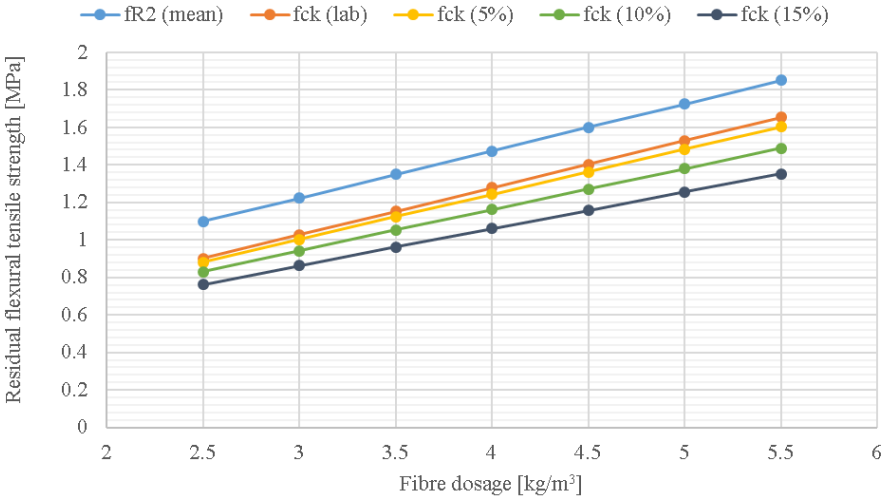

(b) f_{R2}

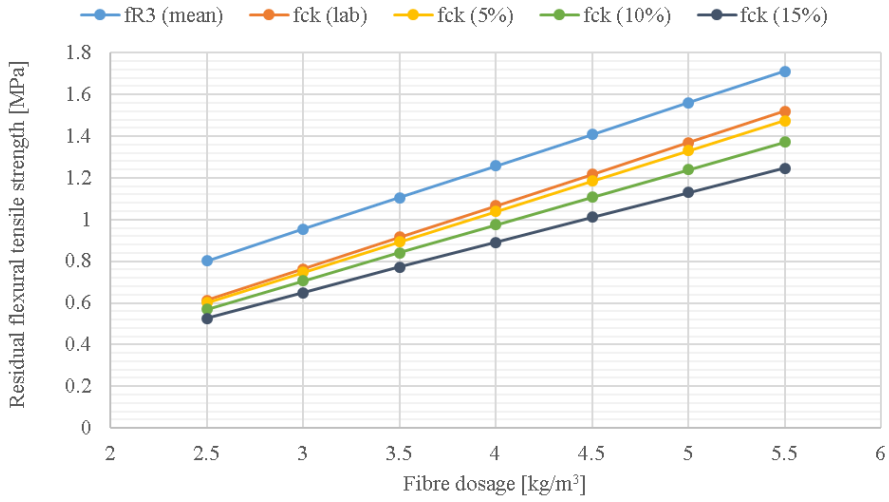

(c) f_{R3}

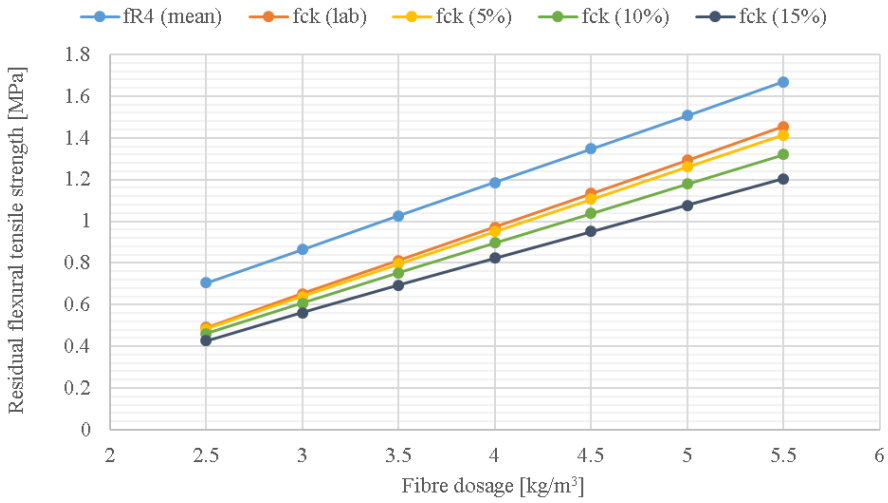

(d) f_{R4}

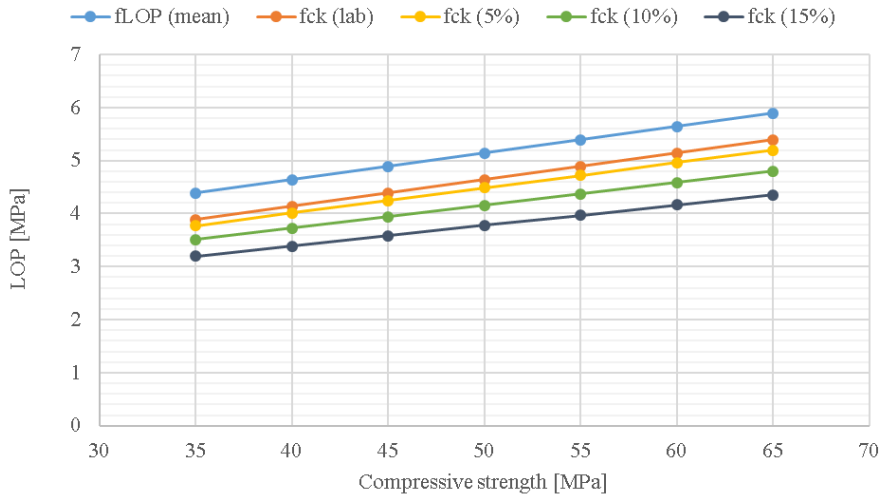

(e) f_{LOP}

Figure 6.3: Mean regression models versus the characteristic regression models predicting the performance parameters, considering the laboratory results as well as the additional standard deviations

Table 6.10: Summary of the linear regression models predicting the mean and characteristic mean values for each performance parameter

Performance Parameter		**Linear regression model**
f_{R1}	mean ($f_{\mu,R1}$)	$0.249 \cdot Fibre\ dosage\ (kg/m^3) + 1.567$
	characteristic ($f_{ck,R1}$)	$0.249 \cdot Fibre\ dosage\ (kg/m^3) + 1.207$
f_{R2}	mean ($f_{\mu,R2}$)	$0.251 \cdot Fibre\ dosage\ (kg/m^3) + 0.47$
	characteristic ($f_{ck,R2}$)	$0.251 \cdot Fibre\ dosage\ (kg/m^3) + 0.274$
f_{R3}	mean ($f_{\mu,R3}$)	$0.303 \cdot Fibre\ dosage\ (kg/m^3) + 0.045$
	characteristic ($f_{ck,R3}$)	$0.303 \cdot Fibre\ dosage\ (kg/m^3) - 0.146$
f_{R4}	mean ($f_{\mu,R4}$)	$0.321 \cdot Fibre\ dosage\ (kg/m^3) - 0.098$
	characteristic ($f_{ck,R4}$)	$0.321 \cdot Fibre\ dosage\ (kg/m^3) - 0.311$
f_{LOP}	mean ($f_{\mu,LOP}$)	$0.05 \cdot f_{cu}\ (MPa) + 2.641$
	characteristic ($f_{ck,LOP}$)	$0.05 \cdot f_{cu}\ (MPa) + 2.139$

6.5 Partial material factors

As a means of adjusting performance parameters so that appropriate values are derived for design calculations, partial factors have emerged within limit state design methodology. The design value method, also referred to as the semi-probabilistic method according to EN 1990 (European Norms, 2002), is an important consideration toward the operational partial factor method. The design value method is directly associated to the basic principle of EN 1990, stating that no limit state may be exceeded when the design values of all basic variables are implemented in the models of structural resistance and action effect (Holicky, 2009).

The partial factor methods, accepted in EN 1990 to 1999, states that the design values can be represented by their characteristic values, with a prescribed or intended probability of being exceeded, and can be expressed as:

$$f_d = \frac{f_{ck}}{\gamma_M} \tag{6.10}$$

where:
f_d = design value
f_{ck} = characteristic value
γ_M = partial factor of material properties

The design value may be modified depending on the type of structural member and construction material, therefore the partial factor γ_M are split into a resistance model uncertainty factor (γ_{RD}), depending on the behaviour of the structural member, and a material property factor (γ_m). For the purpose of this research, γ_{RD} is assumed to be 1 due to the behaviour of the structural elements not being considered, and therefore:

$$\gamma_M = \gamma_m \tag{6.11}$$

The material property factor is determined by the characteristic values and the design values, and can be expressed as (Holicky, 2009):

$$\gamma_m = \frac{f_{ck}}{f_d} = \frac{1 - u_{0.05} \cdot w_x}{1 - u_p \cdot w_x} \tag{6.12}$$

where $u_{0.05}$ and u_p denotes the standard normal variable corresponding to a 95% exceedance probability and a p-fractile which is related to the notional probability of failure, $p = \Phi(0.8 \cdot \beta_R)$, where Φ corresponds to a cumulative normal distribution and β_R referring to the level of reliability which takes account of accepted or assumed statistical variability in action effects, resistance, and model uncertainties, associated with the appropriate reliability class according to SANS 10160-1 (SABS Standards Division, 2011). According to SANS 10160-1, the reference class of structures representing a medium level of consequences of structural failure with ductile and gradual modes of failure, requires a reliability level of $\beta_R \geq 3.0$, where EN 1990 (European Norms, 2002) recommends a β_R value of 3.8 for a reliability class of structures with a medium consequence for loss of human life, economic, social, or environmental consequences. Due to the moderate reliability concerns of FRC structures, a reliability class (RC) of RC2 was considered according to SANS 10160-1. Thus, a β_R value of 3.0 is used to calculate the material property factors. A β_R value of 3.8 is also considered as a comparative measure. The coefficient of variation associated with the variable under consideration is denoted by w_x. Substituting the values of $u_{0.05}$ and u_p, the material property factor has the following form:

$$\gamma_m = \frac{1 - 1.645 \cdot w_x}{1 - (0.8 \cdot \beta_R) \cdot w_x} \tag{6.13}$$

The standard formulation of the coefficient of variation (w_x), i.e. the ratio of the standard deviation to the mean, applies to the interpretation and analysis of a single variable. When interpreting the coefficient of variation associated to the regression models, the w_x is determined as the ratio of the RMSE to the mean of the observed values associated to each performance parameter. Therefore, as a general rule to calculate the w_x associated with each performance parameter, the following equation is implemented:

$$w_x = \frac{RMSE}{\bar{Y}} \tag{6.14}$$

where Equation 6.7 is implemented to calculate RMSE, and $\bar{Y}$ refers to the mean of the observed data for each performance parameter. A comparison between the observed and predicted values for each performance parameter is presented in Appendix C. Table 6.11 provides the w_x coefficients and a comparison between the γ_m factors for each performance parameter, considering the two β_R values implemented for the investigation. It should be noted that Table 6.11 also includes a comparison between the γ_m factors for the different amounts of additional variation, as mentioned in Section 6.4.

Table 6.11: w_x coefficients and partial material factors (γ_m) for each performance parameter

Performance Parameter	$\mathbf{w_x}$	β_R	γ_m			
			mean	**+5%**	**+10%**	**+15%**
f_{R1}	0.085	3.0	1.08	1.15	1.25	1.41
		3.8	1.16	1.32	1.59	2.15
f_{R2}	0.081	3.0	1.08	1.14	1.24	1.39
		3.8	1.15	1.30	1.56	2.08
f_{R3}	0.092	3.0	1.09	1.16	1.27	1.44
		3.8	1.18	1.35	1.65	2.28
f_{R4}	0.109	3.0	1.11	1.20	1.32	1.52
		3.8	1.23	1.43	1.80	2.71
f_{LOP}	0.059	3.0	1.05	1.11	1.19	1.32
		3.8	1.10	1.23	1.43	1.80

From Table 6.11 it is evident that γ_m varies between 1.05 and 1.11 considering the mean values for a β_R value of 3.0, with f_{R4} indicating the largest value. The differences in γ_m can be attributed to the differences in the standard deviation for each performance parameter. It can also be concluded that an increase in the additional variation has a substantial effect on the partial material factor, with an increase of approximately 26 and 37% evident between the mean values (no additional variation) and the adjusted mean values, considering an additional variation of 15% and a β_R value of 3.0. Considering the β_R value of 3.8 according to EN 1990, a substantial increase in the γ_m values is evident for each performance parameter. The material factor is thus sensitive to the implemented reliability index. To be conservative, it is recommended that γ_m, incorporating the additional variation, should be implemented in the design values for each performance parameter. For MSFRC, and depending on the chosen amount of additional

variation and β_R value that should be accounted for, the design values for each performance parameter should be determined by considering a partial material factor (γ_m) as indicated in Table 6.11. For a β_R of 3.0 according to the South African standards (SANS 10160-1) a γ_m value of 1.5 is recommended for MSFRC.

6.6 Concluding summary

Simple- and multiple linear regression analyses are performed to investigate the relationships between the IVs and each DV and ultimately to create linear models predicting the performance of MSFRC.

The simple linear regression analyses indicated that fibre dosage is the only IV having a significant influence on performance parameters f_{R1} to f_{R4}. From the simple linear regression analyses it is also evident that compressive strength is the only IV having a significant influence on performance parameter f_{LOP}.

Fibre dosage is also identified as the only IV having a significant effect on performance parameters f_{R1} to f_{R4} according to the multiple regression analyses, as well as compressive strength being the only IV having a significant effect on f_{LOP}. The multiple linear regression analyses are used to determine the linear generic models predicting the performance parameters which are illustrated in Table 6.8.

To take account of the uncertainties in the construction industry, the linear regression models are adjusted to incorporate the additional variations. The linear regression models are adjusted using a Model Factor (MF) with a μ-value of 1 and three different standard deviations, i.e. 0.05 (5%), 0.10 (10%), and 0.15 (15%). A comparison between the mean regression models and the characteristic mean regression models incorporating the different additional standard deviations, is illustrated in Figure 6.3. Due to the uncertainty regarding the exact amount of additional variation that should be accounted for, the mean regression models and the characteristic mean regression models are presented as the generic models predicting the performance parameters and are indicated in Table 6.10.

As a means of adjusting the performance parameters to derive appropriate design values, material property factors (γ_m) are calculated for each performance parameter. A comparison is illustrated between the γ_m factor for each performance parameter considering the mean values and different reliability indices, as well as the adjusted mean values incorporating the additional variation due to uncertainties in the construction industry. It is concluded that an increase of up to 37% is evident for γ_m by accounting for additional variation, and depending of the chosen amount, the design values for each performance parameter should be determined by considering the stated partial material factors. It is also shown that the γ_m factor is sensitive to the chosen β_R value, with a substantial increase evident for the β_R value of 3.8 according to EN 1990.

Chapter 7

Conclusion and Future Prospects

7.1 Conclusion

The primary objective of this study is to develop generic models which can be implemented to predict the residual flexural tensile performance (f_{R1}-f_{R4}) and the limit of proportionality (f_{LOP}) of macro-synthetic fibre reinforced concrete (MSFRC), calibrated for an experimental macro-synthetic fibre supplied by CHRYSO, specifically for industrial flooring applications. To develop the generic models, research hypotheses are stated and investigated to determine the factors having a significant influence on the performance parameters. The linear regression models derived are based on the three-point bending test (TPBT) results. Additional tests, i.e. shrinkage tests, computed tomography (CT) scans, single-fibre pull-out tests, and scanning electron microscopy (SEM) imaging are also performed to investigate and get a better understanding of the performance of the CHRYSO macro-synthetic (CMS) fibre.

The following subsections include the conclusions drawn from the research presented. It should be noted that the macro-mechanical performance evaluation is based on the linear regression analyses presented in Chapter 6.

7.1.1 Macro-mechanical performance evaluation

- The simple- and multiple linear regression analyses indicate that fibre dosage is the only influencing factor having a significant influence on performance parameters f_{R1} to f_{R4} and compressive strength as the only influencing factor having a significant effect on f_{LOP}.
- The extent of the influence of compressive strength on the LOP is dependent on the cement type and class, with a cement extended with blastfurnace slag indicating an improved LOP.
- An interesting observation is made referring to the effect of mixing time. For both a pan and tilting-drum mixer, mixing time negligibly affected the LOP and f_{R1}. For prolonged mixing times exceeding 10 minutes associated with a pan mixer, performance parameters f_{R2} to f_{R4} significantly decreased. However, for prolonged mixing times associated with a tilting-drum mixer, a negligible effect is evident for performance parameters f_{R1} to f_{R4}.

- Shrinkage tests revealed that the addition of the CMS fibre, at different dosages, do not affect the shrinkage strain compared to the shrinkage strain measured for plain concrete.
- CT scans revealed that an increase in the nominal coarse aggregate size affect the fibre distribution within the concrete matrix, yielding a more prominent non-homologous fibre distribution and an increase in the void content of the MSFRC matrix.
- Determining the linear models predicting the performance parameters, a 52.5N CEM II cement type and a fibre dosage between 2.5 to 5.5 kg/m^3, as well as the effect of mixing time associated with a tilting-drum mixer, is considered. Taking account of the aforementioned conditions, the following linear regression models predict the mean performance parameters according to the multiple linear regression analyses:
  - $f_{\mu,R1} = 0.249 \cdot Fibre\ dosage\ (kg/m^3) + 1.567$
  - $f_{\mu,R2} = 0.251 \cdot Fibre\ dosage\ (kg/m^3) + 0.470$
  - $f_{\mu,R3} = 0.303 \cdot Fibre\ dosage\ (kg/m^3) + 0.045$
  - $f_{\mu,R4} = 0.321 \cdot Fibre\ dosage\ (kg/m^3) - 0.098$
  - $f_{\mu,LOP} = 0.05 \cdot f_{cu}\ (MPa) + 2.641$
    - f_{cu} = cube compressive strength
- To derive appropriate design values, additional variation experienced in the construction industry, as well as a partial material factor (γ_m), should be considered.
- Taking account of the additional variation, a Model Factor (MF) should be implemented which accounts for an additional variation between 5 to 15%.
- A γ_m value of 1.5 is recommended for MSFRC associated with a reliability index (β_R) of 3.0.

7.1.2 Single-fibre performance evaluation

- Compressive strength do not significantly affect the pull-out resistance of the CMS fibre in its virgin fibre state.
- The CMS fibre is affected by the mixing process, indicating an increase in the fibre-matrix bond characteristics, ultimately increasing the interfacial bond stress.
- An increase in the W/C ratio has a positive effect on the pull-resistance experienced by the CMS fibre in its premixed fibre state. No clear explanation could be provided for this phenomenon.
- SEM images revealed extensive fibre deterioration for prolonged mixing times exceeding 10 minutes, associated with a pan mixer. Damage to the CMS fibre is however less susceptible to the mixing process associated with a tilting-drum mixer.

7.2 Future prospects

From the results obtained and the knowledge gained during the this research project, the following aspects need further investigation:

- Large deviations in the results obtained according to the three-point bending test (TPBT) was experienced, specifically investigating the influence of coarse aggregate size and coarse aggregate volume on the macro-mechanical performance. A test method with a larger crack-surface is recommended to investigate the macro-mechanical performance of MSFRC.
- A relationship tends to exist between the LOP and performance parameter f_{R1} and should further be investigated. Due to cement type and class having a significant effect on the LOP, it is suggested that a multiple linear regression analysis is performed considering the effect of fibre dosage and the LOP, incorporating more than one cement type, to explore the multiple effect of fibre dosage and the LOP on performance parameter f_{R1}.
- Unexpected results were obtained for the influence of an increase in W/C ratio on the single-fibre performance. It is recommended to investigate the effect of an increase in fine aggregate volume, associated with an increase in the W/C ratio, on the single-fibre performance of premixed macro-synthetic fibres.
- Extensive research should be done on the exact amount of additional variation, due to uncertainties experienced in the construction industry, that should be considered in design values for MSFRC.
- Due to the limited time frame of the study, the data set used to conduct the multiple linear regression analyses were based on the primary interactions between the considered independent variables. Additional tests should be completed corresponding to W/C ratios, coarse aggregate sizes, coarse aggregate volumes, fibre dosages, and mixing times not considered in this study to create a complete data set which includes the secondary interactions between the independent variables.
- Additional macro-mechanical tests, incorporating different macro-synthetic fibres, should be performed to determine the efficiency of the calculated regression models predicting the performance parameters. The models should be calibrated to incorporate different macro-synthetic fibres.

7.3 Concluding statement

The primary aim of this research project is to develop generic models which can be implemented to predict the performance of MSFRC, calibrated for the CMS fibre, specifically for industrial flooring applications. From simple- and multiple linear regression analyses, incorporating the results obtained during the investigation of the stated research hypotheses, it is indicated that performance parameters f_{R1} to f_{R4} are significantly influenced by fibre dosage (kg/m^3) and

f_{LOP} is significantly influenced by compressive strength (MPa). Based on the results, linear regression models are determined to predict the performance parameters. It is also indicated that the mean regression models should be adjusted to incorporate uncertainties and additional variation experienced in the construction industry, and that appropriate design values should be calculated by considering a partial material factor (γ_m).

References

ACI Committee 302 (1997). 'Guide for Concrete Floor and Slab Construction'. In: *ACI 302.1R*.

ACI Committee 544 (1999). 'Measurement of properties of fiber reinforced concrete'. In: *ACI 544.2R-89*.

— (2002). 'State-of-the-Art Report on Fiber Reinforced Concrete Reported by ACI Committee 544'. In: *ACI Structural Journal* 96.Reapproved.

— (2008). 'Guide for specifying, proportioning, and production of fiber-reinforced concrete'. In: *ACI 544.3R-08*.

ASTM Committee (2010a). 'C1399/C1399M Standard Test Method for Obtaining Average Residual-Strength of Fiber-Reinforced'. In: *ASTM standard C1399/C1399M* c, pp. 1–6. DOI: 10.1520/C1399.

— (2010b). 'Standard Test Method for Flexural Strength of Concrete (Using Simple Beam with Third-Point Loading)'. In: *ASTM standard C78/C78M* C78-02.C, pp. 1–4. DOI: 10.1520/C0078.

— (2013). 'Standard Test Method for Flexural Performance of Fiber-Reinforced Concrete (Using Beam With Third-Point Loading)'. In: *ASTM standard C1609/C1609M-12* April, pp. 1–9. DOI: 10.1520/C1609.

Babafemi, Adewumi John and Boshoff, William Peter (2015). 'Tensile Creep of Cracked Macro Synthetic Fibre Reinforced Concrete'. Ph.D Thesis. Stellenbosch University.

Beaudoin, James J. (1990). *Handbook of Fiber-Reinforced Concrete: Principles, Properties, Developments and Applications*. Park Ridge, New Jersey: Noyes Publications.

Bentur, Arnon and Mindess, Sidney (2007). *Fibre Reinforced Cementitious Composites*. 2nd Edition. Abington, Oxon: Taylor & Francis.

Boshoff, William P., Mechtcherine, Viktor and Zijl, Gideon P A G van (2009). 'Characterising the time-dependant behaviour on the single fibre level of SHCC: Part 2: The rate effects on fibre pull-out tests'. In: *Cement and Concrete Research* 39.9, pp. 787–797. ISSN: 00088846. DOI: 10.1016/j.cemconres.2009.06.006. URL: http://dx.doi.org/10.1016/j.cemconres.2009.06.007.

Boshoff, William Peter (2007). 'Time-Dependant Behaviour of Engineered Cement-Based Composites'. Ph.D Thesis. Stellenbosch University.

Bothma, J (2013). 'The Structural Use of Synthetic Fibres: Thickness Design of Concrete Slabs on Grade'. M.Sc Thesis. Stellenbosch University.

Bouard, Brenton (2015). *Concrete Mix Design Method*. Private interview. September 08, 2015 (Boksburg, South Africa).

British Standards Institution (2004). 'Eurocode 2: Design of concrete structures - Part 1-1: General rules and rules for buildings'. In: *BS EN 1992-1-1:2004*.

— (2009). 'Testing of concrete - Part 8: Determination of drying shrinkage of concrete for samples prepared in the field or in the laboratory'. In: *BS ISO 1920-8:2009*.

Buratti, Nicola, Mazzotti, Claudio and Savoia, Marco (2011). 'Post-cracking behaviour of steel and macro-synthetic fibre-reinforced concretes'. In: *Construction and Building Materials* 25.5, pp. 2713–2722. ISSN: 09500618. DOI: 10.1016/j.conbuildmat.2010.12.022.

Central Analytical Facility, US (2012). *CT Scanner - Information*. URL: http://academic.sun.ac.za/saf/services/services8.html.

DiFrancia, Célene, Ward, Thomas and Claus, Richard (1996). 'The single-fibre pull-out test. 1: Review and interpretation'. In: *Composites Part A: Applied Science and Manufacturing* 27.8 PART A, pp. 597–612.

Domone, Peter (2010). *Construction Materials*. Ed. by Peter Domone and John Illston. 4th Edition. Abington: Spon Press, pp. 83–208.

EFNARC (1996). 'European specifications for sprayed concrete'. In: 44.0, p. 300.

ERMCO (2012). *Guidance to fibre concrete: Properties, specifications and practice in Europe*. Tech. rep. September. European Ready Mixed Concrete Organisation, pp. 1–39.

European Norms (2002). 'Eurocode - Basis of structural design'. In: *EN 1990:2002*. ISSN: 0965-089X. DOI: 10.1680/cien.144.6.8.40609.

— (2005). 'Methods of testing cement - Part 1: Determination of strength'. In: *EN 196-1:2005*.

— (2006). 'Fibres for concrete - Part 2: Polymer fibres - Definitions, specifications and conformity'. In: *EN 14889-2:2006*.

— (2007). 'Test method for metallic fibre concrete. Measuring the flexural tensile strength (limit of proportionality (LOP), residual)'. In: *EN 14651:2005+A1:2007*.

Gilbert, Raymond Ian, Engineering, Civil, Wales, New South, Australian, Council, Fellowships, Professorial, Ranzi, Gianluca, Lecturer, Senior and Engineering, Structural (2011). *Time-Dependent Behaviour of Concrete Structures*. ISBN: 9780415493840.

Gopalaratnam, Vellore S. and Gettu, Ravindra (1995). 'On the characterization of flexural toughness in fiber reinforced concretes'. In: *Cement and Concrete Composites* 17.3, pp. 239–254. ISSN: 09589465. DOI: 10.1016/0958-9465(95)99506-0.

Hair, J.F. (Jr.), Black, W.C., Babin, B.J. and Anderson, R.E. (2010). *Multivariate Data Analysis*. Ed. by Sally Yagan, Julian Partridge and Elizabeth Walne. 7th Edition. Pearson Education, Inc.

Hannant, D.J. (1978). *Fibre Cements and Fibre Concretes*. Chichester: John Wiley & Sons, Ltd.

Hoaglin, D.C. and Iglewicz, B. (1987). 'Fine-tuning some resistant rules for outlier labeling'. In: *Journal of the American Statistical Association* 82, pp. 1147–1149.

Holicky, Milan (2009). *Reliability Analysis for Structural Design*. 1st Edition. SUN MeDIA.

Kobayashi, K and Cho, R (1976). 'Mechanics of Concrete with randomly orientated discontinious fibres'. In: *2nd International Conference on Mechanical Behaviour of Materials*, pp. 1938–1942.

Kovler, Konstantin (1995). 'Interdependence of Creep and Shrinkage for Concrete under Tension'. In: *Journal of Materials in Civil Engineering* 7.2, pp. 96–101. ISSN: 0899-1561. DOI: 10.1061/(ASCE)0899-1561(1995)7:2(96).

Labib, Wafa and Eden, Nick (2006). 'An investigation into the use of fibres in concrete industrial ground-floor slabs'. In: *3rd International Built a. Human Environment Research Week*. Rotterdam, Netherlands: in house publishing, pp. 466–477. URL: http://www.irbnet.de/daten/iconda/CIB9056.pdf.

Larrard, F. de (1999). *Concrete mixture proportioning: A scientific approach*. Ed. by A Bentur and S Mindess. 1st Edition. Vol. 1. Taylor and Francis, p. 421.

Lerch, Jean Oliver (2016). 'Investigation into the Effect of Fibre Geometry on the Performance of Macro Synthetic Fibre Reinforced Concrete'. M.Sc Thesis. Stellenbosch University.

Lin, W.L. (1992). 'Toughness behaviour of fibre reinforced concrete'. In: *Fibre Reinforced Cement and Concrete. Proceedings of the fourth RILEM International Symposium.*

Löfgren, Ingemar (2005). 'Fibre-reinforced Concrete for Industrial Construction - a fracture mechanics approach to material testing and structural analysis'. Ph.D Thesis. Chalmers University of Technology. ISBN: 9172916966.

McKee, Dean Clive (1969). 'The Properties of an Expansive Cement Mortar Reinforced with Random Wire Fibres'. Ph.D. Thesis. University of Illinios.

Mills, Craig (2015). *Aggregates for Industrial Flooring Applications*. Private interview. September 04, 2015 (Eersterivier, South Africa).

Mindess, Sindney and Vondran, Gary (1988). 'Properties of concrete reinforced with fibrillated polypropylene fibres under impact loading'. In: *Cement and Concrete Research* 18.1, pp. 109–115.

Montgomery, D.C. and Runger, G.C. (2007). *Applied Statistics and Probability for Engineers*. Ed. by Jennifer Welter and Nicole Repasky. 4th Edition. John Wiley and Sons, Ltd.

Murugesan, M and Rajpurohit, D (2015). 'ADVANTAGES OF STEEL FIBRE REINFORCED CONCRETE IN INDUSTRIAL FLOORS'. In: *International Journal of Research in Engineering and Technology* 4.10, pp. 243–247.

Neal, F.R. (2002). *Concrete Industrial Ground Floors*. 2nd Edition. Kent, England: Thomas Telford Publishing.

Neville, A.M. (2011). *Properties of Concrete*. 5th Edition. London: Pearson Education, Inc., p. 846.

Odendaal, Courtney Megan (2015). 'Establishment of Performance-Based Specifications for the Structural Use of Locally Available Macro- Synthetic Fibres'. M.Sc Thesis. Stellenbosch University.

Oh, Byung Hwan, Park, Dae Gyun, Kim, Ji Cheol and Choi, Young Cheol (2005). 'Experimental and theoretical investigation on the postcracking inelastic behavior of synthetic fiber reinforced concrete beams'. In: *Cement and Concrete Research* 35.2, pp. 384–392. ISSN: 00088846. DOI: 10.1016/j.cemconres.2004.07.019.

Perrie, Bryan (2009). *Fulton's Concrete Technology*. Ed. by Gill Owens. 9th Edition. Midrand: Cement and Concrete Institute, pp. 329–339.

Prisco, Marco, Plizzari, Giovanni and Vandewalle, Lucie (2009). 'Fibre reinforced concrete: new design perspectives'. In: *Materials and Structures* 42.9, pp. 1261–1281. ISSN: 1359-5997. DOI: 10.1617/s11527-009-9529-4.

Quiroga, PN and Fowler, DW (2004). *The effects of aggregates characteristics on the performance of Portland cement concrete*. Tech. rep. Austin: International Center for Aggreagates Research (ICAR).

Robins, Peter, Austin, Simon, Chandler, Jim and Jones, Peter (2001). 'Flexural strain and crack width measurement of steel-fibre-reinforced concrete by optical grid and electrical gauge methods'. In: *Cement and Concrete Research* 31.5, pp. 719–729. ISSN: 00088846. DOI: 10.1016/S0008-8846(01)00465-3.

Romualdi, J and Mandel, J (1964). 'Tensile strength of Concrete Affected by uniformly distributed and Closely Spaced Short Lengths of Wire Reinforcement'. In: *Journal of the American Concrete Institute* 61.6, pp. 657–671.

SABS Standards Division (2006a). 'SANS 5845:2006 SOUTH AFRICAN NATIONAL STANDARD Bulk densities and voids content of aggregates'. In:

— (2006b). 'SANS 5864:2006 SOUTH AFRICAN NATIONAL STANDARD Concrete tests - Flexural strength of hardened concrete'. In:

— (2011). *SANS 10160-1:2011 SOUTH AFRICAN NATIONAL STANDARD Basis of structural design and actions for buildings and industrial structures Part 1 : Basis of structural design*. ISBN: 9780626266127.

— (2014). 'SANS 5844:2014 SOUTH AFRICAN NATIONAL STANDARD Particle and relative densities of aggregates'. In:

Singh, Sehaj, Shukla, Arun and Brown, Richard (2004). 'Pullout behavior of polypropylene fibers from cementitious matrix'. In: *Cement and Concrete Research* 34.10, pp. 1919–1925. ISSN: 00088846. DOI: 10.1016/j.cemconres.2004.02.014.

Slag Cement Association (SCA) (2013). *Compressive and Flexural Strength*. URL: http://www.slagcement.org/tempComDocs/-76060/no14{_}compressive{_}and{_}flexural{_}strength.pdf.

Stock, A. F., Hannantt, D. J. and Williams, R. I. T. (1979). 'The effect of aggregate concentration upon the strength and modulus of elasticity of concrete'. In: *Magazine of Concrete Research* 31.109, pp. 225–234. DOI: 10.1680/macr.1979.31.109.225. eprint: http://dx.doi.org/10.1680/macr.1979.31.109.225. URL: http://dx.doi.org/10.1680/macr.1979.31.109.225.

Tazawa, Ei ichi and Miyazawa, Shingo (1995). 'Experimental study on mechanism of autogenous shrinkage of concrete'. In: *Cement and Concrete Research* 25.8, pp. 1633–1638. ISSN: 00088846. DOI: 10.1016/0008-8846(95)00159-X.

The Concrete Society (2003). *Technical Report 34: Concrete Inductrial Ground Floors - A guide to design and construction*. Third. Camberley, Surrey: The Concrete Society.

— (2007). *Technical Report 65: Guidance on the use of Macro-synthetic-fibre- reinforced Concrete*. Camberley, Surrey: The Concrete Society.

— (2013). *Technical Report 34: Concrete Industrial Gound Floors - A guide to design and construction*. Fourth. Camberley, Surrey: The Concrete Society, pp. 20–24.

Tukey, J. W. (1977). *Exploratory Data Analysis*. Ed. by Tukey, J. W. Behavioral Science: Quantitative Methods. Addison-Wesley.

Vandewalle, L (2000). 'Design method for steel fiber reinforced concrete proposed by RILEM TC 162-TDF'. In: *Fifth International RILEM Symposium on Fibre-Reinforced Concrete (FRC)*, pp. 51–64.

Vandewalle, L, Van Rickstal, F, Heirman, G and Parmentier, B (2008). 'The round panel test and the 3-point bending test'. In: *7th international RILEM symposium on Fibre Reinforced Concrete* 1, pp. 1–10.

Vijaya Gowri, T., Sravana, P. and Srinivasa Rao, P. (2016). 'On the relationship between compressive strength and water binder ratio of high volumes of slag concrete'. In: *International Journal of Applied Engineering Research* 11.2, pp. 1436–1442. ISSN: 09739769.

Zhao, Guanyu, Prisco, Marco di and Vandewalle, Lucie (2014). 'Experimental investigation on uniaxial tensile creep behavior of cracked steel fiber reinforced concrete Experimental investigation on uniaxial tensile creep behavior of cracked steel fiber reinforced concrete'. In: *Materials and Structures*, pp. 0–11. ISSN: 1359-5997. DOI: 10.1617/s11527-014-0389-1. URL: http://dx.doi.org/10.1617/s11527-014-0389-1.

Zollo, R.F. (1984). 'Collated fibrillated polypropylene fibers in FRC'. In: *Special Publication* 81, pp. 397–410.

— (1997). 'Fiber-reinforced Concrete : an Overview after 30 Years of Development'. In: 19, pp. 107–122.

fib Special Activiy Group (2010). *CEB-fib Model Code 2010 Volume 1*. Tech. rep. Lausanne, Switzerland: International Federation for Structural Concrete (fib), pp. 220–231.

Appendix A

Macro-Mechanical Performance Characteristics

This appendix provides information regarding the specimen characteristics according to the macro-mechanical performance evaluations.

A.1 Compressive strength results

The obtained compression test results, according to the macro-mechanical performance evaluations, are listed in Tables A.1 to A.8.

Reference mix design

Table A.1: Compressive strength test results - Reference mix design

Cement type	Sample no.	Density (kg/m^3)	Strength (MPa)	Average (MPa)	Standard deviation (MPa)	CoV	Slump (mm)
42.5N CEM III	1	2485.05	49.19	50.15	1.8710	0.0373	195
	2	2458.78	50.74				
	3	2468.66	52.47				
	4	2467.04	48.19				
52.5N CEM II	1	2466.87	52.44	52.83	1.3197	0.0250	180
	2	2460.01	51.62				
	3	2455.10	52.57				
	4	2452.70	54.71				

Hypothesis 1

Table A.2: Compressive strength test results - Hypothesis 1 (42.5N CEM III)

W/C ratio	Sample no.	Density (kg/m^3)	Strength (MPa)	Average (MPa)	Standard deviation (MPa)	CoV	Slump (mm)
0.40	1	2479.09	62.57	62.75	0.5804	0.0092	85
	2	2485.86	62.54				
	3	2479.20	62.30				
	4	2475.18	63.61				
0.45	1	2454.87	58.54	58.90	0.7829	0.0133	110
	2	2476.36	58.61				
	3	2484.65	58.38				
	4	2478.38	60.06				
0.50	1	2465.13	57.65	56.79	0.6092	0.0107	105
	2	2469.03	56.25				
	3	2484.22	56.76				
	4	2472.60	56.51				
0.55	1	2470.10	50.20	50.94	1.4261	0.0280	115
	2	2459.53	52.96				
	3	2455.25	50.84				
	4	2441.83	49.73				
0.60	1	2466.09	49.41	47.01	2.0418	0.0434	90
	2	2465.00	44.84				
	3	2439.70	47.89				
	4	2435.45	45.90				
0.65	1	2434.87	42.64	41.97	0.8588	0.0205	70
	2	2420.30	41.85				
	3	2426.90	42.58				
	4	2436.28	40.80				

Continued on next page

Table A.2 – *Continued from previous page*

W/C ratio	Sample no.	Density (kg/m^3)	Strength (MPa)	Average (MPa)	Standard deviation (MPa)	CoV	Slump (mm)
0.70	1	2482.74	40.37	40.46	1.1662	0.0288	70
	2	2455.35	42.13				
	3	2454.57	39.83				
	4	2461.21	39.51				
0.75	1	2440.10	39.62	39.74	0.3462	0.0087	60
	2	2425.43	39.30				
	3	2438.79	40.07				
	4	2455.57	39.96				
0.80	1	2449.19	31.73	32.17	0.7585	0.0236	50
	2	2462.21	33.17				
	3	2441.31	31.46				
	4	2438.83	32.33				

Table A.3: Compressive strength test results - Hypothesis 1 (52.5N CEM II)

W/C ratio	Sample no.	Density (kg/m^3)	Strength (MPa)	Average (MPa)	Standard deviation (MPa)	CoV	Slump (mm)
0.40	1	2477.37	65.63	66.65	1.9418	0.0291	60
	2	2464.52	64.61				
	3	2507.31	67.31				
	4	2499.41	69.03				
0.45	1	2484.22	62.54	59.99	1.7608	0.0294	60
	2	2484.44	59.26				
	3	2479.27	58.53				
	4	2483.35	59.61				
0.50	1	2502.05	58.49	58.49	0.6477	0.0111	85
	2	2478.69	58.76				
	3	2487.35	59.11				
	4	2527.99	57.59				

Continued on next page

Table A.3 – *Continued from previous page*

W/C ratio	Sample no.	Density (kg/m^3)	Strength (MPa)	Average (MPa)	Standard deviation (MPa)	CoV	Slump (mm)
0.55	1	2477.68	55.04	56.05	0.7389	0.0132	65
	2	2473.43	55.98				
	3	2455.33	56.49				
	4	2468.08	56.70				
0.60	1	2419.60	49.31	48.91	0.3173	0.0065	75
	2	2460.71	49.00				
	3	2454.80	48.67				
	4	2442.73	48.64				
0.65	1	2439.50	45.40	44.54	1.0911	0.0245	65
	2	2478.38	43.31				
	3	2499.19	44.91				
	4	-	-				
0.70	1	2447.21	38.17	38.90	1.2915	0.0332	60
	2	2439.80	37.54				
	3	2426.77	40.40				
	4	2432.06	39.52				
0.75	1	2432.06	38.16	38.14	0.9077	0.0238	55
	2	2464.72	36.96				
	3	2462.67	38.24				
	4	2455.38	39.18				
0.80	1	2447.07	32.95	32.93	0.5935	0.0180	60
	2	2439.40	33.15				
	3	2428.04	32.11				
	4	2452.26	33.52				

Hypothesis 2

Table A.4: Compressive strength test results - Hypothesis 2

Nominal coarse aggregate size (mm)	Sample no.	Density (kg/m^3)	Strength (MPa)	Average (MPa)	Standard deviation (MPa)	CoV	Slump (mm)
26.5	1	2456.08	48.58	49.57	4.0743	0.0822	65
	2	2443.70	46.08				
	3	2485.60	54.05				
37.5	1	2482.10	48.50	47.06	4.6991	0.0999	60
	2	2447.45	50.87				
	3	2457.41	41.81				

Hypothesis 3

Table A.5: Compressive strength test results - Hypothesis 3

Nominal coarse aggregate size (mm)	Coarse aggregate volume (l/m^3)	Sample no.	Density (kg/m^3)	Strength (MPa)	Average (MPa)	Standard deviation (MPa)	CoV	Slump (mm)
19	350	1	2478.08	50.47	52.48	2.0453	0.0390	95
		2	2441.51	50.98				
		3	2472.76	54.46				
		4	2458.48	54.01				
	450	1	2459.25	47.08	47.39	1.7954	0.0379	50
		2	2423.82	48.51				
		3	2480.56	44.98				
		4	2492.32	48.98				
26.5	350	1	2383.38	40.84	44.87	4.2925	0.0957	95
		2	2339.07	44.38				
		3	2398.50	49.38				
	450	1	2465.54	47.62	47.99	0.9086	0.0189	100
		2	2471.91	49.03				
		3	2441.46	47.33				
37.5	350	1	2387.39	42.28	41.76	1.3530	0.0324	75
		2	2363.69	40.23				
		3	2318.18	42.78				
	450	1	2453.09	41.91	44.55	2.5420	0.0571	60
		2	2432.24	44.77				
		3	2442.69	46.98				

Hypothesis 4

Table A.6: Compressive strength test results - Hypothesis 4

Fibre dosage (kg/m^3)	**Sample no.**	**Density (kg/m^3)**	**Strength (MPa)**	**Average (MPa)**	**Standard deviation (MPa)**	**CoV**	**Slump (mm)**
2.5	1	2412.46	51.51	50.11	1.2092	0.0241	95
	2	2442.33	48.60				
	3	2443.42	50.42				
	4	2414.85	49.89				
3.0	1	2471.26	51.32	52.15	1.6185	0.0310	85
	2	2486.77	54.18				
	3	2490.55	52.64				
	4	2497.11	50.48				
3.5	1	2470.15	52.96	52.10	0.8267	0.0159	145
	2	2461.62	51.31				
	3	2464.65	52.03				
	4	-	-				
4.5	1	2447.65	55.68	55.32	0.5112	0.0092	80
	2	2463.03	55.52				
	3	2454.07	55.52				
	4	2478.69	54.56				
5.0	1	2431.92	48.62	51.65	2.2044	0.0427	60
	2	2430.05	51.44				
	3	2452.56	53.15				
	4	2449.85	53.41				
5.5	1	2434.50	53.23	53.94	0.7959	0.0148	55
	2	2456.68	53.34				
	3	2436.22	54.32				
	4	2451.06	54.88				

Hypothesis 5

Table A.7: Compressive strength test results - Hypothesis 5 (Pan mixer)

Mixing time (min)	Sample no.	Density (kg/m^3)	Strength (MPa)	Average (MPa)	Standard deviation (MPa)	CoV	Slump (mm)
5	1	2456.78	55.98	55.38	1.0638	0.0192	65
	2	2475.08	56.22				
	3	2425.50	55.47				
	4	2479.30	53.85				
10	1	2458.99	55.83	57.65	1.6833	0.0292	65
	2	2449.05	56.75				
	3	2448.04	58.41				
	4	2466.46	59.60				
20	1	2428.90	53.94	58.23	3.1969	0.0549	80
	2	2459.70	59.05				
	3	2450.25	58.30				
	4	2472.66	61.63				
30	1	2443.03	64.54	62.62	1.6007	0.0256	65
	2	2446.47	60.77				
	3	2480.20	63.14				
	4	2440.61	62.04				
60	1	2457.89	67.07	64.17	2.9335	0.0457	140
	2	2476.58	61.94				
	3	2464.14	61.38				
	4	2460.90	66.31				

Table A.8: Compressive strength test results - Hypothesis 5 (Tilting-drum mixer)

Mixing time (min)	**Sample no.**	**Density (kg/m^3)**	**Strength (MPa)**	**Average (MPa)**	**Standard deviation (MPa)**	**CoV**	**Slump (mm)**
5	1	2459.20	56.63	55.77	0.6044	0.0108	135
	2	2474.70	55.29				
	3	2461.09	55.40				
	4	2457.30	55.76				
10	1	2474.73	48.39	51.05	2.0406	0.0400	145
	2	2451.46	52.22				
	3	2467.17	53.01				
	4	2483.70	50.58				
20	1	2469.56	54.84	53.10	1.6135	0.0304	135
	2	2509.45	52.96				
	3	2468.08	50.98				
	4	2473.17	53.60				
30	1	2477.58	57.61	57.36	1.0807	0.0188	125
	2	2464.42	58.45				
	3	2465.05	57.51				
	4	2469.85	55.87				
60	1	2466.43	56.35	57.72	2.0128	0.0349	65
	2	2478.27	56.35				
	3	2459.90	57.55				
	4	2455.58	60.61				

A.2 Three-point bending test (TPBT) results

The obtained TPBT results, according to the stated research hypotheses, are listed in Tables A.9 to A.19.

Hypothesis 1

Table A.9: TPBT results - Hypothesis 1 (42.5N CEM III)

W/C ratio	**Beam density (kg/m^3)**		**(MPa)**				
			$\mathbf{f}_{R1}$	$\mathbf{f}_{R2}$	$\mathbf{f}_{R3}$	$\mathbf{f}_{R4}$	$\mathbf{f}_{LOP}$
0.40	2466.11	Mean	2.67	1.43	1.29	1.26	8.47
		Std. Dev.	0.35	0.21	0.25	0.22	0.33
		CoV	0.13	0.15	0.19	0.18	0.04
0.45	2448.4	Mean	2.78	1.47	1.25	1.23	7.93
		Std. Dev.	0.35	0.32	0.38	0.41	0.36
		CoV	0.13	0.22	0.30	0.33	0.05
0.50	2436.22	Mean	2.71	1.62	1.48	1.43	6.85
		Std. Dev.	0.36	0.18	0.15	0.19	0.39
		CoV	0.13	0.11	0.10	0.13	0.06
0.55	2421.59	Mean	2.56	1.56	1.39	1.35	6.70
		Std. Dev.	0.55	0.25	0.18	0.17	0.46
		CoV	0.21	0.16	0.13	0.13	0.07
0.60	2434.82	Mean	2.08	1.14	1.02	0.97	5.84
		Std. Dev.	0.28	0.22	0.24	0.22	0.21
		CoV	0.13	0.19	0.23	0.22	0.04
0.65	2430.47	Mean	2.47	1.44	1.24	1.13	5.60
		Std. Dev.	0.42	0.21	0.21	0.19	0.24
		CoV	0.17	0.15	0.17	0.16	0.04

Continued on next page

Table A.9 – *Continued from previous page*

W/C ratio	**Beam density (kg/m^3)**		**(MPa)**				
			$\mathbf{f}_{R1}$	$\mathbf{f}_{R2}$	$\mathbf{f}_{R3}$	$\mathbf{f}_{R4}$	$\mathbf{f}_{LOP}$
0.70	2444.58	Mean	2.10	1.21	1.06	0.99	5.17
		Std. Dev.	0.39	0.17	0.15	0.14	0.58
		CoV	0.19	0.14	0.14	0.14	0.11
0.75	2460.31	Mean	2.83	1.73	1.56	1.54	5.50
		Std. Dev.	0.16	0.26	0.28	0.33	0.28
		CoV	0.06	0.15	0.18	0.22	0.05
0.80	2462.13	Mean	2.36	1.40	1.22	1.17	5.04
		Std. Dev.	0.14	0.14	0.16	0.18	0.23
		CoV	0.06	0.10	0.13	0.15	0.05

Table A.10: TPBT results - Hypothesis 1 (52.5N CEM II)

W/C ratio	**Beam density (kg/m^3)**		**(MPa)**				
			$\mathbf{f}_{R1}$	$\mathbf{f}_{R2}$	$\mathbf{f}_{R3}$	$\mathbf{f}_{R4}$	$\mathbf{f}_{LOP}$
0.40	2453.66	Mean	2.53	1.36	1.16	1.12	6.23
		Std. Dev.	0.32	0.16	0.20	0.21	0.38
		CoV	0.13	0.12	0.18	0.19	0.06
0.45	2463.95	Mean	2.62	1.38	1.10	1.02	5.49
		Std. Dev.	0.27	0.21	0.17	0.19	0.61
		CoV	0.10	0.15	0.16	0.19	0.11
0.50	2452.37	Mean	2.40	1.33	1.08	1.00	5.14
		Std. Dev.	0.23	0.17	0.09	0.09	0.23
		CoV	0.10	0.13	0.09	0.09	0.04

Continued on next page

Table A.10 – *Continued from previous page*

W/C ratio	**Beam density (kg/m^3)**		**(MPa)**				
			$\mathbf{f}_{R1}$	$\mathbf{f}_{R2}$	$\mathbf{f}_{R3}$	$\mathbf{f}_{R4}$	$\mathbf{f}_{LOP}$
0.55	2462.21	Mean	2.84	1.49	1.26	1.19	5.14
		Std. Dev.	0.35	0.21	0.25	0.25	0.62
		CoV	0.12	0.14	0.20	0.21	0.12
0.60	2445.87	Mean	2.59	1.45	1.21	1.12	4.98
		Std. Dev.	0.38	0.27	0.20	0.19	0.42
		CoV	0.15	0.19	0.17	0.17	0.08
0.65	2449.95	Mean	2.28	1.32	1.13	1.08	4.17
		Std. Dev.	0.43	0.20	0.16	0.16	0.44
		CoV	0.19	0.16	0.14	0.15	0.11
0.70	2456.33	Mean	2.50	1.48	1.31	1.19	4.45
		Std. Dev.	0.47	0.32	0.25	0.22	0.09
		CoV	0.19	0.22	0.19	0.19	0.02
0.75	2447.20	Mean	2.63	1.62	1.48	1.42	4.72
		Std. Dev.	0.17	0.14	0.14	0.13	0.46
		CoV	0.06	0.09	0.10	0.09	0.10
0.80	2451.24	Mean	2.10	1.30	1.19	1.12	4.15
		Std. Dev.	0.36	0.23	0.22	0.21	0.24
		CoV	0.17	0.18	0.19	0.18	0.06

Hypothesis 2

Table A.11: TPBT results - Hypothesis 2

Nominal coarse aggregate size (mm)	**Beam density (kg/m^3)**		**(MPa)**				
			$\mathbf{f}_{R1}$	$\mathbf{f}_{R2}$	$\mathbf{f}_{R3}$	$\mathbf{f}_{R4}$	$\mathbf{f}_{LOP}$
26.5	2445.31	Mean	2.92	1.77	1.42	1.29	5.39
		Std. Dev.	0.34	0.28	0.18	0.20	0.20
		CoV	0.12	0.16	0.13	0.15	0.04
37.5	2438.07	Mean	2.40	1.39	1.21	1.15	4.56
		Std. Dev.	0.30	0.19	0.21	0.17	0.20
		CoV	0.12	0.14	0.17	0.15	0.04

Hypothesis 3

Table A.12: TPBT results - Hypothesis 3

Nominal coarse aggregate size (mm)	**Coarse aggregate volume (l/m^3)**	**Beam density (kg/m^3)**		**(MPa)**				
				$\mathbf{f}_{R1}$	$\mathbf{f}_{R2}$	$\mathbf{f}_{R3}$	$\mathbf{f}_{R4}$	$\mathbf{f}_{LOP}$
19	350	2447.34	Mean	2.45	1.41	1.24	1.16	5.25
			Std. Dev.	0.14	0.14	0.16	0.16	0.57
			CoV	0.06	0.10	0.13	0.14	0.11
	450	2470.82	Mean	2.76	1.58	1.47	1.43	5.43
			Std. Dev.	0.42	0.19	0.18	0.19	0.44
			CoV	0.15	0.12	0.12	0.13	0.08
26.5	350	2429.70	Mean	2.75	1.55	1.26	1.14	5.10
			Std. Dev.	0.68	0.44	0.31	0.18	0.29
			CoV	0.25	0.28	0.24	0.15	0.06
	450	2472.02	Mean	2.88	1.58	1.24	1.10	5.14
			Std. Dev.	0.35	0.28	0.23	0.22	0.69
			CoV	0.12	0.18	0.18	0.20	0.13

Continued on next page

Table A.12 – *Continued from previous page*

Nominal coarse aggregate size (mm)	**Coarse aggregate volume (l/m^3)**	**Beam density (kg/m^3)**		**(MPa)**				
				$\mathbf{f}_{R1}$	$\mathbf{f}_{R2}$	$\mathbf{f}_{R3}$	$\mathbf{f}_{R4}$	$\mathbf{f}_{LOP}$
37.5	350	2416.49	Mean	2.25	1.33	1.13	1.03	4.88
			Std. Dev.	0.37	0.16	0.16	0.16	0.80
			CoV	0.17	0.12	0.14	0.15	0.16
	450	2461.03	Mean	2.53	1.51	1.31	1.25	5.17
			Std. Dev.	0.56	0.32	0.26	0.21	0.46
			CoV	0.22	0.21	0.20	0.17	0.09

Hypothesis 4

Table A.13: TPBT results - Hypothesis 4

Fibre dosage (kg/m^3)	**Beam density (kg/m^3)**		**(MPa)**				
			$\mathbf{f}_{R1}$	$\mathbf{f}_{R2}$	$\mathbf{f}_{R3}$	$\mathbf{f}_{R4}$	$\mathbf{f}_{LOP}$
2.5	2466.44	Mean	2.47	1.30	1.07	0.99	5.46
		Std. Dev.	0.18	0.31	0.39	0.43	0.51
		CoV	0.07	0.23	0.36	0.44	0.09
3.0	2459.55	Mean	2.22	1.20	0.98	0.93	5.14
		Std. Dev.	0.45	0.24	0.18	0.17	0.40
		CoV	0.20	0.20	0.18	0.19	0.08
3.5	2461.01	Mean	2.55	1.33	1.12	1.03	5.10
		Std. Dev.	0.61	0.26	0.16	0.13	0.25
		CoV	0.24	0.20	0.15	0.13	0.05
4.5	2460.55	Mean	2.80	1.69	1.47	1.44	5.33
		Std. Dev.	0.28	0.24	0.21	0.19	0.42
		CoV	0.10	0.14	0.14	0.13	0.08
5.0	2460.27	Mean	3.22	1.94	1.75	1.80	5.82
		Std. Dev.	0.38	0.25	0.26	0.25	0.36
		CoV	0.12	0.13	0.15	0.14	0.06
5.5	2437.92	Mean	2.81	1.86	1.68	1.59	5.30
		Std. Dev.	0.68	0.31	0.27	0.23	0.46
		CoV	0.24	0.17	0.16	0.14	0.09

Hypothesis 5

Table A.14: TPBT results - Hypothesis 5 (Pan mixer)

Mixing time (min)	**Beam density (kg/m^3)**		**(MPa)**				
			$\mathbf{f}_{R2}$	$\mathbf{f}_{R2}$	$\mathbf{f}_{R3}$	$\mathbf{f}_{R4}$	$\mathbf{f}_{LOP}$
5	2469.41	Mean	2.49	1.43	1.25	1.26	5.08
		Std. Dev.	0.27	0.30	0.30	0.33	0.28
		CoV	0.11	0.21	0.24	0.26	0.06
10	2465.37	Mean	2.65	1.68	1.51	1.40	5.45
		Std. Dev.	0.32	0.37	0.42	0.40	0.15
		CoV	0.12	0.22	0.28	0.29	0.03
20	2459.71	Mean	2.67	1.58	1.29	1.10	5.72
		Std. Dev.	0.43	0.19	0.17	0.16	0.22
		CoV	0.16	0.12	0.13	0.15	0.04
30	2452.67	Mean	2.56	1.40	1.02	0.76	5.14
		Std. Dev.	0.25	0.10	0.09	0.08	0.51
		CoV	0.10	0.07	0.09	0.10	0.10
60	2471.69	Mean	2.73	0.99	0.57	0.36	5.84
		Std. Dev.	0.31	0.13	0.12	0.11	0.51
		CoV	0.11	0.14	0.21	0.31	0.09

Table A.15: TPBT results - Hypothesis 5 (Tilting-drum mixer)

Mixing time (min)	**Beam density (kg/m^3)**		**(MPa)**				
			$\mathbf{f}_{R2}$	$\mathbf{f}_{R2}$	$\mathbf{f}_{R3}$	$\mathbf{f}_{R4}$	$\mathbf{f}_{LOP}$
5	2484.82	Mean	2.76	1.52	1.22	1.17	5.54
		Std. Dev.	0.45	0.22	0.25	0.26	0.20
		CoV	0.16	0.14	0.21	0.22	0.04
10	2475.39	Mean	2.41	1.41	1.21	1.17	5.25
		Std. Dev.	0.25	0.18	0.20	0.18	0.36
		CoV	0.11	0.13	0.16	0.15	0.07
20	2465.81	Mean	2.50	1.35	1.13	1.07	5.17
		Std. Dev.	0.21	0.28	0.24	0.24	0.44
		CoV	0.08	0.21	0.21	0.23	0.09
30	2460.53	Mean	2.37	1.37	1.22	1.22	5.34
		Std. Dev.	0.21	0.15	0.13	0.15	0.24
		CoV	0.09	0.11	0.11	0.12	0.05
60	2460.07	Mean	2.57	1.50	1.41	1.31	5.80
		Std. Dev.	0.34	0.25	0.27	0.24	0.56
		CoV	0.13	0.17	0.19	0.19	0.10

Additional TPBT results

Table A.16: TPBT results - Additional macro-mechanical tests (Fibre dosage = 3.0 kg/m^3)

W/C ratio	**Beam density (kg/m^3)**		**(MPa)**				
			$\mathbf{f}_{R1}$	$\mathbf{f}_{R2}$	$\mathbf{f}_{R3}$	$\mathbf{f}_{R4}$	$\mathbf{f}_{LOP}$
0.45	2483.03	Mean	2.53	1.48	1.29	1.25	6.40
		Std. Dev.	0.36	0.10	0.10	0.13	0.36
		CoV	0.14	0.07	0.08	0.11	0.06
0.50	2449.53	Mean	2.35	1.35	1.24	1.23	5.61
		Std. Dev.	0.38	0.22	0.27	0.32	0.36
		CoV	0.16	0.16	0.22	0.26	0.06
0.60	2449.07	Mean	2.55	1.41	1.22	1.21	4.69
		Std. Dev.	0.31	0.02	0.21	0.19	0.43
		CoV	0.12	0.01	0.17	0.16	0.09
0.65	2475.49	Mean	2.39	1.31	1.10	1.05	5.03
		Std. Dev.	0.22	0.14	0.15	0.18	0.13
		CoV	0.09	0.11	0.14	0.17	0.03

Table A.17: TPBT results - Additional macro-mechanical tests (Fibre dosage = 3.5 kg/m^3)

W/C ratio	**Beam density (kg/m^3)**		**(MPa)**				
			$\mathbf{f}_{R1}$	$\mathbf{f}_{R2}$	$\mathbf{f}_{R3}$	$\mathbf{f}_{R4}$	$\mathbf{f}_{LOP}$
0.45	2347.43	Mean	2.39	1.34	1.24	1.26	5.38
		Std. Dev.	0.23	0.17	0.17	0.18	0.40
		CoV	0.10	0.13	0.14	0.15	0.07
0.50	2373.40	Mean	2.91	1.63	1.49	1.50	5.39
		Std. Dev.	0.40	0.21	0.18	0.14	0.59
		CoV	0.14	0.13	0.12	0.09	0.11
0.60	2424.05	Mean	2.70	1.61	1.47	1.42	4.97
		Std. Dev.	0.29	0.30	0.35	0.38	0.49
		CoV	0.11	0.19	0.24	0.27	0.10
0.65	2432.50	Mean	3.30	1.86	1.52	1.43	4.88
		Std. Dev.	0.33	0.18	0.20	0.19	0.27
		CoV	0.10	0.10	0.13	0.13	0.06

Table A.18: TPBT results - Additional macro-mechanical tests (Fibre dosage = 4.5 kg/m^3)

W/C ratio	**Beam density (kg/m^3)**		**(MPa)**				
			$\mathbf{f}_{R1}$	$\mathbf{f}_{R2}$	$\mathbf{f}_{R3}$	$\mathbf{f}_{R4}$	$\mathbf{f}_{LOP}$
0.45	2495.34	Mean	3.49	2.09	2.02	2.05	6.55
		Std. Dev.	0.85	0.43	0.37	0.41	0.21
		CoV	0.24	0.21	0.18	0.20	0.03
0.50	2506.62	Mean	2.97	1.84	1.63	1.67	5.43
		Std. Dev.	0.65	0.37	0.32	0.33	0.23
		CoV	0.22	0.20	0.20	0.20	0.04
0.60	2509.80	Mean	2.77	1.55	1.45	1.44	6.60
		Std. Dev.	0.22	0.23	0.23	0.25	0.43
		CoV	0.08	0.15	0.16	0.17	0.07
0.65	2443.31	Mean	3.33	2.07	1.79	1.69	4.69
		Std. Dev.	0.44	0.17	0.03	0.23	0.30
		CoV	0.13	0.08	0.02	0.13	0.06

Table A.19: TPBT results - Additional macro-mechanical tests (Fibre dosage = 5.0 kg/m^3)

W/C ratio	**Beam density (kg/m^3)**		**(MPa)**				
			$\mathbf{f}_{R1}$	$\mathbf{f}_{R2}$	$\mathbf{f}_{R3}$	$\mathbf{f}_{R4}$	$\mathbf{f}_{LOP}$
0.45	2475.93	Mean	3.34	2.15	1.88	1.89	6.34
		Std. Dev.	0.57	0.40	0.10	0.08	0.36
		CoV	0.17	0.18	0.05	0.04	0.06
0.50	2479.57	Mean	2.95	1.82	1.68	1.66	4.64
		Std. Dev.	0.35	0.42	0.45	0.48	1.01
		CoV	0.12	0.23	0.27	0.29	0.22
0.60	2466.09	Mean	3.24	2.02	1.85	1.85	5.10
		Std. Dev.	0.23	0.33	0.38	0.38	0.59
		CoV	0.07	0.16	0.21	0.20	0.12
0.65	2478	Mean	3.26	2.32	2.24	2.22	5.35
		Std. Dev.	0.38	0.37	0.32	0.30	0.29
		CoV	0.12	0.16	0.14	0.14	0.05

A.3 Simple linear regression analysis results

The detailed simple linear regression regression analyses, for each performance parameter, is listed in Tables A.20 to A.24.

Table A.20: Simple linear regression analysis - Response variable f_{R1}

Independent Variable	Data type	Response variable - f_{R1}							
		R^2	Adjusted R^2	SS (Model)	MS (Model)	SS (Residuals)	MS (Residuals)	F_{ratio}	p-value
Compressive strength (MPa) (42.5N CEM III)	Raw values	0.100	0.082	0.856	0.856	7.667	0.156	5.471	0.023
	Average values	0.216	0.103	0.133	0.133	0.485	0.069	1.923	0.208
Compressive strength (MPa) (52.5N CEM II)	Raw values	0.082	0.064	0.602	0.602	6.739	0.132	4.553	0.038
	Average values	0.219	0.108	0.082	0.082	0.293	0.042	1.964	0.204
Coarse aggregate size (mm)	Raw values	0.268	0.222	0.693	0.693	1.896	0.118	5.853	0.028
	Average values	0.733	0.466	0.116	0.116	0.042	0.042	2.745	0.346
Coarse aggregate volume (l/m^3)	Raw values	0.049	0.031	0.517	0.517	10.057	0.193	2.674	0.108
	Average values	0.187	0.071	0.086	0.086	0.374	0.053	1.613	0.245
Fibre dosage (kg/m^3)	Raw values	0.259	0.240	2.539	2.539	7.264	0.186	13.633	0.001
	Average values	0.593	0.511	0.435	0.435	0.299	0.060	7.275	0.043
Mixing time (min) (Pan mixer)	Raw values	0.034	-0.001	0.096	0.096	2.755	0.098	0.977	0.331
	Average values	0.426	0.235	0.016	0.016	0.022	0.007	2.226	0.233
Mixing time (min) (Tilting-drum mixer)	Raw values	0.005	-0.030	0.015	0.015	2.949	0.105	0.146	0.705
	Average values	0.027	-0.298	0.003	0.003	0.093	0.031	0.083	0.792

Table A.21: Simple linear regression analysis - Response variable f_{R2}

Independent Variable	Data type	Response variable - f_{R2}							
		R^2	Adjusted R^2	SS (Model)	MS (Model)	SS (Residuals)	MS (Residuals)	F_{ratio}	p-value
Compressive strength (MPa) (42.5N CEM III)	Raw values	0.003	-0.016	0.011	0.011	3.479	0.068	0.168	0.684
	Average values	0.027	-0.112	0.007	0.007	0.268	0.038	0.192	0.675
Compressive strength (MPa) (52.5N CEM II)	Raw values	0.006	-0.013	0.016	0.016	2.545	0.050	0.317	0.576
	Average values	0.058	-0.077	0.005	0.005	0.082	0.012	0.430	0.533
Coarse aggregate size (mm)	Raw values	0.048	-0.012	0.060	0.060	1.203	0.075	0.800	0.384
	Average values	0.131	-0.737	0.010	0.010	0.066	0.066	0.151	0.764
Coarse aggregate volume (l/m^3)	Raw values	0.021	0.002	0.073	0.073	3.413	0.067	1.098	0.300
	Average values	0.089	-0.041	0.012	0.012	0.117	0.017	0.686	0.435
Fibre dosage (kg/m^3)	Raw values	0.488	0.475	2.647	2.647	2.778	0.069	38.113	0.000
	Average values	0.876	0.851	0.441	0.441	0.062	0.012	35.330	0.002
Mixing time (min) (Pan mixer)	Raw values	0.405	0.384	1.275	1.275	1.870	0.067	19.090	0.000
	Average values	0.761	0.682	0.213	0.213	0.067	0.022	9.566	0.054
Mixing time (min) (Tilting-drum mixer)	Raw values	0.003	-0.032	0.004	0.004	1.365	0.049	0.092	0.764
	Average values	0.030	-0.293	0.001	0.001	0.024	0.008	0.094	0.779

Table A.22: Simple linear regression analysis - Response variable f_{R3}

Independent Variable	Data type	Response variable - f_{R3}							
		R^2	Adjusted R^2	SS (Model)	MS (Model)	SS (Residuals)	MS (Residuals)	F_{ratio}	p-value
Compressive strength (MPa) (42.5N CEM III)	Raw values	0.012	-0.009	0.039	0.039	3.172	0.067	0.583	0.449
	Average values	0.037	-0.100	0.010	0.010	0.246	0.035	0.272	0.618
Compressive strength (MPa) (52.5N CEM II)	Raw values	0.127	0.110	0.286	0.286	1.956	0.040	7.158	0.010
	Average values	0.299	0.199	0.038	0.038	0.089	0.013	2.984	0.128
Coarse aggregate size (mm)	Raw values	0.022	-0.040	0.018	0.018	0.806	0.050	0.352	0.561
	Average values	0.122	-0.757	0.003	0.003	0.021	0.021	0.139	0.773
Coarse aggregate volume (l/m^3)	Raw values	0.055	0.037	0.149	0.149	2.555	0.049	3.038	0.087
	Average values	0.281	0.179	0.025	0.025	0.064	0.009	2.741	0.142
Fibre dosage (kg/m^3)	Raw values	0.662	0.653	3.314	3.314	1.694	0.046	72.402	0.000
	Average values	0.951	0.942	0.643	0.643	0.033	0.007	97.566	0.000
Mixing time (min) (Pan mixer)	Raw values	0.576	0.561	2.671	2.671	1.963	0.070	38.094	0.000
	Average values	0.874	0.832	0.445	0.445	0.064	0.021	20.756	0.020
Mixing time (min) (Tilting-drum mixer)	Raw values	0.111	0.080	0.168	0.168	1.337	0.048	3.510	0.071
	Average values	0.669	0.558	0.028	0.028	0.014	0.005	6.059	0.091

Table A.23: Simple linear regression analysis - Response variable f_{R4}

Independent Variable	Data type	Response variable - f_{R4}							
		R^2	Adjusted R^2	SS (Model)	MS (Model)	SS (Residuals)	MS (Residuals)	F_{ratio}	p-value
Compressive strength (MPa) (42.5N CEM III)	Raw values	0.009	-0.012	0.023	0.023	2.483	0.054	0.428	0.516
	Average values	0.051	-0.085	0.015	0.015	0.273	0.039	0.373	0.561
Compressive strength (MPa) (52.5N CEM II)	Raw values	0.124	0.107	0.273	0.273	1.929	0.038	7.223	0.010
	Average values	0.240	0.132	0.029	0.029	0.093	0.013	2.212	0.181
Coarse aggregate size (mm)	Raw values	0.015	-0.046	0.011	0.011	0.713	0.045	0.251	0.623
	Average values	0.159	-0.683	0.002	0.002	0.010	0.010	0.188	0.739
Coarse aggregate volume (l/m^3)	Raw values	0.069	0.050	0.154	0.154	2.097	0.041	3.757	0.058
	Average values	0.162	0.043	0.021	0.021	0.111	0.016	1.356	0.282
Fibre dosage (kg/m^3)	Raw values	0.697	0.690	4.128	4.128	1.792	0.046	89.846	0.000
	Average values	0.898	0.878	0.722	0.722	0.082	0.016	44.029	0.001
Mixing time (min) (Pan mixer)	Raw values	0.678	0.667	3.899	3.899	1.849	0.066	59.045	0.000
	Average values	0.934	0.912	0.650	0.650	0.046	0.015	42.320	0.007
Mixing time (min) (Tilting-drum mixer)	Raw values	0.077	0.044	0.106	0.106	1.274	0.046	2.329	0.138
	Average values	0.576	0.434	0.018	0.018	0.013	0.004	4.070	0.137

Table A.24: Simple linear regression analysis - Response variable f_{LOP}

Independent Variable	**Data type**	**Response variable - f_{LOP}**							
		R^2	**Adjusted R^2**	**SS (Model)**	**MS (Model)**	**SS (Residuals)**	**MS (Residuals)**	**F_{ratio}**	**p-value**
Compressive strength (MPa) (42.5N CEM III)	Raw values	0.842	0.839	65.777	65.777	12.344	0.237	277.080	0.000
	Average values	0.911	0.898	10.963	10.963	1.077	0.154	71.225	0.000
Compressive strength (MPa) (52.5N CEM II)	Raw values	0.593	0.585	17.390	17.390	11.942	0.234	74.267	0.000
	Average values	0.813	0.787	2.905	2.905	0.667	0.095	30.484	0.001
Coarse aggregate size (mm)	Raw values	0.282	0.237	1.280	1.280	3.256	0.203	6.290	0.023
	Average values	0.577	0.154	0.213	0.213	0.156	0.156	1.364	0.451
Coarse aggregate volume (l/m^3)	Raw values	0.017	-0.002	0.260	0.260	15.111	0.291	0.894	0.349
	Average values	0.077	-0.055	0.043	0.043	0.522	0.075	0.580	0.471
Fibre dosage (kg/m^3)	Raw values	0.016	-0.010	0.134	0.134	8.266	0.218	0.615	0.438
	Average values	0.047	-0.143	0.028	0.028	0.560	0.112	0.248	0.640
Mixing time (min) (Pan mixer)	Raw values	0.166	0.136	1.013	1.013	5.073	0.188	5.389	0.028
	Average values	0.322	0.096	0.163	0.163	0.343	0.114	1.423	0.319
Mixing time (min) (Tilting-drum mixer)	Raw values	0.126	0.095	0.657	0.657	4.542	0.162	4.048	0.054
	Average values	0.423	0.231	0.109	0.109	0.149	0.050	2.199	0.235

A.4 Multiple linear regression analysis results

The detailed multiple linear regression regression analyses, for each performance parameter, are provided in this section.

Univariate test of significance

The detailed univariate tests of significance, for each performance parameter, according to the multiple linear regression analyses, are listed in Table A.25 to Table A.29.

Table A.25: Univariate test of significance - Response variable f_{R1}

	Independent Variables	**SS**	**F_{ratio}**	**P-value**
Restricted parameterisation test	Compressive strength (MPa)	0.097408	2.068632	0.164431
	Coarse aggregate size (mm)	0.000565	0.012003	0.913753
	Coarse aggregate volume (l/m^3)	0.084406	1.792503	0.194293
	Fibre dosage (kg/m^3)	0.402424	8.546179	0.007871
	Mixing time (min)	0.040771	0.865845	0.362207
Best subset solution	Compressive strength (MPa)			
	Coarse aggregate size (mm)			
	Coarse aggregate volume (l/m^3)			
	Fibre dosage (kg/m^3)	0.435210	9.07460	0.005711
	Mixing time (min)			

Table A.26: Univariate test of significance - Response variable f_{R2}

	Independent Variables	**SS**	**F_{ratio}**	**P-value**
Restricted parameterisation test	Compressive strength (MPa)	0.000690	0.04309	0.837468
	Coarse aggregate size (mm)	0.001760	0.10992	0.743368
	Coarse aggregate volume (l/m^3)	0.011560	0.72191	0.404668
	Fibre dosage (kg/m^3)	0.441253	27.55491	0.000029
	Mixing time (min)	0.003409	0.21290	0.649037
Best subset solution	Compressive strength (MPa)			
	Coarse aggregate size (mm)			
	Coarse aggregate volume (l/m^3)			
	Fibre dosage (kg/m^3)	0.441127	31.02840	0.000008
	Mixing time (min)			

Table A.27: Univariate test of significance - Response variable f_{R3}

	Independent Variables	**SS**	**F_{ratio}**	**P-value**
Restricted parameterisation test	Compressive strength (MPa)	0.046700	3.77428	0.064953
	Coarse aggregate size (mm)	0.008493	0.68638	0.416297
	Coarse aggregate volume (l/m^3)	0.025540	2.06413	0.164871
	Fibre dosage (kg/m^3)	0.665540	53.78885	0.000000
	Mixing time (min)	0.015055	1.21671	0.281928
Best subset solution	Compressive strength (MPa)	0.027969	2.25626	0.146119
	Coarse aggregate size (mm)			
	Coarse aggregate volume (l/m^3)	0.025343	2.04444	0.165653
	Fibre dosage (kg/m^3)	0.658395	53.11299	0.000000
	Mixing time (min)			
Forward stepwise solution	Compressive strength (MPa)			
	Coarse aggregate size (mm)			
	Coarse aggregate volume (l/m^3)			
	Fibre dosage (kg/m^3)	0.642926	47.71248	0.000000
	Mixing time (min)			

Table A.28: Univariate test of significance - Response variable f_{R4}

	Independent Variables	SS	F_{ratio}	P-value
Restricted parameterisation test	Compressive strength (MPa)	0.034409	2.07092	0.164208
	Coarse aggregate size (mm)	0.020829	1.25362	0.274938
	Coarse aggregate volume (l/m^3)	0.021976	1.32268	0.262460
	Fibre dosage (kg/m^3)	0.741249	44.61304	0.000001
	Mixing time (min)	0.015007	0.90323	0.352242
Best subset solution	Compressive strength (MPa)			
	Coarse aggregate size (mm)			
	Coarse aggregate volume (l/m^3)			
	Fibre dosage (kg/m^3)	0.721506	42.74827	0.000001
	Mixing time (min)			

Table A.29: Univariate test of significance - Response variable f_{LOP}

	Independent Variables	SS	F_{ratio}	P-value
Restricted parameterisation test	Compressive strength (MPa)	2.978388	28.05340	0.000026
	Coarse aggregate size (mm)	0.025183	0.23720	0.631052
	Coarse aggregate volume (l/m^3)	0.036569	0.34445	0.563249
	Fibre dosage (kg/m^3)	0.001326	0.01249	0.912030
	Mixing time (min)	0.027538	0.25938	0.615617
Best subset solution	Compressive strength (MPa)	3.585880	38.48066	0.000001
	Coarse aggregate size (mm)			
	Coarse aggregate volume (l/m^3)			
	Fibre dosage (kg/m^3)			
	Mixing time (min)			

Parameter estimation

The regression parameter estimates for each performance parameter, considering the various solution processes, are listed in Table A.30 to Table A.34.

Table A.30: Linear regression parameter estimation - Response variable f_{R1}

	Independent Variables	Parameter	Std. Error	P-value	Beta (β)
Restricted parameterisation test	**Intercept**	0.234975	0.863087	0.787969	
	Compressive strength (MPa)	0.009064	0.006302	0.164431	0.264345
	Coarse aggregate size (mm)	-0.000808	0.007378	0.913753	-0.019494
	Coarse aggregate volume (l/m^3)	0.002372	0.001772	0.194293	0.224014
	Fibre dosage (kg/m^3)	0.240450	0.082250	0.007871	0.490502
	Mixing time (min)	-0.003312	0.003559	0.362207	-0.162954
Best subset solution	**Intercept**	1.567086	0.333667	0.000075	
	Compressive strength (MPa)				
	Coarse aggregate size (mm)				
	Coarse aggregate volume (l/m^3)				
	Fibre dosage (kg/m^3)	0.249345	0.082773	0.005711	0.508648
	Mixing time (min)				

Table A.31: Linear regression parameter estimation - Response variable f_{R2}

	Independent Variables	Parameter	Std. Error	P-value	Beta (β)
Restricted parameterisation test	**Intercept**	0.191200	0.503319	0.707678	
	Compressive strength (MPa)	-0.000763	0.003675	0.837468	-0.032047
	Coarse aggregate size (mm)	-0.001427	0.004303	0.743368	-0.049553
	Coarse aggregate volume (l/m^3)	0.000878	0.001033	0.404668	0.119415
	Fibre dosage (kg/m^3)	0.251783	0.047965	0.000029	0.739822
	Mixing time (min)	-0.000958	0.002076	0.649037	-0.067874
Best subset solution	**Intercept**	0.470009	0.181669	0.015623	
	Compressive strength (MPa)				
	Coarse aggregate size (mm)				
	Coarse aggregate volume (l/m^3)				
	Fibre dosage (kg/m^3)	0.251034	0.045066	0.000008	0.737622
	Mixing time (min)				

Table A.32: Linear regression parameter estimation - Response variable f_{R3}

	Independent Variables	Parameter	Std. Error	P-value	Beta (β)
Restricted parameterisation test	**Intercept**	-0.129441	0.442425	0.772591	
	Compressive strength (MPa)	-0.006276	0.003231	0.064953	-0.238192
	Coarse aggregate size (mm)	-0.003134	0.003782	0.416297	-0.098336
	Coarse aggregate volume (l/m^3)	0.001305	0.000908	0.164871	0.160360
	Fibre dosage (kg/m^3)	0.309221	0.042162	0.000000	0.820887
	Mixing time (min)	0.002012	0.001824	0.281928	0.128861
Best subset solution	**Intercept**	-0.269056	0.422981	0.530735	
	Compressive strength (MPa)	-0.004432	0.002951	0.146119	-0.168208
	Coarse aggregate size (mm)				
	Coarse aggregate volume (l/m^3)	0.001300	0.000909	0.165653	0.159739
	Fibre dosage (kg/m^3)	0.307411	0.042181	0.000000	0.816082
	Mixing time (min)				
Forward stepwise solution	**Intercept**	0.045016	0.176865	0.801093	
	Compressive strength (MPa)				
	Coarse aggregate size (mm)				
	Coarse aggregate volume (l/m^3)				
	Fibre dosage (kg/m^3)	0.303062	0.043875	0.000000	0.804536
	Mixing time (min)				

Table A.33: Linear regression parameter estimation - Response variable f_{R4}

	Independent Variables	Parameter	Std. Error	P-value	Beta (β)
Restricted parameterisation test	**Intercept**	-0.236956	0.512685	0.648486	
	Compressive strength (MPa)	-0.005387	0.003744	0.164208	-0.189167
	Coarse aggregate size (mm)	-0.004907	0.004383	0.274938	-0.142484
	Coarse aggregate volume (l/m^3)	0.001210	0.001053	0.262460	0.137628
	Fibre dosage (kg/m^3)	0.326336	0.048858	0.000001	0.801534
	Mixing time (min)	0.002009	0.002114	0.352242	0.119036
Best subset solution	**Intercept**	-0.097652	0.197942	0.625917	
	Compressive strength (MPa)				
	Coarse aggregate size (mm)				
	Coarse aggregate volume (l/m^3)				
	Fibre dosage (kg/m^3)	0.321049	0.049103	0.000001	0.788548
	Mixing time (min)				

Table A.34: Linear regression parameter estimation - Response variable f_{LOP}

	Independent Variables	Parameter	Std. Error	P-value	Beta (β)
Restricted parameterisation test	**Intercept**	1.823849	1.295976	0.173305	
	Compressive strength (MPa)	0.050123	0.009463	0.000026	0.773400
	Coarse aggregate size (mm)	0.005396	0.011079	0.631052	0.068848
	Coarse aggregate volume (l/m^3)	0.001561	0.002661	0.563249	0.078017
	Fibre dosage (kg/m^3)	0.013802	0.123504	0.912030	0.014897
	Mixing time (min)	0.002722	0.005344	0.615617	0.070859
Best subset solution	**Intercept**	2.640715	0.410644	0.000001	
	Compressive strength (MPa)	0.050065	0.008071	0.000001	0.772514
	Coarse aggregate size (mm)				
	Coarse aggregate volume (l/m^3)				
	Fibre dosage (kg/m^3)				
	Mixing time (min)				

Adjusted multiple regression models

The adjusted regression model parameters for each performance parameter are listed in Table A.35.

Table A.35: Comparison between the calibrated and the mean characteristic regression model parameters

Performance Parameter		**Regression model parameters**	
		Intercept	**Regression coefficient (γ)**
f_{R1}	Mean	1.5671	0.2493
	f_{ck} (lab)	1.2068	0.2493
	f_{ck} ($\sigma_y = 0.05$)	1.1902	0.239
	f_{ck} ($\sigma_y = 0.10$)	1.1348	0.2183
	f_{ck} ($\sigma_y = 0.15$)	1.0492	0.1961
f_{R2}	Mean	0.47	0.251
	f_{ck} (lab)	0.2739	0.251
	f_{ck} ($\sigma_y = 0.05$)	0.2817	0.2402
	f_{ck} ($\sigma_y = 0.10$)	0.2838	0.2192
	f_{ck} ($\sigma_y = 0.15$)	0.2711	0.1969
f_{R3}	Mean	0.045	0.3031
	f_{ck} (lab)	-0.1459	0.3031
	f_{ck} ($\sigma_y = 0.05$)	-0.1264	0.2913
	f_{ck} ($\sigma_y = 0.10$)	-0.0949	0.267
	f_{ck} ($\sigma_y = 0.15$)	-0.0714	0.2403
f_{R4}	Mean	-0.0977	0.321
	f_{ck} (lab)	-0.3114	0.321
	f_{ck} ($\sigma_y = 0.05$)	-0.2906	0.3102
	f_{ck} ($\sigma_y = 0.10$)	-0.2507	0.2861
	f_{ck} ($\sigma_y = 0.15$)	-0.2136	0.2583
f_{LOP}	Mean	2.6407	0.0501
	f_{ck} (lab)	2.1386	0.0501
	f_{ck} ($\sigma_y = 0.05$)	2.1151	0.0474
	f_{ck} ($\sigma_y = 0.10$)	2.0076	0.043
	f_{ck} ($\sigma_y = 0.15$)	1.8458	0.0386

Appendix B

Single-Fibre Performance Characteristics

This appendix provides detailed information regarding the specimen characteristics according to the single-fibre performance evaluation.

B.1 Mortar compression test results

The mortar compression test results obtained according to the single-fibre mix designs, are listed in Tables B.1 to B.3.

Table B.1: Mortar compression test results (W/C = 0.45)

Sample no.	**Density (kg/m^3)**	**Compressive strength (MPa)**	**Average (MPa)**	**Standard deviation**	**COV**
1	2223.42	67.03	71.78	6.062	0.084
2	2235.15	66.26			
3	2238.03	75.42			
4	2232.80	78.41			

Table B.2: Mortar compression test results (W/C = 0.55)

Sample no.	**Density (kg/m^3)**	**Compressive strength (MPa)**	**Average (MPa)**	**Standard deviation**	**COV**
1	2140.41	55.24	56.39	1.321	0.023
2	2132.21	55.48			
3	2143.84	56.70			
4	2133.61	58.12			

Table B.3: Mortar compression test results (W/C = 0.65)

Sample no.	Density (kg/m^3)	Compressive strength (MPa)	Average (MPa)	Standard deviation	COV
1	2197.50	52.78	50.35	2.519	0.050
2	2170.61	47.99			
3	2162.45	48.37			
4	2185.83	52.27			

B.2 SFPOT results

The SFPOT results obtained for each specimen, considering the investigation of the fibre performance in its virgin and premixed fibre state, are listed in Tables B.4 to B.6.

Table B.4: SFPOT results (W/C = 0.45)

Fibre state	Sample no.	Mass (g)	Density (kg/m^3)	Length (mm)	l_e (mm)	d_{eq} (mm)	F_{max} (N)	Interfacial bond (MPa)	Average (MPa)	Standard deviation	COV
Virgin	1	0.0174	0.92	50	25	0.694	41.791	0.767	0.803	0.088	0.110
	2	0.0166				0.678	40.908	0.768			
	3	0.0166				0.678	49.737	0.934			
	4	0.0185				0.716	41.791	0.744			
Premixed	1	0.0154	0.92	50	25	0.653	44.145	0.861	0.806	0.158	0.196
	2	0.0148				0.640	10.889	0.217			
	3	0.0153				0.651	32.079	0.628			
	4	0.0158				0.661	48.265	0.929			

Table B.5: SFPOT results (W/C = 0.55)

Fibre state	Sample no.	Mass (g)	Density (kg/m^3)	Length (mm)	l_e (mm)	d_{eq} (mm)	F_{max} (N)	Interfacial bond (MPa)	Average (MPa)	Standard deviation	COV
Virgin	1	0.0174	0.92	50	25	0.694	52.091	0.956	0.854	0.070	0.082
	2	0.0179				0.704	45.028	0.814			
	3	0.0177				0.700	44.145	0.803			
	4	0.0178				0.702	13.244	0.240			
Premixed	1	0.0163	0.92	50	25	0.672	59.449	1.127	1.107	0.029	0.027
	2	0.0117				0.569	47.971	1.073			
	3	0.0155				0.655	57.683	1.121			
	4	0.007				0.440	11.772	0.341			

Table B.6: SFPOT results (W/C = 0.65)

Fibre state	**Sample no.**	**Mass (g)**	**Density (kg/m^3)**	**Length (mm)**	**l_e (mm)**	**d_{eq} (mm)**	**F_{max} (N)**	**Interfacial bond (MPa)**	**Average (MPa)**	**Standard deviation**	**COV**
Virgin	1	0.0183	0.92	50	25	0.712	57.389	1.027	0.822	0.208	0.254
	2	0.0176				0.698	34.727	0.633			
	3	0.0162				0.670	51.208	0.974			
	4	0.0170				0.686	35.022	0.650			
Premixed	1	0.0165	0.92	50	25	0.676	87.996	1.658	1.859	0.208	0.112
	2	0.0143				0.629	102.416	2.073			
	3	0.0168				0.682	98.591	1.841			
	4	0.0087				0.491	96.236	2.497			

Appendix C

Performance Parameters - Observed and Predicted

This appendix provides a detailed comparison between the observed TPBT results for each performance parameter, which is based on the average values, and the predicted values, according to the linear regression models.

Table C.1: f_{R1} - Comparison between the observed values and the predicted values according to the linear regression model

No.	Observed values (Y)	Predicted values (Y')	Residuals (Y-Y')	Squared Residuals
1	2.10	2.56	-0.46	0.215
2	2.56	2.56	0.00	0.000
3	2.50	2.56	-0.07	0.004
4	2.28	2.56	-0.29	0.082
5	2.59	2.56	0.03	0.001
6	2.84	2.56	0.28	0.078
7	2.40	2.56	-0.16	0.026
8	2.62	2.56	0.05	0.003
9	2.53	2.56	-0.03	0.001
10	2.45	2.56	-0.12	0.014
11	2.76	2.56	0.19	0.038
12	2.75	2.56	0.18	0.033

Continued on next page

Table C.1 – *Continued from previous page*

No.	Observed values (Y)	Predicted values (Y')	Residuals (Y-Y')	Squared Residuals
13	2.92	2.56	0.35	0.123
14	2.88	2.56	0.31	0.097
15	2.25	2.56	-0.32	0.099
16	2.40	2.56	-0.17	0.028
17	2.53	2.56	-0.04	0.001
18	2.47	2.19	0.28	0.079
19	2.22	2.32	-0.10	0.010
20	2.32	2.44	-0.12	0.013
21	2.80	2.69	0.11	0.013
22	3.22	2.81	0.41	0.166
23	2.81	2.94	-0.13	0.017
24	2.76	2.56	0.20	0.040
25	2.41	2.56	-0.15	0.023
26	2.50	2.56	-0.07	0.004
27	2.37	2.56	-0.19	0.036
28	2.57	2.56	0.00	0.000

Table C.2: f_{R2} - Comparison between the observed values and the predicted values according to the linear regression model

No.	Observed values (Y)	Predicted values (Y')	Residuals (Y-Y')	Squared Residuals
1	1.30	1.47	-0.17	0.029
2	1.62	1.47	0.14	0.021
3	1.48	1.47	0.01	0.000
4	1.32	1.47	-0.16	0.025

Continued on next page

Table C.2 – *Continued from previous page*

No.	Observed values (Y)	Predicted values (Y')	Residuals (Y-Y')	Squared Residuals
5	1.45	1.47	-0.03	0.001
6	1.49	1.47	0.02	0.000
7	1.39	1.47	-0.08	0.006
8	1.38	1.47	-0.09	0.008
9	1.36	1.47	-0.12	0.013
10	1.41	1.47	-0.06	0.004
11	1.58	1.47	0.11	0.011
12	1.55	1.47	0.08	0.006
13	1.77	1.47	0.29	0.086
14	1.47	1.47	0.00	0.000
15	1.33	1.47	-0.14	0.020
16	1.39	1.47	-0.08	0.007
17	1.51	1.47	0.03	0.001
18	1.30	1.10	0.20	0.041
19	1.20	1.22	-0.02	0.001
20	1.33	1.35	-0.02	0.000
21	1.69	1.60	0.09	0.007
22	1.94	1.73	0.21	0.046
23	1.86	1.85	0.01	0.000
24	1.52	1.47	0.04	0.002
25	1.41	1.47	-0.06	0.004
26	1.35	1.47	-0.13	0.016
27	1.37	1.47	-0.11	0.012
28	1.50	1.47	0.03	0.001

Table C.3: f_{R3} - Comparison between the observed values and the predicted values according to the linear regression model

No.	Observed values (Y)	Predicted values (Y')	Residuals (Y-Y')	Squared Residuals
1	1.19	1.26	-0.06	0.004
2	1.48	1.26	0.22	0.050
3	1.31	1.26	0.05	0.003
4	1.13	1.26	-0.13	0.016
5	1.21	1.26	-0.05	0.003
6	1.26	1.26	0.00	0.000
7	1.09	1.26	-0.17	0.029
8	1.10	1.26	-0.16	0.025
9	1.08	1.26	-0.18	0.031
10	1.24	1.26	-0.02	0.000
11	1.47	1.26	0.21	0.045
12	1.26	1.26	0.00	0.000
13	1.42	1.26	0.16	0.026
14	1.24	1.26	-0.02	0.000
15	1.13	1.26	-0.13	0.017
16	1.21	1.26	-0.05	0.003
17	1.31	1.26	0.05	0.003
18	0.90	0.80	0.09	0.009
19	0.98	0.95	0.03	0.001
20	1.12	1.11	0.01	0.000
21	1.47	1.41	0.06	0.003
22	1.75	1.56	0.19	0.038
23	1.68	1.71	-0.03	0.001
24	1.22	1.26	-0.04	0.002

Continued on next page

Table C.3 – *Continued from previous page*

No.	Observed values (Y)	Predicted values (Y')	Residuals (Y-Y')	Squared Residuals
25	1.21	1.26	-0.05	0.002
26	1.13	1.26	-0.12	0.015
27	1.22	1.26	-0.04	0.002
28	1.41	1.26	0.15	0.023

Table C.4: f_{R4} - Comparison between the observed values and the predicted values according to the linear regression model

No.	Observed values (Y)	Predicted values (Y')	Residuals (Y-Y')	Squared Residuals
1	1.12	1.19	-0.06	0.004
2	1.42	1.19	0.24	0.057
3	1.19	1.19	0.00	0.000
4	1.08	1.19	-0.10	0.011
5	1.12	1.19	-0.06	0.004
6	1.19	1.19	0.00	0.000
7	1.00	1.19	-0.18	0.034
8	1.02	1.19	-0.16	0.027
9	1.04	1.19	-0.15	0.022
10	1.16	1.19	-0.03	0.001
11	1.43	1.19	0.24	0.059
12	1.14	1.19	-0.04	0.002
13	1.29	1.19	0.11	0.012
14	1.01	1.19	-0.17	0.029
15	1.03	1.19	-0.15	0.024

Continued on next page

Table C.4 – *Continued from previous page*

No.	Observed values (Y)	Predicted values (Y')	Residuals (Y-Y')	Squared Residuals
16	1.15	1.19	-0.04	0.002
17	1.25	1.19	0.06	0.004
18	0.81	0.70	0.11	0.012
19	0.93	0.87	0.06	0.004
20	1.03	1.03	0.01	0.000
21	1.44	1.35	0.09	0.009
22	1.80	1.51	0.30	0.088
23	1.59	1.67	-0.07	0.005
24	1.17	1.19	-0.02	0.000
25	1.17	1.19	-0.02	0.000
26	1.07	1.19	-0.11	0.013
27	1.22	1.19	0.03	0.001
28	1.31	1.19	0.13	0.016

Table C.5: f_{LOP} - Comparison between the observed values and the predicted values according to the linear regression model

No.	Observed values (Y)	Predicted values (Y')	Residuals (Y-Y')	Squared Residuals
1	4.15	4.29	-0.14	0.020
2	4.72	4.55	0.17	0.028
3	4.41	4.59	-0.17	0.030
4	4.17	4.87	-0.70	0.496
5	4.98	5.09	-0.11	0.012
6	5.14	5.45	-0.30	0.092
7	5.14	5.57	-0.43	0.184

Continued on next page

Table C.5 – *Continued from previous page*

No.	**Observed values (Y)**	**Predicted values (Y')**	**Residuals (Y-Y')**	**Squared Residuals**
8	5.49	5.64	-0.16	0.025
9	6.23	5.98	0.26	0.066
10	5.25	5.27	-0.02	0.000
11	5.43	5.01	0.41	0.171
12	5.10	4.89	0.22	0.046
13	5.39	5.12	0.27	0.073
14	5.14	5.04	0.10	0.010
15	4.88	4.73	0.15	0.021
16	4.56	5.00	-0.44	0.195
17	5.17	4.87	0.30	0.087
18	5.46	5.15	0.31	0.095
19	5.14	5.25	-0.11	0.013
20	5.10	5.25	-0.15	0.022
21	5.33	5.41	-0.08	0.007
22	5.97	5.23	0.74	0.548
23	5.12	5.34	-0.22	0.047
24	5.54	5.43	0.11	0.011
25	5.25	5.20	0.05	0.003
26	5.17	5.30	-0.13	0.017
27	5.34	5.51	-0.17	0.030
28	5.80	5.53	0.27	0.074